Integrated Systems Biology Analysis;

Exemplified on Potyvirus and Geminivirus interaction with *Nicotiana benthamiana*

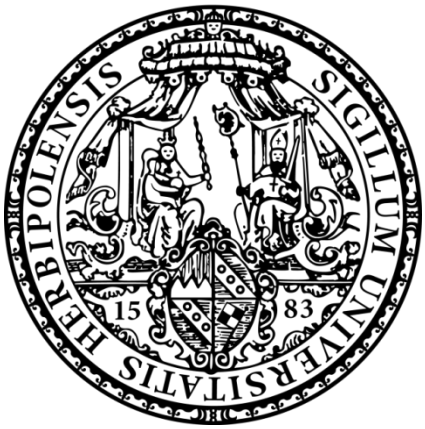

DISSERTATION

zur Erlangung des naturwissenschaftlichen Doktorgrades

der Fakultät für Biologie,

Bayerischen Julius-Maximilians-Universität Würzburg

vorgelegt von

Pirasteh Pahlavan

aus Karaj, Iran

Würzburg, Germany 2017

Eingereicht am:
.....

Mitglieder der Promotionskommission:

Vorsitzender: Prof. Dr. Thomas Rudel

Erster Gutachter: Prof. Dr. Thomas Dandekar

Zweiter Gutachter: PD Dr. Susanne Berger

Tag des Promotionskolloquiums: .....

Doktorurkunde ausgehändigt am: .....

Erklärung (gem. § 4 Abs. 3 S. 3, 5 und 8 der Promotionsordnung)

Hiermit erkläre ich an Eides statt, die Dissertation " Integrated Systems Biology Analyses; exemplified on Potyvirus and Geminivirus interaction with *Nicotiana benthamiana*" eigenständig, d.h. insbesondere selbstständig und ohne Hilfe eines kommerziellen Promotionsberaters, angefertigt und keine anderen als die von mir angegebenen Quellen und Hilfsmittel verwendet zu haben. Ich erkläre außerdem, dass dir Dissertation weder in gleicher noch in ähnlicher Form bereits in einem anderen Prüfungsverfahren vorgelegen hat. Zusätzlich habe oder werde ich nicht versuchen neben diesem Abschluss einen weiteren Abschluss oder Qualifikation mit dieser Doktorarbeit zu erweben.

Ort, Datum

Würzburg, …29.03.2017…….

Dedicated to my beloved parents

Acknowledgements

This study is made by contribution of number of amazing people whom I would like to express my gratitude.

I would first express my deepest appreciation to my incredible supervisor Prof. Dr. Thomas Dandekar. The honour and privilege to have worked with him, without his essential and motivational comments, patience, and consistent encourage neither of these would have happened and his positive impact on my life is invaluable.

I would also like to extend my appreciation to my committee members PD Dr. Susanne Berger and Prof. Dr. Thomas Rudel, for their time, guidance, and kindly comments to improve this study.

I would also like to extend my thanks to my great mentor Dr. Muhammad Naseem for the nice guidance through the work also warmly sharing his deep knowledge and valuable experiences. Along with him, I had a chance to meet great friends and colleagues in department of Bioinformatics in university of Würzburg; my very special gratitude to Robin Hillius and Dr. Elena Bencúrová for their kindly support and kindness on proofreading this thesis. I also thank the helpful discussions with Dr. Meik Kunz, Martin Kaltdorf, and Dr. Chunguang Liang during the project. I also appreciate Eva Fischer and Annette Dorst for the consistent support with all the administrative procedure.

I would also like to seize the opportunity to thank my co-workers in plant virus department of Leibniz-institute DSMZ, Dr. Stephan Winter for giving me the project, more importantly to technical support of Sabine Bonse, Beate Stein, Marianne Koebeler, Anja Butgereitt, and many thanks to Dr. Wulf Menzel for his nice cooperation. I also appreciate the technical assist of IT department and greenhouse facility of DSMZ and JKI in Braunschweig. Very special thanks to Dr. Sven Jechalke for nice revision and Prof. Dr. Smalla for her attentive insights.

I am so thankful to my friends in the campus of Helmholtz Centre for Infection Research, Braunschweig for their contribution rendered to me at different stages of this work; Dr. Cristina Della Beffa, Abhishek Bakuli, Dr. Till Robin Lesker and Dr. Stefan Janssen for all their kindly helps in addition to Dr. Michael Beckstette for his support on central cluster. Also thank the BIC and R club members for the nice open discussions and troubleshooting, especially Dr. Johannes Sikoroski and Dr. Sarah Pohl for their nice suggestions.

In 2014, I spent several months at Max Planck Institute for Molecular Plant Physiology, Potsdam. I would like to show my gratitude to Marek Mutwil, Christian Schudoma, Bjoern Ost Hansen, Sebastian Proost, Neha Vaid, and Jürgen Gremmels for this opportunity, with most memorable experience to work in such an inspiring atmosphere.

My sincere appreciation to Dr. Daniel G. Vassão and Dr. Michael Reichelt, Dept. of Biochemistry, Max Planck Institute for Chemical Ecology, Jena where the HPLC-based

chemical analyses were performed in collaboration. I also thank to Microarray and Deep-Sequencing Core Facility in University Medical Center Göttingen especially heading by Dr. Gabriela Salinas-Riester for the great discussion on the RNA-seq, nice consultant on experiment design and great quality of libraries and sequences.

I very much thank the gracious support of Sophien Kamoun, Joe Win, Steve Wylie, Ken Shirasu, Cristina Azevedo, Guo Huishan for providing transgenic and mutant material. Also I thank Kranthi Mandadi and Manpreet S Katari for their advice throughout the project.

I am very blessed for having the friends who are currently spread all over the world but still ‘have been there for me’; Dorna, Golnar, Shirin, Mehdi, Maxi, Anja, Samad, Laura and Franzisca. The ‘wir brauchen Deutsch’ and ‘Wednesday Poker’ gang especially Angèle, Peitro, Gautier, Filipe, Fernando whom I had the most fun with, away from work.

My family is a treasure that I owe my very deep gratitude and thanks to; my mom and dad for keeping up with strength and hope. They raised me gifted with ‘best brothers ever’ Pedram and Pouyan. Their constant unconditional love, believing in me through, and encouragements have supported my dreams come true.

Thank you all for your beautiful sprit around ….

Summary

Viral infections induce a significant impact on various functional categories of biological processes in the host. The understanding of this complex modification of the infected host immune system requires a global and detailed overview on the infection process. Therefore it is essential to apply a powerful approach which identifies the involved components conferring the capacity to recognize and respond to specific pathogens, which in general are defeated in so-called compatible virus-plant infections. Comparative and integrated systems biology of plant-virus interaction progression may open a novel framework for a systemic picture on the modulation of plant immunity during different infections and understanding pathogenesis mechanisms. In this thesis these approaches were applied to study plant-virus infections during two main viral pathogens of cassava: *Cassava brown streak virus* and *African cassava mosaic virus*.

Here, the infection process was reconstructed by a combination of omics data-based analyses and metabolic network modelling, to understand the major metabolic pathways and elements underlying viral infection responses in different time series, as well as the flux activity distribution to gain more insights into the metabolic flow and mechanism of regulation; this resulted in simultaneous investigations on a broad spectrum of changes in several levels including the gene expression, primary metabolites, and enzymatic flux associated with the characteristic disease development process induced in *Nicotiana benthamiana* plants due to infection with CBSV or ACMV.

Firstly, the transcriptome dynamics of the infected plant was analysed by using mRNA-sequencing, in order to investigate the differential expression profile according the symptom developmental stage. The spreading pattern and different levels of biological functions of these genes were analysed associated with the infection stage and virus entity. A next step was the Real-Time expression modification of selected key pathway genes followed by their linear regression model. Subsequently, the functional loss of regulatory genes which trigger R-mediated resistance was observed. Substantial differences were observed between infected mutants/transgenic lines and wild-types and characterized in detail. In addition, we detected a massive localized accumulation of ROS and quantified the scavenging genes expression in the infected wild-type plants relative to mock infected controls.

Moreover, we found coordinated regulated metabolites in response to viral infection measured by using LC-MS/MS and HPLC-UV-MS. This includes the profile of the phytohormones, carbohydrates, amino acids, and phenolics at different time points of infection with the RNA and DNA viruses. This was influenced by differentially regulated enzymatic activities along the salicylate, jasmonate, and chorismate biosynthesis, glycolysis, tricarboxylic acid cycle, and pentose phosphate pathways, as well as photosynthesis, photorespiration, transporting, amino acid and fatty acid biosynthesis. We calculated the flux redistribution considering a gradient of modulation for enzymes along different infection stages, ranging from pre-symptoms towards infection stability.

Collectively, our reverse-engineering study consisting of the generation of experimental data and modelling supports the general insight with comparative and integrated systems biology into a model plant-virus interaction system. We refine the cross talk between transcriptome modification, metabolites modulation and enzymatic flux redistribution during compatible infection progression. The results highlight the global alteration in a susceptible host, correlation between symptoms severity and the alteration level. In addition we identify the detailed corresponding general and specific responses to RNA and DNA viruses at different stages of infection. To sum up, all the findings in this study strengthen the necessity of considering the timing of treatment, which greatly affects plant defence against viral infection, and might result in more efficient or combined targeting of a wider range of plant pathogens.

Zusammenfassung

Virale Infektionen haben einen signifikanten Einfluss auf verschiedene funktionelle Eigenschaften und biologische Prozesse im Wirt. Das Verständnis dieser komplexen Modifikation des infizierten Wirtsimmunsystems benötigt eine globale und detaillierte Einsicht in den Infektionsprozess. Diese erfordert einen leistungsfähigen Ansatz zur Identifizierung der beteiligten Komponenten, welche eine Pathogen-Erkennung und Antwort vermitteln bzw. eine kompatible Virus-Pflanze-Infektion voraussetzen. Die Anwendung der vergleichenden und integrierten Systembiologie zur Untersuchung dieser Pflanzen-Virus-Interaktionen im Infektionsverlauf kann eine neue Grundlage zum systematischen Verständnis der Modulation des Immunsystems der Pflanze und der Pathogen-Mechanismen während verschiedener Infektionen eröffnen. In dieser Arbeit wenden wir diese Ansätze an, um Pflanzen-Virus-Infektionen der zwei häufigsten viralen Pathogenen von Maniok zu untersuchen, den *Cassava brown streak virus* (CBSV) und den *African cassava mosaic virus* (ACMV).

Dazu rekonstruieren wir den Infektionsprozess durch die Kombination von „omics“ basierten Datenanalysen und metabolischen Netzwerkmodellen um die wichtigen Elemente des viralen Infektionsprozesses zu verschieden Zeitpunkten aufzuklären. Metabolische Flussanalysen geben Einblick in metabolische Umsätze und deren Regulierung. Diese simultanen Untersuchungen erfassen ein breites Spektrum der Virus-vermittelten Veränderungen im Wirt über mehrere „omics“ Ebenen, einschließlich Geneexpression, Primärmetabolite und enzymatischer Aktivitäten, die mit dem charakteristischen Krankheitsentwicklungsprozess assoziiert sind, der in *Nicotiana benthamiana* Pflanzen aufgrund einer Infektion mit CBSV oder ACMV induziert wurde.

Zuerst wurde die Dynamik des Transkriptoms infizierter Pflanzen mittels mRNA-Sequenzierung analysiert um das differentielle Expressionsprofil nach dem Symptomentwicklungsstadium zu untersuchen. Die Expressionsmuster und die biologischen Funktionen dieser Gene wurden im Hinblick auf die Infektionsstufe und den Virus Einheiten aufgelöst. Ein nächster Schritt war die Echtzeit-Expressionsmodifikation ausgewählter Schlüsselprozess-Gene, gefolgt von der Umsetzung im linearen Regressionsmodell. Anschließend wurde der funktionelle Verlust von regulatorischen Genen ermittelt, welche eine R-vermittelte Resistenz auslösen können. Es wurden erhebliche Unterschiede zwischen infizierten Mutanten / transgenen Linien und Wild-typen beobachtet und im Detail charakterisiert. Darüber hinaus entdeckten wir eine massive lokalisierte Akkumulation von reaktiven Sauerstoffspezies und quantifizierten die Expression von Abbauproteinen in den infizierten Wildtyp-Pflanzen relativ zu Mock-infizierten Kontrollen.

Darüber hinaus fanden wir koordinierte regulierte Metaboliten als Reaktion auf eine virale Infektion, gemessen unter Verwendung von LC-MS / MS und HPLC-UV-MS Techniken. Dazu gehören die Analyse der Profile von Phytohormonen, Kohlenhydraten, Aminosäuren, und Phenolika zu verschiedenen Zeitpunkten der Infektion mit den RNA und DNA-Viren. Diese wurden beeinflusst durch die differentielle regulierten

enzymatischen Aktivitäten entlang der Salicylat-, Jasmonat- und Chorismat-Biosynthese, der Glykolyse, Tricarbonsäure und Pentose-Phosphat-Umsetzung, der Photosynthese und Photorespiration, des Transportes und der Aminosäure sowie Fettsäure-Biosynthese. Wir berechneten die Umverteilung des metabolischen Flusses unter Berücksichtigung einer ansteigenden Beeinflussung von Enzymen in den verschiedeneren Infektionsstadien, die von Prä-Symptomen zur Infektionsstabilität reichen.

Zusammengefasst beinhaltet unsere Reverse-Engineering-Studie die Generierung von experimentellen Daten und deren Modellierung mittels vergleichender und integrierter Systembiologie zum Einblick in das Modell-Pflanzen-Virus-Interaktionssystem. Wir lösten die Interaktion zwischen Transkriptom-Modifikation, Metabolitenmodulation und die Umverteilung des metabolischen Flusses während des kompatiblen Infektionsprozesses auf. Das Ergebnis zeigt die globalen Veränderungen in einem anfälligen Wirt auf, sowie die Korrelation zwischen Symptomschwere und der Stärke dieser Veränderungen. Darüber hinaus identifizieren wir im Detail die entsprechenden allgemeinen und spezifischen Reaktionen auf RNA und DNA-Viren in den verschiedenen Stadien der Infektion. Zusammenfassend lässt sich feststellen, dass die Erkenntnisse aus dieser Studie die Notwendigkeit aufzeigen, den zeitlichen Ablauf bei einer Pflanzenschutzbehandlung zu berücksichtigen, welche die pflanzliche Abwehr gegen eine Virusinfektion stark beeinflusst; und insgesamt zu einer effizienteren oder kombinierten Anwendung gegen ein breiteres Spektrum von Pflanzenpathogenen führen könnte.

Content

Figures and Tables

1. Introduction

The complex networks of biological systems are involved during compatible host-pathogen interaction that depends on the entity of pathogen, environmental condition, developmental stage and physiological condition of host, which leads to a wide range of modifications in various biological processes. The common strategies among different microbial pathogens to promote their infection include efficient protein secretion systems. This delivers their virulence effector proteins into the host cell cytoplasm which modulate the host defence mechanisms. Plants pathosystems include definitive combination of host/pathogen responses as well as specific reaction signals associated with the pathogen. Unlike animals which could develop adaptive immune system, plants are dependent on innate responses of individual cells to activate defence by either cell surface or cytoplasmic immune receptors. During pathogen infection progression antagonistic or synergistic modification in plant host results in minimizing the surviving costs in order to optimizing resistance strategies (Koornneef A 2008, Jacob F 2013, Pierce EJ 2013, Sarris P 2015).

According to the common view on plant innate immunity system, which is represented in the schematic 'zigzag' model by Dangl *et al.*, the PTI[1] response caused by recognition of certain conserved M/PAMPs[2] by plant PRRs[3]. MAPK[4] cascades are involved in plant stress responses by mediating M/PAMP signals, while NB-LRR[5] accomplish intracellular either direct or indirect detection of pathogen effectors. That activates the immune signalling pathway ETI[6], an amplified version of PTI that often passes a threshold for induction of HR[7], the oxidative burst, the induction of defence-related genes, and localized cell death. Based on current definitions of innate immunity cascade in case of viruses, virus-associated factors, such as virion components or virus-encoded proteins, could be perceived by putative cell surface PRRs or cytosolic NB-LRR receptors and R proteins to trigger ETI or susceptible ETS[8] responses, culminating in HR, SAR, and/or necrosis phenotypes (Dangl 2006, Botër M 2007, Mandadi KK 2013, Malinovsky FG 2014, Adachi H 2015, Sarris P 2015). In this study we address this model and describe the involved elements during the compatible interaction between two different plant viruses with their susceptible host, the essential bases for developing resistant or tolerant crops.

Plant viruses with their outstanding characteristics are appealing for elucidation of host–microbe interactions due to encoding few proteins and exclusive dependency on host cellular metabolism for multiplication and movement. Various symptomatic manifestations of host immune responses triggered in the infected cells occur with chlorotic lesions or spots, ringspots, and necrotic lesions on leaves, stems, tubers and fruits, and subsequently HR in association with ROS[9], ion fluxes generation, induction of defence-related genes and PCD[10] (Whitham SA 2006, Komatsu K 2010, Kørner CJ 2013). Infection with Potyviruses as a RNA virus involves various molecular processes taking place in several cellular compartments, requiring the participation of many host genes and proteins, and causing modification on signalling networks, likely including Ca^{2+} signalling. This would transduce virus-induced signals to the nucleus, triggering changes in host gene expression. One of the intriguing aspects of this molecular process is to

understand the crosstalk between virus-induced processes in the cytoplasm and host gene expression modification in the nucleus (Ivanov KI 2014). On the other hand, infection with Geminiviruses as a DNA virus consequently reprograms the infected cell cycle followed by replication of both viral and plant chromosomal DNA, redirected protein turnover or blocked host defence and hormone signalling. This is fulfilled through modification on macromolecular trafficking and cell signalling (Hanley-Bowdoin L 1999, Krupovic M 2009).

This study is aimed to address the most important threatening viral diseases in cassava[11] production; cassava brown streak disease (CBSD) and cassava mosaic disease (CMD). These viral infections threat the production of this staple crop by food-insecure populations in sub-Saharan Africa. It is mostly produced for its starchy roots, but the leaves are also part of the diet in several African regions (Vanderschurena H 2014). These viral diseases result in 100% damage in susceptible varieties as well as severely defect on the food security (Monger WA 2001, Mbanzibwa DR 2011). This plant is being less-devoted on adapting new improved varieties with desired virus resistance properties, compared to other staple crops like rice, maize and wheat (Scholthof K-BG 2011). Therefore, it opens the elaborative potential and challenges to analyse the interaction between this important host and viral pathogens.

CBSD is caused by one or two distinct Ipomoviruses belong to Potyviridae, *Cassava brown streak virus* (CBSV) and *Ugandan Cassava brown streak virus* (UCBSV). CBSD is characterised by filamentous flexible particles and a positive-sense single-stranded RNA (+ssRNA) genome, of 10 segments, total size approximately 8.9 to 10.8 kb, and code for a polypeptide with about 2,900 amino acid residues, which is processed into mature proteins and a short overlapping open reading frame (Dombrovsky A 2014, Alicai T 2016). Ipomovirus genome is monopartite, linear, and is about 11,000 nucleotides long. The 3' terminus has a poly (A) tract and the 5' terminus has a genome-linked protein (*VPg*). Genome is organized similar to other members of the Potyviridae family, though it shows some variation in details between the members. It is translated into a single polyprotein of 390 kDa, from which an estimated ten functional products are produced by proteolytic processing: with the 34 kDa coat protein at the C-terminus, *P1* protein[12], *HC-Pro*[13], *P3* protein[14], "*6K1*"[15], *CI*[16], "6K2"[17]; *VPg*[18], *NIa-Pro*[19] and *NIb*[20]. Some members of this genus lack the HC-Pro cistron. In some of these cases there appears to be two (divergent) copies of the P1 protein in its place, while in the cassava-infecting members such as CBSV, an additional *HAM-1* like protein has been identified between the *NIb* and coat protein regions, besides a small ORF (*PIPO*) is generated by frameshifting within the *P3* cistron (Fig. 1).

CMD is caused by a Begomovirus belong to Geminiviridae, *African mosaic virus* (ACMV), which is nominated as one of the top 10 most important plant viruses according to contributors to molecular plant pathology. Geminivirus genomes are arranged with divergent transcription units, and a 5′ intergenic region contains the origin for rolling-circle replication and two RNA polymerase II promoters. Begomovirus can have monopartite genomes or bipartite genomes designated as DNA-A and DNA-B, a single-

stranded DNA (ssDNA) structure which is packaged into virions and replicative dsDNA[21] transcribed in the nucleus of infected plant cells (Hull 2009, Scholthof K-BG 2011, Hanley-Bowdoin L 2013). ACMV was one of the first Geminiviruses which was characterized molecularly. The bipartite genome of two single-stranded DNA consists a DNA-A and DNA-B segment of 2800 nt and 2760 nt, respectively (Fig. 1). The common region also possesses the sequences necessary for the initiation and termination of rolling circle replication, the mechanism by which these viruses replicate. Consequently, both DNAs are required for efficient pathogenicity: while DNA-B encodes two proteins, namely *BC1* and *BV1* which are involved in intracellular and systemic virus movement, DNA-A encodes the virus replication genes as well as encapsidation of viral nucleic acid, in addition to the *AV2* protein which functions as anti-defence protein to inhibit PTGS[22]. BC1 is found on the complementary strand and mediates cell-to-cell movement of the virus and *BV1* is the *NSP* that controls movement of viral DNA between the nucleus and cytoplasm (Hanley-Bowdoin L 1999, Scholthof K-BG 2011, Pierce EJ 2013).

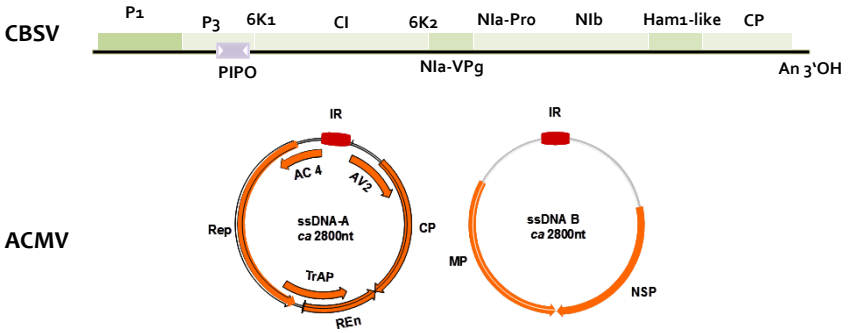

Figure 1. Genome structure of CBSV-Tan70 and ACMV

Notable increment of interest and efforts have been made at studying molecular biology of plant interaction with CBSV and ACMV as the vital step towards developing CBSD/CMD tolerant/resistant varieties. Moreover, these viruses are transmitted by whiteflies, *Bemisia tabaci*, in a semi persistent manner. Therefore, the increased threats of whitefly population due to global warming is another aspect of importance of this study to protect cassava against one or both of these diseases (Scholthof K-BG 2011, Dombrovsky A 2014, Alicai T 2016). We started the investigation in the prime model system for virology and molecular biology with a broad wide range of functionality, *Nicotiana benthamiana* (Nakasugi K 2013, FF 2016).

Nicotiana benthamiana is a native tobacco, an allo-tetraploid with 19 chromosome pairs with 26 exclusively Australian native tobacco relatives. This plant is particularly useful to plant virologists due its susceptible nature to over 500 different viruses. Also, it has been used as a host for VIGS[23], as well as transient transgene expression by agro-infiltration (Nakasugi K 2013). Both ACMV and CBSV infection in *N. benthamiana* occur with plant stunting and typical curled and deformed leaves along with mottled pattern and/or yellow mosaic, vein swelling and enations. However, ACMV infected *N. benthamiana* develops more severe symptoms and earlier reproductive organs. At later stage of infection progress, the old leaves start to turn yellow with necrosis spots. These infection symptoms imply notable manipulation in host which occurs as altered cellular

homeostasis and developmental processes. These symptomatic developments involve different responses such as hypersensitive and necrotic resistance to virus infection, systemic necrosis, systemic acquired resistance, R gene-mediated or defence-related genes expression and ubiquitin proteasome system. To identify these extended changes, the detailed differentially regulated processes involved in response to infection progression with these viruses, transcriptome, metabolome and enzymatic flux levels, have been addressed as an integrated systems biology approach.

Systems biology of host- pathogen interaction includes an integrative genome-wide analyses and modelling of host and/or pathogen responses. That simulates the dynamics of infection processes, together with experimental strategies aimed at understanding interactions across multiple molecular entities (Fernie AR 2004, Durmuş S 2015). Through development of experimental and computational analyses, different robust techniques have been developed for analysing and describing the confrontation of the host with viruses. This research started with reconstruction of the infection process by omics data-based analyses followed by metabolic network modelling, to gain an insight into the major metabolic pathways and elements underlying viral infection progression, as well as the enzymatic flux redistribution to understand the mechanism of regulation in various levels such as transcript and metabolic flow. All the computational analyses accompanied by experimental validation on a broad spectrum of changes in several levels including the gene expression, oxidative activities, and primary metabolites induced in *N. benthamiana* plants due to infection with CBSV or ACMV.

Expression profiling experiments is usually based on measuring the relative amount of mRNA expressed in two or more experimental conditions and tries to help to answer to this question: How does the mRNA concentration change by external signals such as infection, how is it affected in the development stages of the host and its immunity system, and how is it differed in pathogen content? Quantifying the changing expression levels of each transcript during development and under different conditions is one of the main purposes of transcriptomics. For achieving this, various technologies and approaches are developed, including hybridization-or sequence-based approaches. This could help identifying essential virulence determinants and host factors, predicting potential resistance targets, and might provoke evolutionary long-term adaptation and selection of pathogenicity and immune responses. Most importantly, simultaneous monitoring of genes from both host and pathogen at different time points throughout the infection process could be achieved by dual RNA-seq. This way, genes at every single desired snapshot of the disease progression can be monitored (Westermann AJ 2012, Durmuş S 2015). Also, the RNA- or DNA- virus specific induced changes in gene expression contribute to our understanding of host-virus compatible interactions. The time series analyses of infected plant suites of altered expression of various biological processes including transport, catabolism, environmental adaptation, plant-pathogen interaction, phytohormone signalling and biosynthesis, energy metabolism, oxidative phosphorylation, as well as amino acids, lipid, sulphur and nitrogen metabolisms. In addition to the detailed identification of involved genes in specific biological processes, we also made a crosstalk

between viral infection with deterioration and senescence. Moreover, some experimental disciplines including the qRT-PCR complement this recent technique, as we applied it to confirm the expression pattern of selected group of genes during viral infection progression. That is followed by the linear regression modelling of the expression values obtained from RNA-seq and qRT-PCR. That addressed the significantly positive correlation between these methods for transcriptome analyses.

There are many comparative studies on transcriptome alteration of plant hosts in response to viral infections (Whitham SA 2003, Yang C 2007, Ascencio-Ibáñez JT 2008, Pierce EJ 2013, Maruthi MN 2014). Identified general changes in plant gene expression associated with infection by diverse positive-stranded RNA viruses- TVCV[24], ORMV[25], PVX[26], CMV[27] strain Y, or TuMV[28]- at 1, 2, 4, and 5 days after inoculation (DAI) by using DNA microarray. Approximately one-third (35 of 114) of the differentially expressed genes are associated with 'cellrescue, defence, cell death and ageing', including several defence and/or stress-associated genes (Whitham SA 2003). Compared CaLCuV[29] infection profile with the profiles of plants inoculated with TuMV or CMV-Y resulted that plant DNA viruses similar to RNA viruses activate the SA pathway leading to the expression of PR genes and the induction of programmed cell death, genotoxic stress, and DNA repair. These comparisons also identified many genes with opposite expression patterns (Ascencio-Ibáñez JT 2008). Consistent with previous data, TuMV-responsive genes overrepresented in chloroplast which include proteins with functions in light harvesting, photosynthesis, sulphur assimilation, and starch metabolism and protein degradation system (Yang C 2007). Additionally, there are some reports on CBSD and CMD; comparing the transcriptome of a resistant and a susceptible cassava uncovered transcripts putatively involved in disease resistance. This characterization and screening of the resistance level to CBSD of three cassava varieties showed that none of resistant genes with *NBS*[30] or *LRR*[31] domains were significantly regulated (Maruthi MN 2014). The global comparative expression study of TYLCV in *N. benthamiana* and SACMV[32] in Arabidopsis described the host-pathogen interplay earlier infection or in a delay or reduction of infection (Pierce EJ 2013).

Given the similarities between defence mechanisms, the critical role of oxidative burst and its effect on signal transduction pathway is one of the general activities that have been reported in response to various stresses (Maxwell DP 1999, Riedle-Bauer M 2000, Talarczyk A 2002, Xu J 2013). Therefore, detecting the SA-regulating H_2O_2 level as a part of the signalling cascade might determine the induced protection activities against viral infection progression. Thereby, we applied the DAB-staining technique together with Real-Time quantification of ROS scavenging enzymes to identify this part of defence response in infected plants with CBSV and ACMV.

Complementary network modelling of enzyme activities by using the expression values obtained by RNA-seq can help to simulate the flux balance of infected plants relative to mock. Following the previous studies (Cecil A 2015, Fieselmann A 2016), we modelled the broad-spectrum of changes caused by viral infection which implicate in various flux distributions along the carbohydrate, fatty acid and amino acid metabolism, signal

transduction, carbon fixation, photosynthesis and transporting processes. Besides, system-level metabolite profiling can be helpful to obtain a detailed insight into correlation between all metabolites alteration, perhaps in order to induce the immunity and in response to infection. To analyse the dynamic of metabolite profile within the plant-virus interaction system, measurement of a number of phytohormones, soluble sugars, amino acids and caffeoly esters, by using LC-MS/MS and HPLC-UV-MS applied to describe the significantly altered metabolites during infection progress. Various statistical analyses clarified the effect of time point of infection and entity of pathogen on the type and scale of altered metabolite.

Comparing all results, we addressed this question by analyzing early events in CBSV and ACMV infection starting with transcriptome analyses by using next-generation sequencing approaches. That investigated the gene expression changes associated with the characteristic disease development induced in *N. benthamiana* plants and comprises a gradient of stages of infection ranging from pre-symptoms stage towards infection stability and dominance. We attempt to zoom on the plant immunity concept through integration of antiviral immune concepts and definitions in the current general plant defending. Fluxomics and metabolomics following the transcriptomics shed light on the interplay between CBSV/ACMV and their compatible host *N. benthamiana*. Thereby demonstrated JA/SA-dependent defence-like responses, in addition to affected primary metabolite cascade and flux redistribution were observed in details. That helps us to identify host metabolites that contribute to infection progression responses. The assessment of antiviral immunity system of a susceptible host shows their conceivable promising properties to investigate the involved elements in presumably PCD, HR, PTI and ETI in infected *N. benthamiana* with CBSV and ACMV. In this study, gene expression profiling and metabolic modelling integrated with experimental data are also combined as a powerful comparative integrative analysis of the progressive infection system.

2. Material and Methods

This chapter provides the research technical methods of this study. Initially, the transcriptome profiling of plant during infection progression by using RNA-seq was made. Followed by Real-Time quantification of key pathway genes, and also elucidated the viral infection progression in various mutant and transgenic lines, then performed ROS-scavenging systems analyses. It is worth to mention that the metabolite measurement by HPLC-based chemical analyses was performed in collaboration with Max Planck Institute for Chemical Ecology in Jena. Furthermore bioinformatics methods on the simulation of flux distribution and enzyme activities are described.

2.1. Transcriptome profiling of plant during infection progress

2.1.1. Samples preparation of control and infected host plants and viruses

Nicotiana benthamiana was used as the host plants. Plants were grown in a greenhouse on a cycle of 16h light at 30°C and 8h dark at 25°C. As the inoculum source were the pre-infected *N. benthamiana* plants with CBSV-Tan70 and ACMV from DSMZ collection (PC-0925 and PC-0421 respectively). Systemically infected young leaf tissue from infected plants (6-8dpi) was harvested and immediately homogenized with carborundum powder (600 mesh) and 2% w/v polyvinylpyrrolidone (PVP) in 1X inoculation buffer (1ml) (S1.1) to prepare the virus inoculum. The resulted inoculums were diluted 1:20 in 1x inoculation buffer. In order to avoid the excessive evaporation and residual inoculum plants were sprayed with water afterwards.

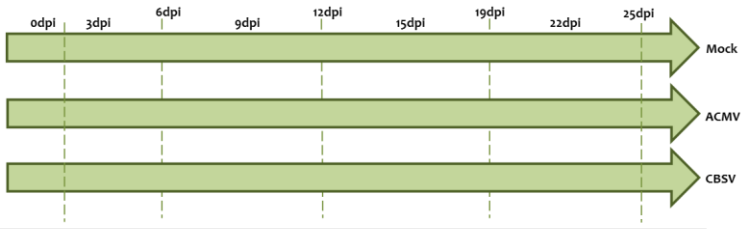

Sampling	1dpi	3dpi	6dpi	9dpi	12dpi	15dpi	19dpi	22dpi	25dpi
ELISA	×	√	√	√	√	√	√	√	×
RNA-seq	×	×	√	×	√	×	√	×	×
qRT-PCR	×	×	√	×	√	×	√	×	×
DAB-staining	√	√	√	√	√	√	√	√	×
VIGS and transgenics	√	×	√	×	√	×	×	×	√
Metabolite profiling	×	×	√	×	√	×	√	×	×

Figure 2. Experimental design and sampling for different experiments; In this study the infection progression of RNA and DNA virus was compared with mock, by applying different approaches, by keeping the pooling method in all the sampling steps

The viral inoculum was rub-inoculated onto the two or three leaves of *N. benthamiana* plants having four or five fully expanded leaves. The experiment was made in separate and clean condition on 420 plants in four blocks: 180 plants inoculated with CBSV-Tan70, 180 plants inoculated with ACMV, 40 plants inoculated with buffer (mock), and 40 plants were left untouched.

The obvious infection symptoms of CBSV-Tan70 and ACMV on *N. benthamiana* were observed at 7 and 8dpi respectively, while mock-inoculated plants showed normal leaf development and no visible effect of buffer inoculation. As it can be seen in Figure 2,

time-series sampling was made in three replicates and randomly; each replicate includes pool of 7 leaves from 7 plants, and 3 pools for each time point. Considering the symptoms progression, we decided to proceed with three time points: i) 6dpi, right before symptoms appeared, ii) 12dpi, the mid-stage when diseases were established in both cases, iii) 19dpi, late stage of infection with different phenotypic status associated with the entity of viruses.

2.1.2. Sample pre-processing and sequencing

RNA extraction, quality evaluation of RNA

Each pool of leaf samples was used for total RNA extraction using TRIzol® Reagent (Invitrogen) following the manufacturer's instructions and subsequently treated with DNase I (Invitrogen). RNA concentration and integrity were measures on Agilent 2100 Bioanalyzer (Agilent Technologies). The unique RIN[33] value was considered for quality assessment of total RNA. The intact RNAs of three technical replicates (belonging to the different pools) were mixed together to further proceed and the final concentration and quality of RNAs was measured by Nanodrop. Pure, intact and quality-checked RNA from 27 samples -three replicates of three samples in three time points- of approximately 1µg were used to proceed with deep sequencing.

mRNA-seq library construction and deep sequencing

RNA-seq library preparation using TruSeq® - Illumina and deep sequencing on HiSeq2000™ -Illumina instruments according to the manufacturer's instructions. Briefly poly(A)-containing mRNAs were purified by using oligo-dT magnetic beads, then were broken into multiple small fragments, primed with random hexamer primers and reverse transcribed to produce cDNA. The second-strand cDNAs were then synthesized by using DNA polymerase I, dNTPs and RNase H. Followed by applying SPRI[34] beads to purify the ds cDNA from free nucleotides, enzymes, buffers and RNA, and then eluting, end repairing and adaptor ligating. The suitable sized fragments were purified and enriched by PCR amplification, using sequences from the adaptors as primers, to obtain the final library. Sequence images were transformed with Illumina Basecaller software to bcl files, which were demultiplexed to fastq files with CASAVA (v1.8.2). Three samples per lane combined for paired-end sequencing (2×101 bp) to attain greater sequencing depth. All these raw reads generated from this study have been deposited in the GEO[35] under ID GSE100295. These data have the accession numbers GSM2677423, GSM2677424, GSM2677425, GSM2677432, GSM2677433, GSM2677434, GSM2677441, GSM2677442, GSM2677443 for mock samples, GSM2677426, GSM2677427, GSM2677428, GSM2677435, GSM2677436, GSM2677437, GSM2677444, GSM2677445, GSM2677446 for CBSV samples, and GSM2677429, GSM2677430, GSM2677431, GSM2677438, GSM2677439, GSM2677440, GSM2677447, GSM2677448, GSM2677449 for ACMV samples at 6, 12 and 19dpi respectively.

Quality control of reads, classification and filtering of viral reads

Quality check of obtained sequence reads was done via FastQC (v0.10.0) which is available online and showed no trimming was necessary (Andrews S 2010). The fastq reads were classified by using Kraken, a novel classification tool, with its standard database followed by a wrapper script to filter the non-viral sequences out, according to viral RefSeq taxonomy ID. Here the target taxon-group ID was 10239, to narrow down the read filtering. All remaining reads corresponding to viral sequences were obtained to perform assembly, were visualized by Krona tool to have a controlled taxonomic overview of the reads (Ondov BD 2011, Wood DE 2014, Schudoma C 2015).

2.1.3. Viral read analyses

Genome assembly

With considering the taxonomy ID, all non-viral reads generated during dual RNA-seq step were removed. The selected reads were assembled with different software, such as Velvet, Oases and Trinity with different k-mer values used to build a de Bruijn graph (Zerbino DR 2008, Grabherr MG 2011, Schulz MH 2012).

Alignment against reference genomes and IGV visualization

All obtained contigs were determined by mapping against viral references (NC_01269836, NC_00146737 and NC_00146838) by using Bowtie v2.0 software with the "very sensitive" flag option and "End to End" as the alignment type and sorted by using Samtools to be visualized by IGV (Langmead B 2009, Li H 2009, Thorvaldsdóttir H 2013).

RNA-seq analyses of viral genes

The filtered viral sequences in fastq format were mapped against CBSV and ACMV viral genomes by using TopHat2, followed by sorting and counting the mapped reads by Samtools and HTSeq, and visualizing in line plot in R (Li H 2009, Kim D 2013, Anders S 2015).

2.1.4. Data processing and RNA-seq analyses

Alignment and Counting

All sequence reads were mapped against the *N. benthamiana* genome (v0.4.4) retrieved from Solgenomics database[39] using TopHat2 and Bowtie v2.0. With HTSeq the alignments were processed to compute the read counts for each transcript. Duplicates were removed by using Samtools followed by removing the low expression values by filtering out the genes with minimum median of 10 in R (Langmead B 2009, Li H 2009, Kim D 2013, Anders S 2015).

Statistical test and differentially expression analyses

The current notion for RNA-seq count data is to assume that each gene follows a negative binomial distribution. Thus two algorithms (DESeq2 and edgeR) were applied to determine differentially expressed genes between conditions. These both assume a NB

distribution and performed using the Bioconductor R packages using re-randomized count data after filtering out the low expressed genes, using default parameters. NB distribution analyses for RNA-seq accounts for both technical and biological variance following normalization, dispersion estimation, fold-change computation and shrinkage also tests to compare conditions, to calculate the proportion of gene expression of each sample.

Data normalization

Normalization step tend to remove systematic errors of the data to allow comparison and combination of data from different biological and technical replicates. Among various normalization methods, we used the TMM[40] techniques which compare individual experimental sample values (infected samples) to aggregated values of controls (mock samples). Raw library sizes were estimated via DESeq2 normalization, applied to the counted clean and mapped reads.

Differential expression analyses and categorization of gene expression

Following the normalization, the expression data was analysed by using edgeR (Robinson MD 2010, R Core Team. 2014) and DESeq2 (Love MI 2014, R Core Team. 2014). In order to reduce the risk of false positives, all p-values were corrected for multiple-testing using recommended approaches (W 2010). For detection of DEGs[41] to consider biological variability within replicates, read sets were compared in a pairwise fashion: grouped biological replicates of the datasets CBSV vs. mock and ACMV vs. mock, followed by calculating the fold-changes of transcript levels between the two groups by using the nbinomWaldTest function in DESeq2 package and the exactTest function in edgeR package. Transcripts with Padj-value<0.05 and log2FC of +2 or greater change in expression were considered as up-regulated and Padj-value<0.05 and log2FC of -2 or lower change in expression were considered as down-regulated.

Annotation enrichment of *N. benthamiana* genome

The assembly of the *N. benthamiana* transcriptome and proteome[42] V0.4.4 was re-annotated with databases such as Pfam (Finn RD 2016) and Uniprot (Apweiler R 2004, Bairoch A 2004) by running BLASTP v2.2.29 (Altschul SF 1990, Camacho C 2008). Moreover, the Mercator automated pipeline of MapMan[43] (Lohse M 2014) was used to obtain categories of metabolic pathways and enzyme functions. Additionally, BLASTKOALA (Kanehisa M 2016, Kanehisa M 2017) was applied to retrieve the KEGG ID of each protein of *N. benthamiana* and with the KO[44] database (Kanehisa M 2000, Kanehisa M 2016, Kanehisa M 2017) collecting the data for molecular-level function analyses of their orthologues in *A. thaliana*. We also employed TRAPID online tool (Van Bel M 2013) in order to functional and comparative analyses for transcriptome data sets of *N. benthamiana's* GO[45] (Ashburner M 2000), where we used *A. thaliana* orthologues description and categorization (Gupta SK 2016).

Functional annotation of differentially expressed transcripts

The re-annotated *N. benthamiana* genome, transcriptome and proteome were used for functional description of differentially expressed genes, to retrieve the protein families

they belong to, their molecular functions, biological process and pathway operations. Pfam, GO, KEGG[46] and MapMan databases were used for deeper annotation of transcriptome profile of *N. benthamiana* plants. Top 100 most significant differentially expressed genes in response to infection with CBSV and ACMV at 6, 12 and 19dpi were determined in the Pfam database and visualized in Pie charts representing the protein families involved in pathogen response.

A broad biological perspective of DEGs dynamic

For global gene expression analyses we used Voronoi treemaps in the web-based java program Voronto (Santamaría R 2012). This type of visualization can display hierarchically structured data of functional categories of infected *N. benthamiana* in a space filling manner. According to orthologue KEGG IDs of *A. thaliana* retrieved from Phytozome 11, expression ratio of CBSV and ACMV samples vs. mock were mapped with specific colour codes (blue for down-regulation, white for unchanged expression and red for up-regulation) onto gene tiles. Homogeneously up- or down regulated gene clusters before removing the duplicates, illustrate the involved cellular and biological functions during viral infection at different time points at two levels.

Differentially regulated pathways in response to infection progression

Among different biological processes which are overrepresented in viral infection, we selected several of them to gain a detailed overview on their modulation over time. Plant-pathogen interaction, plant hormones signal transduction, glycolysis, translation initiation, transporters and biosynthesis of defence metabolites, together with hormone metabolism and ubiquitination and protein degradation pathways according to Mercator categorization. We visualized in heatmap after collecting the associated KEGG/MapMan/UniProt IDs and calculating the average expression values of different isoforms by applying the Euclidean method and heatmap.2 in gplot library of R[47].

2.2. Real-Time quantification of key pathway genes

2.2.1. Primers designing and Real-Time PCR amplification efficiencies

Primer sequences were designed by using QuantPrime (Arvidsson S 2008) according to available dataset of '*N. benthamiana*' in 'TIGR plant TA' and on 'SYBR Green Real-Time qPCR (accept splice variant hits)' mode. Some primers collected from literatures. For each primer pair, the corresponding Real-Time PCR efficiency (E) in the exponential phase was calculated according to the equation: $E = 10^{[-1/\text{slope}]}$. In the investigated 6 step serial dilution in a range from 1 to 10^{-5} μg of genomic DNA input [1, 0.1, 0.01, 0.001, 0.0001, 0.00001] (n = 2). The primers that displayed high linearity also high Real-Time PCR efficiency rates (0.85-1.2) were used for quantitative Real-Time PCR (Pfaffl MW 2001), which are listed in Table S3.

2.2.2. Quantitative Real-Time PCR

RNA was extracted from pooled leaves using RNeasy® purification kits (Qiagen) as recommended by manufacturer. And the integrity and quantity analysis was made with Nanodrop and visualized on 1% agarose gel. RNAs (100 ng) were reverse-transcribed to

cDNAs with M-MLV® Reverse Transcriptase (Invitrogen) as mentioned in Table S3. 5µl of cDNAs were used as template in 20µl PCR reactions containing the KAPA Fast 2X SYBR® Green qPCR Master Mix (KAPA Biosystems) and 3pM of forward and reverse primers. PCR reactions were performed on a Mastercycler® RealPlex2 (Eppendorf) in 96-well plates. PCR conditions were: denaturation at 95°C for 2 min, followed by 40 cycles at 95°C for 5min and 60°C for 20s, in addition to meltingcurve analyses.

RT-qPCR was carried out in two independent technical replicates and for infected *N. benthamiana* leaves with CBSV and ACMV as well as mock retrieved from seven independent plants at three time points 6, 12 and 19dpi. To calculate this expression value, among various established mathematical models, based on the comparison of the distinct cycle determined by various methods, such as CP (crossing points) and Ct (threshold values) at a constant level of fluorescence, which could be either 'without efficiency correction' or 'with kinetic PCR efficiency correction'. The Ct values were used with efficiency correction. Moreover, the 38 cycle were assigned as a threshold for the NTC adjustment and the mean Ct value of every two replicates of each sample (mock/viral inoculated leaves at different time points) was used when discarded the missing values were likely due to technical failure.

2.2.3. Comprehensive stability analyses of housekeeping genes

In Relative quantification Real-Time PCR, the reference gene (also called housekeeping gene, internal or control gene), can be co-amplified in the same plate in a multiplex assay, with induvial treatments and controls (Pfaffl MW 2004). In order to a valid relative quantitative PCR analyses, we made short systematic re-investigation of reference gene stability in *N. benthamiana* under conditions of viral infections. Mainly non-regulated housekeeping genes such as L23, ACT, PP2A and AGO1 were used as control for normalization of qPCR analyses (Liu D 2012). Their stability was evaluated using the web-based comprehensive tool Reffinder (Xie F 2012) based on the Delta CT, BestKeeper, NormFinder and GeNorm algorithms. The most stable endogenous standard gene was used for normalization of the target genes.

2.2.4. Relative quantification of investigated gene transcripts in Real-Time PCR

Ct values of 48 genes were normalized against the housekeeping gene L23 (as well as PP2A) and the relative copy numbers for each gene estimated using Pfaffl equation called 2-ΔΔCt method (Pfaffl MW 2001). Values were expressed as the fold-change between mock and CBSV/ACMV infected samples, which were later transferred to log2 form for visualization and other further analyses. Expression ratio was normalized to the housekeeping genes by using following equation:

$$\text{ratio} = \frac{(E_{target})^{\Delta CP_{target}(control-sample)}}{(E_{ref})^{\Delta CP_{ref}(control-sample)}}$$

2.2.5. Correlation of qPCR and RNA-seq results

The correlation was calculated and presented as the linear regression model between according values. As shown in the box, the linear regression model (lm) was built assuming replicate stand for either RNA-seq or qRT-PCR, value for the log2FC of these selected 48 genes, and time for 6, 12 or 19dpi.

```
lm (formula = value ~ variable * replicate, data = a)
Value= b0 + b1 test + b2 time +b3 replicate *time
```

We intended to calculate the relationship between the detected gene expression values obtained by two different approaches, and if the reflected transcriptome differences between mock-inoculated and viral-infected plants are correlated in these two approaches, followed by hierarchical clustering of expression values of selected genes obtained from qRT-PCR in order to investigate the distance and closeness of these involved genes in response to infection progression.

2.3. Viral infection progression in transgenic plants

2.3.1. Mutant/transgenic lines and VIGS assay

In order to investigate the functional biology of a number of differentially expressed genes during the viral infection progress, we analysed the phenotype and viral accumulation in a natural *RDR1* mutant, *RA4* (Yang SJ 2004, Wylie SJ 2015), transgenic lines of a SA-degrading enzyme salicylate hydroxylase, *NahG* (Ying X-B 2010), and a hypersensitive cell death and resistance mediator *RC3a* (Segretin ME 2014). We received the mutant/transgenic species seeds of *RA4*, *RC3a*, and *NahG* plants and followed the infection progression in these plants relative to the common wild-type as was used for other parts of this study. Surface sterilized seeds were sown in MS culture and transferred to pots 10 days after germination. These plants together with the wild-types were inoculated with CBSV/ACMV/mock at the four-leaf stage, which were grown in pots at 25°C under a 16-h-light/8-h-dark cycle.

We also applied the TRV-VIGS system to silence *SGT1*[48], *RAR1*[49] and *HSP90* genes in *N. benthamiana* (Ratcliff F 2001, Azevedo C 2002, Azevedo C 2006), which induces the hypersensitive response at the infection site. The received fragments of these genes cloned in pTRV2 (RNA2 cDNA of TRV) were used. Mixtures of *Agrobacterium tumefaciens* (strain GV2260) cultures, containing pTRV1 (RNA1 cDNA of TRV) with pTRV2 derivative plasmids were mixed in a 1:1 ratio in infiltration buffer (S1.3) to a final OD_{600} of 1 (S2.2). pTRV2-*NbSGT1*, or pTRV2-*NbRAR1*, pTRV2-*NbHSP90* as well as pTRV2-*NbSGT1-NbRAR1-NbHSP90* T-DNAs were infiltrated onto WT plants (Ratcliff F 2001, Liu Y 2002). In order to examine the efficiency of the transformation system, first we determined the ability of TRV constructs to inhibit the PDS[50] gene in *N. benthamiana*, which is essential for carotenoids production protecting plants from photo-bleaching. Inhibiting the PDS gene by using TRV make the plant tissue turns white (Demmig-Adams B 1992, Kumagai MH 1995, Ruiz MT 1998). As in the trial experiments, the bleaching phenotype started to show up 7-8 days after agro-infiltration. Therefore, day 6 was selected to inoculate the agro-infiltrated plants with viruses. Six days after infiltration, the

upper leaves of these infiltrated plants were inoculated with CBSV or ACMV. These plants were observed and sampled at 6, 12 and 19dpi together with mock relative to infected wild-types. Each of these functional analyses experiments was repeated three times, and each experiment included at least six independent plants for every time point, which were divided into three ELISA bags and analysed twice.

2.3.2. Viral load comparison in transgenic plants compared with wild-types

All the serological detection and measurement of CBSV-Tan70 and ACMV was done with the TAS-ELISA[51] protocol (DSMZ QC-SOP-0087 Anl. 007 and Anl. 005 respectively) (S2.1) on Greiner Bio-One microplates, medium binding (Cat. No. 655001) (Clark MF 1977). TAS-ELISA for detection of CBSV and ACMV, based on polyclonal and specific monoclonal antibodies, was assessed according to spectrophotometric absorbance at 405nm. At each time point, leaf samples were taken from four independent mutant/transgenic and wild-type plants. Infected and mock plants divided into three separated bags, weighed and ground in extraction buffer 1/20 (w/v), pH 8.5 (S1.4) and loaded to plates coated with virus specific capture antibodies. For CBSV (DSMZ AS-1153) in 1:500 dilution and for ACMV (DSMZ AS-0421) in 1:1000 were applied, followed by blocking with 2% skim milk in PBS-Tween, and specific detection by monoclonal antibodies Mab (DSMZ AS-1153/1 and DSMZ AS-0421/2 in 1:50 and 1:1000 dilutions, respectively). Finally the conjugated polyclonal antiserum RAM-AP[52] (Jackson ImmunoResearch 315-055-044) was used in 1:1000 dilution and colorimetric substrate was added to detect the specific viral coat proteins. In every plate, we applied the positive controls (CBSV PC-0925, ACMV PC-0421) and negative control (extraction buffer which later used as normalizing factor for each plate to calculate the viral loads) in four and six wells, respectively. For sampling, three different plants were pooled in three replications at each time point. The samples were loaded in wells of two plates in duplicate wells. Although, we had several biological and technical replicates to minimise the technical error, there were some outlying observations in ELISA measurement, which were removed to obtain stronger statistical analyses.

2.3.3. Statistical analyses

Statistically significant differences in viral load were calculated between infected wild-type plants with CBSV/ACMV and mock in addition to infected mutant/transgenic lines compared with wild-types. We performed the non-parametric version of ANOVA analyses (Kruskal- Wallis test) in order to across-group comparison, using the PMPCR package in R (Pohlert T 2014, R Core Team. 2016). Adjustment for multiple comparisons was done with Bonferroni, and Holm correction. The significance level was defined as if s>0.1: "x", if s<0.0001: "****", if s<0.001: "***", if s<0.01: "**", if s<0.05: "*", otherwise: ".", and visualizations have been presented as boxplots using the package ggplot2 in R. The presented stars in results were obtained from the Pairwise t-test and Bonferroni correction method as a Post-hoc analysis after Kruskal-Wallis test.

2.4. ROS-scavenging systems

2.4.1. DAB staining

The first and second leaves of six different plants (WT, *RA4*, *RC3a* and *NahG*) infected with CBSV, ACMV and mock were taken at 6, 12 and 19dpi, placed in 1mg/ml DAB-HCl, pH 3.8 (Sigma, MO, USA; #D8001) and incubated for 8h at room temperature, with gentle shaking. Subsequently, the leaves were bleached in ethanol (75%) at 80 ºC for 1h. H_2O_2 is visualized as a reddish-brown colouration (Thordal-Christensen H 1997).

2.4.2. qRT-PCR of ROS-scavenging genes

According to the sequences reported by previous studies as involved genes in alternative respiratory pathway (Deng X-G 2016), the primers were designed and the qRT-PCR was performed following the procedure as described in part 2.2.1. This part of analyses was done for the leaves taken from wild-type *N. benthamiana* infected with CBSV and ACMV.

2.5. Metabolite measurement by HPLC-MS and HPLC-UV/Vis

The leaf material pooled from 6 independent plants, inoculated with either CBSV, ACMV and buffer were collected and weighted to 200±20 mg in 6 replicates, and used for metabolome profiling in hormone, amino acids, flavonoids, and mono, di and tri-saccharides levels. The samples were extracted in methanol mixture containing isotope-labelled phytohormone internal standards, and then diluted in an aqueous mixture containing isotope-labelled amino acid internal standards for the amino acid analyses. The samples were analysed by HPLC-MS (triple quadrupole mass spectrometer equipped with a Turbospray ion source as detector, with MRM1 used to monitor analyte parent ion → product ion) for amino acids, sugars and phytohormones, and HPLC-UV/Vis for the phenolic compounds. Quantification for amino acids and phytohormones was based on the internal standards, and for phenolics and sugars on external calibration curves.

2.5.1. Analyses of phytohormone levels

Phytohormones analyses were done by LC-MS/MS: Plant material (≈200 mg) was extracted with 1 ml of methanol containing 40 ng of D6- jasmonic acid (HPC Standards GmbH), 40 ng D4-salicylic acid (Sigma-Aldrich), 40 ng D6-abscisic acid (Santa Cruz Biotechnology.), and 8 ng of D6- jasmonic acid-isoleucine conjugate (HPC Standards GmbH) as internal standards. Separation was made on a with 1200 HPLC chromatography system (Agilent Technologies) with a Zorbax Eclipse XDB-C18 column (50x 4.6 mm, 1.8 µm, Agilent), maintained at 25 ºC, with negative ionization mode on API 5000 tandem mass spectrometer (Applied Biosystems). For data acquisition and processing, Analyst 1.5 software (Applied Biosystems) was used. Phytohormones quantification was relative to the signal of their corresponding internal standard; quantifying the OPDA and OH-JA, was done by internal standard D6-JA and experimental-determined response factors of 1.0 for both, whereas for 12-OH-JA-Ile and COOH-JA-Ile, D6-JA-Ile was applied as the internal standard and equivalent response factor of 1.0 in both cases (Vadassery J 2012).

2.5.2. Analyses of free sugar levels

Sugar analyses were done by LC-MS/MS: A 50 µl aliquot of the methanolic extract of phytohormone analyses step was diluted in water at a ratio of 1:10 (v:v). Chromatography

was performed on an Agilent 1200 HPLC system (Agilent Technologies). Separation was made on a HILIC-HPLC-column (apHera NH2 Polymer; 15 x 4,6mm, 5µm, Supelco) maintained at 25°C, with negative ionization mode on an API 5000 tandem mass spectrometer (Applied Biosystems). The instrument parameters were optimized by infusion experiments with pure standards (D-(+)-glucose, D-(-)-fructose, sucrose, all Sigma-Aldrich). For data acquisition and processing, Analyst 1.5 software (Applied Biosystems) was used. External standard curves generated with dilution series of authentic standards were used for quantification of individual sugars (all from Sigma-Aldrich).

2.5.3. Analyses of amino acid levels

Amino acid analyses were done by LC-MS/MS: Amino acids were extracted with 1 ml methanol, and diluted in a ratio of 1:10 (v:v) in water containing the 13C, 15N labelled amino acid mix (Isotec). An Agilent 1200 HPLC system (Agilent Technologies) was used for chromatography. Separation was made by using a Zorbax Eclipse XDB-C18 column (50x 4.6mm, 1.8µm, Agilent Technologies), maintained at 25 ºC, with positive ionization mode on an API 5000 tandem mass spectrometer (Applied Biosystems). For data acquisition and processing, Analyst 1.5 software (Applied Biosystems) was used. Quantifying individual amino acids was performed by the respective 13C, 15N labelled amino acid internal standard, except for tryptophan, asparagine and ornithine which were quantified using 13C, 15N-Phe, 13C, 15N-Asp, 13C, 15N-Lys applying a response factor of 0.42, 1.0 and 1.0, respectively (Jander G 2004, Crocoll C 2016).

2.5.4. Analyses of flavonoid and caffeoyl quinate ester levels

Flavonoids analyses were done by HPLC-UV-MS: Flavonoids were extracted with 1 ml methanol, and analysed by Agilent HP1100 HPLC-UV system (Agilent Technologies), with a C-18 reversed phase column (Nucleodur Sphinx RP, 250x 4.6mm, 5µm). Quantification of caffeoyl quinates was based on an external standard curve of an authentic standard of trans-5-caffeoylquinic acid applying a relative molar response factor of 1.0. The compounds identifications were based on UV visible absorption and on mass spectra from LC-MS analyses on a Bruker Esquire 6000 IonTrap mass spectrometer (Clifford MN 2003, Clifford MN 2008). Following this procedure, flavonoids were not detected in significant amounts.

2.5.5. Statistical analyses

Statistically significant differences in metabolite between CBSV and ACMV infected compared with mock were calculated as described in part 2.3.3 and visualizations have been presented as barplots by using the package ggplot2 in R (Wickham H 2009, R Core Team. 2016). Here also, the presented stars in results were obtained from Pairwise t-test and Bonferroni correction method as a Post-hoc analysis after Kruskal-Wallis test.

2.6. Flux profiling and enzyme activities simulation during viral infection progress

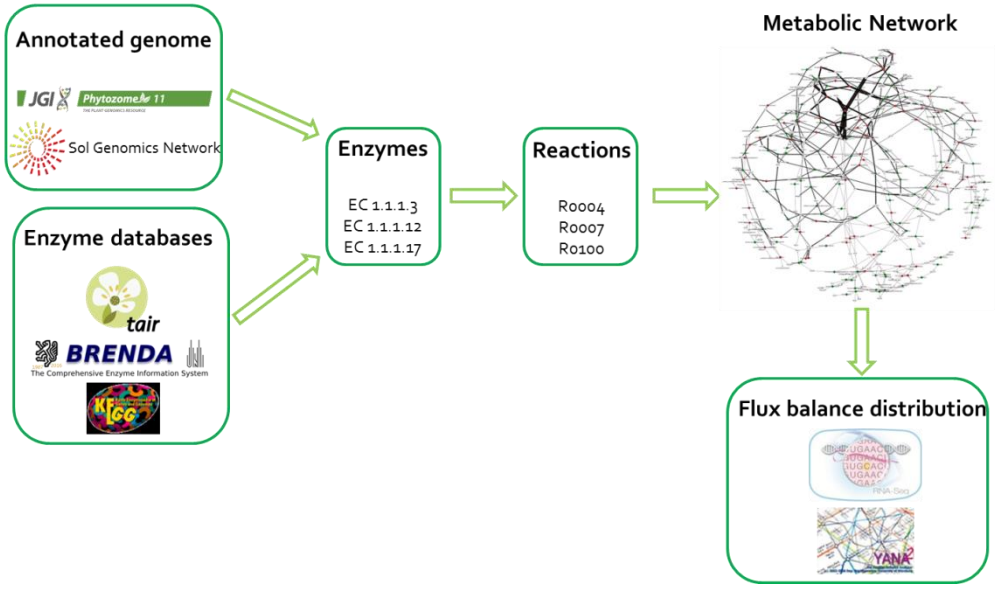

Figure 3. Workflow on enzyme activity simulation

2.6.1. Reconstruction of metabolic networks

We modelled involved metabolic pathways for *N. benthamiana* by following the *Arabidopsis* model provided by Fieselmann *et al.* (Fieselmann A 2016). The model of central metabolism included different primary metabolic pathways such as glycolysis, TCA[53] cycle, PPP[54], photosynthesis and photorespiration, in addition to pathways involve in the biosynthesis of defence molecules such as salicylate and jasmonate, as well as plant-pathogen interactions pathways such as chorismate, shikimate and sphingolipids. Annotation of enzymatic network was made by using BRENDA, TAIR, Uniprot and KEGG databases, describing the enzymes reversibility and localization (Fig. 3). Extreme pathways possible in the annotated enzyme network were calculated to identify actual flux strengths, also to describe a linear combination of all metabolic state of the system analyses (Schilling CH 2000, Schuster S 2000, Cecil A 2015). The preferences of involved metabolites and network reactions are provided in Table S9 and S10. Each reaction in the network is either mediated by a single enzyme or a pool of several isoforms.

2.6.2. Enzymatic flux simulation and metabolic flux modelling

The expression data obtained from RNA-seq were used to estimate the flux strength through the enzymes of the metabolic network (Fig. S5)[55], for CBSV and ACMV infected samples comparing with non-infected conditions (mock) at 6, 12 and 19dpi. We used YANAsquare v1.0.0 and Metatool v4.9.1 (Schwarz R 2005, Schwarz R 2007) to calculate optimal pathway fluxes which best match the constraints for key enzyme activities according to significant induced or inhibited enzyme orthologues expression on transcriptome level. Detailed input files for the pathway models and the simulated enzyme activities of each viral infection at each time point are listed in additional file[56]. The -1 value stand for the unknown/undefined enzyme or its expression value which assure this

enzyme is not the rate limiting step of a pathway and for the program. The calculated activities of the different extreme pathway modes (EMs) for three different time points of infection progression for the *N. benthamiana* leaf samples. In order to calculate the percentage value of each enzyme's activity for each treatment (CBSV or ACMV), we calculated its ratio against the mean of the control (mock) and then calculated the mean of the percentage values and their standard error.

3. Results

This chapter describes the results of comparative and integrated approach we used first on transcriptome analyses of model plant *N. benthamiana* infected with CBSV and ACMV in relative with non-infected plants. The recent fast developing techniques, RNA-seq is applied as a valuable method for transcriptome dynamics analyses in tetraploid *N. benthamiana* to identify several differentially expressed genes, both virus-genera and virus-specific changes. Moreover, here we identify the expression pattern of groups of defence associated genes in addition to various biological processes elements involved in energy metabolism, signal transduction, and ubiquitin proteasome system during infection progression. Among them we present the confirmed Real-Time expression modification of 48 key pathway genes, followed by their regression linear model.

Subsequently, we elucidate the functional loss of numbers of basal regulators genes which trigger R-mediated resistance. The detailed-characterized silenced *RAR1*[57], *HSP90*[58] and *SGT1*[59], in addition to salicylic acid pathway deficiency in *RDR1 and NahG* plants are compared in viral load level along the infection. Then, we provide the analyses output of visualizing the massive localized accumulation of ROS in addition to quantifying the fold change of scavenging genes in the infected wild-type plants compared with mock.

Moreover, the co-ordinately regulated metabolites in response to viral infection measured by using LC-MS/MS and HPLC-UV-MS are described. This includes the profile of the phytohormones, carbohydrates, amino acids, flavonoid and caffeoyl quinate ester at different time points of infection with the RNA and DNA viruses. That could be influenced by differentially regulated enzymatic activities along the salicylate, jasmonate, and chorismate biosynthesis, glycolysis, tricarboxylic acid cycle, and pentose phosphate pathways, photosynthesis, photorespiration, transporting, amino acid and fatty acid biosynthesis. Therefore, we address the simulated flux redistributions comprising a gradient modulation of enzymes along different infection stages, ranging from pre-symptoms towards infection stability.

3.1. Transcriptome profiling of plant during infection progress

Understanding the host response to infection across the time gradients could be helpful to characterize the mechanisms of pathogenesis strategies of host-driven immune reactions. Compatible interactions between susceptible hosts and virulent pathogens frequently lead to altered expression of set of genes belong to defence as well as cellular stress response pathways. Viral infections can interfere with the host hormone biosynthetic and signaling pathways, which in addition to reshaping plant defence could result in developmental defects. These complex plant responses relate to broad spectrum of physiological processes, thus integrated systems biology approaches are optimal solution to capture the complexity of host-pathogen interactions (Whitham SA 2006, Yang C 2007, Ascencio-Ibáñez JT 2008, Lu J 2012).

We performed detailed expression analyses to i) monitor correlation between changes in expression of genes belong to the host and tow viruses ii) host genes involved in response to viral infection response in the course of time, and iii) host mediated differential gene regulation in response to infection with a RNA and DNA virus. Therefore we investigate the infection procedure of CBSV-Tan70 and ACMV in system-level transcriptome by using next-generation sequencing to address the detailed genome-wide gene expression profile of model plant *N. benthamiana*, considering the entity of viruses.

3.1.1. Plant growth, virus inoculation, and RNA isolation

For the gene expression profiling studies, we used the refreshed inoculum of ACMV and CBSV in their compatible host *N. benthamiana*, at the 4- to 6-leaf stage and monitored the symptom development over time. Symptoms of CBSV and ACMV on *N. benthamiana* appear at 7 to 8dpi with all plants showing stabilized symptoms by 12dpi. Both virus symptoms typically include curled, deformed leaves with a yellow mosaic or mottled pattern, vein swelling and enations. Both diseases are visible as chlorosis, patches of yellow areas mixed with normal green colour, and it is often also associated with veinal chlorosis on mature leaves (more prevalent on secondary veins), together with yellow or necrotic vein banding, and sometimes comparatively large yellow or necrotic patches in older leaves. ACMV infection in *N. benthamiana* (Fig. 4, panel B,E,H) in comparison with CBSV (Fig. 4, panel C,F,I) appears with more sever leaf chlorosis followed by distortion and general stunting particularly at the late stage of infection, as well as faster development of reproductive organs. While mock-inoculated plants showed normal leaf development and no visible effect of inoculation (Fig. 4, panel A,D,G).

3.1.2. Sample pre-processing and sequencing

The quality assessment of total RNAs was done according to their RIN values, in addition to integrity evaluating on agarose gel and Nanodrop. Figure S1 shows an example of the representative RNA electropherograms at different time points of infected and mock plants, which indicate the position of 18S and 25S rRNA peaks. The pure, intact and quality-checked RNAs of three technical replicates (belonging to different pools) were pooled together and considered as one replication in sequencing step. Paired-end sequencing (2×101bp) of three combined lanes per samples resulted in a comprehensive deep sequencing of approximately 136 to 177 (min.-max.) MBase data per sample. In total we received 2,956,396,150bp of raw data (table S1).

The quality of the reads was controlled by using FastQC (v.0.10.0) which showed the acceptable quality with no adaptor trace, therefore we did not proceed with any trimming (Andrews S 2010). Various criteria could be assessed in FastQC including basic statistics (Table S1), per base sequence quality, per tile sequence quality, per sequence quality scores, per base sequence content, per sequence GC content, per base N content, sequence length distribution, sequence duplication levels, overrepresented sequences, adapter content and Kmer content (Fig. S2 and S3). All of the obtained raw reads passed all these tests, however the duplication level for all of them was noticeable.

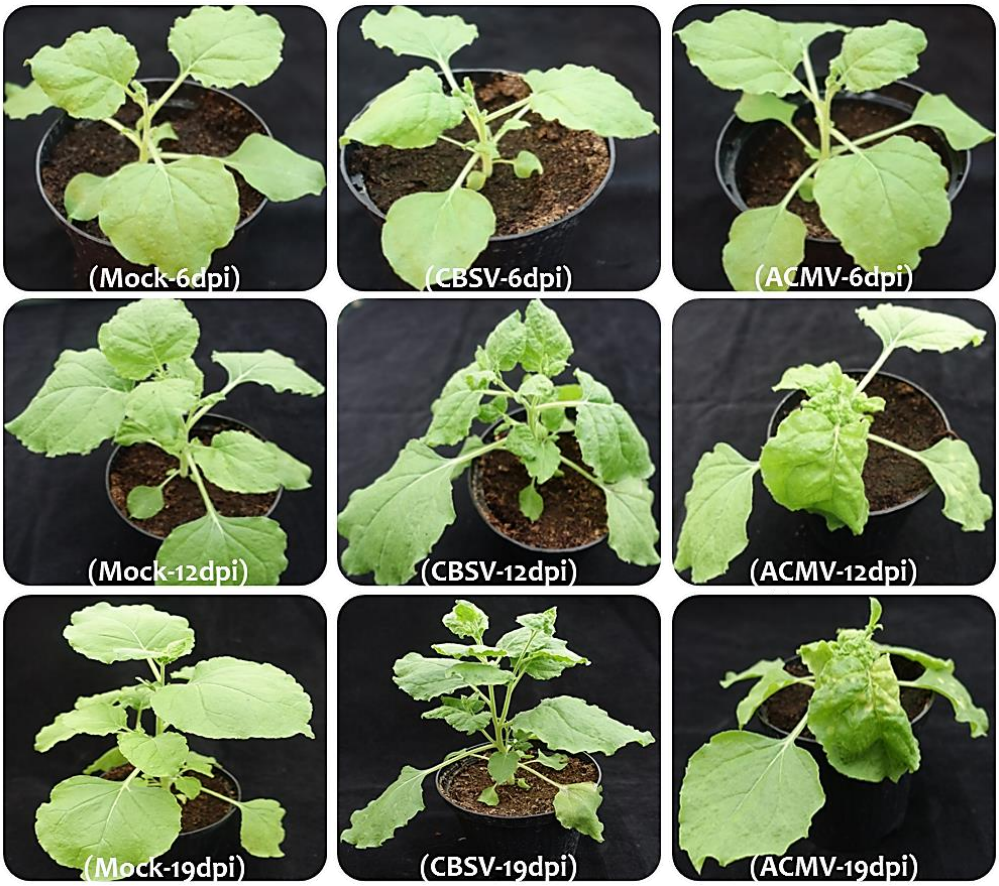

Figure 4. Infection progression observation in infected and control plants; CBSV and ACMV infection in *Nicotiana benthamiana* is associated with plant stunting and a failure to develop normally. Both virus symptoms typically include curled, deformed leaves with a yellow mosaic or mottled pattern, vein swelling and enations.

Classification and filtering of viral reads

In order to assign the raw read data to a taxon and visualize the portion of classified viral reads content at each time point, we used Kraken, Ktoolu and Krona. For instance, the reads obtained from *N. benthamiana* infected with CBSV at 12dpi (Fig. 5A), classified as 6% of the whole read content belonging to viruses, 100% of this content categorized as Ipomovirus (a genus of the family Potyviridae of the group of (+) ssRNA viruses) which matched with the CBSV in a total of 99%. Furthermore, in *N. benthamiana* infected with ACMV at 12dpi (Fig. 5B), 7% of the whole read content and 99% of viral reads belonged to ssDNA viruses, genus of Begomovirus. 4 and 2% of the whole read content classified as ACMV and EACMV respectively, which was 61 and 32% of the viral reads. This could be associated with the high similarity between these two viruses (Oteng-Frimpong R 2012).

Viral genomes assembly, alignment against reference genomes

We filtered the viral read contents out, in order to de novo assembly of viral genomes. Clearly, the elimination of the non-viral reads or of the chimeric portions in the generated reads before assembly was an improvement in terms of speed and accuracy to obtain the whole genome of the considered DNA and RNA virus. We used Velvet, Oases and Trinity in order to assemble the filtered fastq file into fasta contigs. Transcript sequences obtained

by Trinity were much longer compared to the contigs of Oases and Velvet. After indexing they were aligned against the references of interest (ACMV and CBSV) and visualized in IGV. As it can be seen in Figure 6, the efficiency and coverage obtained from Trinity was higher. Therefore we used these contigs to run local blastn (2.2.28+) against the DPV[60] (Adams MJ 2006) as shown is table S2, the hits showed an acceptable E-value, identity percent and bit score.

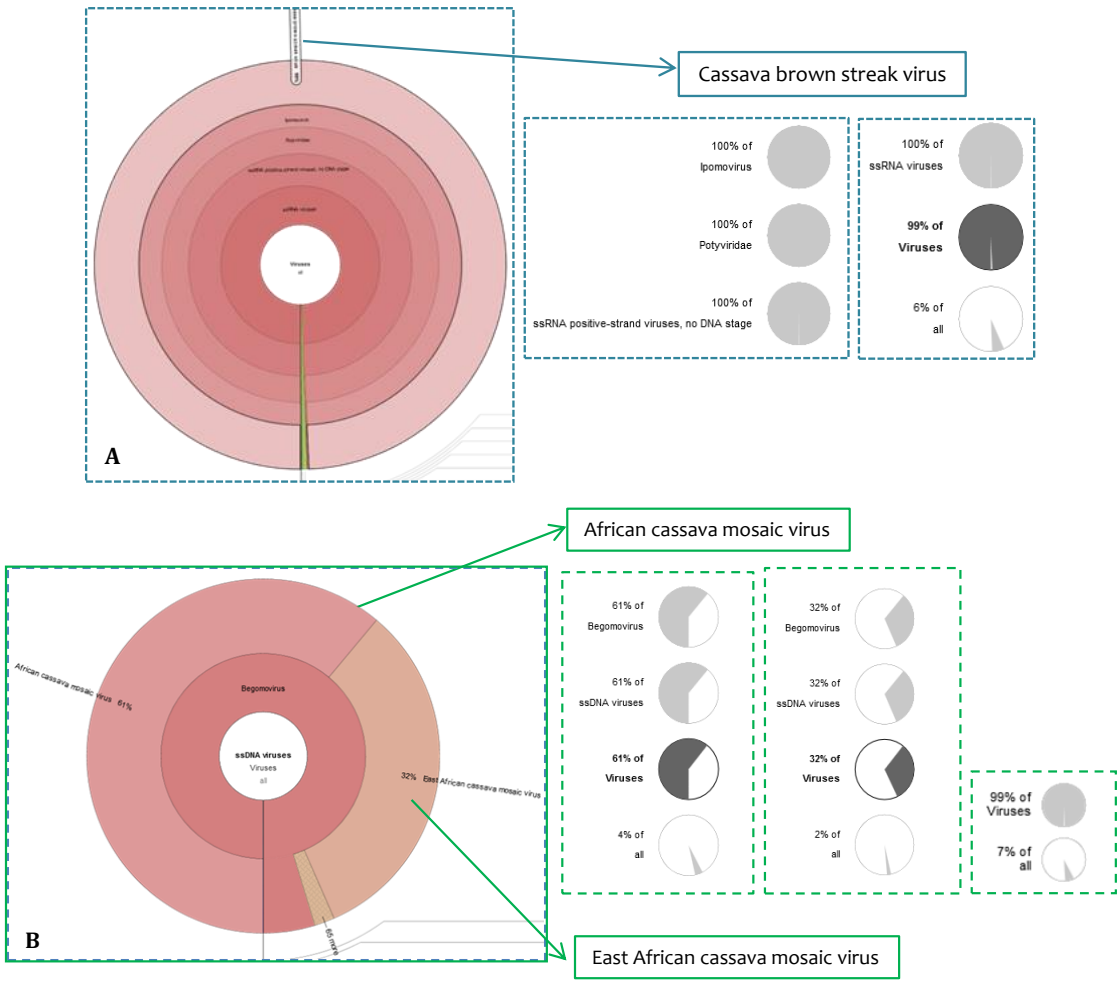

Figure 5. Classification and filtering of viral read; A: Classified reads obtained from infected plant with CBSV, shows that 6% of the total read and 100% of viral read content belong to CBSV, B: Classified reads obtained from infected plant with ACMV, shows that 2 and 4% of total read and 99% of viruses belong to EACMV and ACMV respectively.

RNA-seq analyses of viral genes

We performed a dual expression analyses to describe an association between expression modification of virus genes and their pathogenicity level, or spot directly influenced host genes. Although we did not succeed to get all the viral particles counted, the described genes may be key players involved in regulating pathogenesis and host defence mechanisms after RNA and DNA viral infection. Expression levels of CBSV and ACMV segments correlate with the viral load and may thus be used as surrogates for conventional viral load measurements. This pattern matches with the viral load percentage obtained from Kraken classification as well as the TAS-ELISA measurements. As shown in Figure 7A, in the CBSV samples, the four genes 6K1, VPg, CI, CP were detected: all

with the maximum log2FC at 12dpi, which was 2.136, 2.632, 12.122 and 13.288, respectively. These expression values were decreased at 19dpi however still significantly higher than it was at 6dpi.

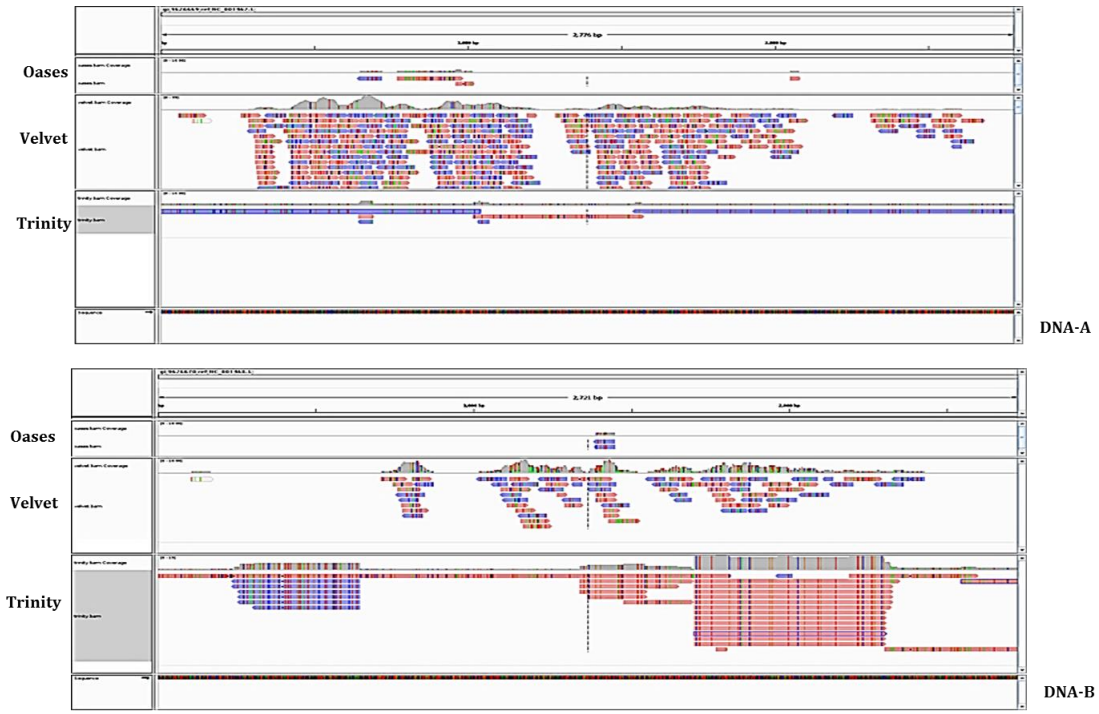

Figure 6. Assembly of virus genomes from RNAseq (ACMV-19dpi); The alignment resulted from Oases, Velvet and Trinity respectively (DNA-A with 2781bp, and DNA-B with 2725bp length) evidently the efficiency of Trinity in terms of the length and coverage of contigs was much higher than Velvet and Oases.

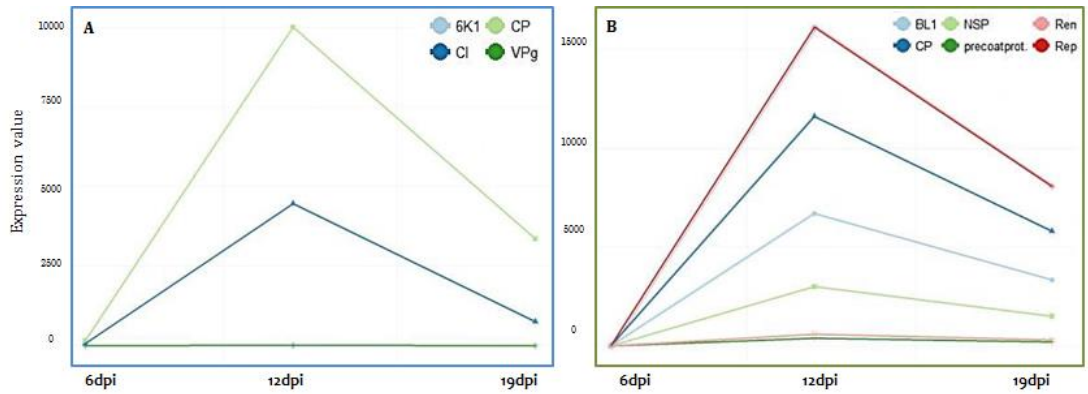

Figure 7. Viral gene expression pattern; A: CBSV genes differentially expressed in the course of time, B: ACMV genes differentially expressed in the course of time; CP and CI of CBSV genome and Rep, CP, BL1, and NSP of ACMV genome were successfully counted after normalizing with mock.

The same pattern was obserevd for ACMV samples: As it can be seen in Figure 7B, at 12dpi the segments including Rep, CP, BL1, NSP, Ren, PreCP. had the maximum log2FC which respectively was 14, 13.5, 12.7, 11.5, 9.2, 8.6. These expression values slightly dropped at 19dpi although remained still higher than at 6dpi. For example Ren gene had -0.16, 9.2, 8.2 very similar to PreCP. -0.16, 8.6, 7.6 at 6, 12, 19dpi.

3.1.3. Data processing and RNA-seq analyses

Data normalization

Correcting the library size of each sample was done by multiplying each library size by a normalization factor, estimated from the raw data following the implemented algorithms in DESeq2. We applied TMM as a batch normalization method, because samples are taken from biologically distinct sources, such as different individuals, the variability between them has often been modelled by negative binomial distribution (sometimes called gamma-Poisson distribution) (Korpelainen E 2014). Then consistency of the data was inspected by boxplot by comparing the distribution before and after transformation and normalization (Fig. 8).

Re-annotation of *N. benthamiana* genome

Towards enrichment of *N. benthamiana* annotation, we re-annotated the assembly of the *N. benthamiana* transcriptome and proteome V0.4.4 in various databases, following the approach mentioned in previous section, resulted in the upgraded annotation of *N. benthamiana*[61].

Differential expression analyses

The expression data was analysed by using edgeR and DESeq2 and the resulting Padj-values to determine log2FC. By using a Padj-value<0.05, and log2FC threshold of 2 and -2 we created Figure 9 which provides a global overview of differentially expressed transcripts including the spreading patterns of various time points and infection causes. Volcano plots summarize these results (Fig. 9 A-F), by presenting the range and level of change and significance[62]. Clearly, there were more up-regulated genes (higher than +2, dots with darkest colours) than down-regulated genes (lower than -2, dots with mid-dark colours) at all these time points of both groups of infected samples. The higher number of induced genes at 12dpi of CBSV and then ACMV, also the highest number of down-regulated genes in ACMV infected samples at 19dpi was evident. As shown in Figure 9, the widest range of differential expression occurred at 12dpi, which there were many genes up- and down-regulated with log2FC +7.26 and -6.88 for CBSV as well as +7.18 and -7.00 for ACMV, distributed in approximately similar pattern. At 19dpi the number and range of induced and repressed genes were higher in ACMV, compare to CBSV infected samples. The margin between induced and repressed genes in response to CBSV infection at 6dpi was very narrow (difference of 10 genes favouring up-regulation) which was much more in ACMV infected plant (difference of 46 genes favouring up-regulation). At 12dpi also this margin was significant until 19dpi where the number of induced genes was 20 times higher (relative to supressed genes) in the CBSV samples at 19dpi, similarly in the ACMV samples was 3 times higher.

As shown in Table 1, an output of 12395, 18150, 13424 and 12529, 18568, 20084 differentially expressed genes with a Padj-value of under 0.05 after normalization of data was obtained in CBSV and ACMV samples at 6, 12 and 19dpi respectively. A total of 2815 and 4237 genes in CBSV and ACMV were common across the three time points indicated. The intersection between ACMV at 12dpi and ACMV at 19dpi was shown to be the highest (11899 genes) whereas for CBSV it was 9077 differentially expressed genes.

The lowest common responding genes were observed between CBSV at 6dpi and CBSV at 19dpi (4155 genes) followed by ACMV at 6dpi and ACMV at 12dpi (5862 genes). The number of identical genes to a particular time point of CBSV infection was 2964 at 6dpi, 7008 at 12dpi and 10781 at 19dpi while for ACMV was 2830, 6590 and 4121, indicating specific significant genes at each time point. Gene overlap was highest between CBSV and ACMV at 12dpi (11560 corresponding genes), followed by 6dpi (9566 genes), with 19dpi showing the lowest intersection between the two time points, indicating a large diversion in transcript expression between mid and late infection phases. Interestingly, maximum levels of gene transcriptional alteration correlated with the peak expression of symptoms, high virus copy number and full systemic virus infection, as ACMV infection at 19dpi and CBSV at 12dpi had highest number of down-regulated genes (573, 469) also CBSV infection at 12dpi and then ACMV at 19dpi had highest number of up-regulated genes (1851, 1649).

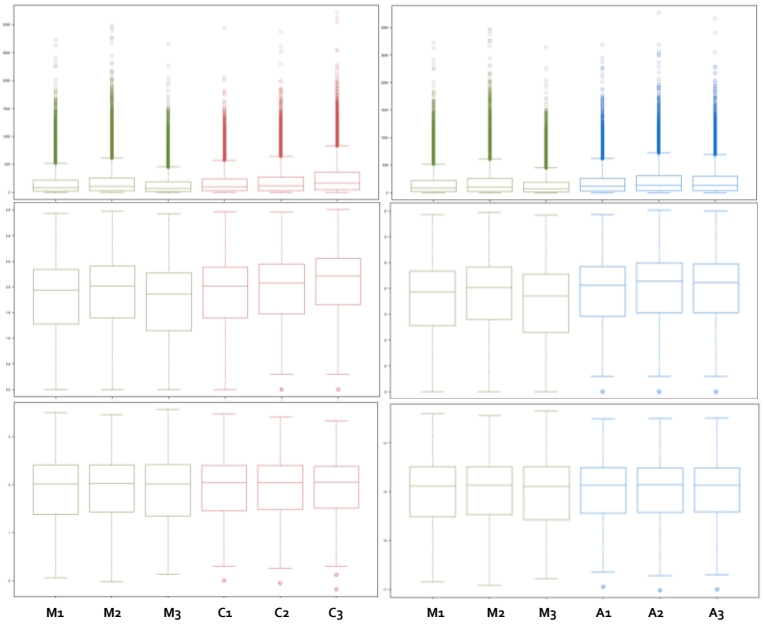

Figure 8. Boxplots of raw data obtained from infected plants with CBSV and ACMV; Before transformation (on top) and before normalization (in middle) and after normalization (in bottom) M: mock, C: CBSV, A: ACMV

28, 73, 1847, and 1140, 979, 1641 significantly up-regulated genes were identified together with 18, 27, 467, and 405, 46, 572 significantly down-regulated genes in CBSV-infected and ACMV-infected versus mock-inoculated *N. benthamiana* in our experimental system respectively at 6, 12 and 19dpi. As it can be seen in Table 1 only relatively few were differentially expressed and accordingly most did not show a considerable change in expression values. During infection progression many of the transcripts occurred to show no change in expression values, as 99.62, 87.25, 92.36% of normalized transcripts from CBSV infected samples with Padj-value<0.05, had log2FC between +2 and -2. Likewise, 99.20, 91.67, 88.98% in ACMV infected samples, at 6, 12, 19dpi respectively.

	CBSV-6dpi	ACMV-6dpi	CBSV-12dpi	ACMV-12dpi	CBSV-19dpi	ACMV-19dpi
Max. of log2FC	3.873	3.447	7.266	7.186	6.360	6.379
Min. of log2FC	-3.134	-2.949	-6.883	-7.001	-3.234	-4.834
Number of padj<0.05	12395	12529	18150	18568	13424	20084
Number of log2FC≤-1	651	555	2249	1904	874	3006
Number of log2FC≥+1	769	1089	4669	4210	3837	5145
Number of log2FC≤-2	18	27	467	405	46	572
Number of log2FC≥+2	28	73	1847	1140	979	1641
Number of total transcripts	41069	41534	43405	43737	42727	42805

Table 1. Statistics report of DEG analyses using DESeq2

The set of over-expressed and under-expressed genes for ACMV and CBSV was different during infection progression. Five different sets were addressed among DEGs: i) set of genes involved in response to infection with CBSV at 6, 12 and 19dpi, ii) set of genes involved in response to infection with ACMV at 6, 12 and 19dpi, iii) set of genes involved in response to infection with CBSV and ACMV at 6dpi, iv) set of genes involved in response to infection with CBSV and ACMV at 12dpi, v) set of genes involved in response to infection with CBSV and ACMV at 19dpi. In the Venn diagrams in Figure 9, we showed the intersection sets between all the transcripts with Padj-value<0.05, which are indicated by blue or green dots (regardless of their brightness level) in Volcano plots. There is an intriguing ratio of them in specific or general cooperation with infection responses. At 6dpi, a very large number (9566) was categorized common between CBSV and ACMV, while 2830 and 2964 were involved in specific response to CBSV and ACMV infection.

3.1.4. Classification of DEGs

To further analyse DEGs that showed specific responses to infection with CBSV and ACMV as well as common up- and down-regulation patterns in both CBSV and ACMV infected plants. Figure 10 shows the number of these genes which are either exclusive to one of the groups or common between other group(s). At 6dpi, 24 out of 30 up-regulated genes in the CBSV samples were also identified in the ACMV samples, whereas in ACMV infected plants there are 49 exclusively up-regulated genes (Fig. 10a-A and B). At 12dpi it is evident that more up- and down-regulated genes in the CBSV samples compared to ACMV, 795 and 316 are commonly elevated (Fig. 10b-A and B) and suppressed (Fig. 10b-C and D) between CBSV and ACMV infected plants, respectively. In contrast at 19dpi more differentially expressed genes are found in ACMV infected plants. The list of top 500 most significantly differentially expressed protein coding genes with their Uniprot, GO and KEGG annotation[63].

Genes distribution in the molecular function GO domains

To elucidate the biological process and molecular effect of RNA and DNA virus infection in *N. benthamiana* plants, we performed GO enrichment analyses using TRAPID, in order to retrieve the annotated DEGs at 6, 12 and 19dpi according to Padj-

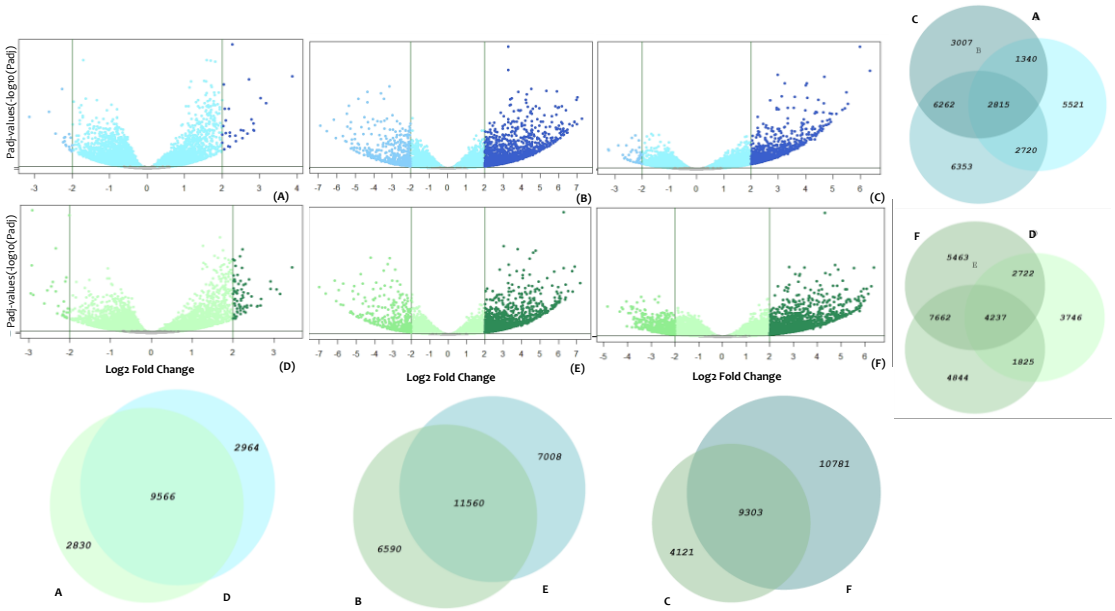

Figure 9. Spread pattern and intersection of differentially expressed genes in response to viral infection progress; **A-F:** Volcano plots of RNA-seq data show the spreading pattern and significance of expressed genes [X axis indicates the log2FC-change of transcriptome profile and Y axis indicates the -log10 (p-value) of each transcript]; The top three most significant differentially protein coding genes in response to CBSV infection are with polysaccharide biosynthetic, M phase, and ATPase activator activities at 6dpi, M phase, nucleic acid binding, and catalytic activities at 12dpi, DNA binding, intracellular membrane-bounded organelle, and immune system process activities at 19dpi. The three most significant differentially expressed genes in ACMV infection are with polysaccharide biosynthetic process and M phase (2 genes) activities at 6 and 19dpi, and from SAUR family protein, autophagy-related protein 2 and acetyl-CoA carboxylase biotin carboxyl carrier proteins at 12dpi. Venn diagrams of differentially expressed genes (Padj-value<0.05) show the intersection between different observations; **A**: CBSV vs. mock - 6dpi, **B**: CBSV vs. mock - 12dpi, **C**: CBSV vs. mock - 19dpi, **D**: ACMV vs. mock - 6dpi, **E**: ACMV vs. mock - 12dpi, **F**: ACMV vs. mock - 19dpi

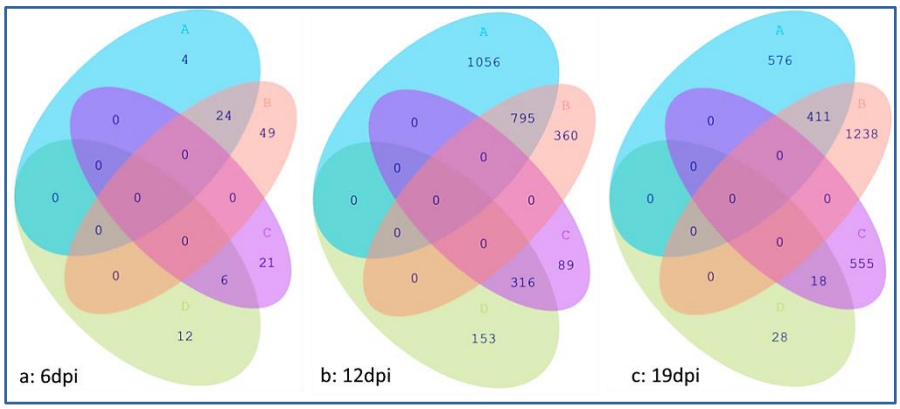

Figure 10- intersection between DEGs according to their log2FC; **A**: up-regulated genes in the CBSV sample with log2FC≥+2, **B**: up-regulated genes in the ACMV sample with log2FC≥+2, **C**: down-regulated genes in the ACMV sample with log2FC≤-2, **D**: down-regulated genes in the CBSV sample with log2FC≤-2

value and log2FC. The identified GO terms of differentially expressed genes, which are specifically and commonly up- or down- regulated in CBSV and ACMV infected plants at 6dpi, is shown in table S6a. In addition, table S6b represents the number of differentially expressed genes at each group of study which did not have any annotation in GO database.

These results indicate that categories for ‘transferase activity’, ‘post-translational protein modification’, ‘intracellular membrane-bounded organelle’, ‘localization’, and ‘transferring one-carbon groups’, ‘cell’, ‘binding’, ‘nucleic acid binding’, ‘microtubule-based movement’, ‘adenyl ribonucleotide binding’, ‘catalytic activity’, ‘cell redox homeostasis’, ‘cellular amino acid and derivative metabolic process’, ‘cellular biosynthetic process’, ‘cellular metabolic process’, ‘DNA binding’, ‘heme binding’, ‘lyase activity’, ‘metal ion binding’, ‘oxidation reduction’, ‘primary metabolic process’, ‘response to stimulus’ are common biological processes which were differentially regulated in the infected plants of our observations and we could not categorize further.

It was evident that ‘purine NTP-dependent helicase activity’ and ‘membrane part’ are the common inhibited biological process in CBSV and ACMV samples at 6dpi, while ‘lyase activity’ and ‘catalytic activities’ are among the up-regulated processes in the CBSV sample at 6dpi, and ‘glucan metabolic process’ was down-regulated. At 12 and 19dpi in CBSV and ACMV infection genes regulated ‘acyltransferase activity’, ‘ATPase activity’, ‘ligase activity’, ‘forming aminoacyl-tRNA and related compounds’, ‘purine NTP-dependent helicase activity’, ‘purine nucleotide biosynthetic process’, ‘cellular component organization’, ‘nucleic acid binding’, ‘passive transmembrane transporter activity’, ‘extracellular region’ and ‘protein metabolic process’, ‘multicellular organismal development’, ‘Immune system process’ were among elevated transcripts. Although ‘purine nucleotide binding’ was shown to be up-regulated in both viruses at 12dpi, at 19dpi it was among both up- and down-regulated genes. Gens related to ‘chromatin modification’, ‘nucleobase, nucleoside, nucleotide and nucleic acid transmembrane transporter activity’ were up-regulated in ACMV infected samples at 12 and 19dpi. ‘Ras guanyl-nucleotide exchange factor activity’, ‘peptidase inhibitor activity’ based genes were up-regulated at 12dpi in CBSV infection and down-regulated in ACMV infection at 19dpi. Similarly the genes which are involved in ‘Tryptophan metabolic process’ were down-regulated in CBSV at 12dpi as well as commonly between two viruses, and up-regulated in ACMV at 19dpi. Genes involved in ‘Oxidoreductase activity’ and ‘acting on single donors with incorporation of molecular oxygen’ were commonly up-regulated in two viruses at 19dpi. Also it was shown that ‘DNA topological change’ was suppressed in ACMV infected samples at 19dpi. The group of genes belongs to ‘Negative regulation of cellular biosynthetic process’ was up-regulated in ACMV infection at 19dpi like ‘nucleotide metabolic process’. Genes related to ‘Glucan metabolic process’ is down-regulated at 6dpi in the CBSV samples, also common in CBSV and ACMV at 12dpi, and up-regulated at 19dpi in CBSV and ACMV. ‘Macromolecule metabolic process’ was suppressed in CBSV and ACMV at 12dpi. In addition, members of the ‘M phase’ biological process were enhanced in ACMV at 19dpi as well as in both viral infections at 12dpi.

Genes with activities with GO annotation ‘Integral to membrane’ were over-expressed in CBSV and ACMV infections at 12dpi and in ACMV at 19dpi, similar to ‘Intracellular part’, ‘clathrin coat assembly’ in the CBSV samples at 12 and 19dpi. Moreover, members of the ‘multicellular organismal development’ were induced only in ACMV infection at

6dpi, while ‘membrane part’ was inhibited in CBSV and ACMV at 6dpi, then increased common in these viruses at the next time points. ‘Plasmodesma’ is suppressed in ACMV at 19dpi, and ‘Extrinsic to membrane’ was down-regulated in CBSV and ACMV at 12dpi. ‘Shoot system development’ was repressed in ACMV at 19dpi, while ‘floral organ development’ was induced in CBSV at 12dpi. ‘Pigment metabolic process’ was up-regulated in CBSV at 12 and 19dpi, ‘response to other organism’ was up-regulated at 12dpi in CBSV and ACMV also in ACMV at 19dpi.

Various GO molecular function categories were represented among the significant genes, which are involved with viral pathogenicity progression across the various functions. Categories corresponding to post-translational protein modification, primary metabolic process, cellular biosynthetic process, localization, catalytic activity, metal ion binding, transferase activity, binding, and heme binding were shown to be differentially and frequently altered between up- or down-regulation due to viral infection.

A Broad Biological Perspective of DEGs Dynamic

At mid-stage of infection, genes involved in ‘peroxisome’, ‘mRNA surveillance pathway’, ‘ubiquitin-mediated proteolysis’ showed higher expression level in the CBSV samples at 12dpi, compared with ACMV. Whereas the expression of genes which mediate ‘RNA transport’, ‘RNA degradation’, ‘spliceosome’ and ‘ribosome’, ‘base excision repair’ and ‘aminoacyl-tRNA biosynthesis’ as well as ‘oxidative phosphorylation’, ‘sulphur metabolism’, and ‘nitrogen metabolism’ were almost on similar levels of expression in both viral infections. More detailed comparison is shown in Figure 11A and B.

At the early stage of infections (Voronoi plot not shown) transcription via spliceosome and transcription factors, translation, replication and repair systems of *N. benthamiana* are induced, whereas the carbohydrate, lipid, all the amino acid metabolism, energy metabolism via oxidative phosphorylation, sulphur and nitrogen metabolism, as well as transport, catabolism and environmental adaptation/plant-pathogen interaction are suppressed.

In the later stage at 12dpi, as can be seen in Figure 11C and D, the genes responsible for the replication and repair (more affected by CBSV infection) as well as carbohydrate metabolism including ‘Glycolysis/Glycogenesis’, ‘starch and sucrose metabolism’ and ‘TCA’ had higher expression values in CBSV at 12dpi, while the group of genes responsible for the metabolism of lipid, terpenoids and polyketides particularly in vitamins and energy metabolisms (more affected by ACMV infection) remain inhibited at 12dpi in infections with these viruses.

A

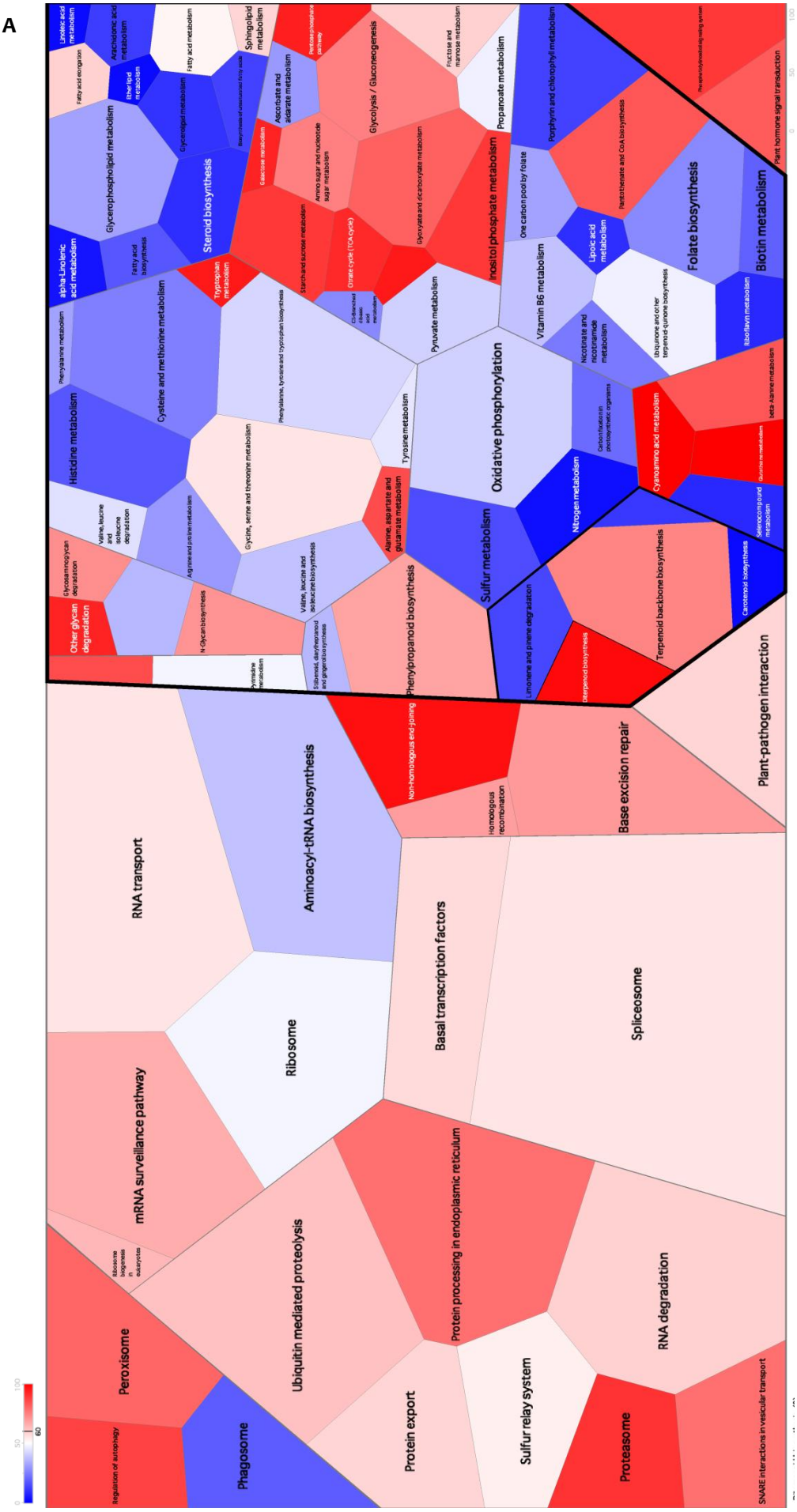
Linoleic acid metabolism
Arachidonic acid metabolism
Fatty acid elongation
Ether lipid metabolism
Fatty acid metabolism
Sphingolipid metabolism
Glycerophospholipid metabolism
Glycerolipid metabolism
Biosynthesis of unsaturated fatty acids
Ascorbate and aldarate metabolism
Pentose phosphate pathway
Galactose metabolism
Glycolysis / Gluconeogenesis
Fructose and mannose metabolism
alpha-Linolenic acid metabolism
Fatty acid biosynthesis
Steroid biosynthesis
Amino sugar and nucleotide sugar metabolism
Propanoate metabolism
Tryptophan metabolism
Starch and sucrose metabolism
Citrate cycle (TCA cycle)
Glyoxylate and dicarboxylate metabolism
Inositol phosphate metabolism
Porphyrin and chlorophyll metabolism
Cutin, suberin and wax biosynthesis
One carbon pool by folate
Phenylalanine metabolism
Cysteine and methionine metabolism
Phenylalanine, tyrosine and tryptophan biosynthesis
Vitamin B6 metabolism
Lipoic acid metabolism
Pantothenate and CoA biosynthesis
Pyruvate metabolism
Nicotinate and nicotinamide metabolism
Ubiquinone and other terpenoid-quinone biosynthesis
Folate biosynthesis
Biotin metabolism
Histidine metabolism
Tyrosine metabolism
Riboflavin metabolism
Plant hormone signal transduction
Glycosaminoglycan degradation
Valine, leucine and isoleucine degradation
Arginine and proline metabolism
Cyanoamino acid metabolism
Other glycan degradation
Glycine, serine and threonine metabolism
Alanine, aspartate and glutamate metabolism
Oxidative phosphorylation
Sulfur metabolism
Nitrogen metabolism
Carbon fixation in photosynthetic organisms
Beta-Alanine metabolism
N-Glycan biosynthesis
Valine, leucine and isoleucine biosynthesis
Pyrimidine metabolism
Steroid, diterpenoid and ginkgolide biosynthesis
Phenylpropanoid biosynthesis
Limonene and pinene degradation
Diterpenoid biosynthesis
Terpenoid backbone biosynthesis
Carotenoid biosynthesis
Selenocompound metabolism
Glutathione metabolism
Plant-pathogen interaction
Base excision repair
Non-homologous end-joining
Homologous recombination
RNA transport
Aminoacyl-tRNA biosynthesis
Ribosome
Basal transcription factors
Spliceosome
Peroxisome
mRNA surveillance pathway
Ribosome biogenesis in eukaryotes
Ubiquitin mediated proteolysis
Protein processing in endoplasmic reticulum
Phagosome
Protein export
Sulfur relay system
RNA degradation
Proteasome
Regulation of autophagy
SNARE interactions in vesicular transport

B


Lipoic acid metabolism
Fatty acid elongation
Arachidonic acid metabolism
Ether lipid metabolism
Fatty acid metabolism
Sphingolipid metabolism
Glycerophospholipid metabolism
Glycerolipid metabolism
Steroid biosynthesis
Biosynthesis of unsaturated fatty acids
Pentose phosphate pathway
Glycolysis / Gluconeogenesis
Fructose and mannose metabolism
Propanoate metabolism
Porphyrin and chlorophyll metabolism
Ascorbate and aldarate metabolism
Glutathione metabolism
Amino sugar and nucleotide sugar metabolism
alpha-Linolenic acid metabolism
Fatty acid biosynthesis
Tryptophan metabolism
Starch and sucrose metabolism
Citrate cycle (TCA cycle)
Glyoxylate and dicarboxylate metabolism
Inositol phosphate metabolism
One carbon pool by folate
Vitamin B6 metabolism
Pantothenate and CoA biosynthesis
Lipoic acid metabolism
Folate biosynthesis
Biotin metabolism
Phenylalanine metabolism
Cysteine and methionine metabolism
Phenylalanine, tyrosine and tryptophan biosynthesis
Co-dienoid oxoic acid metabolism
Pyruvate metabolism
Oxidative phosphorylation
Nicotinate and nicotinamide metabolism
Ubiquinone and other terpenoid-quinone biosynthesis
Riboflavin metabolism
Plant hormone signal transduction
Histidine metabolism
Valine, leucine and isoleucine degradation
Arginine and proline metabolism
Glycine, serine and threonine metabolism
Valine, leucine and isoleucine biosynthesis
Tyrosine metabolism
Alanine, aspartate and glutamate metabolism
Nitrogen metabolism
Carbon fixation in photosynthetic organisms
Cysteine metabolism
beta-Alanine metabolism
Glycosaminoglycan degradation
Other glycan degradation
N-Glycan biosynthesis
Pyrimidine metabolism
Stilbenoid, diarylheptanoid and gingerol biosynthesis
Phenylpropanoid biosynthesis
Sulfur metabolism
Cysteine and methionine metabolism
Cysteine and methionine metabolism
Selenocompound metabolism
Cyanoamino acid metabolism
Limonene and pinene degradation
Terpenoid backbone biosynthesis
Carotenoid biosynthesis
Diterpenoid biosynthesis
Non-homologous end-joining
Homologous recombination
Base excision repair
Plant-pathogen interaction
RNA transport
Aminoacyl-tRNA biosynthesis
Ribosome
Basal transcription factors
Spliceosome
mRNA surveillance pathway
Ribosome biogenesis in eukaryotes
Peroxisome
Ubiquitin mediated proteolysis
Protein processing in endoplasmic reticulum
RNA degradation
Regulation of autophagy
Phagosome
Protein export
Sulfur relay system
Proteasome
SNARE interactions in vesicular transport

C

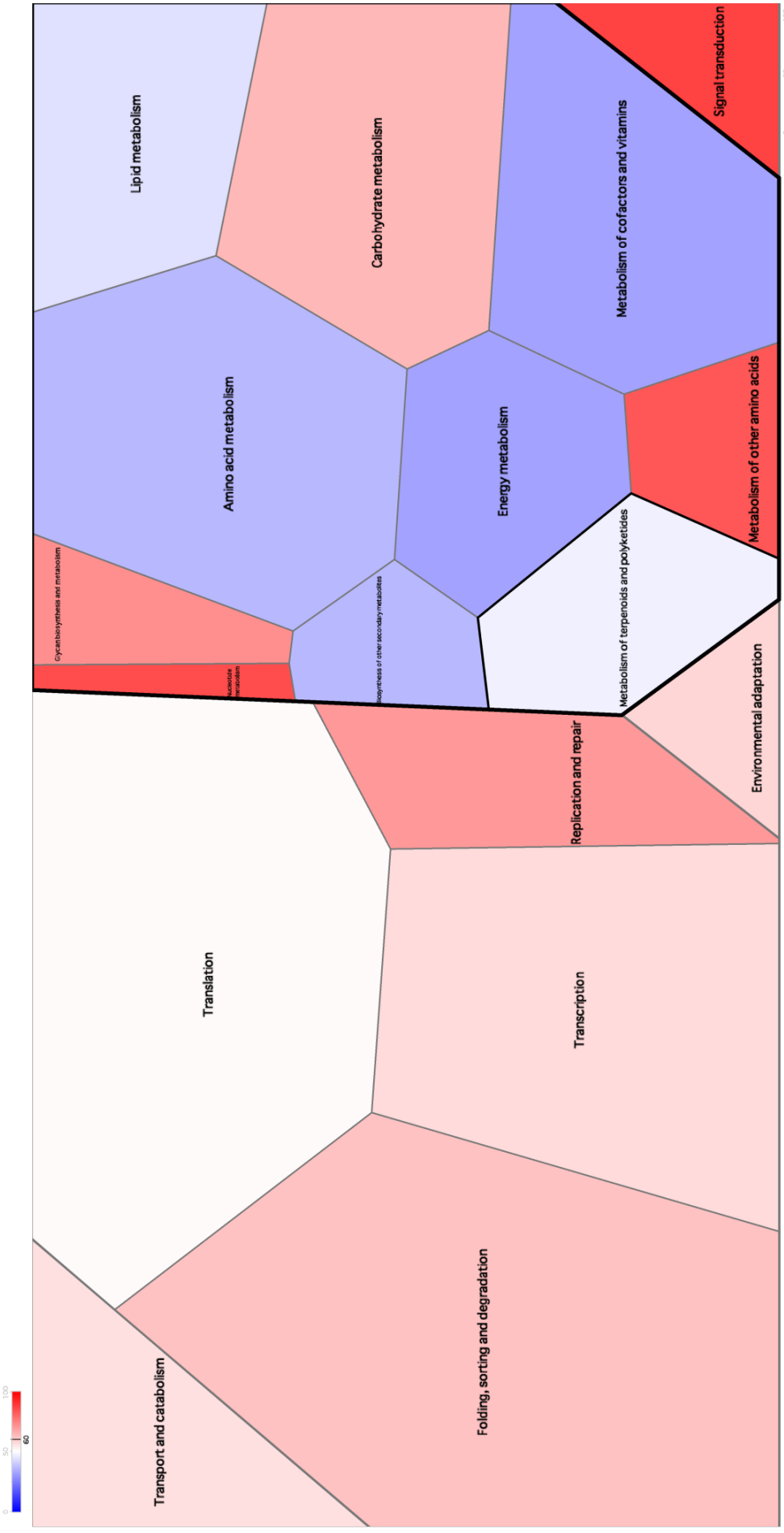
Lipid metabolism
Carbohydrate metabolism
Metabolism of cofactors and vitamins
Signal transduction
Amino acid metabolism
Energy metabolism
Metabolism of other amino acids
Glycan biosynthesis and metabolism
Nucleotide metabolism
Biosynthesis of other secondary metabolites
Metabolism of terpenoids and polyketides
Environmental adaptation
Replication and repair
Translation
Transcription
Folding, sorting and degradation
Transport and catabolism
100
60
50
0

D

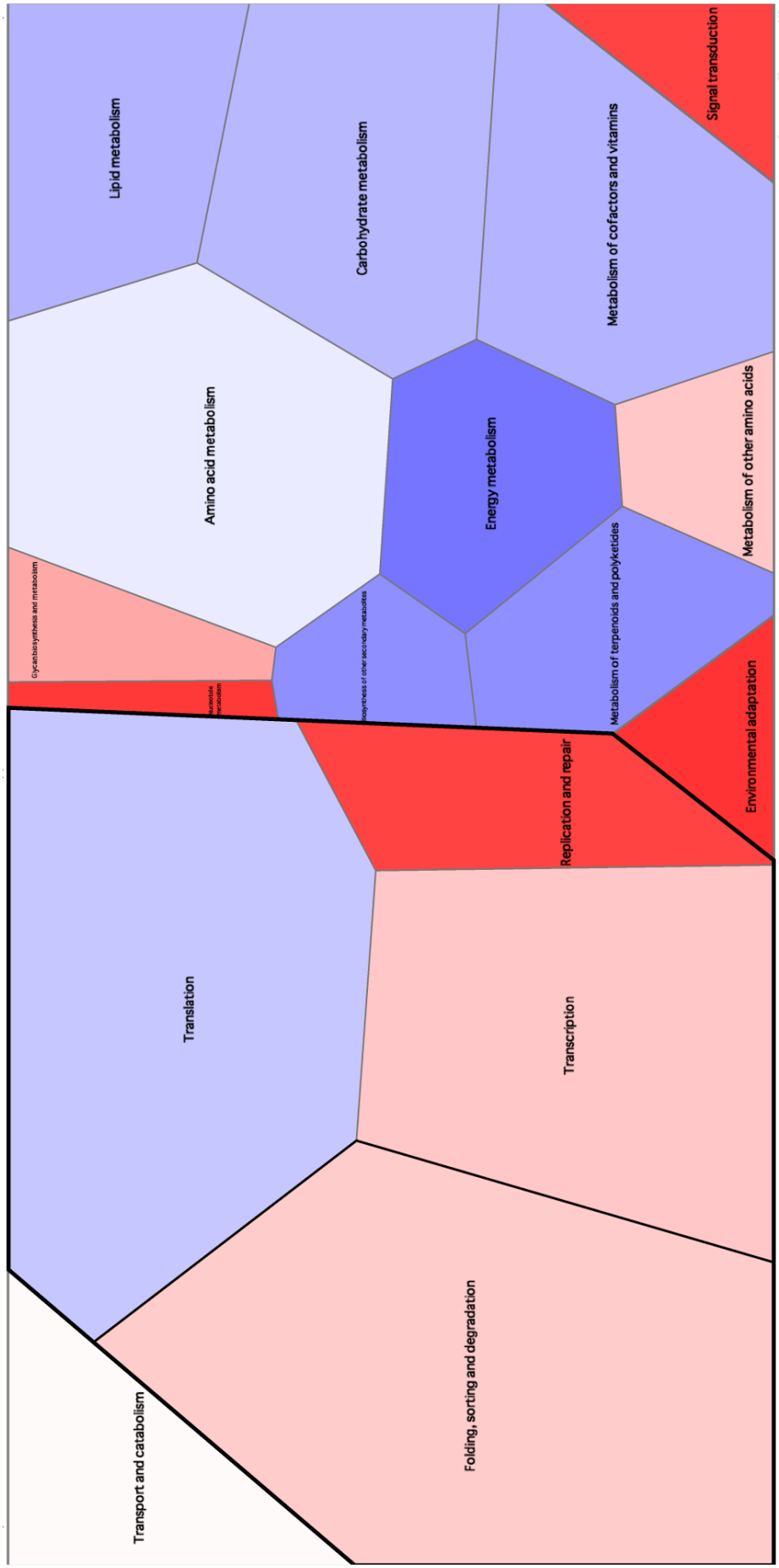
Lipid metabolism
Carbohydrate metabolism
Metabolism of cofactors and vitamins
Signal transduction
Amino acid metabolism
Energy metabolism
Metabolism of other amino acids
Glycanbiosynthesis and metabolism
Nucleotide metabolism
Biosynthesis of other secondary metabolites
Metabolism of terpenoids and polyketides
Environmental adaptation
Replication and repair
Translation
Transcription
Folding, sorting and degradation
Transport and catabolism

Figure 11A-D. Voronoi treemaps of CBSV-12dpi vs. mock-12dpi (A and C) and ACMV-12dpi vs. mock-12dpi (B and D);Genes regulating the function of peroxisome, mRNA surveillance pathway, and ubiquitin mediated proteolysis, as well glycolysis/glyconeogenesis, starch and sucrose metabolism and TCA are shown to be more enhanced in response to infection with CBSV relative to ACMV at 12dpi. Moreover, genes involved in oxidative phosphorylation, sulphur metabolism, and nitrogen metabolism were suppressed in both viral infections. In upper level, as shown in C and D, genes regulating folding, sorting and degradation, transcription, energy metabolism, and lipid metabolism, suppressed equally in addition to the genes involved in signal transduction and environmental adaptation were enhanced equally in CBSV and ACMV infections. Induction of replication and repair system and suppression of translation, also metabolism of terpenoids and polyketide were more noticeable in ACMV infection. Whereas the expression of genes which mediate carbohydrate metabolism were induced in CBSV and reduced in ACMV infected samples relative to mock (Blue for down-regulation, white for unchanged expression and red for up-regulation).

At 19dpi (Voronoi plot not shown) the expression of genes which mediate translation and especially ribosome and aminoacyl-tRNA biosynthesis (more in ACMV), energy and lipid metabolism (more in ACMV), transcription, metabolism of cofactors and vitamins especially biotin and riboflavin (more in ACMV) were repressed, whereas replication and repair (more in ACMV), terpenoids and polyketides, signal transduction (more in ACMV), environmental adaptation (more in ACMV), were induced in both. Transport and catabolism and especially phagosome-regulated genes are suppressed in CBSV and induced in ACMV. At this time point genes which play a crucial role in carbohydrate metabolism are induced in CBSV infected samples, besides of folding, sorting and degradation processes particularly protein processing in endoplasmic reticulum, ubiquitin mediated proteolysis and proteasome are high induced in ACMV infection compared with mock.

Wrapping up the results from this section, various functional processes are shown to be modulated during infection progression of RNA and DNA viruses. According to this colours mapping method, the modification level of some processes such as folding, sorting and protein degradation, spliceosome, translation, signal transduction, phenylpropanoid biosynthesis, oxidative phosphorylation, and different carbohydrate metabolism pathways were strongly differentially expressed that led us for further and more detailed analyses on next steps.

Functional categorization of differentially expressed genes in protein family level

Among the top 100 most significant DEGs of plants infected with ACMV at 6, 12, 19dpi, almost 63, 64 and 76%, and for CBSV infected plants at 6, 12, 19dpi respectively 60, 71, 65% were well-described in Pfam database which was used to make a classification scheme. It is interesting to see more variant protein families are involved in response to ACMV infection, particularly at mid- and late stage of infection. Each pie chart represents the annotated differentially expressed genes, the colours stand for each protein mentioned in the plot and numbers (written also insides the bracket) indicates the number of differentially expressed genes annotated in Pfam database[64]. The classification is given in Figure 12 (A and B) shows that at 6dpi proteins belonging to Kinesin, DUF, Pkinase, PPR[65], Zf[66], F-box, Glyco_hydro and Glutaredoxin families reacted to both ACMV and CBSV infection, while UDPGT[67], cyclin, DDT[68] and WD40 protein families in CBSV and Lipase and Abhydrolase in the ACMV samples were differentially

regulated. Likewise, as shown in Figure 12 (C and D), at 12dpi Pkinase, ABC_trans, IQ and WRKY protein families reacted to both ACMV and CBSV infection, while LRR, Adaptin_N, Zf, DEAD, Peptidase and UDPGT only differently showed up in ACMV infection process similar to DUF, Glyco_transf and NAM families in the CBSV samples. Another category presented in Figure 12 (E and F) belong to protein families involved in response to infections at 19dpi, NAM, Pkinase, ABC_trans, HSP[69] and Sugar_tr. Additionally Auxin_repressed, Asp[70], Ap2[71]-domain, AAA[72], Annexin, HALZ, Hpt, IQ, PTR[73]2 and WRKY families were differentially expressed only in ACMV infection process.

Among the top 100 most significant differential expressed genes, protein families associated with Pkinase and transcription factors (either F-box or WRKY) as well as DUF were observed at all time points and in both groups of samples. Sugar_tr showed differential responses to infection to infection only at 19dpi, while Kinesin, Glyco_hydro and Glutaredoxin only at 6dpi.

Differentially regulated pathways in response to infection progression

Gene expression during infection response is under the control of a complex combination of various pathways, some of which have key roles in other plant processes such as in response to environmental stresses. Among various biological processes which are differentially regulated in response to viral infection a detailed modification pattern of some are presented in Figure 13 (a-b); Elements belong to plant-pathogen interaction (ko04626 KEGG-ID), hormones signal transduction pathway (ko04075 KEGG-ID), mRNA surveillance and transport factors focusing on translation initiation, and glycolysese (EC:3.2.1 KEGG-ID).

Regulated plant hormones signal transduction and plant-pathogen interaction pathways, translation initiation and glycolysis:

Amongst the plant-pathogen interaction, hormones signal transduction, glycolysis and translation initiation pathways, we determined the regulation pattern of a number of involved genes during the symptom development. These include defence-related genes such as SA- and JA- inducible genes, and innate immunity genes which are significantly differentially expressed at mid and late stages of infection. Thus infection with CBSV or ACMV induced the SA and ET signaling pathways, particularly at 12 and 19dpi but repressed the JA signaling pathway at 12dpi.

As shown in Figure 13a, The homologues of the SA-inducible genes such as TGA[74] transcription factor genes as well as NPR1 and PR1 showed much higher expression in CBSV and ACMV infection at 12 and 19dpi relative to 6dpi, particularly PR1 (43-, 33-fold at 12dpi and 4.5-, 21-fold at 19dpi in CBSV and ACMV infected plants). *RDR* was repressed at the early stage of infection up-regulated in response to CBSV (4.2 times) and to ACMV at 19dpi (2.5-fold) at 12dpi. The MYC2[75] transcription factor gene was slightly up-regulated in CBSV and ACMV at 6dpi, whereas WRKY transcription factor 33 was more than 2.5-4 times enhanced in CBSV and ACMV infected plants at 12 and 19dpi.

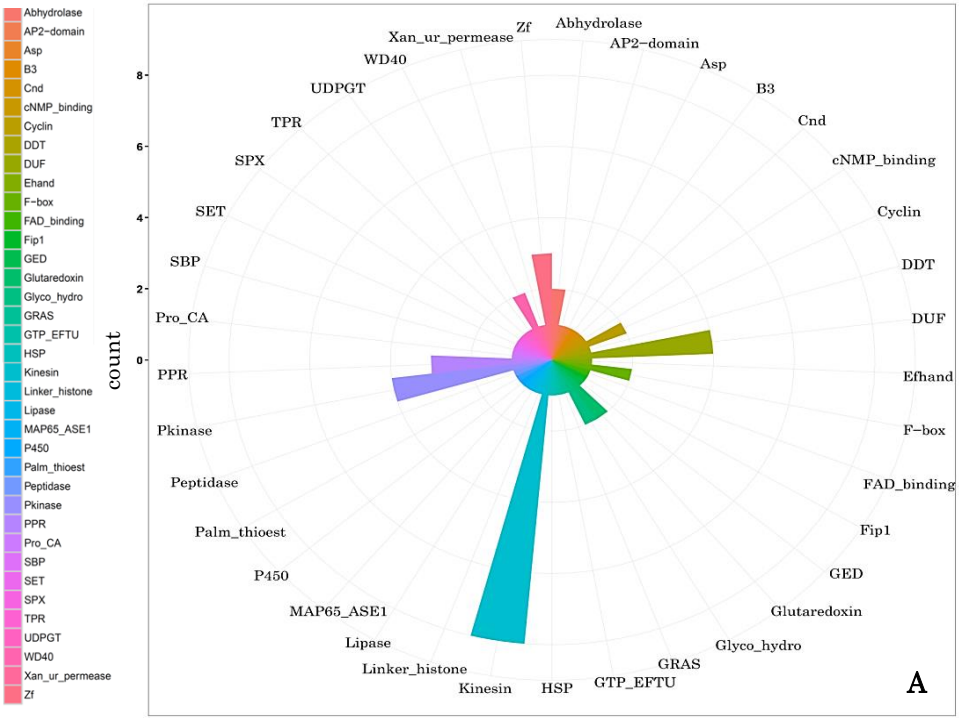

Figure 12a. Pfam Functional classification of top 100 most significant DEGs in CBSV vs. mock - 6dpi; Kinesin (7), Pkinase (4), PPR (3), Zf (3), F-box (2), Glyco_hydro (2), Glutaredoxin (2), UDPGT (2), cyclin (2), WD40 (2) 76

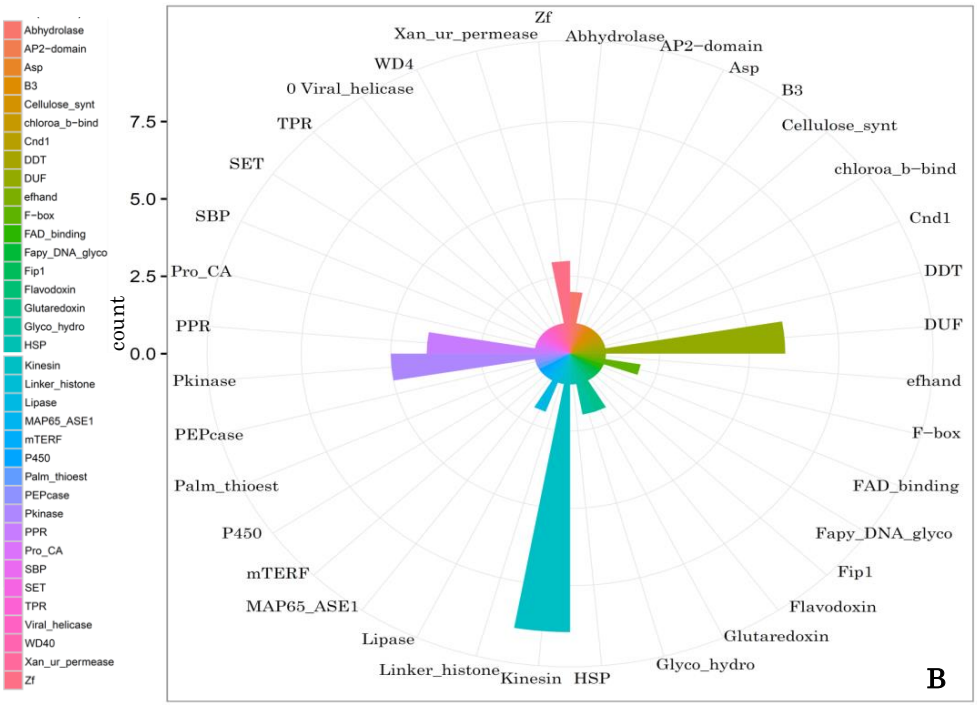

Figure 12b. Pfam Functional classification of top 100 most significant DEGs in ACMV vs. mock - 6dpi; Kinesin (8), Pkinase (5), PPR (4), Zf (3), F-box (2), Glyco_hydro (2), Glutaredoxin (2), Lipase (2), Abhydrolase (2)

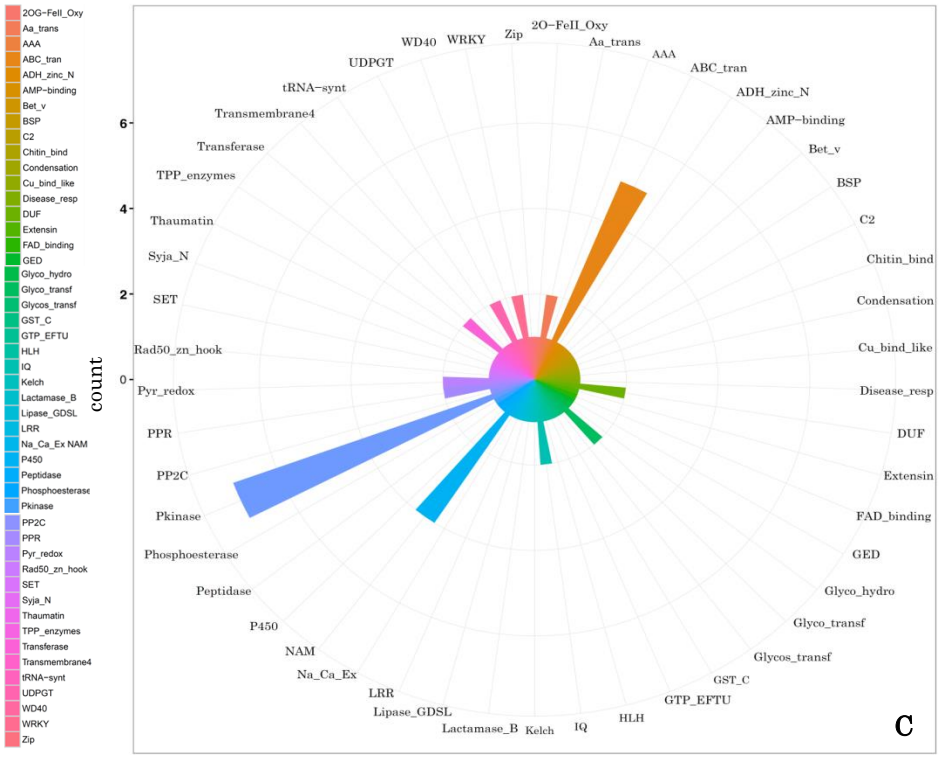

Figure 12c. Pfam Functional classification of top 100 most significant DEGs in CBSV vs. mock - 12dpi; Pkinase (7), ABC_trans (5), NAM (4), Glyco_transf (2), IQ (2), DUF (2), WRKY (2)

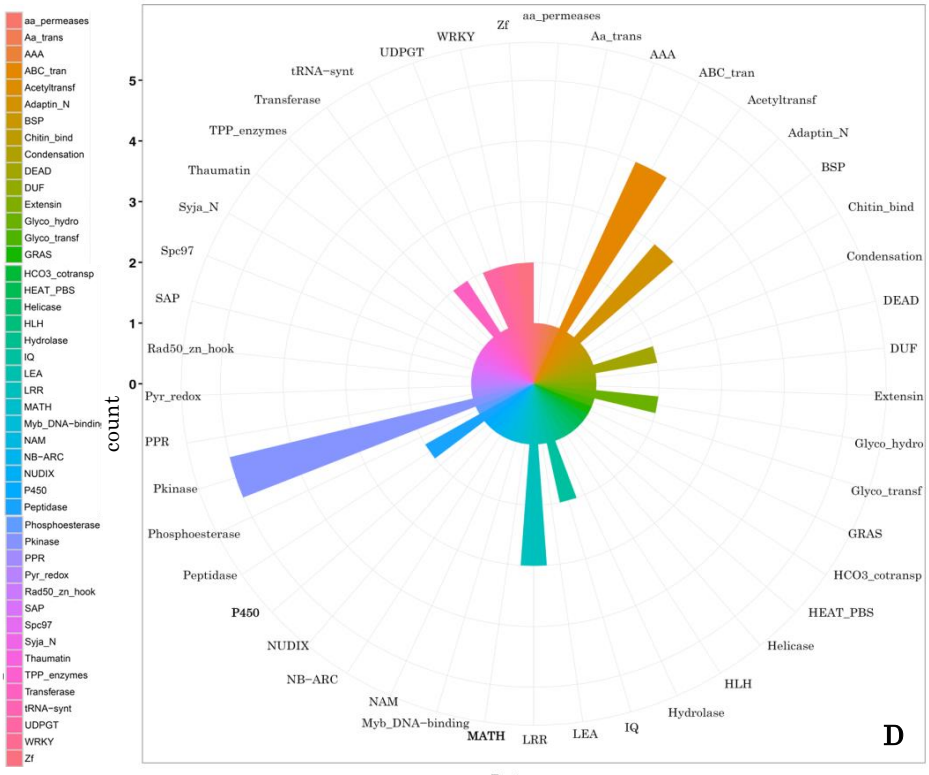

Figure 12d. Pfam Functional classification of top 100 most significant DEGs in ACMV vs. mock - 12dpi; ABC_trans (4), Pkinase (3), LRR (3), Adaptin_N (3), Glyco_hydro (2), IQ (2), WRKY (2), Zf (2), DEAD (2), Peptidase (2), UDPGT (2)

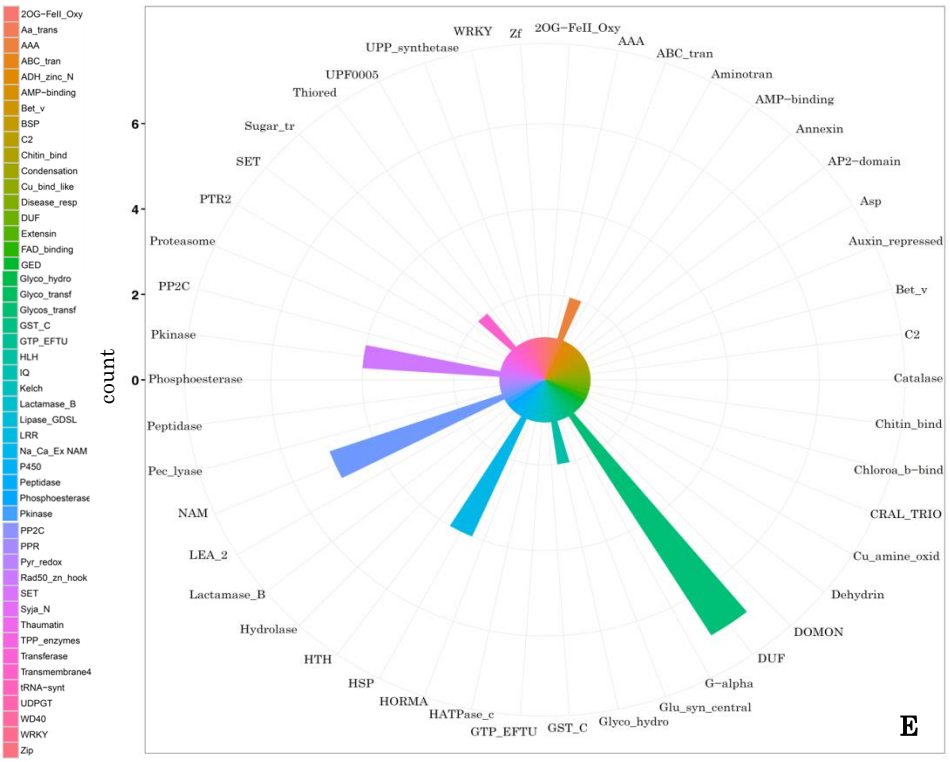

Figure 12e. Pfam Functional classification of top 100 most significant DEGs in CBSV vs. mock - 19dpi; HSP (4), NAM (5), Pkinase (4), Sugar_tr (2), ABC_trans (2)

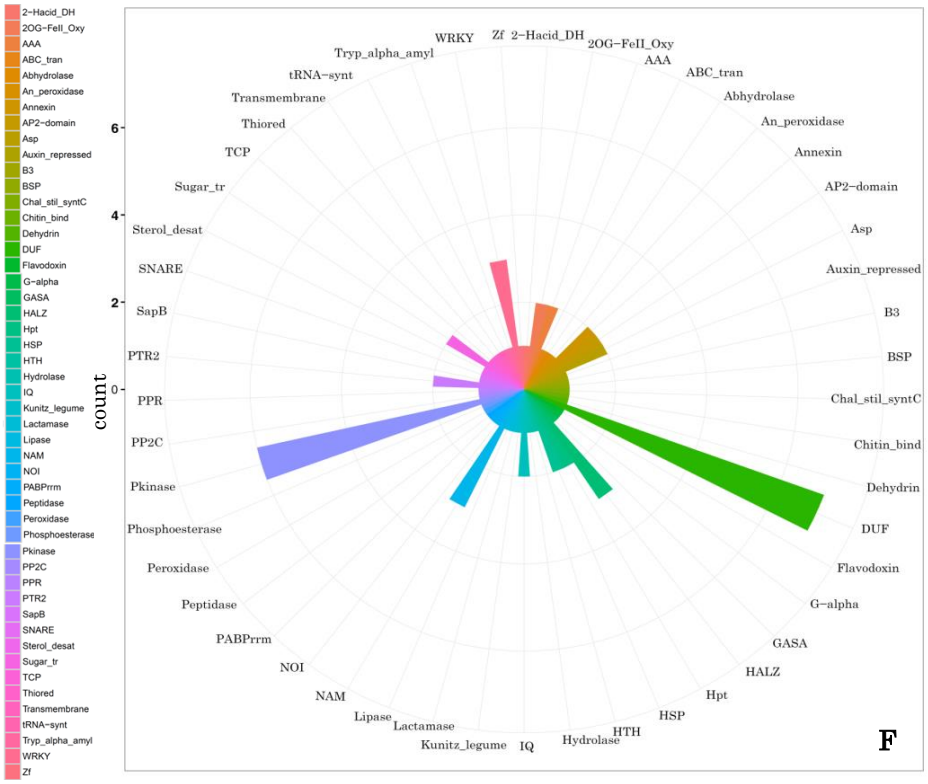

Figure 12f. Pfam Functional classification of top 100 most significant DEGs in ACMV vs. mock - 19dpi; Pkinase (6), HALZ (3), HSP (2), NAM (2), Sugar_tr (2), Asp (2), Ap2-domain (2), AAA (2), Annexin (2), Hpt (4), IQ (2), PTR2 (2), WRKY (3), ABC_trans (1)

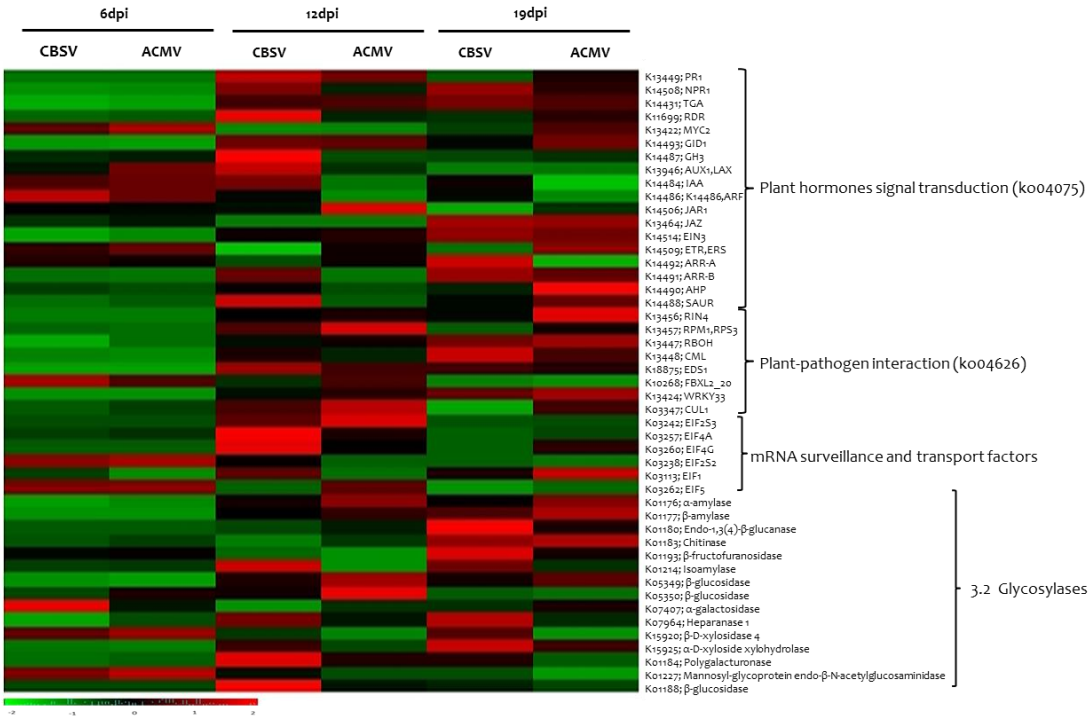

Figure 13a. Regulated plant hormones signal transduction, plant-pathogen interaction pathways, mRNA surveillance and glycosylases; The differentially expressed genes regulating the plant hormones signal transduction (ko04075), plant-pathogen interaction (ko04626), mRNA surveillance and transport factors, and glycosylases are shown in details. The fold change of genes in CBSV and ACMV infections relative to mock are presented in color; green for down-regulation, black for unchanged expression or missing values and red for up-regulation.

The jasmonic acid signaling pathway genes such as JAZ[77] were induced (almost 2.3 times in both) at 19dpi in CBSV and ACMV infected plants, while JAR1[78] remained almost unchanged and OPCL1[79] which is involved in jasmonic acid biosynthesis was induced at 19dpi in both CBSV and ACMV infected plants for 2.4 and 3.7 times (not shown in heatmap). The homologues of ethylene signaling pathway components ERF1, ETR[80], EIN2[81], EIN3[82] were slightly up-regulated in all time points of viral infections; ETR was more responsive at 6dpi, ERF1 was more elevated transcripts at 12dpi (4.3- and 3.1-fold) and 19dpi (2.3 and 5.3 times) in CBSV and ACMV respectively, and EIN3 both time points for both viruses (1.65-fold). EIN2 was up-regulated 1.7-fold in ACMV at 12 and 19dpi while the data for CBSV was not available.

It has been reported that systemic virus infections in plants impair the steady state of auxin and leads to morphogenic alteration (Pennazio S 1996, Park J 2004). CBSV and ACMV infection in *N. benthamiana* plants appear with stunting by 8-9dpi. Analyses of the expression of auxin signaling pathway-related genes indicate that CBSV and ACMV infection to some extent elevated the expression of the auxin transporter AUX1[83] (2.5-fold in ACMV infected plant at 6 and 3.1 times in CBSV infected plant at 12dpi) and PIN[84] (1.3-1-4-fold in CBSV and ACMV infected plants at 6dpi) genes, however the expression values at 19dpi did not show any significant changes of these auxin transporter genes. The expression levels of auxin-responsive genes such as IAA[85], ARF[86] and GH3[87] were slightly up-regulated on infection at 6dpi. Although GH3 stayed enhanced during the infection progression (4.2-, 2.2-fold at 12dpi and 2.3-, 2.4-fold at 19dpi in CBSV and

ACMV samples, respectively), IAA and ARF dropped back to the mock inoculation level or very slightly elevated at 12 and 19dpi. Up-regulation of the negative regulator SAUR[88] gene has been shown to be correlated with virus symptoms development in plants (Park J 2004, Satoh K 2013). Additionally, at 12dpi of CBSV and 19dpi of ACMV in *N. benthamiana* plants the expression of SAUR genes was elevated.

Genes belonging to CK pathway such as IPT[89], ARR-A[90], ARR-B[91], AHP[92], AHK2_3_4[93] were also detected with ARR-A and AHK2_3_4 showing a slight increase in transcripts at 6dpi. CBSV infection at 12dpi induced the expression of AHK2_3_4, ARR-B and AHP, while ACMV at this time point only induced AHK2_3_4. At 19dpi in CBSV infected plants all of the above genes were enhanced, especially ARR-B, AHK2_3_4 and ARR-A (2, 1.8, 1.7 times respectively), similarly in the ACMV samples AHP and AHK2_3_4 were up-regulated (2.3 and 1.35 times respectively). However the expression level of IPT remained unchanged due to infection and gene encoding CK degrading enzyme CKX[94] was significantly increased at late stage of both viruses infection (1.5 and 2.7 times in CBSV and ACMV).

RNA-seq results also described the differential regulation of the innate immunity: At 12dpi of CBSV and ACMV, EDS1[95] was up-regulated 6- and 4.5-fold, similarly RIN4[96] 2.7- and 3.19-fold. Infection with ACMV at 19dpi resulted in induced RIN4, EDS1, RBOH[97], CML[98] and RPM1 by 6.4-, 4-, 2.4-, 1.6- and 1.5-fold, whereas their expression values after CBSV infection were lower with a 2.5-, 4.5-, 2.2-, 2.16- and 0.75-fold. Amongst, disease resistance protein RPM1 was the only gene which was suppressed at 19dpi in the CBSV samples and elevated in the ACMV samples; it might be a regulator of plant survival or sever senescence.

We also had a closer look at the expression profile of the recessive genes which also contribute to plant resistance and encode translation initiation factors. Maruthi *et al* by analyzing the cassava transcript profiles identified the expression of four eIF4E and one eIF4G, where eIF4E transcript was increased two-fold in infected resistant line of cassava compared to healthy and susceptible lines (Maruthi MN 2014). In our dataset, amongst translation initiation factors, subunit 3 of eIF2 was highly up-regulated at 12dpi in both CBSV and ACMV samples (3.7 and 5.6 times respectively) but did not show much difference at other time points, while eIF4A and eIF4G genes were more up-regulated in the CBSV samples at 12dpi.

Among the enzymes with Glycosidase activities alpha-amylase99 and beta-amylase[100] were highly induced (more than 2 times log2fc) in CBSV and ACMV infected plants at 12 and 19dpi, similar to isoamylase[101]. The expression level of beta-glucosidase[102] is induced in both CBSV and ACMV infected plants at 12dpi while isoamylase showed higher expression value for CBSV at 12 and 19dpi. CBSV infected plants at 19dpi also showed elevated expression levels of endo-1,3(4)-beta-glucanase[103] and beta-fructofuranosidase[104]. Infection of ACMV resulted in a more than 4 times down-regulation of expression of beta-fructofuranosidase at 12dpi and a down-regulation of mannosyl glycoprotein endo-beta-N-acetylglucosaminidase at 19dpi.

On the other hand, as shown in Figure 13a, the expression level of many genes dropped at early stage of infection as pathogen-induced response: beta-glucosidase[105] gene expression was suppressed in both virus infections to 0.5-fold, while heparanase 1 [106] was the most suppressed gene in CBSV infection (0.3-fold), which was also expressed at 0.6-fold in the ACMV samples. Alpha-amylase transcript level was declined to 0.6-fold in CBSV infection but unchanged in ACMV. Moreover the expression of some genes decreased almost to the same level in CBSV and ACMV such as Polygalacturonase[107], SAUR, EDS1, RPM1/RPS3, alpha-D-xyloside xylohydrolase[108] (in both viruses 0.6-fold). Other genes including RIN4 and NPR1 (0.6 and 0.7-fold in CBSV and ACMV), TGA (0.5- and 0.6-fold in CBSV and ACMV), GID1 and CML and EIF1/SUI1 (0.7- and 0.6-fold) declined the transcript level differently. At 12dpi, JAZ and beta-fructofuranosidase were suppressed to 0.3- and 0.5-fold in CBSV, and 0.3- and 0.2- in ACMV infection, MYC2 to 0.17-fold in CBSV and 0.2-fold in ACMV. At 19dpi the expression level of MYC2 and EIF5 dropped to 0.55 and 0.66 in CBSV infection, while mannosyl-glycoprotein endo-beta-N-acetylglucosaminidase, ARR-A and EIF2S2 responded to ACMV infection by decreasing the expression to 0.2-, 0.4- and 0.6-fold.

Regulation of ubiquitination and protein degradation:

DNA accessibility is regulated via a complex set of post-translational modifications of histones, also called histone code, and nucleosome remodelling. In CBSV and ACMV infection at 6dpi ELF2C[109] and BARD1[110] as well as most of the chromatin remodelling factors were elevated, although protein degradation pathway via metalloprotease and ubiquitin.E3.SCF.Cullin, deubiquitination via GPS1111 as a COP9 signalosome complex subunit 1, Ubiquitin ligation via RAD51[112] as well as RNAi via ERI2[113] were the most inhibited.

In CBSV and ACMV at 12dpi microRNA pathway via RISC loading complex components including DICER1[114] and ELF2C was induced; together with the BARD1 from BRCC complex as a multi subunit ring-finger type E3 ubiquitin ligase. AAA type of protein degradation pathway was the most activated process and DMAP1[115] from SWR1 complex; Chromatin remodelling factors was the most suppressed gene (with a slightly higher expression value in ACMV) at these samples. Deubiquitination was induced via COPS3[116] as a COP9 signalosome complex subunit 3 with UBL-specific proteases activity in ACMV at 12dpi, as well as chromatin remodelling factors such as SMARCAD1[117] and DEK protein[118]. Cysteine protease, compared with aspartate and serine proteases, was more affected at 12dpi of CBSV infection and 19dpi of ACMV infection.

In response to CBSV infection at 12dpi and 19dpi, ATP-dependent RNA helicase DDX6/DHH1[119] from piRNA/RNA silencing pathway was more than 3-fold enhanced. RNA-dependent RNA polymerase[120] from RDRC[121] and RNAi pathway was induced in response to CBSV at 12dpi and ACMV at 19dpi. Histone deacetylase 1/2[122] from NuRD complex and chromatin remodelling factors was induced in ACMV at 12 and CBSV at 19dpi.

In response to CBSV infection at 19dpi, genes encoding chromodomain-helicase-DNA-binding protein 4[123] were the most induced, whereas ubiquitin.E3.SCF.SKP from protein degradation pathway was inhibited at this time point. In response to ACMV infection at 19dpi, protein degradation via cysteine protease and AAA type elevated transcripts in response to ACMV infection. Histone deacetylase 1/2 from NuRD complex and chromatin remodelling factors, DICER1 from RISC loading complex and microRNA pathway were the most induced transcripts, whereas BARD1 from BRCC complex and multi subunit Ring-finger type E3 ubiquitin ligases as well as histone-binding protein RBBP4[124] from NuRF complex and chromatin remodelling factors were suppressed.

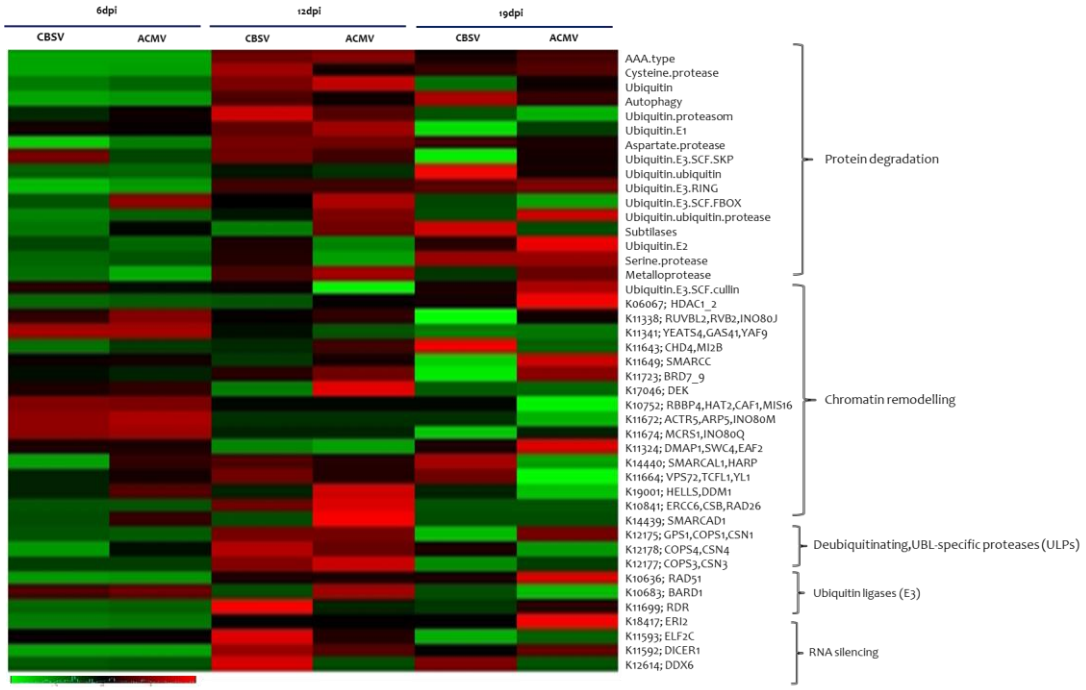

Figure 13b. Heatmap of ubiquitination and protein degradation; The differentially expressed genes regulating the protein degradation, chromatin remodelling, deubiquitinating, UBL-specific proteases (ULPs), ubiquitin ligases (E3), RNA silencing are shown in details. The fold change of genes in CBSV and ACMV infections relative to mock are presented in color; green for down-regulation, black for unchanged expression or missing values and red for up-regulation.

3.2. Real-Time quantification of key pathway genes

Real-Time RT-PCR represents a powerful tool for the detection and quantification of gene expression levels and its high sensitivity, reproducibility, and broad dynamic quantification range rises its widely applications, as the most sensitive method for the detection and quantification of mRNA, in particular for the elucidation of small changes in mRNA expression levels (Pfaffl MW 2004). In general two strategies can be performed in Real-Time RT-PCR, in order to measure the genes expression levels, which are absolute or relative quantitative Real-Time RT-PCR. Absolute quantification, associates the PCR signal to input copy number by using a calibration curve, therefore its reliability depends on the condition of identical amplification efficiencies for both native target and calibration curve in RT reaction, while relative quantification measures the relative change in mRNA expression levels, is based on the expression levels of a target gene versus a housekeeping gene and in theory is adequate for most purposes to address gene

expression levels due to physiological changes, and these relative quantities are comparable across multiple Real-Time RT-PCR experiments.

Relative Real-Time PCR quantification determines the steady expression level of a target gene relative to the level of an internal control. To calculate this expression value, various mathematical models are established, based on the comparison of the distinct cycle determined by various methods, such as CP and Ct at a constant level of fluorescence; these several mathematical models could be either 'without efficiency correction' or 'with kinetic PCR efficiency correction'. In this study, it was decided on following the Pffafl equation and 2-ΔΔCt method, and assessing the Ct values with the efficiency correction approach. In order to confirm the transcriptome data, RT-qPCR was carried out with two independent technical replicates of infected (with CBSV and ACMV) and non-infected (mock) *N. benthamiana* leaves at three time points 6, 12 and 19dpi to analyse the expression pattern and trend of selected genes during infection progression.

3.2.1. Comprehensive stability analyses of housekeeping genes

Among speculated housekeeping genes L23, PP2A, Actin, and Ago1 (Liu D 2012) and according to all the algorithms implemented in Reffinder (Xie F 2012), Delta CT (Fig. S4A), BestKeeper (Fig. S4B), NormFinder (Fig. S4C), and Genorm (Fig. S4D). Finally, it was shown L23 as the most stable endogenous standard gene to apply for normalization of the target genes and verify their RNA-seq expression pattern. Table S5 determines the criteria which were considered by Reffinder to decide on the most stable reference gene.

3.2.2. Relative quantification of investigated gene transcripts in Real-Time PCR

A total relative quantification of 48 genes in comparison to a reference gene and by considering the efficiency of each primer pair were calculated by using the mathematical 2-ΔΔCt method. In general, according to our qRT-PCR data analyses, and as shown in the Figure 14, infected *N. benthamiana* with ACMV faced more notable induction of these selected genes, at 12dpi relative to CBSV, although amongst we found several exceptions.

The genes involved in host defence response were shown to be induced more than 2 fold, such as *ALF5* (2.6-, 4.5-, 2.8-fold in ACMV infection at 6, 12 and 19dpi likewise 3.8-fold in the CBSV samples at 6dpi), *MYC2* (was suppressed at 6dpi, but 4.4- and 2.2-fold in the ACMV samples and 1.2- and 1.1-fold in CBSV infection at 12 and 19dpi), *MAP2K1* (was suppressed at 6dpi, but then got induced to 4.9- and 4.7-fold in the ACMV samples and 2.1- and 1.2-fold in CBSV infection at 12 and 19dpi). The conserved domains of R proteins from different plant species suggest that activation of common signaling pathways occurs upon pathogen perception (Baker B 1997). For example, the functional TIR-NB-LRR class of *R* genes requires *EDS1*, which was induced for 10.9-, 15.4-, 6.4-fold in CBSV infection at 6, 12 and 19dpi, 39.8- 124.9- and 27-fold in ACMV infected samples at 6, 12 and 19dpi, and a subset of the CC-NB-LRR class of *R* genes requires *NDR1*, for resistance to pathogens. We found that the level of *NDR1* was overexpressed to 3.8-, 1.6- and 0.8-fold in CBSV also 1.6-, 17.3-, and 3.8-fold in ACMV at 6, 12 and 19dpi. *RAR1* may represent an example of a signaling component involved in pathways shared by both the CC-NB-LRR and the TIR-NB-LRR resistance gene classes

(Liu Y 2002), which represented as unchanged at 6dpi of CBSV infection, and repressed in the ACMV samples (to 0.72-fold). At 12 and 19dpi it was shown to be over-expressed; 3- and 2-fold in CBSV and 6- and 3.8-fold in ACMV.

Among the genes which are required for PCD triggered by NBS-LRR resistance proteins, the expression level of senescence-associated carboxylesterase 101/*SAG101* in CBSV infection was 7.1-, 3.6-, 2.5-fold and in ACMV infection 2.5-, 46.2-, 9.2-fold was enhanced at 6, 12, 19dpi. Additionally *PAD4* which is required downstream of *MPK4* for accumulation of the plant defence-potentiating molecule (Andreasson E 2005, Wiermer M 2005, Ascencio-Ibáñez JT 2008) was significantly up-regulated at 12dpi of ACMV infection (for 130-fold) with decreasing expression at 19dpi (for 48-fold), while CBSV infection caused the 2.9- and 4.5-fold induction at 12 and 19dpi. This gene was one of few early responding genes to CBSV infection, which showed 6.8-fold increase, while ACMV samples at that time point had 0.6-fold expression of this gene relative to mock.

Other transcription factors such as *TGA* first decreased to 0.9- and 0.15-fold at 6dpi, then got enhanced in response to CBSV infection at 12dpi (to 4.3-fold) and ACMV infection at 12dpi (to 11.6-fold) that was also enhanced at later stage (1.1- and 3.7-fold in CBSV and ACMV samples. Similarly, we observed that *WRKY22* was suppressed at 6dpi to 0.44- and 0.43-fold, and then increased to 1.45- and 8.7-fold at 12dpi also 1.9- and 3.1-fold at 19dpi in CBSV and ACMV infections.

We observed induced transcript level of *BAK1* for CBSV and ACMV at 6dpi (to 4.5- and 10.4-fold), at 12dpi (to 1.5- and 3.2-fold) and 19dpi (for 1.3- and 1.5-fold). *BKI1* showed a suppressed expression at 6dpi (0.8- and 0.7-fold) but then got enhanced at 12dpi (to 2.4- and 10.7-fold), similar to 19dpi (to 3- and 4.5-fold). The level of *MEK2* was highly induced for both viruses at 6dpi as compared to the later time points where it still kept moderately up-regulated (to 251.1-, 13.7-, 5.24-fold in ACMV and 491-, 3.3-, 2.33-fold in CBSV infected samples at 6, 12, 19dpi). Moreover, *F-box* that was induced in CBSV infected plants for 2.3-, 4.3-, and 3.7-fold at 6, 12 and 19dpi also with higher values in ACMV with 7.5- and 3.7-fold at 12 and 19dpi. Moreover, the level of *SKP1* was shown to be differentially regulated in CBSV infection with 1.5-fold at 6dpi, 3.1-fold at 12dpi and 2.1-fold at 19dpi also in ACMV infection with 0.5-fold at 6dpi, 7.5-fold at 12dpi and 10.5-fold at 19dpi. At 6dpi, expression of *SGT1* was suppressed for 0.83-fold in ACMV infection, whereas in CBSV was 3.9-fold induced. At 12 and 19dpi of CBSV and ACMV infected plants, the induction level was about 4.7-, 3.7-, and 8.6-, 5.7-fold respectively.

Amongst the investigated SA pathway involved genes, the transcript level of *RDR1* was induced for 4.8, 1.7, 3.6-fold in CBSV infection and 24.6, 63, 85.4-fold in ACMV infection at 6, 12 and 19dpi. Likewise *PTI6* although was repressed at 6dpi (to 0.7- and 0.4-fold in CBSV and ACMV), got enhanced at 12dpi (to 1.5- and 14.5-fold) and 19dpi (1.7- and 3.3-fold). The expression level of *PR1* dropped to 0.57-, 0.5-, 0.8-fold in CBSV infection at 6, 12 and 19dpi, while in the ACMV samples with high suppression at 6dpi (to 0.15-fold) and 19dpi (0.47-fold) showed induction at 12dpi (to 12.7-fold). On the other

hand, *NPR1* was moderately expressed in CBSV infection (for 1.2-, 1.5-, 1.9-fold) whereas infection with ACMV caused a 0.5-fold reduction at 6dpi, then it was induced for 8.3- and 2.7-fold.

The transcript content of genes belonging to JA pathway was also confirmed to be differentially regulated during infection; interestingly at 6dpi *JAZ* was 20-fold induced in CBSV infection, while in the ACMV sample was 0.4-fold repressed. Then it showed induction to 24.3- and 33.4-fold at 12dpi, likewise to 3- and 8.6-fold at 19dpi of CBSV and ACMV infections. The common transcription factor of ABA and JA signaling pathways, *MYC2* at 12 and 19dpi was up-regulated in CBSV (to 1.2- and 1.1-fold) and ACMV infection (to 4.4- and 2.2-fold), while it showed down-regulation at 6dpi (to 0.6- and 0.7-fold).

The expression of genes involving in the CK pathway were repressed at 6dpi in both infected samples, but at 12 and 19dpi were suppressed (or very slightly enhanced) in CBSV infection, and in contrast significantly induced in ACMV infection; *ARR-B* (reduced to 0.8- and 0.2-fold in CBSV whereas increased to 10.4- and 2.7-fold at 12 and 19dpi), AHP (to 1.2- and 1.7-fold in CBSV infection, 18.4- and 5-fold in ACMV infection), *AHK2_3_4* (to 1.3-fold in both time point of CBSV infections in addition to 7.5- and 1.7-fold in ACMV). In addition, gene encoding CK degrading enzyme such as *CKX* was also differentially regulated, was shown to be induced in some samples (1.4-fold induction at 12 and 19dpi of CBSV infection in addition to 2.5-fold in ACMV infection at 12dpi), however repressed in others (to 0.7-fold in ACMV at 19dpi, 0.5-fold and 0.3-fold of CBSV and ACMV infections at 6dpi).

Genes belonging to auxin pathway also shown to be involved during infection progression, more significantly in infected samples with ACMV. Our experiment showed the suppression of *ILR1* at 6dpi (to 0.9-fold and 0.3-fold in CBSV and ACMV infection) then induction at both 12dpi (to 2.1- and 20.7-fold in CBSV and ACMV infection), and 19dpi (to 1.6- and 4.2-fold in CBSV and ACMV infection). The other gene *IAA* was suppressed at 6dpi (to 0.6-fold and 0.2-fold in CBSV and ACMV infection) then induced at 12dpi (to 1.15- and 3.1-fold in CBSV and ACMV infection), and 19dpi (to 1.3- and 1.4-fold in CBSV and ACMV infection)

The transcript level of genes belonging to Et pathway such as *ERF1* was differently altered at 6dpi (induced to 1.1-fold in CBSV and repressed to 0.7-fold in ACMV), induced at 12dpi (to 1.6- and 3.8-fold in CBSV and ACMV) and 19dpi (to 2.3- and 5-fold in CBSV and ACMV). In addition to *EIN2* which was suppressed at 6dpi (to 0.6- and 0.2-fold), diverse at 12dpi (declined to 0.6-fold in CBSV and increased to 1.7-fold in ACMV infection) and at 19dpi (increased to 1.2-fold in CBSV and decreased to 0.16-fold in ACMV infection).

The RNA level of genes belonging to BR pathways such as *BZR1_2* declined at 6dpi (to 0.6- and 0.4-fold in CBSV and ACMV infections), increased at 12dpi (to 1.3- and 10-fold in CBSV infection and ACMV infection), and then differently altered at 19dpi (slightly declined to 0.8-fold in CBSV infection and slightly induced to 1.6-fold in ACMV

infection). The other gene *BRI1* was similarly repressed at 6dpi (to 0.4- and 0.3-fold in CBSV and ACMV infections), then differently responded at 12dpi (almost unchanged in CBSV and enhanced to 9.6-fold in ACMV infection), followed by slight induction at 19dpi (to 1.6- and 2.3-fold in CBSV and ACMV infection).

Moreover, the differentially expression level of group of genes involved in ROS scavenging and oxidative burst processes was confirmed; at 6dpi suppressed genes such as DNA repair/transcription protein *MET18/MMS19* (0.48- and 0.26-fold in CBSV and ACMV infection) and *NOA1* (to 0.3- and 0.4-fold in CBSV and ACMV infection), like *NTF6* (suppressed to 0.7-fold in CBSV and induced to 1.18-fold in ACMV infection), and *SIPK* (repressed to 0.8-fold in ACMV and induced to 1.5-fold in CBSV infection) were determined. Additionally, other genes were shown to be induced at 6dpi, such as *MEK2* (to 491- and 251-fold in CBSV and ACMV), and at 12dpi like *WIPK* (to 5.2- and 46.8-fold), also at 19dpi by *RBOHA/B* (to 2- and 10.8-fold) and *NTF4* (to 1.9- and 4-fold).

The genes mediating the carbohydrate metabolism, were shown to be differentially regulated, including 4-coumarate/CoA ligase at 6dpi was up-regulated to 2-fold in CBSV infection and down-regulated to 0.8-fold in ACMV infection. Later at 12dpi enhanced to 1.5- and 28.4-fold, then in the late stage at 19dpi to 1.8- and 7.8-fold in CBSV and ACMV infections. Expression of *bglB*/beta-glucosidase was suppressed at 6dpi (to 0.7- and 0.6-fold), then induced at 12dpi (to 1.2- and 3.6-fold) and 19dpi (1.7- and 2.7-fold). Intriguingly, transcript level of basic endochitinase B/*CHIB* was dramatically increased at 6dpi (to 814- and 55.6-fold), 12dpi (to 15- and 1990-fold) and 19dpi (to 39.5- and 354-fold).

Among the genes involved in ubiquitin proteasome system, E3 ubiquitin-protein ligase COP1/E3 ubiquitin-protein ligase *RFWD2***,** from *WD40* repeat-like superfamily protein, was also down-regulated only in CBSV infection at 6dpi (to 0.06-fold), then induced at 12dpi (to 1.4- and 7.7-fold) and 19dpi (to 2.6- and 2.9-fold). In addition, E3 ubiquitin-protein ligase *RHF* was suppressed in all the samples that reached to 0.04-fold in CBSV at 6dpi, 0.6-fold at 12dpi of both viral infections, 0.6- and 0.4-fold at 19dpi of CBSV and ACMV infections. Additionally, ubiquitin-ligase /*BARD1* which was first repressed to 0.4-fold in CBSV infection but highly induced to 39.8-fold in ACMV infection, and then at 12dpi expressed to 0.9- and 3.7-fold, followed by 1.3- and 1.5-fold at 19dpi. On

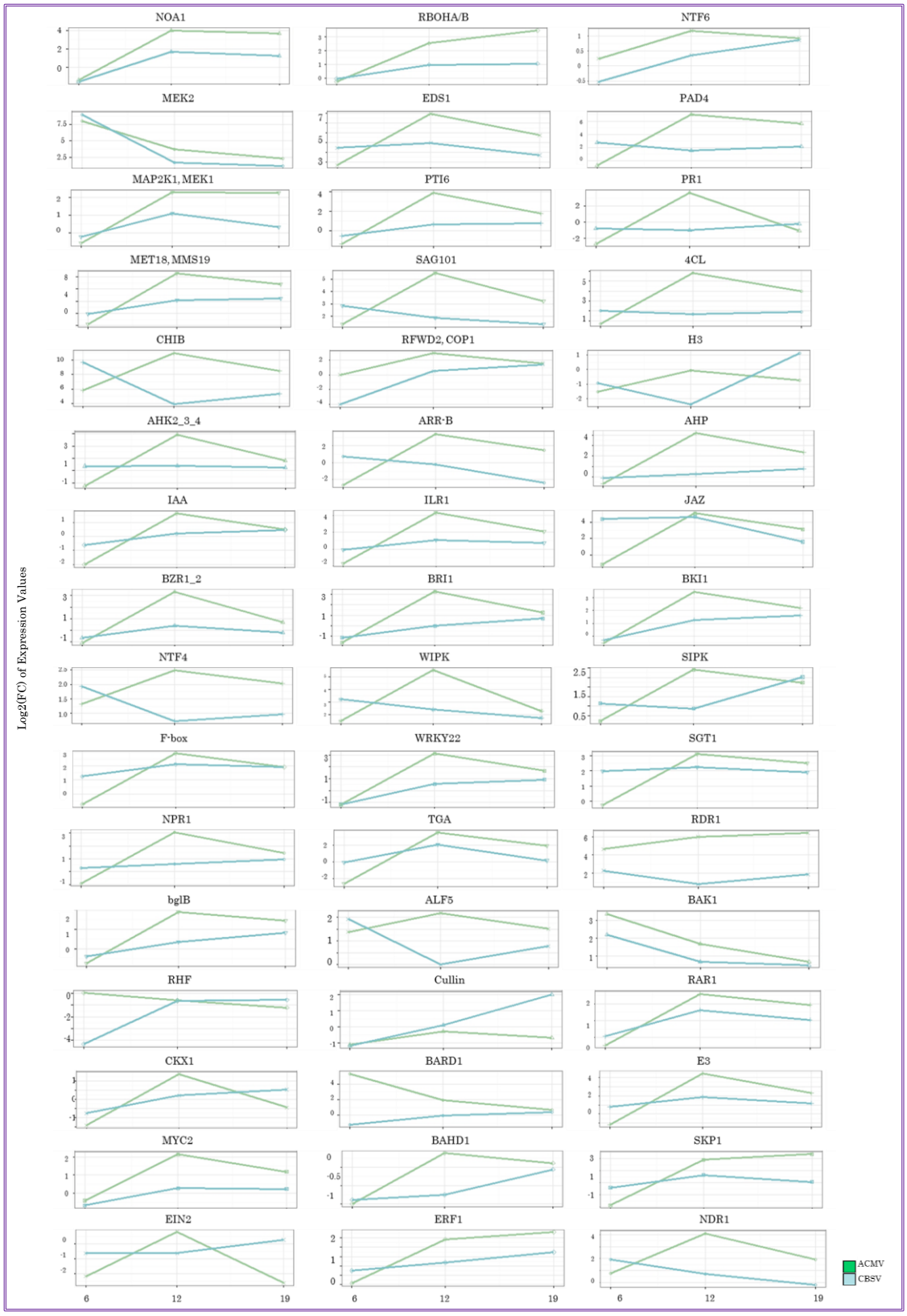

Figure 14. qRT-PCR of genes involved in key pathways, confirming the RNA-Seq data; Expression patterns of selected *N. benthamiana* genes in response to CBSV (blue) and ACMV (green) infection, as determined by qRT-PCR. The x-axis shows the time point of infection. The y-axis shows the log2FC-change of expression levels of the transcripts. Normalization of expression was performed using the L23 gene as the reference. Ct cycles versus cDNA concentration input were plotted to calculate the slope (mean ± SD; n = 3). The corresponding Real-Time PCR efficiencies were calculated according to the equation: $E = 10^{[-1/\text{slope}]}$ (Rasmussen R 2001).

the other hand, *Cullin* was suppressed in all the CBSV and ACMV samples (equally to 0.4-fold at 6dpi and only 0.8-fold in ACMV infection), except at 19dpi of CBSV infection was 3.9-fold enhanced.

Taken together, induction of the selected genes was the highest at 12dpi in the plants infected with ACMV, whereas at 6dpi most of the analysed genes are moderately regulated. However we showed the significant regulation of minority of genes, which presumably are essential for the first line of defence against virus infections. It is worth noting that most of the genes are not comparably regulated by CBSV at 12dpi to the extent of ACMV. Although, the expression level of ACMV regulated genes declined at 19dpi but stay above the expression level at 6dpi. It is therefore inferred that both DNA and RNA viruses differentially regulate the host transcriptional landscape and thus devise

3.2.3. Regression analyses of RNA-seq and qPCR results

We observed a similar coefficient of determination (R^2=0.018 in CBSV and 0.02 in the ACMV samples) of RNA-seq and qRT-PCR of various genes (Fig. 15). These results suggest the statistical similarity in calculated log2FC of gene expression between CBSV and ACMV-infected (vs. mock) plants detected by RNA-seq and qRT-PCR. The thicker confidence interval for ACMV group indicates the greater variability in the observed samples as compared to the expression data obtained from CBSV infected samples.

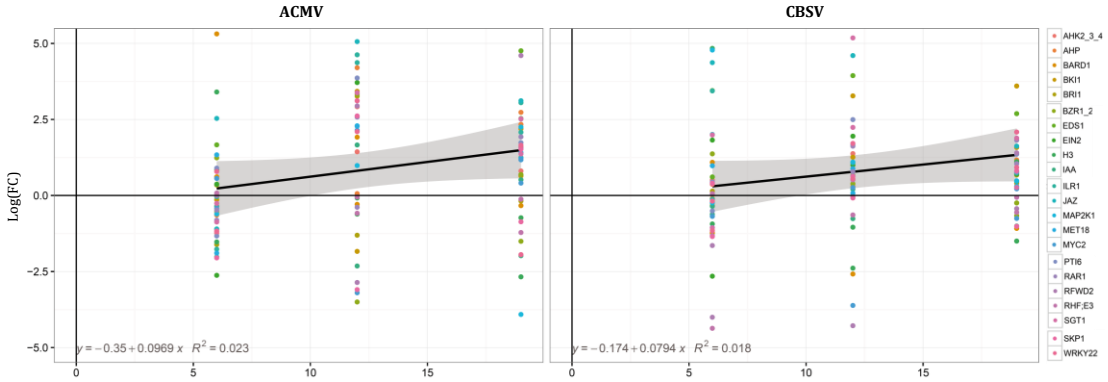

Figure 15. Linear regression model to analyse the correlation between expression values obtained from RNA-seq and qRT-PCR; The slope of regression line (R^2=0.018 in CBSV and 0.02 in the ACMV samples) indicates the positive correlation between the expression value of key pathway genes (each dot stands for one gene) obtained from RNA-seq and qRT-PCR

The results are obtained by fitting the observed values of log2FC based on the linear regression model. The independent variables of interest are the interaction of time points and two replicates (RNA-seq and qRT-PCR). To correct the p-values permutation testing was done on the above model. As presented in details in table S7, the result indicates that the coefficients of the interaction effects between replicates as well as the effect of each replicate are not significantly different from zero. However the effect of time is shown to be positive and significantly different from zero, with an average upward trend across both replicates. Thus we can conclude about the positive correlation of the overall log2FC values across RNA-seq and qRT-PCR.

Overall comparing across both groups CBSV and ACMV, the similarity of log2FC across these groups, lead us to conclude about overlapping confidence intervals and similar trend values between two approached for expression pattern analysis.

3.2.4. Hierarchical cluster analyses of qRT-PCR results

According to the log2FC of expression values of selected genes obtained from qRT-PCR and matrix clustering, we grouped these genes to analyse the closeness and distance of genes in response to infection progression of CBSV and ACMV in *N. benthamiana*.

At 6dpi the expression level of some genes were observed to be induced in response to both viral infections, such as *MEK2* (491 and 251-fold in CBSV and ACMV respectively), *CHIB* (814.4 and 55.6-fold in CBSV and ACMV respectively), *RDR1* (4.8 and 24.6-fold in CBSV and ACMV respectively) and *BAK1* (4.5 and 10.4-fold in CBSV and ACMV respectively). Moreover, the transcript content of some genes was suppressed, such as *Cullin* which was decreased to 0.4-fold in response to infection with CBSV and ACMV, similar to *NOA1* (to 0.35- and -0.40-fold), *PR1* (to 0.5- and 0.15-fold), *TGA* (to 0.9- and 0.15-fold), *EIN2* (to 0.6- and 0.2-fold) and *IAA* (to 0.6- and 0.2-fold), *BRI1* (to 0.45- and 0.33-fold).

CBSV infection at 6dpi declined the expression of *RHF* (0.05-fold), *RFWD2/COP1* (0.06-fold), *NOA1* (0.3-fold), *BARD1*, *Cullin*, *WRKY22* and *BRI1* (0.4-fold), likewise *MET18/MMS19*, *BAHD1*, *PR1*, *H3* and *CKX1* (0.5-fold), together with *MYC2*, *BZR1_2*, *EIN2* and *IAA* (0.6-fold), in addition to *NTF6*, *PTI6*, *bglB* and *BKI1* (0.7-fold) *MAP2K1/MEK1* (0.8-fold). Moreover, this stage of infection caused the overexpression of many genes, such as *CHIB* (814.47-fold), *MEK2* (491-fold), *JAZ* (20.7-fold), *EDS1* (10.9-fold), *WIPK* (9.2-fold), *SAG101* (7.17-fold), *PAD4* (6.8-fold), *RDR1* (4.8-fold), *BAK1* (4.5-fold), *SGT1* (3.9-fold).

On the other hand ACMV caused more notable reduction in transcriptome level of *PR1* (0.15-fold), *TGA* (0.16-fold), *ARR-B* (0.16-fold), *EIN2* (0.22-fold), *IAA* (0.25-fold), *MET18/MMS19* (0.27-fold), *ILR1* (0.29-fold), *H3* (0.35-fold), *CKX1* (0.37-fold), *PTI6* (0.40-fold), *AHK2_3_4* (0.42-fold), *WRKY22* (0.44-fold), *E3* (0.45-fold), *BZR1_2* (0.46-fold), *JAZ* (0.47-fold), *BAHD1* (0.50-fold), *SKP1* (0.55-fold), *PAD4* (0.6-fold), *RAR1* (0.72-fold), *SGT1* (0.83-fold). The detailed clustered genes are plotted in Figure 16a.

In CBSV infected samples, at 12dpi the most suppressed genes were *H3* (0.19-fold), *PR1* (0.5-fold), *BAHD1* (0.6-fold), *RHF* (0.64-fold), *EIN2* (0.65-fold), *ARR-B* (0.8-fold) and *BARD1* (0.9-fold) which are clustered together in the dendrogram. On the other hand the induced genes such as *JAZ* (24.3-fold), *EDS1* (to 15.4-fold), *CHIB* (to 15-fold), *WIPK* (5.2-fold), in addition to *SGT1* (4.7-fold), *F-box* and *TGA* (4.3-fold).

In the plants infected with ACMV our analysis revealed up-regulation of many genes including *CHIB* (1990-fold), *PAD4* (130-fold), *EDS1* (124.9-fold), *RDR1* (63-fold), *WIPK* (46.8-fold), *SAG101* (46.2-fold), *JAZ* (to 33.4-fold), *4CL*;CoA ligase (28.4-fold), *E3* (21.5-fold), *ILR1* (20.7-fold), *AHP* (18.4-fold), *NDR1* (17.3-fold), *NOA1* (15.8-fold), *PTI6* (14.5-fold), *MEK2* (13.7-fold), *PR1* (12.7-fold), *TGA* (11.6-fold), *BKI1* (10.7-fold),

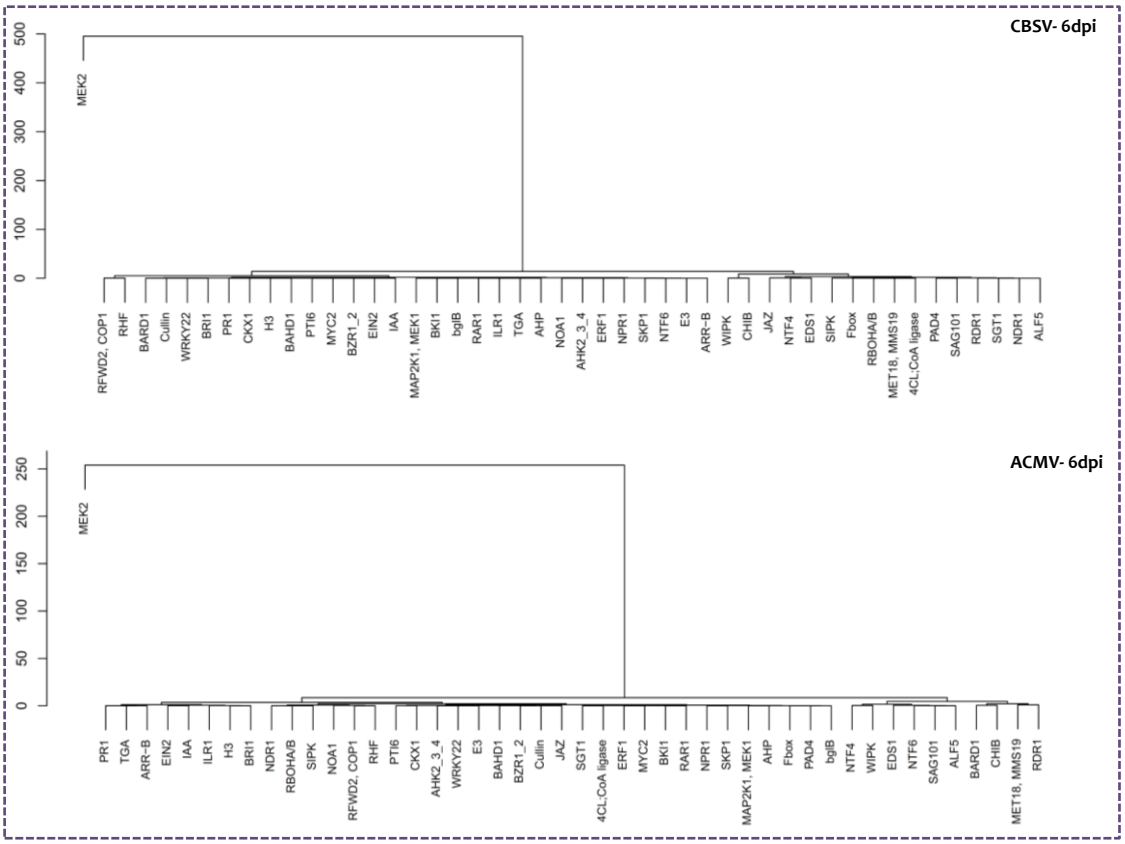

Figure 16a. Clustering of qRT-PCR results of genes involved in key pathways, at 6dpi

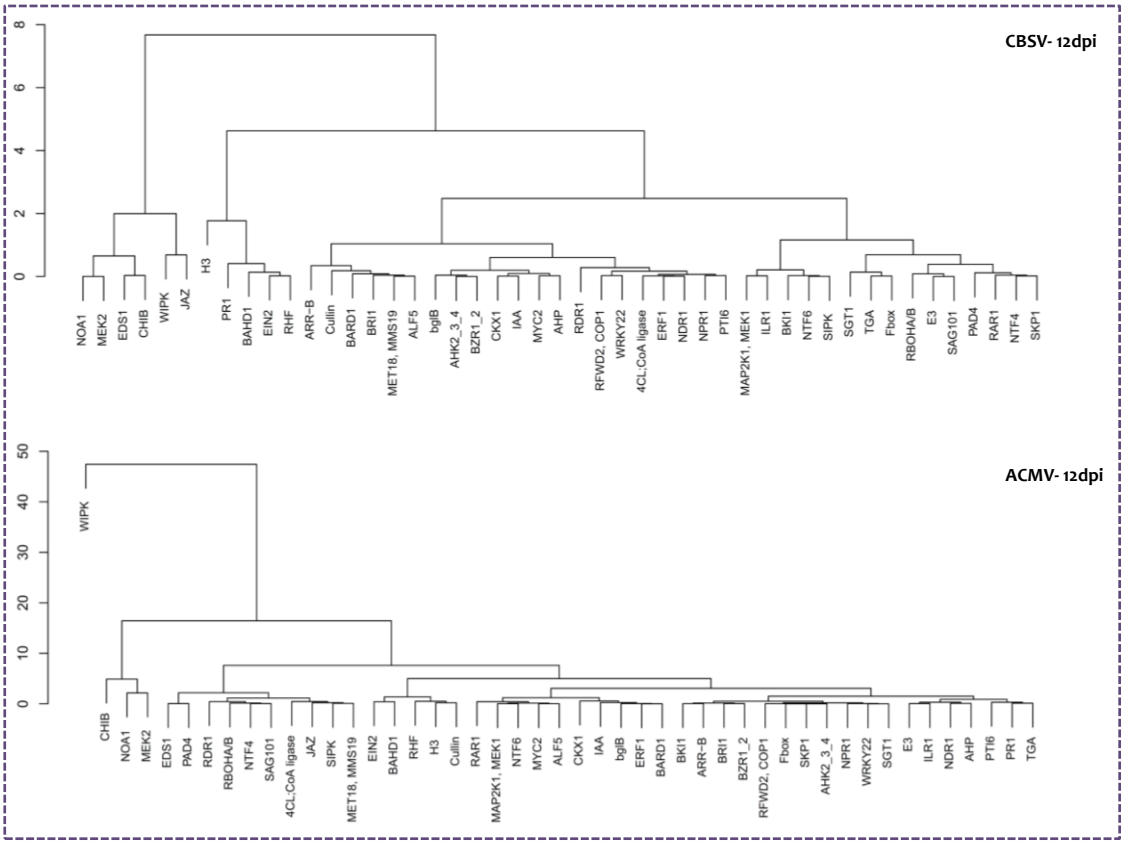

Figure 16b. Clustering of qRT-PCR results of genes involved in key pathways, at 12dpi

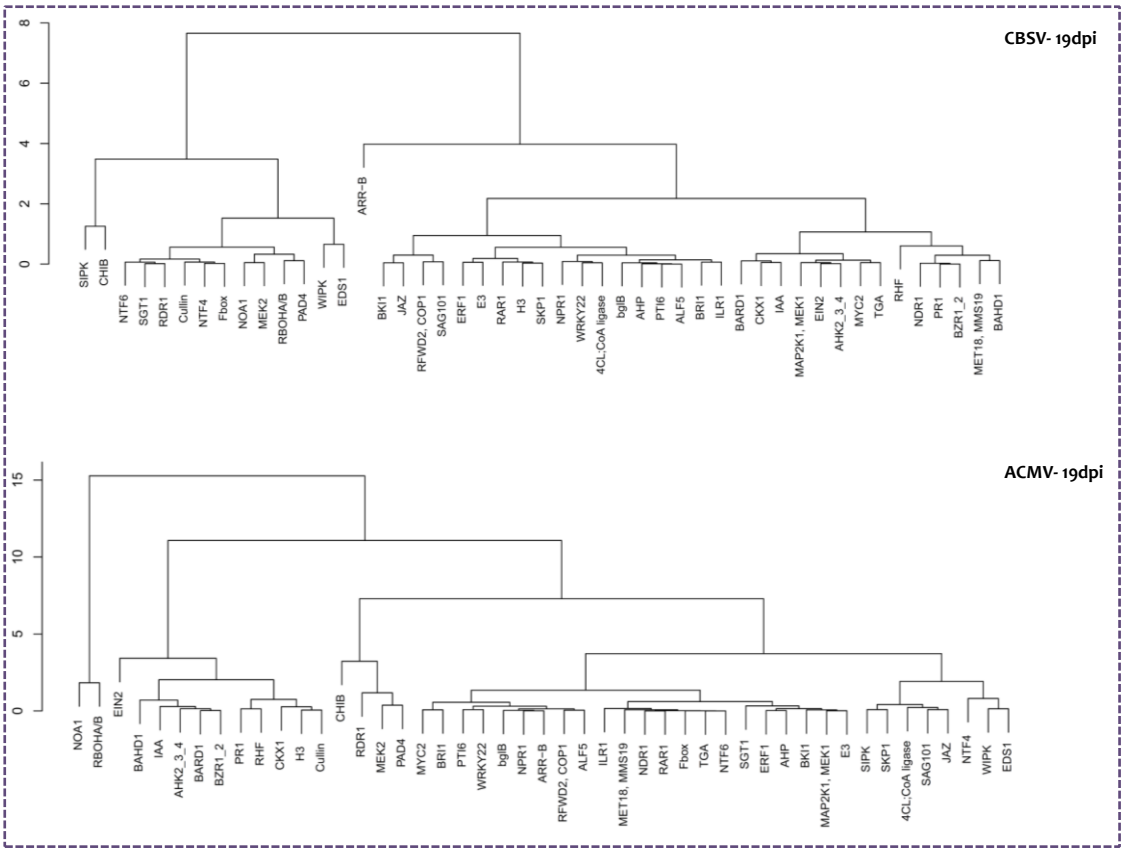

Figure 16c. Clustering of qRT-PCR results of genes involved in key pathways, at 19dpi

WRKY22 (8.7-fold), *SGT1* (8.6-fold), *F-box* (7.5-fold), *SIPK* (5.2-fold), beside of the suppressed genes including *RHF* (0.6-fold), *Cullin* (0.8-fold) and *H3* (to 0.9-fold). The detailed clustered genes are plotted in Figure 16b.

The late stage of infection at 19dpi of ACMV showed down-regulation of *EIN2* (0.16-fold), *RHF* (0.43-fold), *PR1* (0.47-fold), *H3* and *Cullin* (0.6-fold), and *CKX1* (0.7-fold) genes which were modified in transcript level. On the other hand, at this stage high up-regulation of other genes such as *CHIB* (354.4-fold), *RDR1* (85.4-fold), *PAD4* (48.9-fold), *EDS1* (27-fold), *NOA1* (12.7-fold), *RBOHA/B* (10.8-fold), *SKP1* (10.5-fold), *SAG101* (9.2-fold), *JAZ* (8.7-fold), *4CL*;4-coumarate/CoA ligase(7.9-fold), *SGT1* (5.7-fold), *MEK2* (5.2-fold), *AHP* (5.1-fold), *ERF1* (5-fold) were observed compared with mock. Among the overexpressed genes due to infection with CBSV, at 19dpi *CHIB* (39.5-fold), *EDS1* (6.46-fold), *PAD4* (4.5-fold), *SIPK* (4-fold), *Cullin* (3.97-fold), F-box (3.8-fold), *SGT1* (3.7-fold), *RDR1* (3.66-fold), *WIPK* (3.35-fold), *JAZ* (3-fold), *BKI1* (3-fold) are shown to be categorized closely, similar to the suppressed gene *ARR-B* (0.2-fold), *RHF* (0.68-fold), *BZR1_2*, *NDR1* and *PR1* (0.8-fold).

In other point of view, at 19dpi, *CHIB* (39- and 354-fold in CBSV and ACMV respectively), *EDS1* (6.4- and 27-fold in CBSV and ACMV respectively) and *PAD4* (4.5 and 48.8-fold in CBSV and ACMV respectively) were shown to be induced in both viral infections. In addition, the elevated transcripts represented *4CL*;CoA ligase, *AHP*, *BKI1*, *E3*, *ERF1*, *ILR1*, *JAZ*, *MEK1*, *MEK2*, *NOA1*, *NTF4*, *RBOHA/B*, *RDR1*, *SAG101*, *SGT1*, *SKP1 and WIPK* for 7.8-, 5-, 4.5-, 4.8-, 5-, 4.2-, 8.6-, 4.7-, 5.2-, 12.6-, 4-, 10.8-, 85.4-,

9.20-, 5.7-, 10.5- and 4.9-fold in response to infection with ACMV as well as only SIPK for 4-fold in CBSV infected samples. The detailed clustered genes are plotted in Figure 16c.

3.3. Viral infection progression in transgenic plants

To investigate further on acquired results from RNA-seq and qRT-PCR, we analysed the symptom development and viral load on three transgenic lines; i) a defence-related gene regulator such as *RDR1*, ii) a SA-degrading enzyme such as salicylate hydroxylase, and iii) a hypersensitive cell death and resistance mediator such as *RC3a*, was considered to study the functional biology of differentially expressed genes during viral infection progression. In this experiment, the transgenic *N. benthamiana* with malfunctioned proteins are referred as *RA4*, *NahG and RC3a.* were address the susceptibility level of these lines to RNA and/or DNA virus, relative to wild-type and mock plants. That might occur with enhanced symptoms and presumably in parallel with virus accumulation.

Moreover, we used a TRV[125]–based VIGS technique as a gene knockout system to examine the biological role of *SGT1*, *RAR1*, and *HSP90* in N-mediated resistance to CBSV/ACMV. VIGS is initiated when a plant is infected with recombinant TRV carrying an insert homologous with a host gene. Endogenous gene transcripts homologous with the VIGS vector insert are degraded by a post-transcriptional gene silencing mechanism or by co-suppression (Ratcliff F 2001). VIGS is a rapid, transient assay with the phenotype of the silenced plant mimicking a loss-of-function phenotype (Liu Y 2002). The efficiency of this system was examined by starting off with PDS knockout experiment on wild-type *N. benthamiana*. PDS is essential for the production of carotenoids that protect plants from photo-bleaching, therefore plants tissues in which PDS is inhibited turn white due to photo-bleaching. For these experiments, a 409-nucleotide cDNA fragment of PDS was cloned into pTV00 to form pTV:PDS (Ratcliff F 2001). While the MMA-buffer infiltrated plants did not exhibit any difference, plants infiltrated with these Agrobacterium *tumefaciens* (strain GV2260) containing this construct started to develop typical systemic white leaves from top also stems, axillary shoots and sepals at 7-8 days after infiltration. However even at the end of the experiment still part of these plants remained green. Figure 19a shows a progression of this process at 6, 12, 19 and 25dpi. This observation was consistent with previous reported studies. Based on these results, '6 days after infiltration' accounted as a starting point of TRV gene containing expression. Thus at this stage, in the LOF[126] experiment, the top two leaves of infiltrated plants were inoculated at this stage.

3.3.1. The response of *RA4* plants to viral infection

RDRs contribute to silencing mediated turnover of transcripts encoded by endogenous plant genes and transgenes (Hunter LJR 2013). The expression of a functional *RDR1* enhances the susceptibility of *N. benthamiana* to different viruses. This natural loss-of-function mutation on Nb*RDR1* in *N. benthamiana* might be the outcome of coevolution during a long-term host-virus interaction. This together with strong selection pressure for a fully active *RDR6*-mediated antiviral system is considered as a consequence of the

hypersensitivity of *N. benthamiana* to many viruses (Yang SJ 2004, Ying X-B 2010). Herewith comparing these mutant lines with wild-type *N. benthamiana* plants referred as *RA4*, which carry a natural dysfunctional variance of *RDR1*, considering the time series of infection process, showed mutation could result in the hypersensitivity of *N. benthamiana* to DNA and RNA viruses (Ying X-B 2010). To determine the effect of loss-of-function of *RDR1* in response to CBSV and ACMV infection progress, 80 T2 plants from received seeds were inoculated with CBSV and ACMV as well as buffer (mock) in addition to wild-types of each. Almost similar systemic chlorosis and mosaic symptoms were observed (Fig. 17a, b); although the symptom development in CBSV infection seemed to be faster in RA4 plants relative to wild-types, as they started to appear one day earlier in all infected plants and in both independent experiments. However there is no claim these wild-type plants which were used as a control to normalize the observations, contain the functional *RDR1* genes.

To elucidate whether the symptom development and higher susceptibility is detectable by measuring the accumulation of viral coat proteins, we performed the TAS-ELISA in three biological and two technical replicates in wild-type and the transgenic line, relative to mock at similar time points. These results ran counter to our initial idea of lacking the *RDR1* in *N. benthamiana* could bring higher susceptibility against RNA and Potyvirus infection, although this observation was more evident at 6dpi of infection (Fig. 18a). Interestingly, CBSV-infected-*RA4* plants increased viral load to almost the same level as the wild-type infection in later stages, which is in consistency with the qRT-PCR expression value and the steady increasing pattern in ACMV infection. In contrast, in *RA4*-ACMV samples the CP level at the early stage of infection stayed significantly lower than infected wild-type; however at mid-stage it showed higher viral accumulation towards the end to values almost equal to wild-types (Fig. 18 a-c).

3.3.2. The response of *RC3a* plants to viral infection

NbNRC3 is the casual *N. benthamiana* protein that has been shown to contribute to hypersensitive death following Pto^{127} perception of AvrPto and seems not to be required for the response elicited by Rx (Wu C-H 2015). By using the NbRC3 transgenic seeds, observing the induced hypersensitive cell death during the infection progression to RNA and DNA viruses was made. Therefore 80 T2 plants from received seeds were inoculated with CBSV and ACMV as well as buffer (mock) besides of wild-types of each. As shown in Figure 17a and b, almost similar systemic chlorosis and mosaic symptoms were observed; although it seemed that the symptom severity of CBSV infection at 12 and 19dpi was higher than wild-type appeared with stronger necrosis and chlorosis in *RC3a*-infected plants. But ELISA analyses of the wild-type and *RC3a* plants indicated that the viral load in *RC3a*-CBSV was significantly lower than WT-CBSV at12dpi (Fig. 18b) while in *RC3a*-ACMV was almost similar to the wild-type also like *RA4* plants at 6dpi was as low as the mock samples (Fig. 18a).

3.3.3. The response of *NahG* plants to viral infection

It has been shown that enhanced susceptibility of *NahG* plants exhibit to a wide range of pathogens including viruses is not due to absence of SA. As shown that several mutations with defects in SA signaling, remained resistant to pathogens such as *Psp*[128]. Moreover, the

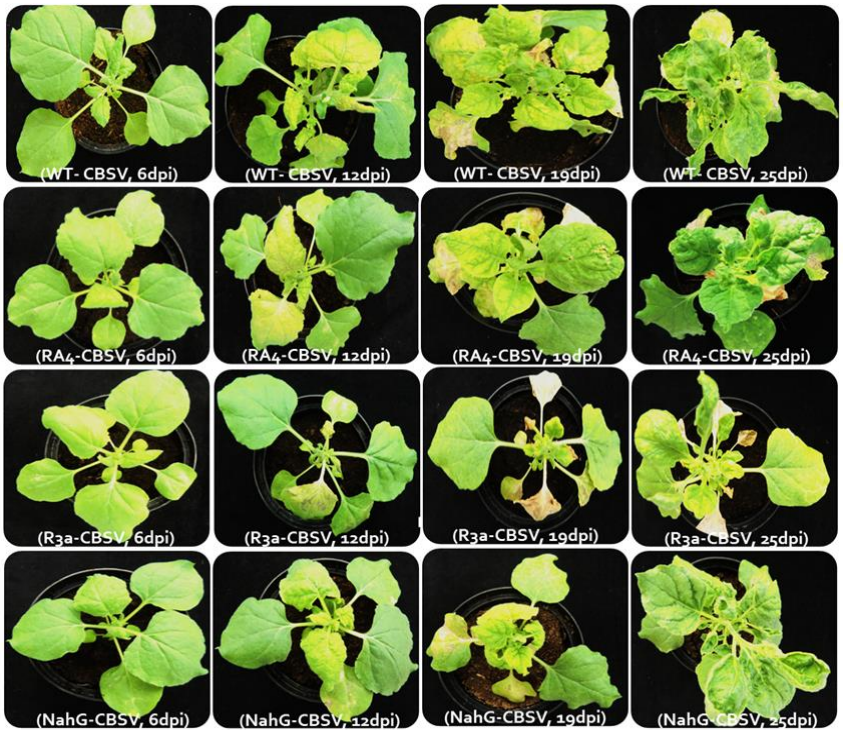

Figure 17a. The average phenotype observed in different lines in response to CBSV infection[129];Wild-type (row 1), *RA4* (row 2), *RC3a* (row3) and *NahG* (row 4) *N. benthamiana* plants infected with CBSV at 6dpi (column 1), 12dpi (column 2), 19dpi (column 3) and 25dpi (column 4).

Figure 17b. The average phenotype observed in different lines in response to ACMV infection; Wild-type (row 1), *RA4* (row 2), *RC3a* (row3) and *NahG* (row 4) *N. benthamiana* plants infected with ACMV at 6dpi (column 1), 12dpi (column 2), 19dpi (column 3) and 25dpi (column 4).

phenotypes of *NahG* plants might be direct effects of decreased SA levels, suggesting a requirement for SA in many aspects of plant defence responses, as they display greatly reduced expression of *PR* genes (Gaffney T 1993, Delaney TP 1994, Van Wees SC 2003, Takahashi H 2004, Baebler S 2014, Alazem M 2015). To examine the SA-mediated host defence effect on CBSV/ACMV systemic spread, 80 T2 plants from received *NahG* seeds were inoculated with CBSV and ACMV as well as buffer (mock) together with wild-types of each. In these plants compared with mock (Fig. 17c), the stunt phenotype was obvious similar to the wild-type infected plants. Although, there was no obvious difference in symptoms severity observed between the infected wild-type and *NahG* plants (Fig. 17a, b), the *NahG*-ACMV samples at early stage showed significantly lower viral load relative to wild-types (Fig. 18a), similar to mid-stage (Fig. 18b) and late stage (Fig. 18c). While the viral CP load at 12dpi in *NahG*-CBSV infected plants was shown to be higher than wild-types. This proves the effect of defeated SA-mediated defences on CBSV infection particularly at the establishment of infection in *N. benthamiana*.

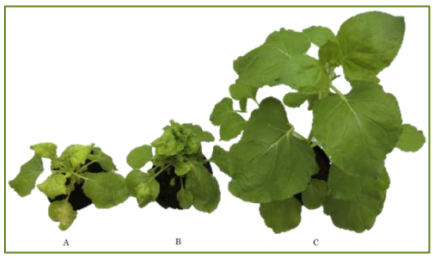

Figure 17c. Infected NahG plants with CBSV (A), ACMV (B) and mock (C), at 19dpi; The stunt infected plants compared with mock-inoculated plants, similar to the observed phenotype observed in wild-types

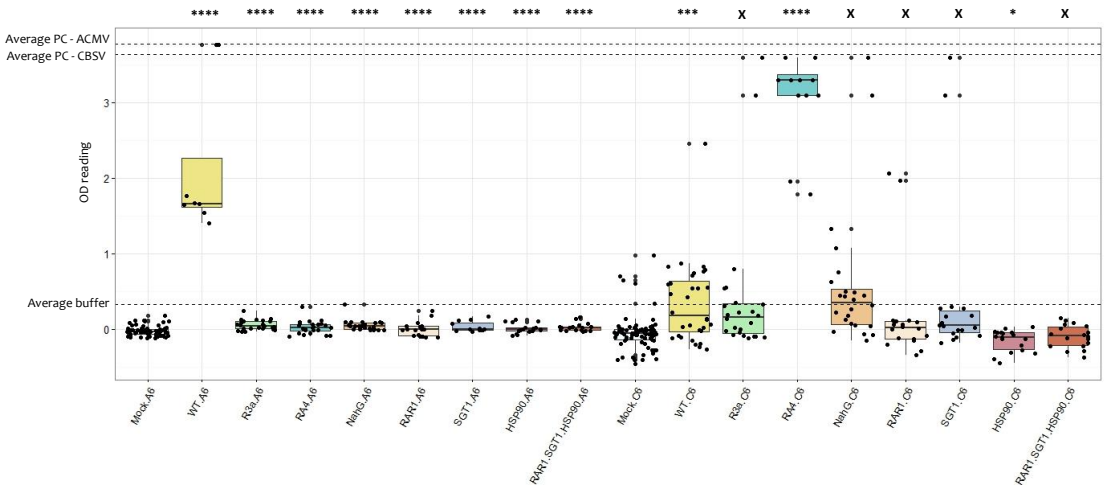

Figure 18a. The viral load of mutant/transgenic plants compared with wild-type and mock at 6dpi; The significant different CP accumulation in wild-type infected with ACMV (WT-A6) and CBSV (WT-C6) is presented relative to mock (Mock-A6 and Mock-C6). The other observations are analysed compared with wild-types of each. The average buffer-OD-reads was subtracted to normalize the reads on each plate.

3.3.4. The effect of deficient *SGT1/RAR1/HSP90* chaperone on viral infection

To assess whether the association of different *SGT1/RAR1/HSP90* components, as the R-mediated resistance moderators, play a role in RNA and DNA viral infection progression, we performed a loss-of-function study by transiently expressing these genes by using TRV-VIGS approach. This is a reverse genetics technique, in order to study the function of a gene whose knockouts lead to a lethal phenotype (Ratcliff F 2001, Liu Y 2002). First we examined the efficiency of this transformation system by observing the ability of TRV constructs to inhibit the PDS gene in *N. benthamiana* and appearing with photo-bleaching phenotype as inhibiting the PDS gene by using TRV result in white tissues in plant (Demmig-Adams B 1992, Kumagai MH 1995, Ruiz MT 1998). This bleaching phenotype as can be seen in Figure 19a, started to show up 7-8 dpa[130], so it was

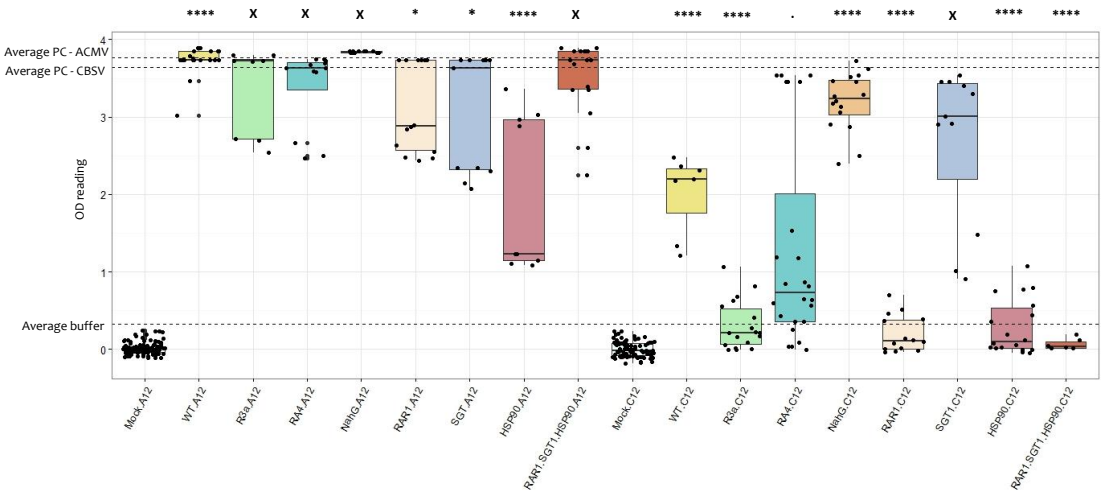

Figure 18b. The viral load of mutant/transgenic plants compared with wild-type and mock at 12dpi; The significant different CP accumulation in wild-type infected with ACMV (WT-A12) and CBSV (WT-C12) is presented relative to mock (Mock-A12 and Mock-C12). The other observations are analysed compared with wild-types of each. The average buffer-OD-reads was subtracted to normalize the reads on each plate.

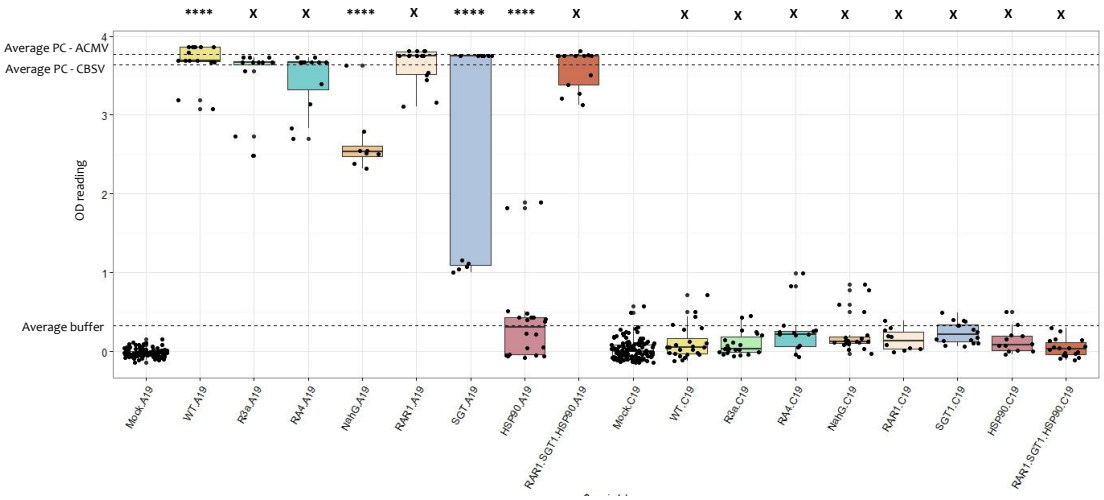

Figure 18c. The viral load of mutant/transgenic plants compared with wild-type and mock at 19dpi; The significant different CP accumulation in wild-type infected with ACMV (WT-A19) and CBSV (WT-C19) is presented relative to mock (Mock-A19 and Mock-C19). The other observations are analysed compared with wild-types of each. The average buffer-OD-reads was subtracted to normalize the reads on each plate.

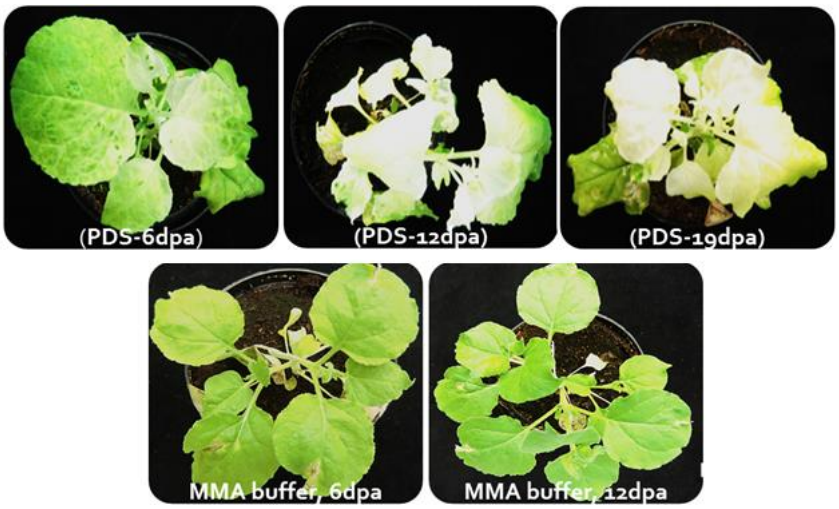

Figure 19a. PDS inhibition and viral infection progression in wild-type *N. benthamiana;* PDS-6dpa shows the clear photo-bleaching phenotypes 6 days after agro-infiltration. This stage is considered to be inoculated the infiltrated leaves with CBSV and ACMV. Typical systemic white leaves appearance was observed until 19 days after infection. The second row represents the normal developmental shape of plants after buffer-infiltration.

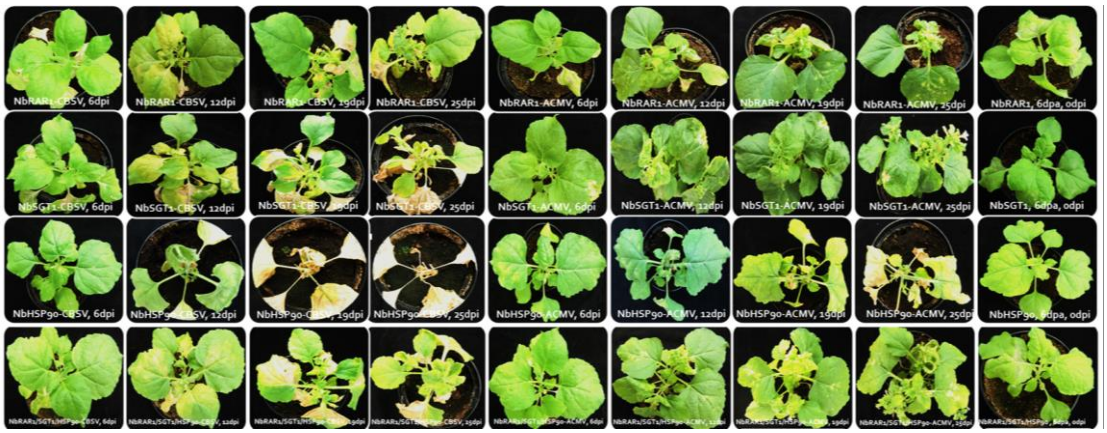

Figure 19b. The average[131] phenotype observed in different lines; Transient silenced *RAR1* (row 1), *SGT1* (row 2), *HSp90* (row 3) and *RAR1/SGT1/HSp90* (row 4) in *N. benthamiana* plants infected with CBSV and ACMV at 6dpi (column 1 and 5), 12dpi (column 2 and 6), 19dpi (column 3 and 7) and 25dpi (column 4 and 8). The last column represents the shape of the plants 6days after infiltration and 0dpi (the day they were inoculated)

decided to pick up the day 6 to inoculate the agro-infiltrated plants with viruses. The upper leaves of transiently silenced *SGT1, RAR1, HSP90* and *SGT1/RAR1/HSP90* plants were infected with CBSV or ACMV. These plants together with mock and infected wild-types were sampled at 6, 12 and 19dpi for further analyses. Then the viral load of top three leaves of these in *N. benthamiana* plants were compared with wild-types (Fig. 18 a-c).

At 6dpi, silenced *RAR1, SGT1, HSP90* and *RAR1/SGT1/HSP90* plants showed very low viral load of ACMV similar to CBSV (more significantly in HSP90 samples) in relative to the wild-types (Fig. 18a). At 12dpi, in CBSV and ACMV samples, silenced *HSP90* exhibited significant lower load of these RNA and DNA viruses relative to wild-type (Fig. 18b). It is worth to mention that *HSP90* samples, particularly in the CBSV samples, at this time point towards the end showed very severe yellow-wilting symptoms

(Fig. 19b), which could be the main reason on unpredicted ELISA outputs. Likewise the measured viral content in silenced-*RAR1* plants in response to both infections and *SGT1* in ACMV infected plants was shown to be significantly lower than wild-types.

More interestingly the mixture of *RAR1/SGT1/HSP90* silencing caused the significant decline in CBSV content in contrast with the high accumulation of ACMV as in wild-type. Similarly at 19dpi, CBSV infection appeared to be undetectable by ELISA, like all other infected samples including the wild-types which showed the same viral load as in the mock plants (Fig. 18c). On the other hand in the ACMV samples, *SGT1, RAR1* and *RAR1/SGT1/HSP90* silenced plants showed high viral load as the wild-type, whereas again HSP90 silencing caused lower load of this DNA virus.

Altogether, the components of *RAR1/SGT1/HSP90* chaperone seem to be responsive in susceptible interaction with RNA virus at mid-stage onwards. And more specifically silenced *HSP90* caused obvious PCD in infected *N. benthamiana* plants with CBSV. On the other hand infection with DNA virus was more affected in these silenced plants at the late stage (19dpi), where increment loads of ACMV were measured, but perhaps it occurred due to limited sensitivity of ELISA.

3.4. ROS-scavenging systems assessment

3.4.1. DAB staining

The DAB staining method was applied to detect putative changes in H_2O_2 distribution in the infected wild-type and transgenic *N. benthamiana* relative to mock during the infection progression. DAB taken up enables us to detect H_2O_2 in the detached infected leaves, indicating the cells undergoing HR, where proteins are cross-linked by H_2O_2 (Thordal-Christensen H 1997, Talarczyk A 2002). Leaves inoculated with CBSV, ACMV and buffer were collected 6, 12 and 19dpi and then DAB stained to detect areas of tissues subcellular localizations and concentrations of hydrogen peroxidases and catalases.

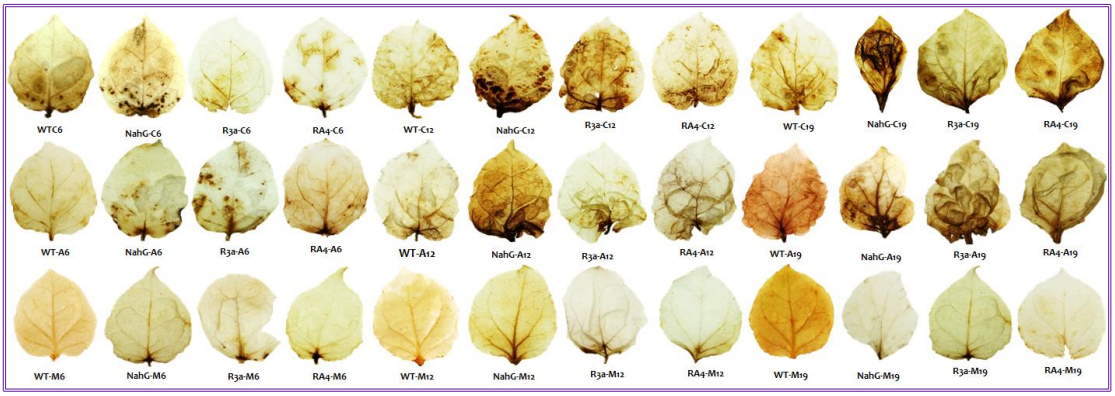

Figure 20. Oxidative activity assay (DAB staining); First row show the infection with CBSV at 6dpi (first four leaves, indicated with C6), 12dpi (second four leaves, indicated with C12), 19dpi (third four leaves, indicated with C19)- second row show the infection with ACMV at 6dpi (first four leaves, indicated with A6), 12dpi (second four leaves, indicated with A12), 19dpi (third four leaves, indicated with A19)- third row show the mock samples at 6dpi (first four leaves, indicated with M6), 12dpi (second four leaves, indicated with M12), 19dpi (third four leaves, indicated with M19); the H_2O_2 concentration was evident to be increasing in the course of time in wild-type plants relative to mock, also in transgenic plants compared to wild-types.

Reddish-brown pigments were observable at sites of the enzyme activity due to instant and local DAB polymerization.

As shown in Figure 20, infected wild-type plants exhibited distinct brown rings compared to mock, at all time points. The highest DAB-uptake was observed in CBSV and ACMV samples at 12dpi, followed by 19dpi and 6dpi. Somehow in the CBSV samples more sever lesions were evident, while mostly in neither of mock plants any pigments were observed. The indicated presence of high concentration of H_2O_2 was more evident in *NahG* transgenic plants, *RC3a* and *RA4* plants, which partially negates the defence response of *N. benthamiana* to CBSV and ACMV. At all the studied time points, a stronger ROS activity in these transgenic plants relative to wild-type, particularly at *NahG*-CBSV infected plants at 19dpi, was observed.

3.4.2. Expression of ROS-scavenging involved genes during infection progression

The aim of this analysis is to gain further knowledge on the AOS[132] accumulation level during the viral pathogenesis progression. Analyses of oxidative stress biomarkers and quantification of ROS-scavenging capacity in infected wild-type and transgenic *N. benthamiana* plants with CBSV and ACMV compared with their mock were carried out at three times post-infection (6, 12, 19dpi). We detected the increased elicited antioxidant responses by ACMV and CBSV infection, also in wild-types. Additionally, its association with expression pattern of number of ROS-scavenging enzymes and alternative respiratory pathway such as *WIPK*[133], *SIPK*[134], *RBOH*[135]*A/B*, *NTF4*, *NTF6* and *NOA1* genes measured by qRT-PCR, which are shown before in Figure 14.

Relative to mock, the represented RNA level of *WIPK* was counted as 9.2-, 5.2-, 3.3-fold in CBSV and 2.8-, 46.8-, 4.9-fold in ACMV at 6, 12 and 19dpi. Moreover, *SIPK* 1.55-, 1.2-, 4-fold in CBSV and 0.8-, 5.2-, 3.3-fold in ACMV were expressed. *RBOHA/B* and *NOA1* exhibited the suppressed expression at 6dpi in CBSV and ACMV infection, followed by enhanced values at 12 and 19dpi; the RNA level of RBOHA/B in infection with CBSV was up to 1.9- and 2-fold also in ACMV up to 5.7- and 10.8-fold, while *NOA1* up to 3.3-, 2.3-fold in CBSV and 15.8- and 12.6-fold in ACMV infection at 12 and 19dpi, respectively. *NTF4* and *NTF6* were also differentially regulated during infection progression of CBSV and ACMV; *NTF4* showed 3.8-, 1.6-, 1.9-fold in CBSV infection and 2.5-, 5.6-, 4-fold in ACMV infection at 6, 12 and 19dpi, and represented expression values of *NTF6* were 0.7-, 1.2-, 1.8- and 1.18-, 2.2- and 1.9-fold.

3.4.3. Superoxide activities between PPD[136] in cassava and viral infection in *N. benthamiana*

Infections with CBSV and ACMV, both cause notable losses in cassava production, especially in tubers. Here we aimed at correlating the superoxide activities in cassava roots and *N. benthamiana* leaves during PPD and viral infection. The expression level of reported oxidase, peroxidase, catalase, reductase and dehydrogenase enzymes in a recent study (Vanderschurena H 2014) was used to detect their orthologues and calculate the average expression values[137], which is shown in Table 3. According to our RNA-seq data, and comparing the infected plants with mock, the transcript level of peroxidase and

catalase decreased at 6dpi, and then increased at 12 and 19dpi. While glutathione peroxidase, L-ascorbate peroxidase, peroxiredoxin and monodehydroascorbate reductase were down-regulated during the whole infection progression, in contrast with respiratory burst oxidase.

In addition, it is noteworthy that *α-DOX1*[138] (cassava4.1_003891m and NbS00012114g0006), a fatty acid dioxygenase catalysing the primary oxygenation of fatty acids (De León IP 2002), was more than 64- and 32-fold up-regulated in CBSV and ACMV (as shown in Table S8). Up-regulation of this enzyme at 12 and 19dpi might be indicative of fatty acid degradation through α-oxidation, as it was evident in PPD progression as well (Vanderschurena H 2014). Expression of this gene is dependent on both JA and ethylene pathways and was also slightly down-regulated in the *NahG* plants, which has been shown to also have a role in oxylipin production protecting plants from oxidative stress and cell death (De León IP 2002). The expression of the *alpha-DOX1* gene require the presence of the SA pathway, which probably leads to JA and other oxylipin biosynthesis was shown to be declined in the absence of JA and ethylene signals and this may indicate a feedback control of this signaling pathway (Buchanan-Wollaston V 2005). As it was shown in MS profiling results the amount of SA in the ACMV sample at 19dpi is much higher than CBSV that is totally consistent with the expression of the fatty acid dioxygenase activity during infection progression of CBSV and ACMV.

	CBSV-6dpi	ACMV-6dpi	CBSV-12dpi	ACMV.12dpi	CBSV-19dpi	ACMV.19dpi
Peroxidase	0.83	0.98	1.76	1.16	1.60	1.29
Glutathione peroxidase	0.90	0.86	0.79	0.70	0.80	0.82
L-ascorbate peroxidase	0.88	0.84	0.80	0.72	0.90	0.76
Peroxiredoxin	0.88	0.81	0.67	0.65	0.68	0.47
Catalase	0.85	0.87	1.55	1.37	1.85	1.73
Monodehydroascorbate reductase	0.82	0.78	0.89	0.81	0.96	0.88
Respiratory burst oxidase	1.05	1.11	1.56	1.40	1.53	1.34

Table 3. The expression level of the selected genes according to RNA-seq analyses; The transcript level of peroxidase and catalase decreased at 6dpi, then increased at 12 and 19dpi, while glutathione peroxidase, L-ascorbate peroxidase, peroxiredoxin and monodehydroascorbate reductase were down-regulated during the whole infection progression, in contrast with respiratory burst oxidase.

3.5. Metabolite measurement by HPLC-MS and HPLC-UV/Vis

Here, systems-level experimental approaches such as metabolomics are applied to decipher the pathogen–host nutritional interactions, in phytohormones, sugars, amino acids and flavonoids levels. This study indicates that viral replication within specific cells initiates a series of metabolic events over several days, following infection.

3.5.1. Viral infection and phytohormones biosynthesis and signaling

Viral infection significantly altered phytohormones metabolism. which have long been known for their roles as response regulating elements during biotic stresses, such as SA, JA and Et are involved in defence pathways, by exhibiting antagonistic inter-relations (Alazem M 2015). RNA and DNA viruses typically activate the antagonistic SA/JA cooperating pathway, although depending on the snapshot time point of disease progress, might be in different level. As shown in Figure 21a, at early stage of our observation,

6dpi, salicylic acid was declined in both ACMV and CBSV infected leaves, compared to mock, while ACMV infected plants had significantly increased JA and OH-JA. At 12dpi, the SA accumulation was enhanced in CBSV and ACMV infected plants, whereas CBSV infection decreased the JA level. The last step of our observation identified that SA in ACMV infected plants and JA in the CBSV samples were significantly increased.

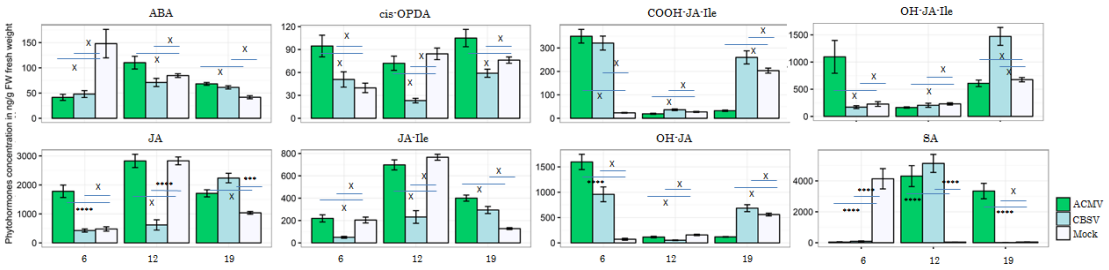

Figure 21a. Hormone–virus inter-relations: general effects of hormones on plant defence against viruses; Amongst, SA, JA and OH-JA showed significant alteration at least in one of observations (The data obtained from two experimental repetition and measurement of six technical replicates)

3.5.2. Viral infection and carbohydrates metabolism

Sugars such as glucose, fructose, and sucrose are recognized as signaling molecules in plants, in addition to their typical roles as carbon and energy sources (Rolland F 2006, Bolouri Moghaddam MR 2012). Viral infection significantly changed carbohydrate metabolism that could be associated with starch content alteration. The inhibition of starch accumulation and/or starch degradation is probably due to the increased demand for soluble sugars (mainly glucose) required for maintaining the high respiration rate (Shalitin D 2000). Our carbohydrate profiling demonstrated that before symptoms appearance on *N. benthamiana* leaves the defeated defence system accompanied by the dropped level of carbohydrates content. Subsequently, decline in fructose, glucose and sucrose contents were observed at early stage of infection (6dpi) (Figure 21b).

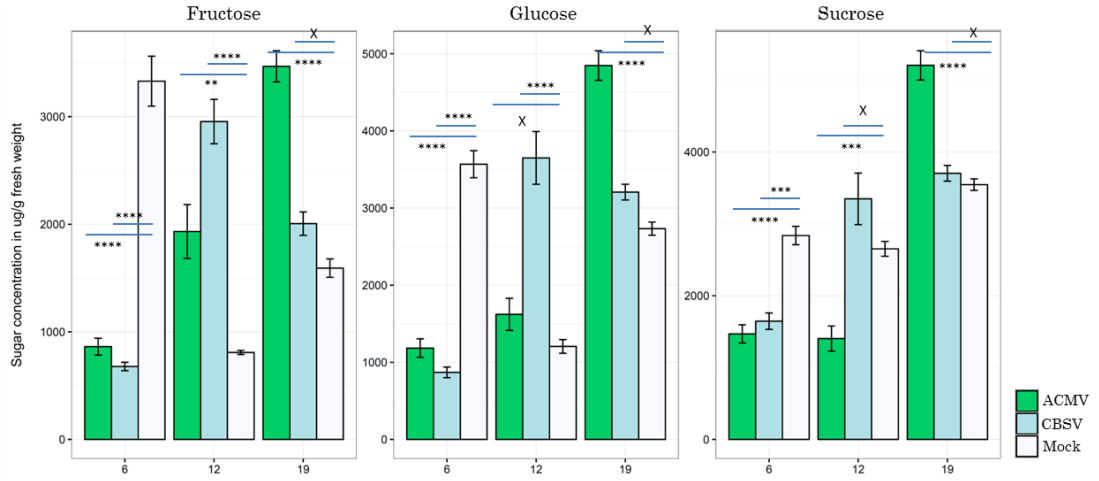

Figure 21b. Sugar–virus inter-relations: general effects of sugars on plant defence against virusesAmongst, Fructose, Glucose and Sucrose showed significant alteration during CBSV and ACMV infection progression (The data obtained from one experimental repetition and measurement of six technical replicates)

Infected leaves with CBSV at 12dpi showed a sharp increase in the concentrations of fructose and glucose, while ACMV infection significantly decreased sucrose and increased fructose. Although, the infection progression incorporates with less fixed carbon into structural carbohydrates also with more into soluble sugars, this detailed analyses in *N. benthamiana* plants addressed that at 19dpi of infection progression infection with ACMV caused notable induction in fructose, glucose and sucrose loads. Here, we can determine the relationships between viral accumulation, entity of virus, sugars/starch content, carbon fixation and energy metabolism.

3.5.3. Viral infection and amino acid biosynthesis and signaling

Amino acid catabolism is essential for the conservation of nitrogen and for maintaining physiologic concentration of amino acids, and represents an important strategy that can be successfully exploited by pathogens for conquest of their host. Each degradative pathway is characterized by a rate-limiting enzyme, whose expression is normally subjected to strict regulation. In higher organisms, catabolism of most amino acids normally occurs due to the infection, with the exception of branched-chain amino acids (leucine, isoleucine and valine) (Grohmann U 2010), which interestingly in our amino acid profiling were not identified as significantly altered. In general, viral infection significantly altered amino acids metabolism; Infected leaves with CBSV and ACMV at 6dpi, showed a sharp decline in the concentrations of alanine, serine, proline, glutamine, however at next stage of infection (12dpi) glutamine had notable increase in CBSV and ACMV infection as well as asparagine in the ACMV samples. At 19dpi, the glutamine level stayed high in CBSV and ACMV infected plants, compared to mock; as did proline in CBSV infected leaves. The presented results in Figure 21c are from the second replicate of experiment, because in the merged data from two repetitions, only glutamine was shown to be significantly decreased at 6dpi and increased at 12 and 19dpi. These alterations might imply the existence of critical enzymes which are involved in regulating the various metabolic processes as an opportunity for targeted intervention aimed at relieving the negative effects on the immune system (Grohmann U 2010).

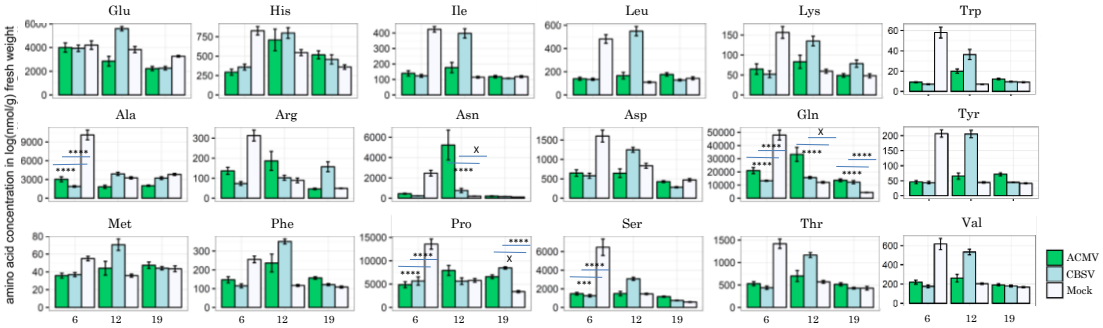

Figure 21c. Plant amino acids–virus inter-relationsgeneral effects of amino acids on plant defence against viruses; Amongst, Alanine, Asparagine, Glutamine, Proline and Serine showed significant alteration during CBSV and ACMV infection progression (The data obtained from one experimental repetition and measurement of six technical replicates)

3.5.4. Viral infection and caffeoyl ester biosynthesis and signaling

As shown in Figure 21d, among the measured caffeoyl quinate esters, accumulation of trans-4-caffeoylquinic acid and trans-5-caffeoylquinic acid was inhibited at 6dpi infected ACMV and CBSV. While at 12dpi, only trans-5-caffeoylquinic acid was significantly enhanced due to CBSV infection, both trans-5-caffeoylquinic acid and trans-4-caffeoylquinic acid were notably increased in CBSV and ACMV samples at 19dpi.

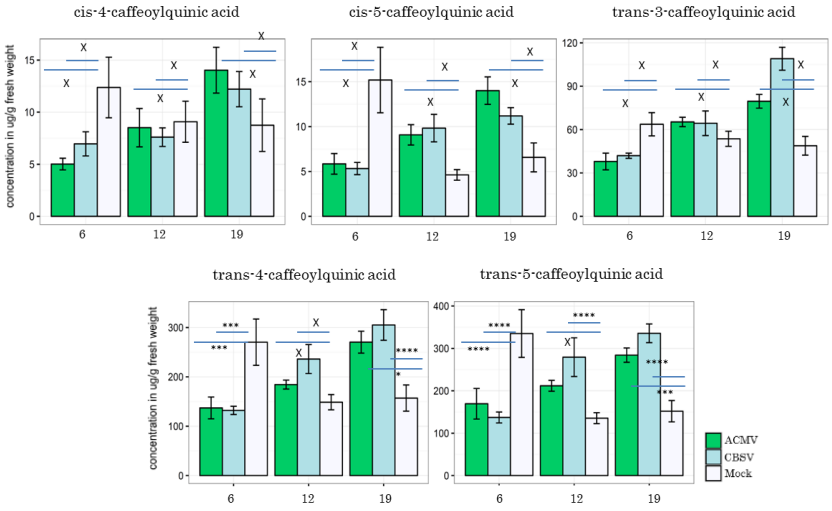

Figure 21d. Caffeoyl quinate–virus inter-relations: general effects of phenolic on plant defence against viruses; Amongst, trans-4-caffeoylquinic and trans-5-caffeoylquinic acids showed significant alteration at least in one of observations (The data obtained from two experimental repetition and measurement of six technical replicates)

3.6. Flux profiling and enzyme activities simulation during viral infection progress

Hereby applying several bioinformatics tools such as Metatool and YANAsquare we calculated the flux distribution and simulated the enzyme activities, hoping this large-scale metabolic flux analyses in plant systems would connect macroscopic phenomena such as leaf senescence, chlorosis and necrosis to intracellular metabolic fluxes. In this way, metabolic processes underlying observed developmental failures can be better understood. This approach applies different levels of automation in Flux Balance Analyses (FBA) and Metabolic Flux Analyses (MFA) for numerically determination of optimal steady-state flux distribution in the metabolic network (Junker BH 2014).

3.6.1. Reconstruction of metabolic networks, enzymatic flux simulation of infected plants

In order to get a more complete overview from these genes expression data, we used the *Arabidopsis* supervised and targeted model of the involved pathways network[139]. We managed to identify affected enzymes which are not apparent from transcriptome data, by applying YANAsquare and a custom-made routine written in R for calculating metabolic-flux changes (Schwarz R 2007) during RNA and DNA viral infection progression. This metabolic modelling allowed us to consider all possible flux and metabolic changes of the central metabolism, including i) defence metabolites, such as salicylate and jasmonate, chorismate, shikimate and sphingolipids, ii) carbohydrates metabolism pathways such as

glycolysis, tricarboxylic cycle and pentose phosphate pathways, iii) photosynthesis as well as photorespiration, iv) transporters. Combined data indicates that both viruses interfere with many of these enzymatic activities with different significance depending on the stage of infection progression and host physiological development.

3.6.2. Modulation of metabolic pathways involved in pathogen defence during infection with CBSV and ACMV

Activity of enzymes which mediates the biosynthesis of salicylic acid in chloroplast including isochorismate-pyruvate lyase[140] [isochorPyrL_H] and isochorismate synthase[141] [isochorS_H] simulated to be declined to 12 and 15% at 12dpi in addition to 17 and 20% at 19dpi of CBSV and ACMV infection, respectively whereas they remained almost unchanged at 6dpi. Moreover, as can be seen in Figure 22a, amongst enzymes involved in sphingolipid biosynthesis in endoplasmic reticulum, activity of 3-dehydrosphinganine[142] [3dehydrosphinganineRed_ER] and serine C-palmitoyltransferase[143] [SerCpalmitoylTran_ER] showed an increase of 8% at early stage of infection with CBSV.

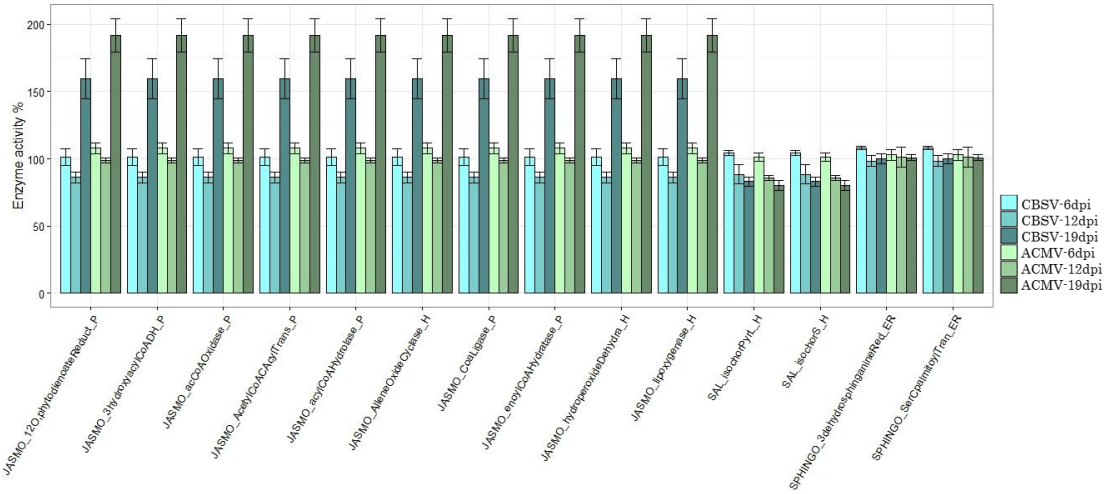

Figure 22a. Defending enzyme activity modulation during infection progression of CBSV and ACMV; Simulated activities of the enzymes in the pathways i) jasmonic acid biosynthesis (marked by the prefix "JA_"), ii) salicylic acid biosynthesis (indicated by the prefix "SAL_") at the three time points 6dpi, 12dpi and 19dpi each after the infection with the two pathogens ACMV and CBSV; Biosynthesis of salicylic and jasmonic acids modulated by mediating the defence pathways. SA biosynthesis showed reduction, JA increased especially at 12 and 19dpi, whereas sphingolipid did not undergo very notable changes. Salicylic fluxes in chloroplast through isochorismate-pyruvate lyase and isochorismate synthase were shown to be suppressed for 15 and 20% in ACMV as well as 12 and 17% in CBSV. In peroxisome jasmonate fluxes through 12-oxophytodienoate reductase, 3-hydroxyacyl-CoA dehydrogenase, acyl-CoA oxidase, acetyl-CoA C-acyltransferase, acyl-CoA hydrolase, allene oxide cyclase, CoA ligase, enoyl-CoA hydratase, hydroperoxide dehydratase, and lipoxygenase in chloroplast showed 59 and 91% induction in CBSV and ACMV infected samples at 19dpi.

At 19dpi, in peroxisomes enzymes which mediate the biosynthesis of jasmonic acid, including 12-oxophytodienoate reductase[144] [12O,phytodienoateReduct_P], 3-hydroxyacyl-CoA dehydrogenase[145] [3hydroxyacylCoADH_P], opc-8 acyl-CoA oxidase[146] [acCoAOxidase_P], acetyl-CoA C-acyltransferase[147] [AcetylCoACAcylTrans_P], acyl-CoA hydrolase[148] [acylCoAHydrolase_P], OPC8 CoA ligase[149] [CoaLigase_P], and enoyl-CoA hydratase[150] [enoylCoAHydratase_P] are

identified to be induced by 59 and 91% in CBSV and ACMV infection, similar to allene oxide cyclase[151] [AlleneOxideCyclase_H], hydroperoxide dehydratase[152] [hydroperoxideDehydra_H], and lipoxygenase[153] [lipoxygenase_H] in chloroplast. They are also affected in other time points; 6dpi of ACMV infection caused 7% induction whereas 12dpi of CBSV infection had 14% repression.

3.6.3. Modulation of carbohydrate metabolic pathways during infection with CBSV and ACMV

Amongst the pathways related to carbohydrate metabolism, which are (in-) directly associated with the innate immunity, enzymatic activities of glycolysis, TCA and PPP also showed some modulation in response to infection progress, that have been shown to be enhanced defence-responsive fluxes.

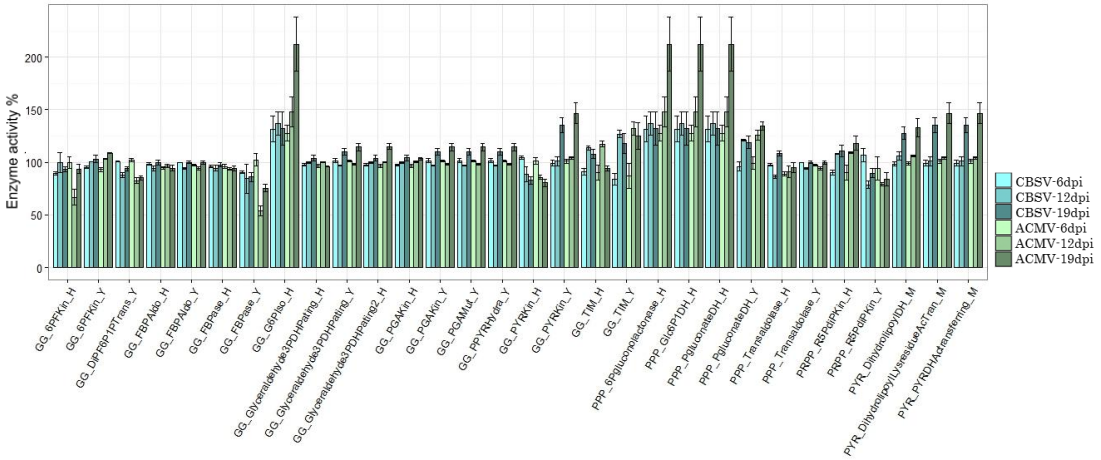

Figure 22b. Glycolysis, PPP and pyruvate pathways enzyme activity modulation during infection progression of CBSV and ACMV; Simulated activities of the enzymes in the pathways i) glycolysis/gluconeogenesis (marked by the prefix "GG_"), ii) pentose phosphate pathway (indicated by the prefix "PPP_"), iii) pyruvate pathway (indicated by the prefix "PYR_") at the three time points 6dpi, 12dpi and 19dpi each after the infection with the two pathogens ACMV and CBSV; Glucose-6-phosphate isomerase in chloroplast showed induced activity to 136 and 132% in CBSV, 148 and 212% in ACMV at 12 and 19dpi, in addition to pyruvate kinase in cytosol to 134 and 146% in CBSV and ACMV at 19dpi. Trios-phosphate isomerase in cytosol activated to 126 and 118% in CBSV, and 132 and 125% in ACMV at 12 and 19dpi. Activity of fructose-bisphosphatase in cytosol and 6-phosphofructokinase in chloroplast dropped by 46, 34% at 12dpi of ACMV infection also fructose-bisphosphatase in cytosol and pyruvate kinase in chloroplast by 25, 20% at 19dpi of ACMV infection. Pentose phosphate pathway fluxes in chloroplast such as 6-phosphogluconolactonase, glucose-6-phosphate 1-dehydrogenase, phosphogluconate dehydrogenase (decarboxylating) elevated to 148 and 212% in response to infection with ACMV at 12 and 19dpi, likewise 136 and 132% in response to CBSV infection. Moreover, transaldolase which was suppressed by 16% in the CBSV samples at 12dpi and 11% in the ACMV samples at 6dpi. In mitochondria, pyruvate pathway fluxes such as Dihydrolipoyllysine-residue acetyltransferase and Pyruvate dehydrogenase (acetyl-transferring) were equally increased by 34 and 46% in CBSV and ACMV at 19dpi.

According to our analyses, and as shown in Figure 22b the flux distribution of non-oxidative part of the pentose phosphate pathway (noxPPP) catalyzed by transaldolase[154] [Transaldolase_H/Y] in chloroplast of CBSV and ACMV infected plants was decreased to 97, 86, 108% and to 89, 90, 94% relative to mock at 6, 12 and 19dpi respectively. Whereas in cytosol of CBSV infection at 12dpi, ACMV infection at 6dpi, ACMV infection at 19dpi it was suppressed to 94, 97 and 94% active, and in other samples was equal to mock. However many of oxidative section of the PPP which converts glucose-6-

phosphate into ribulose-5-phosphate, catalyzed by phosphogluconate dehydrogenase[155] (decarboxylating) [PgluconateDH_H/Y] in cytosol was slightly declined to 94% at 6dpi of CBSV infection, and then increased to 121 and 125% at 12dpi also 118 and 134% at 19dpi. However the activity of this enzyme in chloroplast was induced in all time points to 127 and 131% at 6dpi, 136 and 148% at 12dpi, 132 and 212% at 19dpi in CBSV and ACMV infection. Activity of glucose-6-phosphate, 1-dehydrogenase[156] [Glc6P1DH_H] and 6-phosphogluconolactonase[157] [6Pgluconolactonase_H] in chloroplast were similarly increased to 131 and 127% at 6dpi, 136 and 148% at 12dpi and 132 and 212% at 19dpi of CBSV and ACMV infection, relative to mock.

Among the simulated phosphoribosyl pyrophosphate (PRPP[158]) fluxes, activity of Ribose-phosphate diphosphokinase[159] [R5PdiPKin] decreased at 6dpi in chloroplast to 90% in both infections, at 12dpi showed a slight induction to 107 and 109%, and then at 19dpi to 110 and 118% in CBSV and ACMV infections. While in cytosol it altered to 107 and 94% at 6dpi then suppressed to 78 and 79% at 12dpi, followed by 89 and 83% of reduction at 19dpi of CBSV and ACMV (Fig. 23b).

Interestingly, Glycolysis fluxes distribution via 6-phosphofructokinase[160] [6PFKin_H/Y] in chloroplast reduced to 90% in CBSV infection at 6dpi and to 66% in ACMV infection at 12dpi, then to 93% at 19dpi in both viruses. However, in cytosol it was not very notable; at 6dpi declined to 95 and 93%, at 12dpi it was 100 and 103% active, and then at 19dpi increased to 103 and 108%. Diphosphate-fructose-6-phosphate 1-phosphotransferase[161] [DiPF6P1PTrans_Y] activity in cytosol showed reduction at 12dpi (to 87 and 82% CBSV and ACMV respectively) and 19dpi (to 94 and 85% in CBSV and ACMV respectively). Activity of glucose-6-phosphate isomerase [GG_G6dpiso] in chloroplast increased to 131 and 127%, 136 and 148%, 132 and 212% in CBSV and ACMV infection at 6, 12, 19dpi. Fructose-bisphosphate aldolase[162] [FBPAldo_H/Y] showed slight reduction in activity in both chloroplast and cytosol; at the highest to 94% in response to CBSV infection at 12dpi (in both cytosol and chloroplast), as well as ACMV at 6 and 19dpi (in chloroplast), and ACMV at 12dpi (in cytosol) while remained unchanged in both organelles in CBSV infection at 19dpi.

In addition, Phosphopyruvate hydratase[163] [PPYRHydra_Y] showed slight increased activity at 19dpi to 109 and 114% at 19dpi in CBSV and ACMV infection, while was almost unchanged at 6 and 12dpi. Fructose-1,6-bisphosphatase[164] [FBPase_H/Y] in cytosol was the most suppressed enzyme at 12dpi to 84 and 54% in CBSV and ACMV infection, similarly at 19dpi to 86 and 75%, while at the early stage showed 90% suppression in CBSV and unchanged in ACMV infection. In chloroplast, it was slightly declined in response to all the infections, which might not be notable. Likewise, activity of glyceraldehyde-3-phosphate dehydrogenase (NAD(P))[165] (GAPDH) [GG_Glyceraldehyde3PDHPating] at 6 and 12dpi in chloroplast was repressed by 3-4% which is not notable whereas at 19dpi was different; in cytosol induced to 110 and 114%, and in chloroplast altered to 104 and 96% in response to CBSV and ACMV infections, respectively. Plus activity of glyceraldehyde-3-phosphate dehydrogenase, type2 (TDH2) [GG_Glyceraldehyde3PDHPating2] in chloroplast was slightly suppressed by 3-4% at

6dpi and induced by 4 and 14% at 19dpi in response to CBSV and ACMV infections. Phosphoglycerate kinase[166] was shown to be at 6dpi less-activated by 3-4% whereas at 19dpi over-activated by 3-4% in chloroplast and 10-14% in cytosol of CBSV and ACMV infected plants. Likewise activity of phosphoglycerate mutase[167] [PGAMut_Y] in cytosol was also induced to 110 and 114% at 19dpi. Pyruvate kinase[168] [PYRKin_H/Y] was induced in cytosol at 19dpi to 134 and 146% compared with mock while was shown to be suppressed in chloroplast at 12 and 19dpi to 88, 85% and 83, 80% in CBSV and ACMV infections. Activity of triose-phosphate isomerase[169] [TIM_H/Y] at 6dpi of infection was reduced equally to 90% in chloroplast, 83 and 86% in cytosol, and then induced at 12dpi to 113 and 117 in chloroplast in addition to 126 and 132% in cytosol, whereas at 19dpi was shown to be in 108 and 94% of activity in chloroplast and 118 and 125% active in cytosol.

Mitochondrial enzymes belonging to pyruvate pathway were high-activated by 25-40% in response to infection with CBSV and ACMV at 19dpi. Dihydrolipoyllysine- residue acetyltransferase[170] [PYR_DihydrolipoylLysresidueAcTran] showed the induction to 134 and 146% in CBSV and ACMV infection, similar to pyruvate dehydrogenase (acetyl-transferring)[171] [PYR_PYRDHActransferring]. It is also noteworthy that activity of dihydrolipoyl dehydrogenase[172] [DihydrolipoylDH_M] in pyruvate and TCA fluxes was the most activated enzyme in infected samples with ACMV and CBSV at 19dpi with 27 and 32% increased activity.

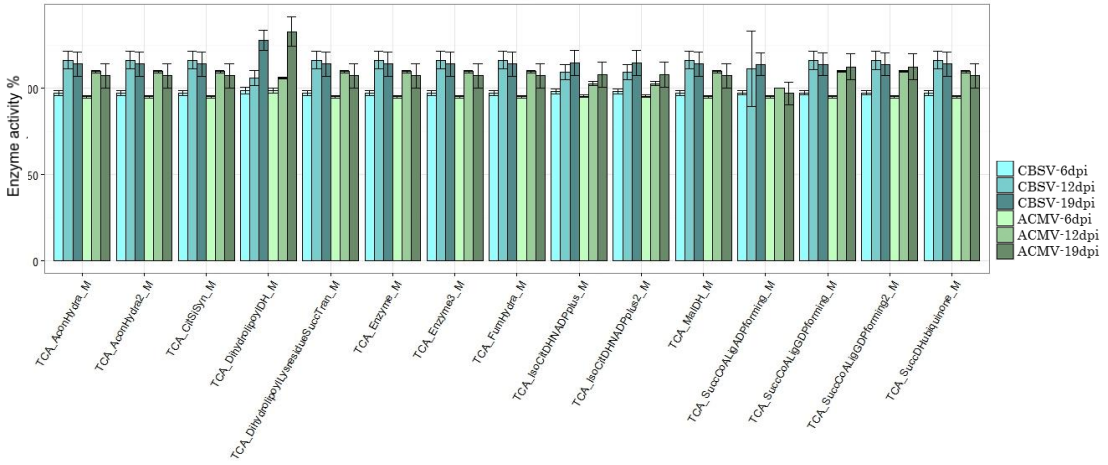

Figure 22c. TCA enzyme activity modulation during infection progression of CBSV and ACMV; Simulated activities of the enzymes in the trichloroacetic acid pathways (indicated by the prefix "TCA_") at the three time points 6dpi, 12dpi and 19dpi each after the infection with the two pathogens ACMV and CBSV; Most of these enzymes showed reduction at 6dpi for 5 and 3% in CBSV and ACMV infection, maximum increased activity was for dihydrolipoyl dehydrogenase at 19dpi. Most of these enzyme were more responsive at 12 and 19dpi to CBSV (induced for 16 and 14%) also to ACMV (induced for 9 and 7%), amongst isocitrate dehydrogenase ($NADP^+$) 1 and isocitrate dehydrogenase ($NADP^+$) were modified more in response to CBSV in a higher level compared with ACMV, although by following the same trend.

Among the TCA enzymes as shown in Figure 22c, aconitate hydratase[173] 1 [AconHydra_M] and aconitate hydratase 2 [AconHydra2_M], citrate (Si)-synthase[174] [CitSiSyn_M], dihydrolipoyllysine-residue succinyltransferase[175] [DihydrolipoylLysresidueSuccTran_M], oxoglutarate dehydrogenase (succinyl-transferring)[176] [TCA_Enzyme_M and TCA_Enzyme3_M], Fumarate Hydratase[177]

[FumHydra_M], malate dehydrogenase[178] [MalDH_M], succinate-CoA ligase[179] (GDP) 1 [SuccCoALigADPforming_M], succinate-CoA ligase (GDP) 2[SuccCoALigADPforming2_M] and succinate dehydrogenase (ubiquinone)[180] [TCA_SuccDHubiquinone_M] at 6dpi were simulated to be very slightly repressed by 3-5%, but then induced at the next points to 116 and 109% at 12dpi of CBSV and ACMV infections, likewise to 113 and 107% at 19dpi. Activity of isocitrate dehydrogenase ($NADP^+$) 1[181] [IsoCitDHNADPplus_M] and isocitrate dehydrogenase (IDH) ($NADP^+$) 2 [IsoCitDHNADPplus2_M] showed 114 and 107% enhancement at 19dpi of CBSV and ACMV. At this time point, activity of dihydrolipoyl dehydrogenase [DihydrolipoylDH_M] increased by 27 and 32% in response to CBSV and ACMV. Succinate-CoA ligase (ADP-forming) [SuccCoALigADPforming_M] was more responsive to CBSV infection; as it showed 111 and 113% activity at 12 and 19dpi.

According to our analyses, almost all the TCA cycle fluxes, which are mitochondrial enzymes, increased due to both viral infection at 12 and 19dpi, whereas very slightly decreased at 6dpi. This can lead us to assume, these changes in the proportion of glucose uptake, reflect the re-prioritizing the maintenance and biosynthesis for the energy consumption of infected plants. The induction level of most these enzymes was evidently simulated to be higher in CBSV infection at 12 and 19dpi, however some of them such as isocitrate dehydrogenase ($NADP^+$) 1 and isocitrate dehydrogenase ($NADP^+$) were responsive to CBSV slightly higher.

3.6.4. Modulation of metabolic pathways involved in Photosynthesis during infection with CBSV and ACMV

Figure 22d shows that activity of photosystem I[182] [PSI_H] and photosystem II[183] [PSII_H], ATPase - which acts as a primary transporter via proton pumping-, ferrodoxin-$NADP^+$ reductase[184] [ferrodoxinNADPReduct_H] - which transfers electrons during photosynthesis from photosystem I to NADPH-, similar to plastoquinol-plastocyanin reductase[185] [plastoquinol_plastocyaninReduct_H] declined to 89% in response to CBSV infection, and to 55% in ACMV infection at 12dpi. The activities of these enzymes reduced to 82 and 80% at the next time point, although were slightly induced at early stage for 4 and 10%. Activity of fructose-bisphosphate aldolase [FBPAldo2_H] and fructose-bisphosphatase [FBPase_H] in chloroplast was declined by 4% at 6dpi, almost unchanged at 12dpi and increased by 3.7 and 5% t 19dpi of CBSV and ACMV infection. Simulated fluxes in chloroplast such as Phosphoribulokinase[186] [PHOTO_PribuloKin] slightly (2-3%) decreased at 6 and 12dpi, and then increased at 19dpi to 2-3%. In addition Transketolase[187] 1 was suppressed by 4 and 6%, equally 3%, then increased by 4 and 3% in CBSV and ACMV infected plants. Transketolase 2 was most affected at 19dpi for 10 and 16% in response to CBSV and ACMV infection.

Activity of ribose-5-phosphate isomerase[188] [Ri5PIso_H] in chloroplast was suppressed by 13-14% at 12dpi of CBSV and ACMV infection, in addition to 10% in ACMV infection at 19dpi. Whereas in cytosol this was induced by 22 and 23%, 11 and 17% active in infected samples with CBSV and ACMV at 12, 19dpi, respectively, while it

showed 106 and 94% activity at 6dpi. Likewise, Ribulose-phosphate 3-epimerase[189] [RuP3Epi_H] in chloroplast only changed 2-3% in activity, whereas in cytosol showed more significant alteration; equally decreased by 2% at 6dpi, increased by 9 and 12% at 12dpi, similarly 10 and 20% induction at 19dpi in CBSV and ACMV infection.

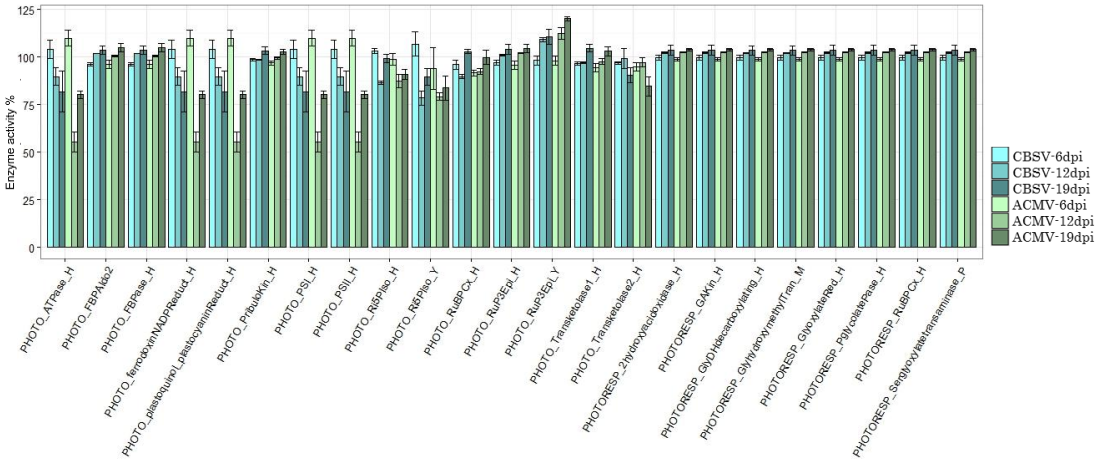

Figure 22d. Photosynthesis enzyme activity modulation during infection progression of CBSV and ACMV; Simulated activities of the enzymes in the i) photosynthesis pathways (indicated by the prefix "PHOTO_"), and ii) photorespiration (indicated by the prefix "PHOTORESP_") at the three time points 6dpi, 12dpi and 19dpi each after the infection with the two pathogens ACMV and CBSV; Activity of Photosystem I and photosystem II, ATPase, ferrodoxin- NADP+ reductase and plastoquinol-plastocyanin reductase are shown to be decreased at 12dpi of infection for 11 and 45% at 12dpi, also 18 and 20% at 19dpi. Ribulose-phosphate 3-epimerase at 19dpi was induced for 10 and 20% in CBSV and ACMV infection. Photorespiration fluxes did not show very significant alteration in response to both infections.

Activity of ribulose-bisphosphate carboxylase[190] [PHOTO_RuBPCx] in photosynthesis fluxes was shown to be decreased to 89% at 19dpi of CBSV infection while was unchanged in response to ACMV, moreover in photorespiration fluxes only 2-3% reduced. Photorespiration represents a converging point for carbohydrate and amino acid metabolic pathways. Recent studies have reported that, in addition to the physiological function as a salvage pathway for carbon loss, photorespiration is also involved in defence responses (Rojas CM 2014). Photorespiration fluxes in chloroplast including Glycine dehydrogenase (decarboxylating)[191] [GlyDHdecarboxylating], glyoxylate reductase[192] [GlyoxylateRed_H], glycerate dehydrogenase[193], hydroxypyruvate reductase[194], 2-phosphoglycolate phosphatase [195] [PglycolatePase_H], glycerate 3-kinase[196] [GAKin_H], (S)-2-hydroxy-acid oxidase[197] [2hydroxyacidoxidase_H] equally have undergone a 1% reduction at 6dpi, 2 and 3% increase at 12 and 19dpi, similar to the activity of glycine hydroxymethyltransferase[198] [GlyhydroxymethylTran_M] in mitochondria and serine-glyoxylate transaminase[199] [Serglyoxylatetransaminase_P] in peroxisome.

3.6.5. Modulation of metabolic pathways involved in transporting and amino acids metabolism during infection with CBSV and ACMV

As presented in Figure 22e, biosynthesis of chorismate in chloroplast via 3-phosphoshikimate 1-carboxyvinyltransferase[200] [3PShi1carboxyvinylTran_H], chorismate synthase[201] [ChorSyn_H], 3-dehydroquinate dehydratase[202] [DHQdeHydra_H], 3-dehydroquinate synthase[203] [DHQSyn_H], in addition to shikimate reactions enzymes

such as shikimate dehydrogenase[204] [ShiDH_H] and shikimate kinase[205] [ShiKin_H], 3-deoxy-7-phosphoheptulonate synthase[206] [3deoxy7PheptuSyn_H] were simulated to be declined by 17 and 20% at 19dpi, 12 and 15% in CBSV and ACMV infections, respectively whereas they were slightly induced (1 and 4%) in CBSV and ACMV samples at 6dpi. Amongst other amino acids metabolism enzymes, activity of phosphoserine phosphatase[207] [SER_3PSerPhosphatase_H], phosphoglycerate dehydrogenase[208] [SER_PGlycerateDH_H], phosphoserine aminotransferase[209] [SER_PSerAminoTransf_H] had undergone a slight change; 2% increase in response to CBSV infection at 6 and 19dpi similar to ACMV infection at 12 and 19dpi.

Moreover, the transporter enzymes such as the copper transporter Mcf1 [TRANSPORT_MCF1] was simulated to be enhanced in CBSV and ACMV infection at 19dpi to 34 and 46%. Activity of peroxisomal ATP-binding cassette transporter PXA1 [TRANSPORT_PXA1] at 19dpi was to 59 and 91% induced, while at 12dpi showed to be to 86% inhibited in CBSV infection, after 107% activity at the early stage of infection with ACMV. Moreover glycolate glycerate transporter PLGG1 [TRANSPORT_PLGG1] and unknownGenes 6, 8 and 9 decreased only showed a 1-3% modification in activity during infection progression. PEP/phosphate translocator [TRANSPORT_PPT] also had undergone a slight induction at 6dpi to 4 and 1% at 6dpi, followed by suppression to 12 and 15% at 12dpi, 17 and 20% at 19dpi of CBSV and ACMV.

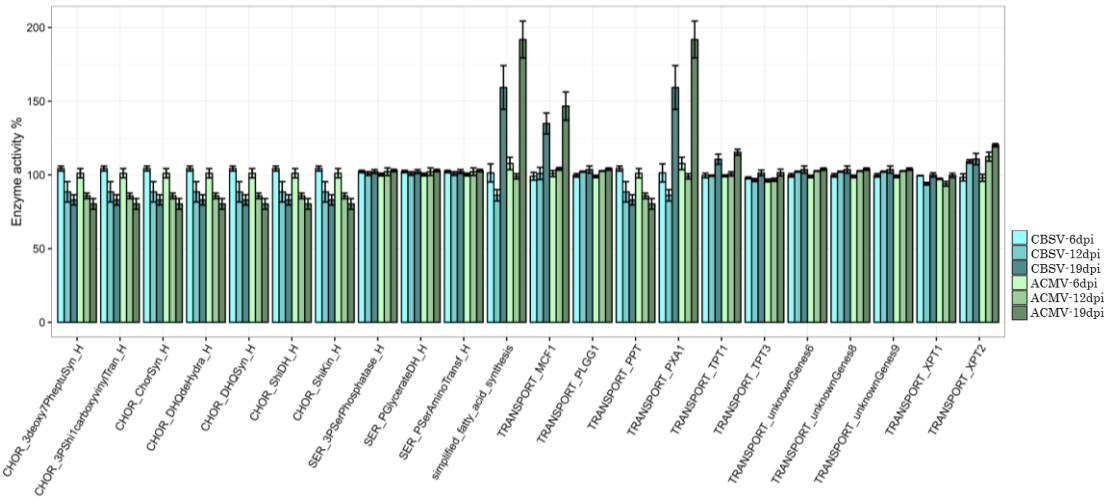

Figure 22e. Transporters and other enzyme activities modification during infection progression of CBSV and ACMV; Simulated activities of the enzymes in the i) amino acids metabolism pathways including chorismate biosynthesis pathway (indicated by the prefix "CHOR_"), and other pathways (indicated by the prefix "SER_"), ii) transporters (indicated by the prefix "TRANSPORT_"), and a fatty acid biosynthesis element at the three time points 6dpi, 12dpi and 19dpi each after the infection with the two pathogens ACMV and CBSV; Activity of chorismate biosynthesis enzymes such as 3-deoxy-7-phosphoheptulonate synthase, 3-phosphoshikimate 1-carboxyvinyltransferase, chorismate synthase, 3-dehydroquinate dehydratase, 3-dehydroquinate synthase, shikimate dehydrogenase, shikimate kinase were simulated to be suppressed to 17 and 20 in CBSV and ACMV infection at 19dpi. Activity of fatty acid synthesis enzyme and transporter PXA1 were reduced the most at 12dpi of CBSV infection (equally for 14%), although interestingly were enhanced the most at 19dpi for 60% in response to infection with CBSV and for 90% in response to infection with ACMV. Likewise, activity of TRANSPORT_PPT was suppressed in both viral infections at 12dpi (12 and 15%) and 19dpi (17 and 20%).

The activity of single simulated fatty acid synthesis enzyme (simplified_fatty_acid_synthesis) was enhanced to 59 and 91% at 19dpi of CBSV and

ACMV infection. This flux was suppressed by 14% in the CBSV samples at 12dpi also induced by 7% in the ACMV samples at 6dpi.

4. Discussion

In this section, we discuss about the analysed plant patho-system which share a common set of functional responses besides of the specific characteristics according to every host-pathogen interaction. This suppressed innate immunity, which may have resulted by induction and inhibition of various signalling and defence metabolites, might lead to the triggered immunity response in infected plants towards the late stage. The general pathogen responses address dramatic changes in gene expression level, enzymatic flux distribution and metabolite production to provide the defencins and R proteins systematically and particularly to young tissues such as meristems. Our data identified a small set of genes which likely play important roles in the establishment of the HR response in interaction with these viruses, focusing on the nature of their genome. We also try to describe the extent and complexity of these responses with their reflection on the ongoing PTI, ETI and programmed cell death at different time points of infection with RNA or DNA viruses.

Here, integrating novel approaches help us to utilize an comprehensive study of systems biology of plant-virus interaction during infection progression. That enables a deeper understanding on infection effects and at the same time leading to a complex cooperation network of various substances, in response to infection. This section provides the detailed characterized correlation between gradient stage of infection and signaling pathways, protein synthesis, glycolysis flux distributions, and oxidative activity also Rx signalosome compartments. Targeting the common responsive transcript, metabolite or enzymatic flux at the precise stage of infection might become an unravelling potential for resistant line development, drug discovery.

4.1. Transcriptome profile of infected plant

Various technologies have been developed to deduce and quantify the transcriptome, including hybridization- or sequence-based approaches. This could lead to identify essential virulence determinants and host factors, predict potential resistance targets, and perhaps provoke evolutionary long-term adaptation and selection of pathogenicity and immune responses. The advent of high-throughput sequencing coupled with advances in bioinformatics technologies have paved the way towards system-level studies that were previously intractable to approach. Such methods as RNA-seq include the sequencing of cDNA libraries from individuals experiencing various physiological challenges, with no prior knowledge of the genes' identity or sequence. Expression profiling experiments consist of measuring the relative amount of mRNA expressed in two or more experimental conditions to investigate the effected biological processes, functional genes and their expression trend differing in the course of time. The advent of high-throughput sequencing coupled with advances in bioinformatics technologies such as RNA-seq has paved the way for genomic studies in systems that were previously intractable to research. This includes the sequencing of cDNA libraries from individuals experiencing various physiological challenges, with no prior knowledge of the genes' identity or sequence. Here we quantify the changing expression levels of each transcript during development and under different conditions which provide the basis for new molecular insights into the

mechanisms of pathogenesis and the corresponding immune responses (Westermann AJ 2012, Durmuş S 2015).

4.1.1. Symptom development and sample preparation

N. benthamiana plants were observed to be fully symptomatic at 12dpi, although mild symptoms started appearing at 7-8dpi. Severe symptoms such as entire stunning, distortion, etching and leaf malformation were easily detected in CBSV and ACMV infected plants. The typical symptoms of Cassava brown streak disease on cassava plants develop on leaves, stems, and roots. However, depending on the cassava varieties and age of the plant, sometimes the symptoms disappear or become undetectable on neither leaves nor tubers. On *N. benthamiana* the symptoms can only be observed on leaves which appear as patches of yellow areas mixed with chlorosis. Advanced symptoms on the leaves are detected as an irregular yellow blotchy chlorosis which is characterized by overall stunting. Upper leaves became narrower, smaller, curled and displayed a reticulated chlorosis beginning at the base. Symptoms of African cassava mosaic disease occur as characteristic leaf mosaic patterns that affect discrete areas in addition to leaf chlorosis, which might be pale yellow or nearly white with only a shade of green, or just noticeably paler than normal-. The chlorotic areas are usually clearly defined and vary in size from that of a whole leaflet to small flecks or spots. Distortion, reduction in leaflet size and general stunting can be secondary effects that are associated with symptom severity. Chlorotic symptoms may be the direct result of the plants attempt to rescue resources from infected tissues via basal resistance mechanisms. If chlorosis is absent in infected tissues, this usually indicates a loss of basal resistance (Pierce EJ 2013). The appearance of mild chlorosis at 12dpi in all CBSV and ACMV infected *N. benthamiana* leaves represent an inhibited innate basal defence which results in susceptibility to the virus. This develops into severe symptoms at 19dpi of ACMV infection, due to inhibited basal resistance.

An increase in viral load which was detected during the infection progression of ACMV, confirms the positive correlation between symptoms development and viral titre. In the case of CBSV the viral load declined at 19dpi, which might be due to the slight possibility of successful immunity response or physiological condition of host at older age. It has also been shown that infected soybean plants with SMV^{210} had two-fold higher levels of virus at 14dpi compared with 7dpi (Babu M 2008). Similar to observed higher viral load from 4 to 14dpi in TMV response genes in *Arabidopsis Shahdara* (Golem S 2003), 5 and 6-fold increase of SACMV titre was detected between time points 14, 24 and 36dpi, respectively (Pierce EJ 2013). All together confirm that high viral load is in correlation with symptom severity, since CBSV symptoms 12dpi to 19dpi became moderate whereas in the case of ACMV the infection phenotypes remained very severe. In our study we could not estimate exact fold change of ACMV accumulation between 12 and 19dpi, due to the sensitivity of ELISA test, which could not measure the values higher than 4 (It was decided to consider the n.a. reads as 4). Plant viral loads are identified by normalization against extraction buffer (negative control of ELISA) and reads of mock-

inoculated controls (negative control of biological experiment), ensuring that alterations are solely caused by CBSV or ACMV infection.

The best approach to limit the variation in profiling is pooling the top two youngest leaves close to the meristem tip (which contain active Poty/Begomovirus). Sampling from independent various plants, also carrying out the three technical replicates and three biological replicates was considered. The quality-confirmed RNAs from three different pools were mixed together for further analyses including RNA-seq, qRT-PCR and LC-MS/HPLC-UV-MS.

For dual RNA-seq experiments, sequence coverage required is currently at the upper limit of sequencing capacities. The RNA samples were not depleted for rRNA, as each individual depletion step not only removes rRNA but also decreases the final yield of non-rRNA transcripts. Instead, increasing the read numbers of non-rRNA transcripts was achieved simply by increasing the overall sequencing depth of polyA enriched mRNAs (Westermann AJ 2012). Therefore it seems that the maximum possible depth of high throughput sequencing (3GB) would be sufficient to perform the transcriptome analyses of plant host and viral pathogen simultaneously. Although the quality control of obtained raw reads was satisfying, still a large amount of reads could not be mapped to the reference genomes (6.5-7.5%). There could be several reasons for the unmapped reads, such as sequencing errors, failure to remove the adapter, the presence of contaminated sequences that could not be detected in the filtering processes or an incomplete reference genome.

4.1.2. Differential expression analyses

By applying dual RNA-seq approach, we had a goal on understanding the Potyviral and Begomoviral pathogenicity mechanisms. Such tools may describe involvement of different compartments of the RNA and DNA virus to induce and establish the infection. The individual viral components, which were counted in these infected samples, open potential function of these genes to more learned about in future on their pathogenicity regulation. Also how they redirect the eukaryotic protein-synthesizing and translation system to establish the infection.

Several RNA plant virus studies have indicated that in compatible interactions suppression of host transcription defence response is a prerequisite for infection (Pierce EJ 2013). In our finding, of all the differentially expressed transcripts, the percentage of repressed genes compared to total number of altered genes at each time point was notable. This maximum number of repressed genes appeared at 19dpi in the ACMV samples and 12dpi in the CBSV samples. Inhibition of many host-responsive genes at mid- and late stage of infection with DNA-virus as well as mid-stage of infection with RNA-virus might be consistent with symptom severity and established infection. This trend has been previously demonstrated in several plant host-virus interactions in *N. benthamiana* also senescence-related responses (Postnikova OA 2012, Pierce EJ 2013). As the number of inhibited transcripts decreased between 12 and 19dpi, the CBSV viral load between these time points declined, whereas the accumulation of ACMV remained high from mid- to

late stage. The increase in down-regulated genes at 12dpi in the CBSV samples and 19dpi in the ACMV samples is also indicative of successful ACMV attempt to redirect many host cellular processes for its own benefit, which resulted in repression of a large number of genes. While in CBSV it might represents the slight recovery or enhanced defence system due to the physiological stage of infected plants. On the other hand, a percentage of induced genes increased from 6 to 19dpi like 0.06, 4.25, and 2.3% in CBSV infection and 0.17, 2.6 and 3.8% in ACMV infection; the same trend with constant increasing for ACMV infection and decreasing for CBSV infection between mid and the later stage of pathogenesis as occurred for down-regulated genes. The higher number of induced genes at 12dpi may reflect more of a general non-specific innate host response to virus invasion by the activation of stress and defence-like genes.

4.1.3. Differentially regulated biological activities in response to viral infection

Notably but unsurprisingly, there were many biological processes frequently and non-specifically involved in response to viral infection. It is important to emphasize three key points when relying on the GO terms in analyzing expression profiles: their generality, their obvious redundancy and their incompleteness. Within the obtained GO annotation from TRAPID, it was decided to choose only the first associated biological process, which might be the issue to consider. Redundant annotations and multiple descriptions of the same biological mechanisms represent special concern undermining an effort to address consistency in characterization of gene products (Postnikova OA 2012).

All GO molecular function categories were represented among the significant genes, which are involved with viral pathogenicity progression: categories corresponding to ‘transferase’, ‘ligase’, ‘lyase’, ‘ATPase’, ‘oxidative and catalytic activities’. Similarly protein and DNA/RNA metabolism via ‘M phase’ in addition to ‘chromatin organization processes’ such as ‘posttranslational modifications’ and ‘histone modification’ were altered in response to infection progression. It indicates the involvement of various biological processes during multiplication and movement of RNA and DNA viruses. We found chromatin organization (histone modification) only annotated in the up-regulated gene set of ACMV infected plants at 12 and 19dpi, as its crucial role in the regulation of genes expression is proven (Kouzarides 2007, Postnikova OA 2012). Genes regulating ‘tryptophan metabolic process’ were down-regulated at 12dpi of infection with both viruses, and up-regulated in ACMV at 19dpi. It is associated with providing the precursors for the synthesis of key secondary metabolites such as auxin, IAA[211], and other molecules that help protect plants against pathogens and herbivores (Postnikova OA 2012). Late stages of pathogenesis, when plants are systemically infected, are characterized by repression of the majority of the stress-responsive pathways activated at the early phases, such as ‘response to abscisic acid stimulus’, ‘response to wounding’, ‘innate immune response’, ‘response to oxidative stress’, ‘response to auxin stimulus’, ‘callose deposition in cell wall’ and ‘glycosinolate metabolic process’. Genes involved in ‘Oxidoreductase activity’ and ‘acting on single donors with incorporation of molecular oxygen’ were shown to be up-regulated at 19dpi in both viruses particularly in response to ACMV.

Down-regulation of biological functions is presumably due to the virus overtaking host defence-related pathways and causing physiological changes associated with the disease symptoms (Yang C 2007, Postnikova OA 2012) such as 'macromolecule metabolic process' that was suppressed in CBSV and ACMV at 12dpi. Additionally, 'glucan metabolic process' was down-regulated at 6dpi in CBSV, also both in the CBSV and ACMV samples at 12dpi. 'Plasmodesma', 'Ras guanyl-nucleotide exchange factor' and 'peptidase inhibitor activity' based genes were inhibited in ACMV infection at 19dpi, similar to 'extrinsic to membrane' at 12dpi of CBSV and ACMV. In our impression, the number of suppressed biological processes was higher at 12dpi of CBSV infection and 19dpi of ACMV infection compared to other time points and categories, which is consistent with the symptoms severity and viral loads addressed in previous section.

4.1.4. Differentially responsive protein family during viral infection progression

The massive shift in gene expression patterns and metabolic functions that occurs during infection progression is reflected in the substantial increase in transcript abundance of putative proteins. Overrepresentation of protein categories from biological process was investigated during viral infection progression using the list of regulated proteins. We used the Pfam database (Finn RD 2016) and the list of top 100 most significant differentially expressed genes (including up and down-regulated ones) to identify and analyse the protein families and enzymes that were significantly regulated during the onset and progression of viral pathogenicity depending on the genome entities. The protein categories responding to infection in *N. benthamiana* and pathogenicity progression of CBSV and ACMV are described here. Similarities as well as differences were found between these two compatible interactions, in the early response to inoculation through the gradient of infection. This Pfam enrichment analyses revealed protein families that are necessarily involved in responding to the infection establishment of these viruses, and might show how two different viruses trigger different cascades of molecular changes through protein expression.

The number of encoding putative transcription factors showed the most significant differentially expression. These include *F-box*, *WRKY*, *AP2* domain proteins, zinc finger proteins and other DNA- and RNA-binding proteins. Transcription factors *ERF1* and *ORA59* form part of the (*AP2/ERF*[212]) superfamily. The *AP2/ERF* domains bind to a GCC promoter box of stress-responsive genes, and can act as either activators or repressors of stress responsive genes (Finn RD 2016, Abiri R 2017). *ERF1* expression elevated transcripts at 12 and 19dpi in both viral infection conditions, as well as *EIN*s. Similar to the *WRKY* family, which are involved in the regulation of pathogen defence, senescence and the biosynthesis of secondary metabolites such as anthocyanin pigmentation (Adachi H 2015, Finn RD 2016). This has also been confirmed in our qRT-PCR experiment, where the WRKY22 is up-regulated particularly at 12dpi of CBSV and ACMV (almost 2- and 8-fold respectively). The RNA-seq results show the induced expression values of WRK33[213] at 12 and 19dpi to both viral infections (almost 2.5-3-fold at 12dpi and 4-4.5 fold at 19dpi). Likewise, F-box was more frequently observed in involved protein families at 6dpi, and showed only slight induced expression pattern during the whole infection

progression of both viruses. These proteins function in mediating protein-protein interactions in a variety of contexts, such as polyubiquitination. Through the *F-box*, *LRR*s and the *WD* repeats are linked to the *Skp1* protein and the core of *SCF*[214]s complexes. The protein degradation system also includes the ubiquitin E2 and E3 proteins and mark different proteins for degradation (Bai C 1996, Duplan V 2014, Finn RD 2016). The expression of E2 was shown to be up-regulated at 19dpi, whereas most of the ubiquitin E3 components showed a constant induction pattern during viral pathogenicity.

The LRR family proteins were more frequently expressed at 12dpi of ACMV, that might imply the involvement of a variety of biological processes, such as signal transduction, DNA repair, RNA processing, apoptosis, and the immune or resistance response (Tameling WI 2007, Hofberger JA 2014, Finn RD 2016). In addition, 5-7% of the members of the NAM[215] proteins (NAC domain) show differential expression in our protein family analyses, particularly at 12 and 19dpi of infection. This protein family has been implicated in developmental processes, including formation of the shoot apical meristem, floral organs and lateral shoots, as well as in plant hormonal control and defence. It is evident that binding of AL3 of *Geminiviruses* to a NAC transcription factor enhances viral DNA replication. A NAC domain protein (SINAC1) was reported to be in positive interaction with the Rep[216] of TLCV[217] in tomato, to promote viral replication. Furthermore, interaction of TMV replicase protein with a NAC domain transcription factor (ATAF2) has also been shown to be associated with suppression of systemic host defences, promoting systemic virus accumulation. However in SACMV, down-regulation of ATAF1 at 24dpi occurred to be in contradictory with TMV and TLCV studies (Buchanan-Wollaston V 2005, Selth L , Ascencio-Ibáñez JT 2008, Wang X , Pierce EJ 2013, Finn RD 2016), in our analyses, both viruses and more CBSV seemed to be interacting with these transcription factors (in terms of number of involved NAM). Besides, kinases belong to a very extensive family of proteins were also differentially regulated. This family share a conserved catalytic core common with both serine/threonine and tyrosine protein kinases. They are one of the dominant protein families at all time points of infection progression of RNA and DNA viruses. The expression values from our RNAseq and qRT-PCR analyses of this family members (including *BAK1*, *BRI1*, *BSK*[218], *BIN2*[219], *MPK6 and EIF2AK4*[220]) confirms their higher cellular catalytic activity, similar to the dual specificity proteinases (e.g. *MEK* - phosphorylates both Thr and Tyr on target proteins). They are involved in protein phosphorylation biological process, by catalysing the gamma phosphate transferring from nucleotide triphosphates (often ATP) to amino acid residues of proteins, causing a conformational change affecting protein function (Hanks SK 1988, Finn RD 2016). On the other hand, HPt[221] domain occurred as more significant in ACMV infected plants at 19dpi compared to other samples, and mediates phosphorelay signal transduction system in biological process. *AHP*, as the most important member of this family, showed induced expression at 19dpi in the ACMV samples (2.3-fold) and at 12dpi in the CBSV samples (1.2-fold) (Laub MT 2007, Finn RD 2016). In addition, Kinesin family as microtubule-associated force-producing proteins were evidently one of the top significant infection-responding protein families at 6dpi. They are ATP binding and function in organelle

transport and microtubule-based movement biological process (Brady ST 1995). Similar to PPR[222] proteins, which have roles in mitochondria or plastid and are essential in post-transcriptional processes within organelles and thought to be sequence-specific RNA-binding proteins (Small ID 2000, Finn RD 2016). Znf or Zf domains bind zinc, or other metals such as iron or no metal at all. They function in gene transcription, translation, mRNA trafficking, cytoskeleton organisation, epithelial development and cell adhesion. This protein family represented as one of the most significant differentially expressed families in ACMV at 12dpi as well as at 6dpi and 19dpi of both CBSV and ACMV. They are essential for protein folding, chromatin remodelling and zinc sensing (Laity JH 2001, Finn RD 2016). Asp[223] with their aspartic-type endopeptidase activity are involved in proteolysis biological process (Kirchhausen T 1997, Finn RD 2016) and were among the top most involved protein families at 6 and 19dpi of CBSV and ACMV. In addition, IQ[224] (CaM[225]), which are protein-binding and recognized as major calcium (Ca^{2+}) sensor and their interaction with a diverse group of cellular proteins, were responsive to infection at 12dpi in CBSV and ACMV and similarly at 19dpi in ACMV infection (Rhoads AR 1997, Finn RD 2016). The auxin repressed protein family contains several plant dormancy-associated proteins. Amongst, the expression of the DRM/ARPs as a responsive protein to stress and environmental factors (Finn RD 2016) were found at 19dpi of CBSV and ACMV differentially expressed. Likewise, *DEAD* and *DEAH* box helicases were also identified among the top100 most differentially regulated. They are involved in various aspects of RNA metabolism, including nuclear transcription, pre mRNA splicing, ribosome biogenesis, nucleocytoplasmic transport, translation, RNA decay and organellar gene expression (Aubourg S 1999, Finn RD 2016).

At this level of analyses, it occurred that elevated transcripts of plant defence proteins such as *BAK1*, *BRI1*, *BSK*, *BIN2*, *MPK6*, *MEK2*, *EIF2AK4* and *HPSE* illustrate a common trend in expression patterns to both RNA and DNA viral stress responses. In general, among the differentially expressed genes at 6, 12 and 19dpi of CBSV and ACMV infected plants with a Padj-value cut-off of 0.05, *HSP/HSC* proteins, transporters, proteasome and proteins that are involved in regulation of cellular oxidative state were among the most significantly differentially regulated proteins in response to infection. The involvement of genes are which potentially essential in signal transduction - such as protein kinases, DNA binding proteins and different transcription factors such as AP2 domain-containing, *WRKY* and *F-box* at early towards late stage of infection - is evident. Moreover, the up-regulation of a range of amino acids and peptides transporters, also sugar synthases and glucosyl transferases reflects the new function of a chlorotic/mosaic symptomatic leaves, as they become a source tissue for the mobilization of nutrients to the rest of the plant.

4.1.5. Differentially regulated functions in response to viral infection

The global investigation on viral infections affects in transcriptome level may help to find the key elements of morphological changes in addition to the modified innate immunity system in infected plants. Common physiological and biochemical alterations include a decline in energy metabolism and photosynthesis, an increase in respiration, the accumulation of nitrogen and sulphur compounds, and repressed oxidase phosphorylation.

These modifications are accompanied by cellular surveillance activities including the replication and repair, transcription, translation, protein degradation and export, RNA degradation and transport. According to our RNA-seq data obtained from progression of CBSV and ACMV infection and the previous studies, the viral infection is accompanied by significant modification in a wide range of biological processes: declined biosynthesis of carotenoid, fatty acid, steroids, histidine, nitrogen, sulphur and lipoic acid also porphyrin and chlorophyll metabolism. In addition the elevated phenylalanine, tryptophan, glyoxylate and dicarboxylte also inositol phosphate, TCA and penthose phosphate pathway also occurred. Late stage of infection (at 19dpi) with ACMV faced a significant reduction of carbon fixation, pyruvate, fructose and mannose, amino-sugar and nucleotide sugar. CBSV infection progression caused inhibition in metabolism of biotin and riboflavin, histidine and sphingolipid, and an enhanced metabolism of arginine, proline, tyrosine, cyanoamino acid and glycolysis/glucogenesis. Moreover, we observed that viral infection activates transcription of genes encoding ribosomal proteins, although it might occur not equally among all the paralogues. Inside the cell nucleolus, where the whole ACMV genome and Potyviral NIa accumulates, the rRNA synthesis and ribosome biogenesis takes place. Consistent with previous studies, like infection of *N. benthamiana* with PPV[226] activated transcription of genes encoding proteins of both ribosomal subunits. Likewise various members of the ribosomal protein family were differentially induced in TuMV-infected *Arabidopsis* plants (Yang C 2007, Rajamäki ML 2009, Ivanov KI 2014). The strongest effects on gene expression were observed in cells with the highest levels of virus accumulation. According to KEGG functional categorization which was visualized as Voronoi plots, at 12dpi these activities were highly elevated, the time point with higher viral load according to ELISA and viral RNA-seq data, also more significantly in the ACMV samples, then decreased at next time point.

Additionally, comparison of the translation activities profile in CBSV/ACMV infected and mock inoculated *N. benthamiana* showed that transcripts are elevated at 6dpi and inhibited at 19dpi; subcategories by mRNA surveillance pathway, RNA transport, ribosome, aminoacyl-tRNA biosynthesis and ribosome biogenesis. As an additional line of our investigation, at mid-stage of infection, RNA transport (up-regulated) and aminoacyl-tRNA biosynthesis (down-regulated) and ribosome (down-regulated stronger in ACMV) were similarly overexpressed in infection with these viruses, although mRNA surveillance pathway got inhibited in ACMV and induced in CBSV at this time point. This observation is in contradiction with polysome profiles of TuMV-infected Arabidopsis, where did not show any significant difference compared with healthy plants. That led the authors to the hypothesis that Potyvirus infection did not globally inhibit translation (Moeller JR 2012, Ivanov KI 2014), which is rejected here. Induced transcription at 6 and 12dpi but reduced at 19dpi in association with the RNA/DNA virus infection. This demonstrates the modified translation activity through spliceosome, also basal transcription factors (which remain active constantly in the course of time).

Among the mRNA surveillance pathway, the translation initiators play a crucial role, as it was shown in the recent study that these recessive genes also contribute to plant

resistance. All encode translation initiation factor genes such as *eIF4E* transcript cassava4.1_016601m, which was increased in infected Kaleso (cassava variety resistant to CBSV) compared to healthy and Albert (cassava variety susceptible to CBSV) controls (Maruthi MN 2014). Our analyses of *N. benthamiana* transcriptome profiles identified the expression of one *eIF1*, two *eIF2S*, one *eIF4A*, one *eIF4G* and one eIF5. Among these, at the early stage of infection, the transcript level of *eIF2S3*, *eIF2S2* and *eIF4A* was increased, and at 12dpi *eIF2S3*, *eIF4A* and *eIF4G* were highly expressed, followed by the expression of *eIF2S3* in both viral infection also *eIF4G* in the ACMV samples at 19dpi.

In plants, mRNA degradation and RNA silencing mechanisms overlap both spatially and functionally. Plants with a mutated *DCP2*[227], which is a key component of the mRNA decay pathway, show an enhanced silencing phenotype. The phenotype can be reversed by infecting the plant with TuMV, presumably through the action of the RNA silencing suppressor *HC-Pro* (Christie M 2011, Thran M 2012, Ivanov KI 2014). According to our transcriptome analyses, RNA silencing was highly elevated at 12dpi especially in the CBSV samples. Similarly, the RNA degradation was constantly up-regulated during CBSV and ACMV progression, and reduced at 19dpi of CBSV infection. All silencing pathways involve cleavage of dsRNA into siRNAs by Dicer that are potentially involved during viral infections (Hanley-Bowdoin L 2013). Although the expression level of *DCR1*[228] gene increased at 12dpi of both CBSV and ACMV infected plants, however was more induced in response to ACMV. And at 19dpi only the ACMV sample overrepresented the expression of this gene. Among the RNAi components the transcript level of *DDX6*[229], which belongs to the piRNA pathway, was enhanced in CBSV indicated by high value of 3-fold. *AGO*[230] and *RDR* expressions were induced at 12dpi in CBSV and ACMV infected plants, in higher levels in CBSV (1.8- and 2-fold respectively). These results together imply the correlation between RNA silencing and mRNA decay. It might suggest that the infection progression of Potyvirus as well as Begomovirus can be affected by both pathways, or vice versa the elevated transcripts of these pathways might be a sign of a progressive infection, as was evident in ACMV.

4.1.6. Modulated immunity system in response to viral infection progression

The tobacco[231] *N* genes belong to *TIR-NB-LRR*[232] class of resistance genes, which can confer resistance to TMV in heterologous plants like tomato and *N. benthamiana*. According to studies on *N*-mediated signaling, *EDS1*, *RAR1* and *NPR1* genes play an important role in TMV resistance. *EDS1* and *NDR1* define a converging point in disease resistance signaling (Liu Y 2002). *EDS1* which is required for the function of the *TIR-NB-LRR* class of *R* genes, was very enhanced at 6dpi (10.9- and 3.1-fold in CBSV and ACMV respectively), highest at 12dpi (15- and 124-fold in CBSV and ACMV respectively), also at 19dpi (6.4- and 27-fold in CBSV and ACMV), whereas *NDR1* that is required for the function of a subset of *CC-NB-LRR* class of *R* genes, represented induction in CBSV at 6dpi (3.8-fold) and ACMV at 12 and 19dpi (17- and 3.8-fold) respectively.

Mutants in the central PTI regulator *BAK1* has been previously showed more susceptible reaction to three different RNA viruses, namely ORMV, TMV, and TCV in

parallel with ethylene production and *MAPK* activation. *BAK1* is a central regulator of plant immunity and is involved in PCD control and positively regulates the BR-dependent plant growth pathway and negatively regulates the BR-independent cell-death pathway. It is reported that the disruption phenotype in *bak1* mutant accompanied with semi-dwarfed, altered leaf morphology, enhanced chlorosis and lesion formation upon pathogen infection (Kemmerling B 2007, Postel S 2010). The expression of this gene was elevated to 4.5- and 10.4-fold in CBSV and ACMV at 6dpi as well as 3.2-fold in ACMV infected plants at 12dpi. consistent with former reports on *NSP* of another Begomovirus, ToYSV[233] interacts with the kinase domain of tomato BAK1 in yeast two-hybrid assays, suggesting that it might be an important virulence target for plant viruses (Kørner CJ 2013).

BRI1 belongs to a small family of LRR-receptor kinases, with a dual specificity kinase activity, which is activated by serine and threonine phosphorylation and regulates in response to brassinosteroid binding. The disruption phenotype includes dwarfed and aberrant leaf shape morphology (Noguchi T 1999, Belkhadir Y). It is reported that *BRI1* was down-regulated in response to SACMV infection at 14dpi (0.43-fold), whereas in infection with a homologous Begomovirus ACMV it was differentially expressed to 0.32-, 9.6- and 2.3-fold, and in CBSV infection to 0.45-, 0.97-, 1.6-fold at 6, 12 and 19dpi. Since, brassinosteroid signal transduction requires heterodimerisation of *BRI1* and *BAK1* to elicit transcriptional activation of responsive genes, this downstream deactivation of the *LRR-RLK BRI1* by ACMV at early stage of infection and CBSV at mid- and late stage, may contribute to failure to activate transcription of resistance-related responsive genes as was also interpreted for SACMV. C4 segment of BCTV[234] suppresses antiviral host defence by disrupting *LRR-RLK* activity, preventing the brassinosteroid-associated signal perception, which might be an assumption for ongoing interplay between CBSV and ACMV at the early stage of infection with their susceptible host (Piroux N 2007, Pierce EJ 2013). Other genes such as *BZR1_2*[235] which functions as a negative regulator of BR signaling, was also differentially expressed in our analyses; it was repressed at 6dpi (0.6- and 0.4-fold) and induced at 12dpi (1.3- and 10-fold), while at 19dpi it was different (0.8-, 1.6-fold) in CBSV and ACMV, respectively. In *bzr1-1D*, weak dwarf phenotype with declined hypocotyl and petiole lengths and dark green curled leaves when light-grown, increased cell elongation in the dark and Hypersensitive to BR was shown to be evident (Zhao J 2002, He JX 2005). That is in contradictory with the viral infection symptoms in our experiment, in particular in infection with ACMV at late stage. Moreover, *BKI1*[236] is the negative regulator of brassinosteroid signaling, associated with the membrane, and limits the interaction of *BRI1* with *BAK1* by binding to the kinase-inactive form of *BRI1* (Wang X 2006). The expression of this gene was suppressed at 6dpi to 0.8- and 0.7-fold, and then over-expressed at 12dpi to 2.3- and 10.7-fold, also 3- and 4.5-fold at 19dpi in the CBSV and ACMV samples, respectively.

In general the expression level of genes which are categorized with ‘plant-pathogen interaction’, including *RBOH, CML, RIN4, RPM1* and *EDS1* were identified to be inhibited at the early stage of infection, then gradually they enhanced at 12 and 19dpi. Most of the analysed genes in plant-pathogen interaction pathways followed the same

trend in CBSV and ACMV infections; although some of them (such as RPM1 at 19dpi) were suppressed in CBSV and induced in ACMV. As was previously the decreased level of R protein *RPM1* in response to AVR-induced resistance is proven. *RIN4* protein also appears to function with *RPM1* in the recognition of its corresponding AVR products, and this protein level was shown to be decreased in the absence of the *RIN4* protein (Boyes DC 1998, Dodds PN 2002). It seems following this model, early stage of viral infection also accompanied by inactivation of R protein in cooperation with another. These resistant signals at 19dpi are in parallel with the different observations in CBSV and ACMV samples, where the recovery and severe symptoms.

4.1.7. Modulated DNA repairing, ubiquitination and protein degradation pathways in response to viral infection

BARD1, with an ubiquitin-protein transferase activity functions in DNA damage response and repair via homologous recombination also with negative regulation of fatty acid biosynthetic process (Reidt W 2006). It was differently responsive to infection with CBSV and ACMV; was shown to be suppressed in CBSV at 6 (0.42-fold), 12 (0.9-fold) then slightly enhanced at 19dpi (1.3-fold), whereas highly over-expressed in ACMV infection at 6dpi (39.8-fold), slight decline at 12dpi (3.7-fold) and 19dpi (1.5-fold). *MET18/MMS19* is a DNA repair/ transcription protein which was suppressed in RNA level at 6dpi to 0.4-and 0.2-fold in CBSV and ACMV, and then unchanged in CBSV at 12dpi with 4.8-fold over-expression in ACMV, followed by 1.1- and 2.6-fold at 19dpi. ACMV as a Begomovirus, depends on host replication machinery to amplify its circular genome via a combination of RCR[237] and RDR[238] and its accumulation in infected nuclei may be perceived as a DNA damage (Ascencio-Ibáñez JT 2008). Histone H3, expressed during the S phase: Histones thereby play a central role in transcription regulation, DNA repair, DNA replication and chromosomal stability and has been shown to be in interaction with various Geminiviruses particles, including NSP, MP and AL1 that are also likely to impact plant gene expression mechanisms. Interaction of NSP of Geminiviruses with host histone H3 suggesting that viral DNA movement as a minichromosome; it is likely that viral double-stranded DNA is packaged into nucleosomes and further compacted by NSP binding to the amino-terminal tail of H3. Viral MP interacting with H3 has been detected in plasmodesmata of infected cells, brings up the possibility that viral DNA moves between cells in association with nucleosomes (Hanley-Bowdoin L 2013). Moreover, interactions between AL1 and a putative mitotic kinesin or histone H3 might contribute to the altered chromosomal structure characteristic of infected cells and indirectly influence host gene expression (Ascencio-Ibáñez JT 2008). The RNA level of this gene was repressed in infected plants with ACMV (0.3-, 0.9- and 0.9-fold at 6, 12 and 19dpi) as well as CBSV (0.5- and 0.2-fold at 6 and 12dpi) while was elevated to 2.1-fold at 19dpi. However in spite of our expectation, RNA-seq data did not show any difference on the replication and repair processes during ACMV infection compared with CBSV infection. The only overexpressed subcategory was non-homologous end joining with elevated transcripts at 6dpi and a notable increase at 12 and 19dpi. Base excision repair enhanced at 6 and 12dpi then repressed at 19dpi in both vi-

ruses infections. Unfortunately we could not address the expression pattern of the genes encoding this repair machinery. However the global overview confirms the enhanced DNA repairing process in infected host regardless of the entity of the pathogen.

Another addressed biological process in this category was chromatin remodelling (histone modification) which was found in differentially regulated gene sets. However, we may generalize that at 6dpi the expression of most of these genes were enhanced particularly in ACMV infected samples while towards 19dpi they showed a trend to a suppressed state. Chromatin structural features and posttranslational modifications are vital in the regulation of gene expression, spreading over vast regions of chromosomes that can be modified due to stress (Postnikova OA 2012). Proteasome and ubiquitin-mediated proteolysis are represented as enhanced processes during infection, particularly at 12dpi of both viruses. Protein processing in endoplasmic reticulum was slightly repressed at early stage of infection with both viruses, although this process was enhanced during next stages. Viruses alter the ubiquitin and ubiquitin-like protein machineries to achieve a full infection, as some of viral proteins can be modified by these proteins, and some can function as enzymes in the ubiquitylation pathway. This enzymatic machinery include *COP9* signalosome which is essential in mediating *SCF*-type E3 ubiquitin ligase function. In addition to F-box proteins as a variable component of an ubiquitin ligase complex and different E3 ligase complexes that allows the targeting of specific proteins for degradation and serves as a substrate receptor for ubiquitination and subsequent degradation. Infection is impaired when there is a reduction in the expression of any of these enzymatic elements (Liu Y 2002, Buchanan-Wollaston V 2005, Hanley-Bowdoin L 2013), which happened constantly but oppositely at 12dpi of our observation, when the diseases were established. The MapMan functional annotation demonstrated that many of the genes involved in ubiquitin-mediated proteolysis process showed an increased accumulation of their transcripts especially at 12 and 19dpi. Ubiquitin E2 was up-regulated at 19dpi, likewise most of the ubiquitin E3 components showed a constant induction pattern during the whole viral pathogenicity. This includes the *RING, F-box* and proteasome which were enhanced in all the samples, in contrast Cullin was suppressed in response to RNA and DNA virus infection. Cystein and aspartate protease have been also identified to be repressed at 6dpi and then was significantly enhanced at next time points. On the other hand, the C2 proteins of a few Geminiviruses down-regulate the JA-responsive genes by interfering with SCF complexes, thereby affecting certain hormonal responses (JA, ABA or Aux) via ubiquitination (Lozano-Duran R 2011, Alazem M 2015).

E3 ubiquitin-ligases have been shown to be involved in the regulation of the signaling responses downstream of pathogen perception through targeting vesicle trafficking components or nuclear transcription factors. They appear to modulate perception of pathogen-associated molecular patterns by pattern-recognition receptors at the plasma membrane and to regulate the accumulation of nucleotide-binding leucine-rich repeat-type intracellular immune receptors. E3 ubiquitin ligases accept ubiquitin from an E2 ubiquitin-conjugating enzyme in the form of a thioester and then directly transfer the ubiquitin to targeted substrates (Holm M 2002, Shin B 2002). There has been reported

some microbial effector proteins that are able to target host E3 ubiquitin-ligases, or to act themselves as E3 ubiquitin-ligases, in their attempt to subvert the host proteasome to promote disease (Duplan V 2014). The RNA level of E3 in CBSV infection was enhanced in all time points (1.7-, 3.6- and 2.2-fold at 6, 12 and 19dpi), as well as at 12 (21.5-fold) and 19dpi (4.8-fold) of ACMV infection. In addition, E3 ubiquitin-protein ligase *RHF*[239] is a RING-finger E3 ligases has ubiquitin protein ligase and transferase activity. The rhf1a-rhf2a double mutants are defective in the formation of male and female gametophytes due to interphase arrest of the mitotic cell cycle (Liu J 2008) was shown to be suppressed in all the samples of observation, except for ACMV samples at 6dpi, which had unchanged expression of this gene. besides, *RFWD2/COP1*; E3 ubiquitin ligase, that acts as a repressor of photomorphogenesis by mediating ubiquitination and subsequent proteasomal degradation of light-induced transcription factors such as *HY5*, *HYH* and *LAF1*. This protein is involved in the pathway protein ubiquitination, which is part of protein modification (Holm M 2002, Shin B 2002) and clearly also in response to infection with RNA and DNA viruses; as we determined the expression value of 1.4- and 2.6-fold in CBSV and 7.6- and 3-fold in ACMV at 12 and 19dpi respectively.

4.1.8. Modulated signaling transduction pathway in response to viral infection

Developmental defects are an obvious consequence of viral infection resulting from interference of viral infection with genes which are involved in plant growth and development, leading to infection symptoms. In susceptible plants, viral infections result in hormonal disruption, which manifests as the simultaneous induction of several antagonistic hormones. These hormones which primarily regulate plant defence to pathogens include SA, JA, Et, ABA and Aux (Whitham SA 2006, Alazem M 2015).

ABA plays a crucial role in plants in adaptive stress responses also in the modulation of plant responses to many abiotic stresses, in addition to its antagonistic roles in defence hormone pathways, such as SA and JA/Et. ABA–virus interaction was first studied in the context of the effect of TMV on ABA accumulation in *N. tabacum* and tomato. It has also been reported to be restricting the cell-to-cell movement of viruses such as TNV[240], by increasing the callose deposition on plasmodesmata. However, metabolite profiling did not show any significant alteration during infection progression of CBSV and ACMV, and similarly it was not induced in response to WClMV[241] infection in *Phaseolus vulgaris*. ABA levels also did not differ between uninfected or infected potato cultivar resistant to PVY[242], but tomato plants expressing the conferring resistance (TMV Tm-1) gene contained elevated levels of ABA compared with susceptible lines. Thereby it was shown that ABA is active against BaMV[243] in inoculated leaves of *A. thaliana*, such an effect was only evident in systemic leaves against TMVcg[244]. The defensive role of ABA against viruses is mediated through inhibition of the basic β-1,3-glucanase, which is responsible for the degradation of β-1,3-glucan (callose). The subsequent release of β-1,3-glucan is deposited on plasmodesmata and strengthens them against virus movement. In the analysed RNA-seq data, it was evident that the expression of the gene encoding for this enzyme was suppressed at 6dpi, then shifted up to 2 and 4-fold in CBSV and ACMV samples at 19dpi. This is consistent with the defeated defence system at the early stage

and late-activated signals after infection establishment. It might also be related to overexpression of zeaxanthin epoxidase at 6dpi and repression at the next time points. As well as the expression trend of short chain alcohol dehydrogenase (ABA2) that was induced in CBSV and suppressed in ACMV infections at 12dpi. On the other hand, ABA might suppress ROS production and SA or JA signaling transduction, thereby negating defences controlled by these two pathways. It has been shown to decline plant resistance against infection with necrotrophic pathogens by weakening JA mediated gene expression and its production. In addition, ABA antagonizes the SA pathway therefore reduces resistance at local sites of infection by repressing HR induction, decreasing the production of ROS and SA, and attenuating distal SAR and siRNA systems (Clarke SF 2002, Mauch-Mani B 2005, Asselbergh B 2008, Iriti M 2008, Kovac M 2009, Ton J 2009, Kunz M 2013, Alazem M 2014, Alazem M 2015). Here, although the chemical assays did not succeed on detecting the differed amount of ABA, the subsequently altered level of SA, ROS and HR responses was obvious.

JA seems to support plant defence at early stages of infection, as the metabolite profile of ACMV infected plants significantly enhanced JA and OH-JA production that was followed by significant reduction at 12dpi and induction at 19dpi of CBSV infection. Remarkably, JA treatment at early stages of PVY–PVX double infection enhanced resistance, but later application increased susceptibility, probably as a result of the antagonistic effect of JA on SA. It has also been shown that the treatment of *N. benthamiana* plants with JA or SA induced systemic resistance to TMV, and that resistance was further increased by pre-treatment with JA followed by SA. In contrast, exogenous application of MeJA[245] reduced local resistance to TMV and permitted systemic movement, implying that such treatment abolished *N* resistance to TMV (Oka K 2013, Alazem M 2015). Genes encoding to JA pathway components such as JAZ which substrates of the COI1[246]–based SCF complex (Tiancong Qi 2011), was shown to be involved in viral pathogenicity responses; at early stage of infection showed high induction in CBSV infection (with 20.6-fold) whereas was repressed in ACMV infection (0.4-fold) and then at 12dpi 24.3- and 33.4-fold like 19dpi with 3- and 8.6-fold , in CBSV and ACMV infection. According to the MapMan data analyses, the JA signal transduction was inhibited at 6 and 12dpi of infections while later at 19dpi shifted towards an up-regulation in CBSV and ACMV samples. The transcript level of the biosynthetic precursor of jasmonic acid, 12-oxo-PDA[247] reductase was induced at 12dpi of ACMV and 19dpi of CBSV, similarly also reported to be increased in senescing leaves. In contrast, the expression level of catalysing enzyme lipoxygenase was suppressed at 6dpi and then increased at 19dpi. Notably, plants impaired in the JA pathway failed to accumulate SA in the leaves or phloem, and exhibited increased susceptibility, whereas impairment of the SA pathway did not affect JA levels, but increased susceptibility (Zhu F 2014).

Interestingly, both viral infections inhibited the accumulation of SA at 6dpi, followed by induced levels in CBSV infection at 12dpi and ACMV infection at 19dpi, which could be another evidence of ongoing challenge between defence system and progression of viral pathogenicity. SA as a phenolic compound that is synthesized in response to a wide

range of phytopathogens is essential for the establishment of local and systemic resistance, and activation of SAR in distal tissues that declines the effects of secondary attacks. It has been reported that the over-expression of SA biosynthesis genes often improves plant basal immunity by delaying the onset of viral infection and lessening the disease severity, similar to the positive correlation between SA-mediated defence and the siRNA[248] antiviral machinery. The exogenous application of SA has been reported to reduce the CP levels of TMV and PVX during their compatible interactions with *N. benthamiana* plants. A significant increase in SA in the inoculated and systemic leaves of resistant tobacco plants was observed after infection with TMV[249]. Similar observations were made in Ny-1-resistant potatoes after infection with PVY (Mayers 2005, Alamillo JM 2006, Ishihara T 2008, Lee 2011, Hunter LJR 2013, Peng HT 2013, Baebler S 2014, Alazem M 2015). According to the MapMan data, SA glucosyltransferase ether bond making SAG was inhibited at 6dpi and induced at 12 and 19dpi of both viral infections. Remarkably this data is consistent with the KEGG observation on SGT1[250] expression trend. Moreover, the early stage of infection with CBSV and ACMV, as well as 19dpi of ACMV (almost to 2-fold) induced the degradation process of SA. The transcript level of SA methylesterase was elevated at 19dpi in the ACMV samples to 6.6-fold. This enzyme converts MeSA to SA and its activity is feedback inhibited by SA, and MeSA is required for SAR signaling, in correlation with reduced expression of PR genes (Manosalva PM 2010).

It is evident that CKs are involved in various developmental processes, including transduction of nutritional signals and delay of senescence. Together with SA, plant-derived CKs stimulate defence responses to biotrophs; CKs activate the transcriptional regulator *ARR2*[251] by interacting with the SA-responsive factor *TGA3*[252] and by binding directly to the promoters of *PR1* and *PR2* positively modulating SA signaling. Therefore CKs can play a role in plant resistance to viruses; There have been reports that knock-down of *SAHH*[253], which mediates the methylation of the 5′ end of some viral RNAs such as PVX, CMV and TMV, led to enhanced plant resistance, since it is a prerequisite for the replication of these viruses. Interestingly, PVY, which does not require *SAHH*, was also unable to replicate in these transgenic lines with three-fold increase in CKs content in root exudates. The exogenous treatment with the CK in *P. vulgaris* infected with WClMV, resulted in the declined levels of viral RNA and CP, inconsistent with any significant effect on the SA-responsive genes, such as *PR1* and *NPR1*, and exogenous application of SA declined WClMV RNA and CP levels (Galis I 2004, Choi J 2011). Our Real-Time quantification of CK genes also confirmed the involved of this signalling pathway in immunity system; *CKX* is a FAD-containing oxidoreductase that catalyzes the degradation of cytokinins bearing unsaturated isoprenoid side chains. It catalyzes the oxidation of CKs. This gene was down-regulated at 12dpi in both viruses particularly in CBSV and up-regulated at 19dpi in both viruses, particularly in ACMV, involved in in controlling cytokinin levels in plant tissues (Werner T 2001). The transcript level of *AHK2_3_4* and *ARR-B* was also elevated in response to CBSV infection at 12 and 19dpi. *AHK*[254]s are play a principal role in perceiving the CK via a two-component phosphorelay system; the signal of phosphorylation is transduced from receptor to AHP[255]s in the cytoplasm. Additionally, ARR-B/type2 is a positive regulator of cytokinin signaling, functions in

interaction with TGA3 in the regulation of disease marker gene *PR1* against biotrophic infections in plants (Naseem M 2012). Whereas *ARR-A* was suppressed at 12dpi in the CBSV samples also at 19dpi in ACMV infection (unlike in CBSV). Notably, the transcript accumulation of *IPT* was repressed in both infections at the late stage of infection. There is also a significant interaction between CK and SA signaling, where CK signaling enhances the contribution of SA-mediated immunity in hormone disease networks, which seems to be a genome-wide transcriptional reprogramming (Naseem M 2012, Naseem M 2012). These all together might be integrated into MapMan functional annotation where showed that CK signal transduction and synthesis degradation were suppressed at 6dpi and then induced towards the end of the infection progression, in parallel with induced defence system.

On the other hand, GA may serve to facilitate defence to biotrophs or necrotrophs by partially modulating the balance between SA- and JA/Et-mediated signaling pathways. This hormone also promotes plant growth by inhibiting *DELLA* proteins, which are negative regulators of plant growth. Loss-of-function mutants of *DELLA* increase plant resistance to biotrophs, such as Pst DC3000, but exhibit hypersusceptibility to infection with necrotrophs. The gibberellin biosynthesis via ent-kaurene synthase was induced at 6dpi in response to both viruses. Ent-kaurene is the first cyclic diterpene intermediate of gibberellin biosynthesis in both plants and fungi. There have also been reports regarding the ent-kaurene oxidase, as a key factor in the biosynthesis of gibberellins that interacts with the P2 outer capsid protein of RDV[256]. Infected Rice with RDV exhibited a dwarf phenotype with reduced levels of ent-kaurene oxidase and *GA1*. The RNA-seq data of ACMV samples at 12 and 19dpi described the inhibited expression of ent-kaurene acid hydroxylase/oxygenase, which is consistent with dwarf phenotype and high viral load of ACMV-infected plants. Hypothetically, the interaction between P2 and ent-kaurene oxidase type proteins may interfere with the biosynthesis of phytoalexins, thus promoting viral replication (Kawaide H 1997, Zhu SF 2005, Robert-Seilaniantz A 2007).

Moreover, the MapMan analyses revealed a couple of induced and inhibited BR metabolism involved processes; The induced signal transduction via *BRI*[257] at 6 and 12dpi, in addition to *BZR*[258] at the early stage, 12dpi of CBSV and 19dpi of ACMV infection; The inhibited expression of *DWF1* and *DWF4*, thereby reduction of BRs among all the samples was calculated, similar to *DET2*[259] (which encodes a reductase and acts at the first step of the proposed biosynthetic pathway and CPD[260]). BRs are reported to be essential for plant basal immunity during compatible interactions with RNA viruses. For example, TCV, ORMV and TMV accumulated to higher levels in the *bak1-4* and *bak1-5* mutants than in WT plants. *BRI1* is a BR receptor, the LRR-RLK[261], which interacts with BAK1 upon brassinosteroid perception, initiating the signaling pathway involved in growth and development related processes. In potato, BRs reduced viral infection in starting plant materials at various stages of development until the second tuber generation, also declined TMV level and other biotrophs in tobacco plants (Choe S 1999, Nakashita H 2003, Bari R 2009, Ohnishi T 2012, Korner CJ 2013, Alazem M 2015). According to this study, it

seems that BR is involved in late-defence response against both RNA and DNA viruses, which was shown to be inhibited in general.

Et is involved in certain developmental stages, such as senescence, as well as in the defence response to necrotrophic pathogens. As previously reported, in *N. tabacum* plants resistant to TMV or TNV, *ACC*[262], the precursor of Et accumulates locally around necrotic areas, indicating a possible contribution to lesion formation. Mutants of the Et pathway such as *acs1*[263,] *erf106*[264] and *ein2*[265] were resistant to TMVcg, independent of the ACC application which enhanced TMVcg accumulation in treated plants. Although, Et may support symptom development in of CaMV infection and systemic movement of TMVcg, similar to CMV infection in cucumber. Likewise, according to this RNA-seq data, ACC synthase was suppressed among all the samples, except at 19dpi of ACMV infected sample, whereas ACC oxidase showed a very significant induction at 12 and 19dpi after reduction at 6dpi, which is correlated with ethane emission during PPD (Clarke SF 1998, Knoester M 2001, Sansregret R 2013, Vanderschurena H 2014, Alazem M 2015). Moreover genes specifying Et biosynthetic enzymes and signaling components such as EIN2[266] and ERF1 had differentially regulated their RNA levels. EIN2 was inhibited at 6 and 19dpi due to infection with ACMV, however its expression level slightly was increased (to 1.7-fold) at 12dpi, also it was suppressed by CBSV at 6dpi then induced at 12dpi, with increase to 1.2-fold expression at 19dpi. EIN2 acts downstream of ET receptors, and upstream of ethylene regulated transcription factors and recognized as a molecular link between previously distinct hormone response pathways; as it is required for cytokinin-mediated processes and implicates in cross-talk between ET, JA and other pathways. It is a central component in signaling pathways regulated by ET, and involved in various processes including development, plant defence, senescence, nucleotide sugar flux, and tropisms (Alonso JM 1999). Amongst the significant overlap between the CaLCuV expression profile and senescence-associated genes, EIN2 as the implicating enzyme of ET signaling in programmed cell death as well as the pathogen response was addressed (Buchanan-Wollaston V 2005, Ascencio-Ibáñez JT 2008).

Some viruses interfere with certain Aux factors (with the function in apical dominance) to manipulate their functions and subcellular localization therefore to promote their own replication and systemic spread, as it has been proven for TMV. In general, if a biotrophic infection induces Aux, the HR is usually down-regulated and the SA signaling pathway is repressed, which indicates a possible repressive role of Aux on SA. SA-mediated stabilization of the auxin signaling repressor AUX/IAA renders the plant host resistant to biotrophic infections. Aux/IAA proteins are short-lived transcriptional factors that function as auxin transporters, protein kinases and phosphatases, components of a ubiquitin-proteosome pathway, and transcriptional regulators (Liscum E 2002). The Real-Time expression of this gene was identified with 0.6- and 0.2-fold at 6dpi, 1.1- and 3.1-fold at 12dpi, 1.3- and 1.4-fold at 19dpi in CBSV and ACMV infection. Aux/IAA proteins were also shown to be down-regulated by PPV in *Arabidopsis*, as the 126 and 183 kDa replicase of TMV disrupts interacting Aux/IAA proteins, which leads to promoting disease development (Padmanabhan MS , Babu M 2008, Pierce EJ 2013). ILR1[267] is an

conjugate-amidohydrolase of IAA, including IAA-Leu and IAA-Phe. Thereby it functions in auxin metabolic process and peptide catabolic process (Ludwig-Müller J. 2011) and followed the same trend as IAA; suppressed at 6dpi (0.9-and 0.3-fold), and induced at 12dpi (2.1- and 20.7-fold) as well as 19dpi (1.6- and 4.2-fold) in CBSV and ACMV infected samples. On the other hand, increased auxin levels not only increase the concentration of JA but also enhance JA signaling, which in turn weakens the plant defence against biotrophic pathogens. Many viral infections result in aberrant phenotypes, such as stunting, leaf curl and loss of apical dominance, which resemble those of mutants with compromised Aux biosynthesis and/or signaling. For example, CMV and ToMV[268] infections of tomato cause tomato shoestring mosaic disease which has symptoms that resemble the phenotype of *wiry* mutants, where the levels of tasiRNAs[269] regulator of *ARF3*[270] and *ARF4* were reduced. The proven manipulation of ARFs by viruses accounts for the phenotypic defects in parallel with dysfunctions which often affect symptom severity and dissemination (Kazan K 2009, Jay F 2011, Naseem M 2012, Pratap D 2012, Yifhar T 2012, Alazem M 2015). This RNA-seq analyses detected auxin-responsive genes to be activated by infection, suggesting that symptom and disease progression was allowed to continue in infected *N. benthamiana*. At 6dpi, infected plants compared with mock were identified with higher expression level of *AUX1*, *IAA*, *ARF* and *GH3* whereas *SAUR* proteins were inhibited. Indeed, these auxin-responsive proteins remained up-regulated until next time point of infection. At 19dpi, only *GH3* was equally elevated in both CBSV and ACMV samples. At this stage, a slight induction of *ARF* expression in the CBSV samples and *SAUR* transcript level in ACMV infection was also observed. The rest of examined genes were notably repressed at this time point. MapMan analyses revealed that the Aux signal transduction was enhanced at 6dpi and suppressed at 19dpi in both CBSV and ACMV infection; however the transcript accumulation of Aux-degradation activity was higher in the ACMV samples at 19dpi. Altogether might have resulted in the different stunting symptoms in *N. benthamiana* infected with CBSV at 12dpi and ACMV at 19dpi.

Notably, all these hormones may exhibit some sequential accumulation in response to infection. Viral infection establishment is accompanied by interrupted signaling pathways, including those of phytohormones, causing misregulation of many host-genes expression leading to abnormal growth and development. Therefore the examining of hormone levels of infected plants with different viruses might lead us to formulate their general or specific role during host-virus interactions (Whitham SA 2006, Alazem M 2015). In addition, identifying the interplay between hormone biosynthesis and signalling pathways will help to determine the detailed mechanisms by which plants defeat or defeated by the infection at different stages of infection; starting with HR responses before symptom development towards the end with slight recovery (in the CBSV sample at 19dpi) or presumably PCD (in the ACMV sample at 19dpi).

4.2. Viral infection progression on defected defence system condition

4.2.1. The response of *RA4* plants to viral infection

The natural mutation of the *RDR1* gene (contains a 72-nucleotide insert with consecutive in-frame stop codons in the 5′ half of the *RDR1* open reading frame) in *N. benthamiana* results in extreme susceptibility to virus infection and hence serves as model system for plant-virus interaction studies. Yang *et al.* showed that transgenic *N. benthamiana* expressing Mt*RDR1* gene displayed enhanced resistance to TMV[271], TVCV, and SHMV[272] (tobamoviruses) but not to CMV and PVX and therefore suggested that the extreme susceptibility of *N. benthamiana* to a wide range of viruses is due to the lack of virus-inducible *RDR1* (Yang SJ 2004), hence inability of these plants to accumulate SA upon virus infection. NtRDR1 transgenic plants displayed no obvious differences in susceptibility to two different tobamoviruses (TMV-GFP and ToMV), but showed hypersusceptibility to non-tobamoviruses such as PPV, CMV, PVX and PVY (Ying X-B 2010, Hunter LJR 2013). Moreover it has also been shown that the expression of *RDR1* in tobacco is induced by the SA which thereof points to a link between RNA silencing and SA-mediated-resistance mechanisms such as HR and SAR (Xie Z 2001). *RDR1* might have a dual role, on one hand contributing to SA-mediated antiviral defence, and on the other hand suppressing the *RDR6*-mediated antiviral RNA silencing. *NtRDR1* enhances antiviral RNA silencing via silencing suppressor activity also suppressing *RDR6*-dependent S-PTGS, which may play indirect roles in plant defence via silencing-mediated regulation of cellular mRNAs encoding resistance factors (Ying X-B 2010, Hunter LJR 2013). The fact that down-regulation of *NtRDR1* in transgenic tobacco enhanced susceptibility to PVX and PVY is in contrast with elevated PVX and PVY accumulation and symptoms in *N. benthamiana* expressing *NtRDR1*. These results suggest that PVX and PVY are restricted in this tobacco by an efficient *RDR1*- and SA-mediated defence pathway, but this antiviral mechanism was not able to compensate for the suppression of the *RDR6*-mediated antiviral silencing in the *NtRDR1*–expressing *N. benthamiana* plants (Alamillo JM 2006, Ying X-B 2010). The dependence on *NPR1* of SA-induced *RDR1* expression provides additional evidence on major contribution of SA dependent *RDR1* induction in virus resistance. Knowing the increased *NtRDR1* transcript accumulation due to TMV infection in tobacco cultivar Xanthi (*nn* genotype), which could not be mediated by SA, since infected plants does not induce SA accumulation (Xie Z 2001). Moreover *AtRDR1* gene expression is regulated by various phytohormones including SA, JA, ABA and Et, which might imply its role in co-ordination of resistance to both biotic and abiotic stresses (Hunter LJR 2013). According to the qRT-PCR analyses, the highest point of expression level of *RDR1* in CBSV infection was at 6dpi, and in ACMV infection at 19dpi. That is in accordance with the phenotypic and viral load elucidated in natural dysfunction condition of this gene. *RDR1* seems to be more affecting the plant susceptibility to RNA virus at the early stage, followed by a decreasing level of CBSV content at 12dpi towards 19dpi when it is almost equal to wild-type. Whereas infection with the DNA virus is not affected significantly, as ACMV CP load stayed at the same level with mock and then as high as the wild-type at 12 and 19dpi. It is worth noting that exogenous application of methyl-JA and JA resulted in up-regulation of *TPS10*[273] and *RDR1*[274], respectively, confirming that the JA-dependent signaling monitors the expression level of *RDR1* (Hunter LJR 2013). Both related marker genes of SA and ABA

levels such as PR1a and NCED[275] were enhanced in the mutant *vtc1*[276] with ascorbic acid deficiency, which was resistant to infection by certain RNA viruses such as TMV and BaMV (Barth C 2004, Alazem M 2014, Alazem M 2015). In our findings, the NCED transcript level increased at 19dpi of ACMV infection, when the CBSV samples were shown to repress this gene in transcript level and enhanced the expression of PR1 to 2.1- and 4.4-fold. These results all together indicate the extensive role of *RDR1* in defence responses during viral infection progression more specifically of RNA virus, which are consistent with the SA and JA level together with ROS accumulation.

4.2.2. The response of *NahG* plants to viral infection

Accumulation of SA in the local tissue is required for SAR. The grafting experiments showed that tobacco leaves infected with TMV could transmit a SAR signal despite the presence of bacterial salicylate hydroxylase encoded by the *NahG* gene. By contrast, expression of this SA degrading enzyme in systemic tissue abolished SAR signal perception (Vlot AC 2008). *CPR1*[277] encodes an F-box protein which negatively regulates SA in Arabidopsis. The *cpr1* and *cpr5* mutants caused plants resistance to certain DNA viruses such as CaLCuV, as a result of the constitutive elevation of SA and its related genes (Ascencio-Ibáñez JT 2008, Baebler S 2011, Baebler S 2014, Alazem M 2015). Of a note, BaMV RNA levels were greater in the SA mutants *eds1* and *sid2-1* at 10dpi (Satoh K 2011, Alazem M 2014, Alazem M 2015), inferred that the phenotype of transgenic Arabidopsis *NahG* plants was identical to that of *eds1*, *pad4*, *eds5*, *sid2*, and *npr1* mutants even though they all had defects in SA signaling. After pathogen challenge, SA levels in mutants *eds5* and *sid2* were shown to be as low as those in *NahG*, accompanied by pathogen-induced PR1 expression and production of the phytoalexin camalexin, in contrast to *PR2* and *PR5* expression which were shown to be blocked in *NahG* plants (Van Wees SC 2003). Likewise, it has been shown that *NahG* potato plants exhibited faster onset of PVY^{NTN} viral infection and developed stronger PVY symptoms, when compared with non-transgenic lines. However, this difference was observed only in inoculated leaves at early stages of infection, and diminished with infection progression. In systemic leaves, no difference was observed between *NahG* and WT potato plants, in terms of viral titre or expression of defence-related genes (Alazem M 2015). All these previous studies seem to be consistent with the accumulated viral CP in particularly ACMV samples, which was lower than wild-types at all stages of infection. It also describes the susceptibility and phenotype that we observed in our experiments. The symptoms of *NahG*-CBSV infection at 12dpi were more severe and the viral load was measured to be significantly higher than wild-types. That perhaps was resulted by lower accumulation of SA in *NahG* plants, compromising in defeated defence system against the viral infection.

4.3. Viral infection progression on defected resistant mechanism

4.3.1. The response of *RC3a* plants to viral infection

Paralogs of *NRC1* such as *NRC2a, NRC2b* and *NRC3a* are required for hypersensitive cell death and resistance mediated by Pto. They are not essential for the cell death triggered by Rx and Mi-1.2, while *NRC2a/b* and *NRC3a* weakly contribute to the

hypersensitive cell death triggered by Cf-4 (Wu C-H 2015). We investigated the cell death phenotype induced by CBSV infection due to the *NRC3a* silencing that was not consistent with the observed low viral load at 12dpi. Whereas ACMV infection in these transgenic lines followed an opposite trend with the increasing viral load due to infection progress, except at 6dpi where a lower CP content relative to wild-type was observed. By using the NbRC3-TRV-VIGS transgenic approach, we aimed at observing the induced hypersensitive cell death during plant infection to RNA and DNA viruses. This resulted that the impact of *NRC3a* on infection with DNA virus is more moderate than RNA virus.

4.3.2. The effect of deficient *SGT1/RAR1/HSP90* chaperone on viral infection

Pathogen effector detection and recognition by R proteins activates a common defence mechanism including HR accompanied by oxidative burst, localised cell death and induction of defence-related genes, suggesting the convergence of signaling pathways. The *SGT1/RAR1/HSP90* complex, as a molecular chaperone assures proper folding and stability of R proteins therefore promote R protein recognition of pathogen elicitors. There have also been reports regarding the interaction between *SGT1* and *HSP90* that is required for the accumulation of Rx (a potato R protein), in addition to *RAR1* which may enhance this interaction by acting as a bridge and prompting ternary complex formation. Altogether, *SGT1/RAR1/HSP90/R* protein mediates downstream of MAP kinase activation followed by defence genes expression also hormone levels manipulation (Austin MJ 2002, Botër M 2007, Mandadi KK 2013). It is vital to understand the roles of Rx, *SCF*, and the *COP9* signalosome in other R gene–mediated resistance signaling pathways during viral infection progress, perhaps identifying their targets for plant defence by using different approaches such as VIGS knockout system.

One potential application of the TRV-VIGS approach is to provide a simple, rapid means of assigning and inducing gene silencing in a wide range of *Solanacae*. The TRV vector induces very mild symptoms, infects large areas of adjacent cells and silences gene expression in growing points. This is a RNA-mediated defence which is triggered by the virus vectors carrying host-derived sequence inserts, targeting both the viral genome, and the host gene corresponding to the insert. Therefore, the symptoms in the infected plant feature characteristic loss-of-function or declined-expression mutants in the host gene (Ratcliff F 2001). We aimed at examining the biological role of the *SGT1, RAR1,* and *HSP90* on *R*-mediated responding to CBSV and ACMV infection in the course of time. Following the symptoms development, the viral load in transiently suppressed *SGT1*, *RAR1*, *HSP90* and *SGT1/RAR1/HSP90* in *N. benthamiana* plants was compared with wild-types. In general, we have succeeded on using this approach as a silencing vector in *N. benthamiana*, since the three phenocopy replicates of PDS and all *RAR1, HSP90* and *SGT1* silencing vectors had the least variation between experiments in the proportion of plants that appeared with silencing phenotype. Although in ELISA analyses we also faced some outlying observations that were removed, might be consistent with the previous observation in Arabidopsis with high variation between replicates.

RAR1 and *HSP90* are both *SGT1* binding proteins, and all required to stabilize R proteins. Azevedo's detailed studies proved that SGT1 is necessary to stabilize the Rx resistance protein in its pre-activation state, similar to *RAR1* and *HSP90* (Azevedo C 2006). It has also been demonstrated that *SGT1* and *RAR1*, which are required for many R-gene-mediated HR, play an important role in the restraint of virus multiplication and the induction of PCD, which is a type of ER[278] and postulated to have a negative effect on the growth of biotrophic pathogens such as viruses. However, some studies suggest that PCD may not play a primary role in restraining viruses, ectopic expression of the Rx protein and the viral elicitor for ER (PVX CP[279]) induces PCD which restraint on pathogen multiplication and can be induced through distinct pathways (Liu Y 2002, Peart JR 2002, Komatsu K 2010). The mixture of silenced *RAR1/SGT1/HSP90* led to an interesting effect on induced infection with ACMV especially at 12 and 19dpi, whereas the viral load in the CBSV samples was measured to be as low as in mock which was particularly at 12dpi significantly lower than wild-types. As in experiment replicates, we used the same infiltration stock for all the plants, and then had chosen them randomly to inoculate with CBSV or ACMV. This is unlikely to consider any technical error as the reason for different responses, which might open potential for further detailed analyses in future to apply more precise methods than ELISA to detect the exact content of proteins with a higher standardization.

SGT1 is a conserved eukaryotic protein, interacting with different protein complexes and having multiple functions in various biological pathways. *SGT1* contains three distinct domains: the *SGS*[280] motif, a *TPR*[281], the CS motif[282]. The *SGS* motif of yeast *SGT1* mediates interaction with the LRR domains of *CYR1/CDC35*. Intriguingly, the TPR domain is dispensable in both resistance and auxin responses (Takahashi A 2003, Bansal PK 2004, Azevedo C 2006). The CS motif also interacts with the *CHORD-II* domain of *RAR1* and is a novel subunit of *SCF*[283]. This ubiquitin ligase complex mediates the degradation of multiple proteins involved in diverse signaling pathways through ubiquitin-proteasome pathway. Moreover, it is evident that *SGT1* is essential for Rx accumulation, also monitoring the stabilization of R proteins (Austin MJ 2002, Liu Y 2002, Azevedo C 2006). At mid-stage of infection, *SGT1* knockout resulted in higher accumulation of virus, relative to the wild-type, in consistency with the observed phenocopy which was sever particularly in CBSV. Silencing of *NbSGT1* results in reduced steady-state levels of Rx (Lu R 2003, Azevedo C 2006), which seems to be triggered by the infection progress of RNA (at 12dpi) and DNA viruses (at 12 and 19dpi).

NbRAR1 interacts directly with *NbSGT1* of the *SCF* ubiquitin ligase complex (Shirasu K 1999, Peart JR 2002). Both *NbRAR1* and *NbSGT1* associate with the *COP9* signalosome. The N gene plants that are knocked out for the expression of *NbSGT1*, *NbSKP1*, and the *COP9* signalosome are compromised in their resistance response to TMV (Austin MJ 2002, Azevedo C 2002, Liu Y 2002). *RAR1* contains two highly conserved zinc-binding domains called CHORD[284]-I and *CHORD-II*. There have also been reports regarding the *CHORD-I* of *RAR1* binding to the molecular chaperone *HSP90* and this direct association of *RAR1* with *HSP90* that might stabilizes R proteins. Also in

the absence of *RAR1*, R proteins can accumulate as a consequence of the *HSP90–SGT1* interaction (Hubert DA 2003, Takahashi A 2003, Bansal PK 2004, Bieri S 2004, Schulze-Lefert P 2004, Azevedo C 2006). The knockout *RAR1* in CBSV and ACMV infection represented a contradictory effect on the susceptibility of host to infection, as in both cases at 12dpi of infection the viral load was measured to be lower than in wild-types. At next stage, the viral content was as low or high as in wild-types in CBSV and ACMV infected samples respectively. This altogether was in contrast with the observed phenotype, since the CBSV infection showed more severe symptom in comparison, but ELISA measurement failed to present consistent observation.

A fine balance between *RAR1* and *SGT1* on *HSP90* is crucial to determine the fate of a R protein (Botër M 2007). Moreover accumulation of different types of *HSP*s such as *HSP101* has been reported as a host factor for efficient translation of the TMV genome which is accompanying enhanced tobamoviral infection similarly in TVCV and ORMV infections (Wells DR 1998, Whitham SA 2003). *HSP* protein family were also identified differentially regulated at 19dpi and more frequently in CBSV infection. $Hsp90^{285}$ is one of the most common chaperone proteins and stabilizes proteins against heat stress, and aids in protein degradation. This assists other proteins to fold properly, similar to *HSP70*. Other subfamilies such as *HSP20*s are evolutionarily related to alpha-crystallin and *HSP33*s are cytoplasmically localized proteins with highly reactive cysteines that respond quickly to changes in the redox environment (Craig EA 1989, Csermely P 1998, Maaroufi H 2013). In our experiments, the silenced HSP90 in *N. benthamiana* displayed very clear dominant infection more plausibly at 12dpi onwards, as it has been observed with faint and dead plants in both CBSV and ACMV infection, although the phenotype was more identical in infected plants with CBSV. Surprisingly, the ELISA reads was not in parallel with the visual observation, probably due to the failed leaves quality. The efficient function of HSP90 was also detectable in mixed infiltration study (data not shown), as the silenced *SGT1/HSP90* and *RAR1/HSP90* appeared with severe infection symptoms particularly more evidently in CBSV infection at 19 and 25dpi with necrosis and wilted leaves. A previous study showed that silencing *HSP90* resulted in greater reduction of Rx protein levels compared to those in *NbSGT1* silenced plants, suggesting that *HSP90* may also affect other processes, such as translation of Rx (Lu R 2003, Azevedo C 2006), and this is consistent with the dramatic loss in both RNA and DNA viral infected plants, even though the ELISA did not succeed with identifying the same output.

In total, as it is evident in tobacco *RAR1* and *SGT1* associate with the *COP9* signalosome, which is a multiprotein complex involved in the protein degradation through the 26S proteasome (Liu Y 2002). The least effective immune sensing R proteins were detected at 12dpi of infection, with the induced symptoms in deficient *HSP90*, *SGT1* and *RAR1* conditions. HSP90 forms a chaperone complex with *SGT1* and *RAR1* to stabilize client proteins, and the chaperone complex components contribute to ETI (Takahashi A 2003, Kadota Y 2012, Adachi H 2015). According to the expression pattern of genes of interest and this experiment, it is clear that at 12dpi of CBSV ETI is activated, similarly at 12 and 19dpi of ACMV infection. In addition, although the PCD phenotype of *RC3a*

could not be interpreted by ELISA measurement, *RDR1* and *NahG* plants appear with significant output. The comparative experiment of these mutant/transgenic with wild-type plants showed a stronger role of SA-dependent response to infection with RNA virus at mid-stage of infection.

4.4. Modulated oxidative activity during viral infection progression

4.4.1. Virus-induced oxidative activity

In-situ accumulation of superoxide (O^{2-}) and hydrogen peroxide (H_2O_2) are visually detectable with NBT[286] and DAB[287] staining procedures. DAB-taken up in infected leaves in relative to mock-leaves among wild-types and transgenic lines, is useful for determining the presence and amount of endogenous peroxidase activity as an indication of induced defence responding (Thordal-Christensen H 1997, Talarczyk A 2002, Deng X-G 2016). After exposure of target tissues to DAB, a strong DAB reaction was evident in detached infected leaves, which implies a peroxidase and oxidase activity. The present study was carried out to investigate the role of ROS metabolism in symptom development and pathogenesis in *N. benthamiana* plants upon infection with two viruses, CBSV and ACMV. In compatible plant–virus interactions, ROS-scavenging enzymes are crucially involved in the phytopathogenic response activation. Declining the antioxidant enzymes activity- which leads the increased ROS level- appears as a necessary element on infection establishment, through replication and spread of the virus. In ZYMV[288]-infected *Cucurbita pepo* and CMV-infected *Cucumis sativus plants*, speculation of oxidative activity showed that ROS-formation enhanced by virus-induced-peroxidation is necessary in infection establishment and symptom development such as mosaic and yellowing infected tissues (Riedle-Bauer M 2000). Hernández research on PPV infected resistant and susceptible cultivars of *Prunus armeniaca,* concluded that ROS activates defence-related genes and regulates the antioxidant enzymes which are important in determining the susceptibility or resistance to a virus (Hernández JA 2001, De Gara L 2003, Hakmaoui A 2012). While an alternative respiratory pathway in mitochondria invokes the plant adaptation process to environmental stresses, in chloroplast the reactive ROS production is elevated by an interrupted photosynthetic electron transport chain due to viral infection (Díaz-Vivancos P 2008, Hakmaoui A 2012, Deng X-G 2015, Kühn K 2015). This ROS oxidative activity occurs biphasically during both PTI and ETI; The first burst due to PTI is rapidly and transiently induced almost right after PAMP recognition and does not require protein synthesis, whereas ETI causes the massive second burst continuously after pathogen attacks, depends on *de novo* protein synthesis and regulates the HR cell death (Mur LA 2008, Segonzac C 2011, Adachi H 2015). Thus it could lead us to conclude the beginning of viral infection follows the PTI pattern followed by ETI with higher load of oxidative burst activity, since we observed the steady increased concentration of H_2O_2 accumulation due to infection progression in CBSV and ACMV infection relative to mock.

Moreover, this in-situ DAB-based H_2O_2-detection was also applied to detect the elicited antioxidant responses during infection progression in wild-type compared with

three transgenic lines including *RA4*, *RC3a* and *NahG* plants. The *LRR* mutation in *RC3a* plants similar to *RDR* and *NahG* transgenes plants partially negates the defence response of *N. benthamiana* to CBSV and ACMV. At all the studied time points, a stronger ROS activity in these transgenic plants compared to the wild-type, particularly at 19dpi was evident. For instance, introduction of the *NahG* gene ends up with degradation of SA into catechol, suppressed plant defences and increased lesion size, consequently results in the higher virus accumulation and systemically movement (Alazem M 2015). As in our analyses, *NahG* plants infected with CBSV and ACMV at 19dpi occurred with very significant DAB-uptake, and more severe dark lesions in CBSV leaves. These results match with the context of introducing the *NahG* into incompatible interaction between resistant tobacco and ToRSV[289], also between resistant potato and PVY (Baebler S 2014, Alazem M 2015). Reactive oxygen species, and in particular H_2O_2 has a critical role in perception and transmission of the signals during stress response in plants, in addition to essential role in peroxidase-catalysed modification of plant cell walls. These could result in strengthening the cell walls and thus obstructing the establishment of pathogenicity. ROS can lead to an irreversible protein oxidation through carbonylation, causing structural and functional modification, and H_2O_2 can hypothetically induce alternative respiration as secondary messenger of signal transduction pathway (Neill S 2002, Hakmaoui A 2012, Deng X-G 2015).

4.4.2. Differentially regulated ROS-scavenging genes during viral infection

Plant *MAPK*[290] cascade play a role downstream of pathogen perception, also function to transmit signals within the cell via differential phosphorylation (Malinovsky FG 2014). *MAPK* signaling cascade, including *MAPKKKα* and *MEK2*, is specifically involved in PCD during both Rx-mediated HR triggered by PVX and systemic necrosis induced by PlAMV[291] infection. However, that *MEK2* silencing in N-transgenic plants leads to the loss of PCD and allows the greater TMV RNA accumulation. This suggests that MEK2 is involved in the pathways leading to both PCD and the restraint of virus multiplication in the N-TMV system (Komatsu K 2010). Evident on the represented RNA of *MEK2* in CBSV and ACMV infected leaves at 6dpi which was 491- and 251-fold, and then 3.3- and 13.6-fold at 12dpi, decreased to 2.3- and 5.2-fold at 19dpi. In addition, tobacco NtMEK2 as an upstream *MAPK* kinase preferentially phosphorylates the *SIPK* and *WIPK*. Involvement of *SIPK, WIPK, NtMEK2* activation during the defence response to TMV and other pathogens has been proven. Two *MAPK*s, *WIPK*[292] and *SIPK*[293] have been reported activated in *NN* tobacco plants after infection with TMV. It has been also shown that *WIPK* was regulated at the transcriptional, post-transcriptional and translational level, in contrast with *SIPK* (Deng X-G 2016). Although in our study, *SIPK* also was enhanced in plants infected with CBSV at 19dpi (to 4-fold) also with ACMV at 12 and 19dpi (to 5.2- and 3.3-fold), the expression level of *WIPK* was more notable, as it showed up-regulation in all the samples; in CBSV 9.2-, 5.2-, 3.3-fold and in ACMV 2.8-, 46.8- and 4.8-fold at 6, 12 and 19dpi, respectively. Notably, the expression of other cascade member *MAP2K* was inhibited during infection with CBSV and only was enhanced in the ACMV samples at mid- and late stage of infection, with 4.8- and 2.6-fold. These *MAPK* cascade

components are involved in both PCD and the restraint of virus multiplication in the N-mediated HR to TMV. Additionally, they function in the restraint of virus multiplication in the Rx-mediated HR to PVX and in PlAMV-induced systemic necrosis (del Pozo O 2003, Jin H 2003, Komatsu K 2010).

ROS burst is an early biochemical consequence after plant sensing of pathogens infection, which function as a second messenger in phytohormone signaling and other important biological processes. ROS in particular H_2O_2 is generated by NADPH oxidases encoded by *RBOH* genes, and regulated by various cascades of kinases in transcription level, all together are very important for the plant responding network to biotic and abiotic stresses. Moreover, to utilize ROS as signaling molecules, non-toxic levels must be maintained in a delicate balancing act between ROS production and scavenging pathways (Deng X-G 2015, Deng X-G 2016). In tobacco, *SIPK, NTF4, WIPK*, and *NTF6* are characterized as pathogen-responsive *MAPK*s (Ren D 2006, Ishihama N 2011). Here, we studied the post-infection ROS scavenging enzyme activities by qRT-PCR. Amongst the genes of interest, the expression of some were significantly inhibited at early stage of infection; such as *NOA1* in both CBSV and ACMV, PAD4, SIPK, RBOHA/B in ACMV also *NTF6* in CBSV infection, together with *EDS1, WIPK, NTF4* which were 11-, 9.2-, 3.8-fold in CBSV and 3.1-, 2.8-, 2.5-fold in ACMV up-regulated. *PAD4* had a different behaviour in RNA and DNA virus infection as was 6.8- and 0.6-fold differentially expressed in CBSV and ACMV. Active oxygen species are indispensably involved in many vital processes of defence responses to pathogenicity. Massive AOS accumulation can be prompted by both systemic necrosis as well as HR-related necrosis involve PCD and result in hindering the pathogenesis pace (Thordal-Christensen H 1997, Mandadi KK 2013, Deng X-G 2015).

RBOH as a plant NADPH oxidase is involved in local and systemic resistance signaling against plant pathogens, and located on the plasma membrane. *RBOHD* and *RBOHF* in *Arabidopsis thaliana* and *RBOHA* and *RBOHB* in *N. benthamiana* facilitate ROS generation in response to pathogen attacks and PAMPs which regulated at the transcriptional and posttranslational levels, resulted by activated INF1 perception, also on MAPK-mediated up-regulation (Yoshioka H 2003, Zhang J 2007, Asai S 2008, Suzuki N 2011, Yoshioka H 2011). The RNA level of this enzyme was significantly elevated at 19 and 12dpi of ACMV and CBSV infection, respectively. Hakmaoui *et al.* elucidated the role of RBOH genes in the regulation of the alternative pathway in BR signaling, by knocking down *NbRBOHA* and *NbRBOHB* using a TRV-based VIGS system in *N. benthamiana* and concluded that *RBOHB*-dependent H_2O_2 accumulation is required for the BR-induced alternative respiratory pathway in response to viral infection with PMMoV (Hakmaoui A 2012, Deng X-G 2015).

ROS production through *RBOH* transcription is regulated by various MAPK signaling cascade, including *MEK2*. This is confirmed to be specifically involved in inducing PCD resulted by both PVX-triggered Rx-mediated-HR and PlAMV-induced systemic necrosis (Yoshioka H 2003, Asai S 2008, Komatsu K 2010). Typically, activation of *MEK1/2* mediates NADPH oxidase-dependent ROS generation in response to stresses, and the fact

that *MEK1/2* promotes ABA-induced stomatal closure by elevating H_2O_2 generation in conjunction with inactivating anti-oxidases (Jiang J 2008), was over-expressed in a very high level up to 490- and 251-fold in CBSV and ACMV at the early stage of infection. It was shown that expression of *NtMEK2DD*, a constitutively active mutant of a tobacco *MAPKK* upstream of WIPK and SIPK, prompts the HR-like cell death in tobacco, transactivation of *RBOHB*, and ROS burst also the activation of a subset of defence genes, demonstrating that the *NtMEK2-SIPK/WIPK* cascade, which is highly conserved in diverse plant species and controls multiple defence responses during plant disease resistance. This demonstrated that *MAPK* cascades are involved in transcriptional activation of *RBOHB* and may lead to the second burst, downstream of which *MEK2* acts to induce PCD (del Pozo O 2003, Komatsu K 2010, Deng X-G 2016). *MEK2* silencing in N-transgenic plants resulted in suppressed PCD and therefore higher TMV RNA accumulation, suggesting that *MEK2* is involved in the pathways leading to both PCD and the restraint of virus multiplication in the N-TMV system (del Pozo O 2003, Jin H 2003, Komatsu K 2010). Similarly, the *NPK1-MEK1-NTF6* pathway is another MAPK cascade involved in TMV resistance, as the results from VIGS-based silencing of other *MAPK* components *NPK1*, *MEK1*, or *NTF6* led to declined resistance mediated by N genes and Pto (Yoshioka H 2003, Asai S 2008, Deng X-G 2016). NTF4 is also another stress responsive component downstream of *NtMEK2* in the *MAPK* cascade, which can be activated by cryptogein, a proteinaceous elicitin from oomycetic pathogen *Phytophthora cryptogea*, while Tobacco recognition of cryptogein leads to rapid pathogen-induced HR cell death (Ren D 2006). Moreover, some *WRKY* transcription factors also appear to be regulated by *MAPK*s at the transcriptional and posttranscriptional levels in defence-related signaling pathways and positively or negatively regulate defence responses (Yang K-Y 2001, Eulgem T 2007, Tanaka S 2009, Ishihama N 2014). Interaction of *RBOHB* via the *MAPK-WRKY* pathway is required for ROS burst resulted; *MAPK*-mediated *WRKYs* phosphorylation accelerates WRKY-dependent *RBOHB* expression via binding to the cognate promoter of *W-box*. Four *WRKY*s, including *WRKY8* phosphorylated by *MAPK*s, bind to the W-box in the *RBOHB* promoter in plants and positively regulate the *RBOHB*. *WRKY8*, a group I *WRKY* transcriptional factor in *N. benthamiana*, is a substrate of pathogen-responsive *MAPK*s and is specifically phosphorylated by *SIPK* and *WIPK* in plants (Adachi H 2015).

4.4.3. Comparative oxidative process in different physiological conditions

The two cassava viruses, CBSV and ACMV, both cause notable losses in the tubers of cassava. Thereby at this step we made a relative comparison between superoxide stimulation during PPD and viral infection. The data obtained from proteomics analysis of cassava roots and RNA-seq of *N. benthamiana* leaves.

The expression level of typical oxidase enzyme *RBOH* was shown to be induced from the early stage and increase at later stage up to 1.5-fold in CBSV infection at 12 also 19dpi and 1.4- and 1.3-fold in the ACMV samples at 12 and 19dpi. Ascorbate/glutathione cycle enzymes, such as *APX* were differentially modulated in PPD; L-ascorbate peroxidase[294] protein level was strongly up-regulated 6 h after harvest. APX2 was

expected to be up-regulated at the mRNA level, but its levels did not change significantly during PPD progression (Vanderschurena H 2014). Ascorbate/glutathione pathways have limited capacity to scavenge ROS. Recent work using transgenic cassava storage roots over-expressing catalase and superoxide dismutase demonstrates that limiting the accumulation of ROS independently from the ascorbate pool can effectively decline PPD onset (Xu J 2013). In infected *N. benthamiana* the mRNA level of *APX* as well as glutathione peroxidase[295] was repressed relative to mock (in average of 0.7-0.8-fold), over time. While the increase or decrease of RNA abundance does not correlate with increased enzyme activities during early PPD or viral progression, similar to previous studies our study also revealed that levels of enzymes involved in the reduction of ascorbate and dehydroascorbate are not even significantly up-regulated, but clearly inhibited in expression level (Vanderschurena H 2014).

Number of peroxidases that were reported to be differentially regulated at the transcript level during PPD such as *PER12* and *PX3* had corresponding protein level changes (i.e., cassava4.1_010796m and cassava4.1_011662m) (Vanderschurena H 2014). Peroxidases orthologues in *N. benthamiana*[296] represented an induced expression pattern at 12 (1.75- and 1.15-fold in CBSV and ACMV infection) and 19dpi (1.6- and 1.2-fold in CBSV and ACMV infection) after a slight suppression at the early stage. This correlates with the trend we observed in the expression pattern of catalases[297], moreover the detected peroxiredoxin[298] expression level during viral infection progression showed a significant repression in all the samples, particularly in ACMV infection at 19dpi (0.4-fold). In addition, Glutathione *DHAR*[299] and *MDHAR*[300] levels were not significantly changed or even slightly down-regulated at 6 and 12 h after harvest (Vanderschurena H 2014). In CBSV and ACMV infected *N. benthamiana* expression level of *MDHAR*[301] was observed to be down-regulated to almost 0.8-fold at all time points.

Concisely, the expression analysis was carried out to investigate the role of ROS metabolism in symptom development and pathogenesis in *N. benthamiana* plants upon infection with two cassava viruses, CBSV and ACMV. At 6dpi they induced a strong defence response through up-regulation of *RBOH* which resulted in ROS generation, and was more detectable at 12 and 19dpi; ACMV conducted a better maintenance of high levels of *RBOH* regulators such as *MEK2*, *SIPK*, and *WIPK*. Moreover, surprisingly, there was a decline in oxidized glutathione and ascorbate level changes based on the RNA-seq data at all the stages of CBSV and ACMV infection. The antioxidant response and the extent of oxidative stress in *N. benthamiana* plants correlates to the severity of the symptoms elicited by either viruses of CBSV and ACMV; and the high capacity of ACMV-infected plants for stronger PCD and senescence, compared with CBSV-infected plants (Hakmaoui A 2012).

4.5. Metabolic effects of viral infection

Within host-pathogen interaction framework, many immune responses can be considered as metabolic defences that inhibit pathogen's replication and movement, in addition to variant metabolic pathways used by the pathogen to circumvent them, which

are counted as virulence strategies. These competitive metabolic pathways are crucial for immunity responses that are often focused on few essential nutrients, such a subset of metabolites we measured to get deeper understanding on the battle between pathogens and host at the metabolic interface. The leaf-associated pathogens modify biosynthesis pathways of primary and secondary metabolites such as phytohormones, carbohydrates, as well as amino acids and organic acids of leaves (Trouvelot S 2014). We applied one of the most reliable approaches for robust metabolite profiling, HPLC-MS and HPLC-UV/Vis which allows the quantification of various metabolites including a range of primary and secondary metabolites within a single extract. We took a snapshot of the complex regulatory incorporation of metabolites initially by using system-level metabolite profiling to obtain a global insight into correlation between all metabolites alteration and innate immunity in response to infection. Wide range and fundamental approach of data analyses is used by comparing the metabolites in quantitative level between treatments (infected leaves with CBSV and ACMV) and control (mock) sampled in the course of time. Followed by statistics assessment of significant differences, focus could go on individual metabolites alteration among different samples and time points, which can be built into networks including these correlative incorporations of gene and protein expression (Fernie AR 2004).

4.6. Applied network modelling and detailed analysis of plant-virus interaction

The host undergoes drastic changes in enzyme activities due to infection in order to maintain a metabolically active state; this means that in addition to upholding the metabolism of crucial metabolites also defence metabolites and their precursors have to be produced. The direct functional link between host metabolism and pathogen virulence is also supported by the metabolic could become a candidate target for anti-microbial strategies studies. Therefore large-scale quantification of intracellular metabolic fluxes is on the wish list of many researchers in functional genomics. Therefore well-established bioinformatics methods to reconstruct the metabolic network, based on DNA genome sequences are highly valuable for understanding the physiology of the pathogen, e.g., the biosynthesis of various required substrates to establish their pathogenicity. These methods are useful for simulating of the host survival capabilities and the influence of pathogens on host metabolome with the flux-balance approach (Orth JD 2010, Junker BH 2014, Durmuş S 2015).

In this systematic study, a targeted metabolic model of *N. benthamiana* was reconstructed according to *Arabidopsis* network model, which covered various metabolic pathways consists of a total of 155 metabolites and 111 reactions. Since the viral pathogenicity process triggers depletion, induction or modification of different metabolites in the host, enzymatic flux distribution can help us to understand the basics of infection mechanisms. Flux balance simulation approaches are applied here to decipher the plant-virus interactions, in carbohydrate metabolism, photosynthesis and defence pathways during infection with ACMV and CBSV. We predicted host metabolite network modulations during infection, to analyse response mechanisms and differentially regulated pathways. With this we hope to better understand the modified status of infected and

mock-inoculated responses in enzymatic flux level, from central carbon metabolism to fatty acid and amino acid metabolisms.

4.7. Modulated defence system in response to viral infection

The infected host may be attempting to divert metabolites such as those involved in immunity processes, such that lead to the biosynthesis of salicylate, jasmonate and chorismate. Potyviruses and Geminiviruses could influence host gene expression by altering signal transduction pathways through interactions with host protein kinases. The expression of defence-associated genes which are regulated in response to viruses in susceptible interactions, is controlled through signaling pathways that involve SA (Whitham SA 2003). Mid- and late stage of infection with both a RNA and DNA virus was accompanied by an inhibited activity of chorismate and salicylate pathways enzymes, and an induction in the jasmonate pathway, while sphingolipid pathway had not undergone notable changes.

Salicylic pathway flux activity in chloroplast through isochorismate-pyruvate lyase and isochorismate synthase were shown with a suppression of 12-15 and 17-20% in CBSV and ACMV infections at 12 and 19dpi, respectively. In addition to the chorismate enzymes such as 3-deoxy-7-phosphoheptulonate synthase, 3-phosphoshikimate 1-carboxyvinyltransferase, chorismate synthase, 3-dehydroquinate dehydratase, 3-dehydroquinate synthase, shikimate dehydrogenase, and shikimate kinase were simulated to be suppressed by 17 and 20% in CBSV and ACMV infection at 19dpi. The production of *PR*[302] proteins, as the main executioners of this part of plant immunity, was firstly identified in TMV infected tobacco plants. However later it has been shown that their synthesis can be induced by pathogens and also immune signals such as SA. A crucial step leading to the activation of the SA marker gene *PR1* and the establishment of SAR involves the SA-induced nuclear translocation of the ankyrin repeat protein *NPR1*, which interacts with *TGA* transcription factors. *NPR1* is required to counteract the negative regulator *SNI1*[303], as revealed by the re-establishment of SA-induced *PR1* expression and SAR in the *sni1/npr1* double mutant (Spoel SH 2012). Interestingly, our experimental data showed that the expression of *PR1* got inhibited in all the samples except in ACMV infected plants at 12dpi (to 12.7-fold), which was not in predicted correlation with RNA-seq expression values. Similarly, *PTI6*[304], which activates the expression of a wide array of PR genes and play distinct roles in plant defence (Gu YQ 2002), was also shown to be involved in viral infection responses in this study. In CBSV and ACMV infected plants, *PTI6* after the suppression in the early stage of infection (0.7- and 0.4-fold), was elevated at both 12dpi (1.5- and 14.5-fold) and 19dpi (1.7- and 3.3-fold) time points. This data confirms the interplay between PR1 and PTI6 in innate immunity response, which was more evident at 12dpi of ACMV infection. PAD4 as one of specifying SA biosynthetic enzymes, was addressed with induced expression in qRT-PCR data with 130- and 3-fold at 12dpi, 48 and 4.5-fold at 19dpi in the CBSV and ACMV samples respectively also 6.8 fold in the CBSV samples at 6dpi together with *SAG101* showing 2.4-, 46.2- and 9.2-fold in ACMV at 6, 12 and 19dpi as well as 7.1-, 3.6- and 2.5-fold in the CBSV samples at same time points. As the recurring theme which was also observed in the CaLCuV expres-

sion data analyses, the increased expression of the *EDS1/PAD4/SAG101* complex and downstream genes encoding biosynthetic enzymes, transcriptional regulators, and PR proteins and suppression of the *MPK4* signaling pathway provided strong evidence for the activation of a pathogen response through the SA pathway (Andreasson E 2005, Wiermer M 2005, Ascencio-Ibáñez JT 2008).

NPR1/NIM1 is reported to be involved in controlling of defence genes expression and downstream of SA, also emerged as a critical modulator of the second important plant defence pathway, which is triggered by the signaling molecule JA. NPR1 is involved in SA/JA antagonism by repressing genes of the JA biosynthesis pathway. also has been shown to be interacting with bZIP[305] family of transcription factors like *TGA2/3/6* (Després C 2000, Gao Q-M 2015). These are the associated signals of induced-HR at the site of TMV infection in *NN* plants triggers SAR through its key signal which is SA. Mutants with defects in *NPR1* fail to respond to various SAR-inducing treatments, displaying little expression of PR genes and exhibiting increased susceptibility to infections (Cao H 1997, Ndamukong I 2007). Surprisingly, NPR1 was significantly enhanced in the ACMV samples at 12 and 19dpi to 8.3- and 2.7-fold. TGA RNA level was observed at 4.2- and 11.6-fold in the CBSV and ACMV samples at 12dpi, while at 19dpi only ACMV induced the expression of this transcription factor to 3.7-fold. In addition to TGA factors, Myb and WRKY transcription factors have been shown previously to be induced during *N*-mediated resistance to TMV (Liu Y 2002). Our Real-Time experiment also confirmed that several transcription factors are involved in host defence response, such as MYC2 and WRKY which were differentially expressed during infection progression of CBSV and ACMV; MYC2 which is encoded by JIN1, is as a master regulator of most aspects of the JA signaling pathway in Arabidopsis, and coordinates JA-mediated defence responses by antagonistically regulating two different branches of the JA signaling pathway that determine resistance to pests and pathogens, respectively. It also functions in the regulation of crosstalk between the signaling pathways of JA and other phytohormones such as ABA, SA, GAs, and IAA (Kazan K 2013). Back to our study, expression of MYC2 was repressed in response to CBSV infection, but was 4.4- and 2.2-fold over-expressed in the ACMV samples at 12 and 19dpi, similar to the trend we observed for WRKY expression, as it was 8.6- and 3.1-fold in ACMV at 12 and 19dpi. Expression profiling in *Arabidopsis* reveals that WRKYs are the second largest family with leaf senescence-associated transcription factors, which justifies its vital role in the dark-induced senescence signal transduction pathways. WRKY22 participate in regulation of plant development, signal pathways in response to abiotic stress (Zhou X 2011). Altogether this group of immunity-inducing transcription factors seemed to be more responsive at 12 and 19dpi of ACMV infection. Another transcriptional activator, ERF1[306] positively regulates the expression of the group of genes involved in defence responses against pathogens and is repressed by MYC2. It seems to be a key integrator of ethylene and jasmonate signals in the regulation of ethylene/jasmonate-dependent defences transcription. ERF1 was significantly differentially expressed in response to infection with CBSV and ACMV; at 6dpi (1.18- and 0.7-fold), 12dpi (1.6- and 3.8-fold) and 19dpi (2.35- and 5-fold), indicating a possible

activation of transcription of JA signaling molecules. Concomitant functioning of JA and Et response pathways have been shown in previous studies to be required for induction of a plant defensin genes (Berrocal-Lobo M 2002, Lorenzo O 2004, Lorenzo O 2005, Pierce EJ 2013).

The flux redistribution along the jasmonate pathway in peroxisome of 19dpi-ACMV infected plants increased by 40%, whereas in the CBSV samples a 10% enhancement was observed; 12-oxophytodienoate reductase, 3-hydroxyacyl-CoA dehydrogenase, acyl-CoA oxidase, acetyl-CoA C-acyltransferase, acyl-CoA hydrolase, allene oxide cyclase, OPC8 CoA ligase, enoyl-CoA hydratase, hydroperoxide dehydratase, plus lipoxygenase in chloroplast. Jasmonate pathway enzymes were also affected by CBSV and ACMV at early time points; at 6dpi an increase of 7% in ACMV and at 12dpi an inhibition of 14% in CBSV.

Amongst the sphingolipid enzymes in ER[307], activity of 3-dehydrosphinganine and serine C-palmitoyltransferase showed 8 and 3% of increase in the CBSV and ACMV samples at 6dpi. As it is evident that accumulation of sphingolipids and phospholipids trigger the process of PCD through the generation of ROS followed by the onset of the HR during plant defence responses (Rojas CM 2014).

The slight suppression of flux balance of salicylic acid and chorismate together with induced jasmonic acid and sphingolipid enzymatic activities is not in high consistency with phytohormone profile. Although altogether strongly describe the involved elements and components in recovered and defeated conditions at 12 and 19dpi (in case of CBSV and ACMV infections).

4.8. Modulated energy metabolism response to viral infection

Induction of carbohydrate metabolism with concomitant repression of photosynthesis is a general protecting consequences against pathogenicity. Infection progression of both RNA and DNA viruses, trigger the pathophysiological dynamics in order to conserve energy through central carbon metabolism among others, glycolysis and gluconeogenesis, pentose-phosphate pathways, and carbohydrate metabolism, similar to the observation shown in response to Geminivirus SACMV (Pierce EJ 2013). Subsequent to biotic stresses, sugar starvation and metabolism disorders may be caused by pathogen attack, as it was also demonstrated that in rice infected by *Magnaporthe grisea* where sensitive cultivars had a lower level of metabolites involved in energy metabolism than cultivars resistant to that fungus (Baena-Gonzalez E 2010, Morkunas I 2014).

Glycosyltransferase as the essential protein families in biosynthesis of disaccharides, oligosaccharides and polysaccharides, were differentially regulated. These enzymes catalyse the transfer of sugar moieties from activated donor molecules to specific acceptor molecules, forming glycosidic bonds (Campbell JA 1997). According to the RNA-seq analyses sucrose synthase[308] and UGT73C[309] are up-regulated at 12dpi and 19dpi, especially in the CBSV samples more than 3-fold. UDPGT[310] (with transferase activity of hexosyl groups and involved in metabolic process) was also up-regulated at 12dpi in response to both viruses, whereas the expression values of HUGT[311], glgP[312] and malZ[313]

did not undergo significant change during infection. Amongst the enzymes that hydrolyse O- and S-glycosyl compounds, beta-glucosidase from Glyco_hydro1, Glyco_hydro_3 and Glyco_hydro_3_C subfamilies were 4.3- and 3-fold induced in CBSV and ACMV infection respectively, similarly beta-amylase and alpha-mannosidase[314] from Glycol_hydro and Glyco_hydro_38 subfamilies were slightly elevated in both viral infection conditions. Endo-1,3(4)-beta-glucanase from Glyco_hydro_81 subfamily was shown to be suppressed at 12dpi in both infections particularly in ACMV, by more than 2-fold, however it increased at 19dpi especially in the CBSV sample, whereas HPSE from Glyco_hydro_79n subfamily was more involved in the CBSV samples at 12 and 19dpi.

PR2/BG2/bglB is another essential element in carbohydrate metabolic process and systemic acquired resistance, mediated by salicylic acid with defence responses, also in viral life cycles (Zavaliev R 2013). Antisense inhibition of a tobacco BG2, which hydrolyzes callose is associated with plasmadesmatal gate modifications[315], and inhibits partially cell-to-cell viral movement while its over-expression appears to facilitate viral movement. Previously, its activity has been implicated in enhancing movement of RNA viruses such as TVCV, ORMV, PVX, CMV, and TuMV, all demonstrated elevated ß-1,3-glucanase activity increasing exponentially over the time course of infection also found to over-expressed by SACMV at all the time points, especially at 14dpi (3-fold) showing the highest expression (Whitham SA 2003, Pierce EJ 2013). Accordingly, the expression level of bglB in our qRT-PCR was equal to 3.6- and 2.7-fold in ACMV infected plants at 12 and 19dpi, as well as 1.2- and 1.7-fold in the CBSV samples at 12 and 19dpi. This can be counted as another evident on modified carbohydrate metabolism associated with defence system.

Another interesting gene 4CL[316] is involved in cell wall modification via lignification and monolignol biosynthesis. It ligates CoA[317] with hydroxycinnamic acids, and was reported be up-regulated at one stage in PPD progression, consistently, at 14 and 24dpi in response to infection with SACMV but then down-regulated at 36dpi. 4CL in Real-Time experiment was over-expressed in the ACMV samples at 12dpi (28.4-fold) and 19dpi (7.8-fold) as well as in the CBSV samples at 6dpi (2-fold), 12dpi (1.5-fold) and 19dpi (1.8-fold). These observations together indicate a synergistic interplay with ß-1,3-glucanase, in viral cell-to-cell movement via cell wall modifications. Up-regulation of ß-1,3-glucanase and callose breakdown strongly supports involvement in cell wall modification at the plasmodesmata location. That facilitates Geminivirus and Potyvirus cell-to-cell movement, associated with cell-wall loosening as a general conserved plant response to many RNA and DNA virus infections. This also correlates with the high viral load at 12dpi, and therefore higher induction of this gene and subsequent processes (Hu Y 2010, Pierce EJ 2013, Vanderschurena H 2014).

Among the carbohydrate metabolism fluxes, in chloroplast notable induced simulated activities of glycolytic enzyme glucose-6-phosphate isomerase was observed. This enzyme interconverts glucose-6-phosphate and fructose-6-phosphate, in both viral infections and all time points were observed to be induced; similar to PPP enzymes as the main generator of cellular NADPH such as 6-phosphogluconolactonase, glucose-6-

phosphate, 1-dehydrogenase, and phosphogluconate dehydrogenase (decarboxylating), where they showed double activity (increased to 212%) at 19dpi of ACMV infection, and 148% of increase at 12dpi, likewise to 132 and 136% in the CBSV samples. Moreover, in cytosol, activity of other glycolytic enzyme pyruvate kinase, together with mitochondrial pyruvate enzymes including dihydrolipoyllysine- residue acetyltransferase, and pyruvate dehydrogenase (acetyl-transferring) were induced to 134 and 146% at 19dpi in infected plants with CBSV and ACMV.

On the other hand, glycolytic enzyme fructose-bisphosphatase in cytosol was suppressed by 46 and 25% at 12 and 19dpi of ACMV infection also 16 and 14% in the CBSV samples. Similarly 6-phosphofructokinase in cytosol and chloroplast was inhibited by 34% at 12dpi of ACMV infection, and triose-phosphate isomerase by 17% in the CBSV samples at 6dpi. Pyruvate kinase at 19dpi decreased almost by 20% at 12dpi of CBSV and ACMV infections, similar to PRPP cytosolic enzyme ribose-phosphate diphosphokinase.

CHIB^{318} is also involved in amino-sugar metabolic process and polysaccharide catabolic process. In general seems to be implicated in resistance to jasmonate-inducing pathogens and particularly functions in defence against chitin-containing fungal pathogens. Ethylene induces high level of systemic expression of basic chitinase with expression increasing with plant age. Locally and systemically induced by JA and pathogens such as *Alternaria brassicicola* and *P. syringae*, particularly in case of HR (Thomma BP 1998, Apweiler R 2004). It was highly up-regulated in CBSV and ACMV infections; 814.4-, 15- and 39.5-fold in CBSV in addition to 55.6-, 1990.5 and 354.4-fold in the ACMV samples in the course of time.

To sum up, as pathogen infection cause releasing NADPH to the extracellular compartment leading to oxidative burst, Ca^{+2} in flux as well as accumulation of SA (Xiong Y 2009, Spielbauer G 2013), the suppression of these enzymatic activities leads to less delivered carbon to intermediate for the biosynthesis of amino acids, nucleic acids, lignin, and polyphenols. However it is noteworthy that carbohydrate metabolism positively regulates the expression of defence-related genes and elucidation of the flux distribution implies that the induced enzymatic activities at 12dpi of CBSV samples and 19dpi of ACMV infection are consistent with the slight recovery of CBSV samples at late stage of infection and late-induced thus defeated defence mechanism to ACMV infection, similar to TCA flux redistribution that reflects the re-prioritizing the maintenance and biosynthesis for the energy supply of infected plants.

Effect of viral infection on photosynthetic system

In order to establish a energy balance for fitness cost of defence responses, the up-regulation of defence-related pathways is compensated by the down-regulation of genes involved in other metabolic pathways, for example via genes involved in photosynthesis and chlorophyll biosynthesis that have been reported to be repressed upon challenge by infection as well as pathogen-derived elicitors (Rojas CM 2014). Therefore we expected that the induced carbohydrate metabolic processes and defence pathways in response to

the progression of RNA and DNA viral pathogenicity to occur together with inhibited photosynthesis. As we have addressed the simulated activity of Photosystem I and photosystem II, ATPase, ferrodoxin-$NADP^+$ reductase and plastoquinol-plastocyanin reductase to be declined by 11 and 45% at 12dpi, also at 19dpi by 18 and 20%, although ribulose-phosphate 3-epimerase at 19dpi was induced by 10 and 20% in CBSV and ACMV infection. Moreover the suppressed activity of RUBISCO, a key enzyme for carbon fixation events in the Calvin cycle, is identified here that might indicate the less provided sugars to create a defence-positive amplification loop or the oxygenase reaction leading to photorespiration (Rojas CM 2014).

This general suppression of photosynthesis may be either triggered by pathogen effectors or feedback regulation mediated by sugar signals. Regardless of the mechanism, down-regulation of bioenergetics processes (photosystem I and II fluxes and electron transport chain) presumably cause physiological changes associated with the disease symptoms also alleviates the energy expenditure associated with the up-regulation of other pathways that provide such energy, all due to the virus overtaking host defence-related pathways (Postnikova OA 2012, Rojas CM 2014).

Effect of viral infection on sugar biosynthesis and signaling

The required essential energy for effective plant responses to biotic and abiotic stresses is provided by sugar signaling system which regulates the defence genes. This referred as sugar- elevated immunity as a potential key part of plant immunity and indicator of defence system outcome, since for instance sugar importers determine the efficiency of plant–pathogen interaction (Bolouri Moghaddam MR 2012, Trouvelot S 2014). Sugars are referred to small carbohydrates such as mono/disaccharides including glucose, sucrose and fructose, and residues interconnected by glycosidic linkages to form oligo- and polysaccharides which are natural complex carbohydrates with biological regulatory functions (Albersheim P 1983, Trouvelot S 2014). It is well-established that leaf carbohydrate metabolism is involved in viral infection response, as the infected leaves decrease their photosynthetic rate and that result in reduced sugars concentration and starch accumulation (Goodman RN 1986, RSS 1987, Tecsi LI 1994, Tecsi LI 1994). Additionally, the defected functionality of plasmodesmata by viral movement proteins which can especially in plants with symplasmic loader feature influence the phloem loading process (Shalitin D 2000).

In tobacco, sucrose, glucose, and fructose induce the transcription of PR-protein including *PRQ* and *PAR1* in a SA-independent pathway. Whereas contrarily in Arabidopsis, sucrose or glucose trigger the expression level of different PR-genes such as PR2 and PR5, and their associated proteins through a SA-dependent pathway (Herbers K 1996, Thibaud MC 2004, Trouvelot S 2014). Sunflower infection with a necrotrophic fungus (*Sclerotinia sclerotiorum) in* cotyledon, resulted in 100, 85 and 20% declined level of sucrose, fructose and glucose, respectively. Similarly declined amounts of sugar were observed in tomato plants infected with *Botrytis cinerea* (Berger S 2004, Jobic C 2007, Morkunas I 2014). Here, we argue that it depends on the stage of the infection and its

severity, because in our study plants at the middle and latest stage of the analyses incremented the sugars levels and managed to somehow survive.

Content of glucose which triggers the expression of various PR genes dropped at 6dpi of both CBSV and ACMV infection. The induction of the defence-related genes is catalysed by HXK1[319] that is well-known as glucose sensor, similar to glycerol-3-phosphate which acts as an innate immunity signal in response to pathogenicity. RGS1[320] is another glucose sensor, located in the plasma membrane and plays a major role in the induction of extracellular glucose signaling, indicating its involvement in defence responses against rice blast fungus, for instance by stimulating the ROS synthesis (Morkunas I 2014). Moreover it is evident that decreased level of glucose subsequently caused the defeated innate immunity, HR and increased ROS production. However the increased glucose content at 12dpi of CBSV and 19dpi of ACMV infections also fits into these interactions. Sucrose is vital element as a stress-responding process with regulatory role in growth and development, and transporter of carbohydrates. This main product of photosynthesis whether in endogenous or exogenous form, functions as signaling molecule in plant innate immunity in rice and evidently in *N. benthamiana.* The accumulation of this carbohydrate declined at 6dpi in response to both infections with CBSV and ACMV, in parallel with defeated immunity signaling. Exogenous applying of sucrose to root before infection to *Fusarium* significantly induced expression of defence-related genes (such as PR1, PBZ1, PR5) in leaves to deal with *Fusarium* in lupin. This can be related to simulated accumulation of isoflavanoids and anthocyanins, important components of the defence system with the antimicrobial functionalities (Boddu J 2006, Gómez-Ariza J 2007, Bolouri Moghaddam MR 2012, Morkunas I 2014), at early and mid-stage of infection with ACMV and CBSV, the content of this carbohydrate was measured to be decreased relative to mock plants, which is consistent with the progressive patho-genicity of this virus and therefore defeated immunity signaling. Although a notable increase of sucrose concentration inside the phloem has been reported due to CMV infection, and intriguingly this was also obvious in the phloem content of leaves with no-viral-load, determined that the affected phloem sugars load is not associated with viral particles content. Sucrose is localized in the vacuoles, perhaps CMV infection may cause a irregular sugar localization in the phloem cells (Shalitin D 2000). And that might be in consistency with high sucrose load at 19dpi of ACMV infected plants. Sugar signaling and sugar level regulating enzymes such as invertases, including CWI[321]s are referred as PR proteins with function as extracellular enzymes to break sucrose into glucose and fructose. This can be considered as a potential indicator of priming process, that is pre-prepared respond without actual defence responses therefore can profit from the declined actual defence cost (Roitsch T 2003, Conrath U 2011, Bolouri Moghaddam MR 2012). Intriguingly, the observed pattern in fructose content is very much similar to glucose, where it also decreased at 6dpi and increased at 12dpi in both infections, in addition to ACMV at 19dpi. There have also been other reports regarding the reduced sugars and starch content due to virus infection which enhance the starch hydrolase and inhibit ADP-Glc pyrophosphorylase activities (Shalitin D 2000).

4.9. Effect of viral infection on phenolic biosynthesis and signaling

Flavonoids are hydroxylated phenolic compounds, synthesized via the phenylpropanoid pathway. They function as transcriptional regulators of growth, and as secondary antioxidant defence substances in plant tissues exposed to different abiotic and biotic stresses. Moreover they are located within centre of ROS generation in the nucleus of mesophyll cells, and involved in monitoring the activity of IAA-oxidase with different effects based on their chemical structure. Under these conditions the activity of ROS detoxifying enzymes may be significantly reduced in the chloroplast, which in turn up-regulates the biosynthesis of ROS scavenging flavonoids (Buchanan-Wollaston V 2005, Fraser CM 2011, Kumar S 2013). Some of these phenolic compounds also seem to serve in defence of plants against invading pathogens such as insects, bacteria, fungi, and viruses. Chlorogenic acid[322] is an abundant polyphenolic natural product abundant in a variety of plants, which displays many of the typical biological properties of polyphenolics in diet, such as antioxidant and anti-carcinogenic effects, and inhibition of DNA damage (Lee 2010). Plant BAHD acyltransferases constitute a large family of acyl CoA-utilizing enzymes whose products include small volatile esters, modified anthocyanins, as well as constitutive defence compounds and phytoalexins (D'Auria JC 2006). In Real-Time experiment only slightly showed to be up-regulated in ACMV infection for 1.3-fold, while it was suppressed in other time points and CBSV infection. In the present study the content alteration of some phenolic compounds belonging to caffeoyl quinate ester group were demonstrated to be significant during viral pathogenicity progress, as it has been shown to be effective against inhibiting the growth of both gram-positive bacteria including *Bacillus* (Cetin-Karaca H 2011). This includes trans-5-caffeoylquinic as an extremely active compound which in phosphate buffer (pH 7.4), first isomerizes to trans-4-caffeoylquinic acid and then to trans-3-caffeoylquinic acid by intramolecular acyl migration. The accumulation of these phenolic compounds was declined at 6dpi relative to mock, and then notably increased at 12 and 19dpi. There have been reports on exposing to UV light, which led trans-3, -4-, and -5-caffeoylquinic acids to undergo cis/trans isomerization and formed cis isomers, dependent on the pH of the matrix, the incubation temperature, and independent of metabolic enzymes (Xie C 2011). consistent with the ROS production pattern and other HR signaling immunity, the content of trans-4-caffeoylquinic acid and trans-5-caffeoylquinic acid had dropped at 6dpi of CBSV and ACMV infection, and then both of them were notably increased at 19dpi, while it is also noteworthy that at 12dpi only accumulation of trans-5-caffeoylquinic acid was significantly induced due to CBSV infection.

4.10. Modulation of transporting system during viral infection

As we mentioned above and according to the literature, induced activity of carbohydrate transporters might be counted as one of the up-regulated pathways which provides energy for cost of fitness in response to pathogen infection. Transporters were also enriched in the fraction of modulated protein families. Many genes increased the transcript levels during infection. They include a number of several sugar and ABC[323] transporters, and peptide, amino acid and cation transporters, many of which are

associated with metal transport of H^+ exchange. Sugar transporters are a subfamily essential for transmembrane transporting and as an integral component of membranes with a role in binding and transport of various carbohydrates and organic alcohols (Yan N 2015). In the RNA-seq data, the expression pattern of SLC2A8[324] and FAR[325] (the sugar transporters in our study) showed a slight up-regulation (1.3-fold) at 19dpi in both CBSV and ACMV infected samples also at 12dpi of ACMV infected plants. Another group of transporters, ABC transporters consist of at least two conserved regions, a highly conserved ABC and less conserved TMD[326] region. With ATP binding and ATPase activity they energise diverse biological systems by providing essential nutrients through their import systems. They are also involved in the extrusion of noxious substances via their export systems are, as well as in exporting the extracellular toxins and the targeting of membrane components (Saurin W 1999). ABC transporter family include several defence and/or stress-associated genes, for example, Cf-2 resistance gene-like, PAD3, PAD4, PR1, PR5, and BG2. We confirmed the involvement of several of these family members to viral infection response with qRT-PCR. These proteins were also among the most significant responding families at 12 and 19dpi. Additionally, AA[327] transporters including UNC-47[328] and MTR[329], proline transporters and amino acid permeases (McIntire SL 1997) were also identified among the proteins involved in infection at 12dpi in CBSV and ACMV infected plants. Amongst those that identify the over-activated enzymatic elements due to defeated defence process, transporters Mcf1 and PXA1 were simulated to be induced in CBSV and ACMV infection at 19dpi, although with higher activity in the ACMV samples, like the suppressed activity of PEP/phosphate translocator at 12dpi (by 12 and 15%) and 19dpi (by 17 and 20%) of CBSV and ACMV infections.

The efflux transporter ALF5**,** member of MATE[330] family is essential for the root protection from inhibitory compounds and environmental toxins. In our experiments the RNA level of ALF5 was elevated to 2.6-, 4.5- and 2.8-fold in ACMV infected plants at 6, 12 and 19dpi, while in the CBSV samples was induced to 3.8-fold at early stage of infection then repressed at mid- and late stage. According to the previous studies both transcriptional and translational fusions of ALF5 to the β-glucuronidase reporter gene show that ALF5 is expressed strongly in the root epidermis, a tissue in direct contact with the external environment. Moreover, the Arabidopsis *alf5* loss-of-function phenotype resulted in sensitivity to compounds that fail to affect the growth and development of wild-type plants (Diener AC 2001).

4.11. Effect of viral infection on amino acid and fatty acids biosynthesis and signaling

Common pathways are emerging that can explain the susceptibility of cells of the adaptive immune system to control circuits activated by amino acid deprivation and/or by-products originated from amino acid catabolism. The existence of critical enzymes regulating these metabolic processes offers an opportunity for targeted intervention aimed at relieving the negative effects on the immune system. It looks like cells of the innate immune system might differ from each other in their ability to activate either single or multiple catabolic pathways (Grohmann U 2010). During viral pathogenesis interaction, it

is very likely that macromolecules degradation and metabolites mobilization activities undergo a significant differential expression. It has been reported that inoculation with an avirulent strain of *Pseudomonas syringae* pv. tomato DC3000 (*hrp*$^-$mutant) revealed increased accumulation of tryptophan, tyrosine, lysine, valine, and leucine, and a decrease in glutamate in comparison with mock-inoculated plants, while inoculation with the virulent strain caused higher accumulation of isoleucine, threonine, alanine, phenylalanine, tyrosine, and glutamine (Ward JL 2010, Rojas CM 2014). Here we conducted the amino acid profiling in order to understand how RNA and DNA might reconfigure their susceptible host metabolism. It is likely that particular amino acids, especially those that are accumulated or declined during infection progress, are involved in plant defence. The accumulation of some amino acids or their metabolic byproducts triggers resistance responses against pathogens that can be dependent or independent of SA- and ROS-mediated defence pathways (Rojas CM 2014).

Intriguingly it was evident that glutamine is the most affected amino acid in response to infection to both viruses. Glutamine is non-essential amino acids which may become essential due to physiological stress or critical infection. As a major nitrogen and energy supply for immune system cells, play vital role in protein synthesis as well as cytokine. It is extensively catabolised through glutaminolysis pathway to generate primarily glutamate as well as aspartate, alanine, lactate, pyruvate and CO_2 in the immune cells. Up-regulation of several genes encoding enzymes involved in glutamate/glutamine metabolism due to senescence has been proven, such as two glutamate decarboxylase genes, two glutamate receptor proteins and three cytosolic glutamine synthetases. Adding 4 and 8% glutamate to a glutamine-/glutamate-free diet induced the delayed-type hypersensitivity responses in rats recovering from methotrexate treatment. Glutamine which is showed an increased level in the ACMV samples at 12 and 19dpi also CBSV at 19dpi relative to mock, is a major source of glutamate, regulates the synthesis of glutathione, a tripeptide crucial for defending cells from oxidative stress (Li P 2007, Olive AJ 2016).

Moreover, it has been shown that genes encoding amino acids degrading enzymes such as lactoylglutathione lyase and proline oxidase which are involved in threonine degradation and proline degradation respectively were induced due to senescence (Buchanan-Wollaston V 2005, Grohmann U 2010), consistently we observed the significant reduction in proline content at 6dpi and induction at 19dpi, but our data did not demonstrate any difference between threonine content in infection and mock. Proline has a vital role in wound healing and recovery, mediated by the immune system. In addition, it is utilized in various cellular mechanisms with responsibility for protecting lymphocytes from apoptosis, arousing cell growth and inducing antibody production. H_2O_2, as a major product of proline oxidation functions as a signaling molecule and a cytotoxic agent for pathogenic response (Li P 2007), which subsequent to suppressed level, failed to respond at the early stage of infections with CBSV and ACMV, besides of being activated at the late stage.

Alanine, whose content was also declined at early stage of infection with CBSV and ACMV, also influences the function of the immune system in mammalians as a significant

substrate for the hepatic synthesis of glucose. It play a vital role by Inhibition of apoptosis and is involved in inhibition of protein degradation in immunocytes, similar to prompting antibody production, probably through cellular signaling pathways (Li P 2007). Similarly, content of serine which plays an important role in one-carbon unit metabolism was declined at 6dpi. It involves in the synthesis of glycine, ceramide and phosphatidylserine, which are structural components also signaling molecules of cell and function in response to an immunological challenge. There is evidence that supplementation with of 2mM-serine to the culture medium prevented apoptosis, increased cell growth and enhanced antibody production in lymphocytes (Li P 2007). Similarly, deficient asparagine due to exogenous asparaginase used to be counted as an immunosuppressive, although now we know it might also contribute in glutamine depletion, since asparaginase compromise the glutaminase activity. There is evidence that adding of 2mM- asparagine to the culture medium decreased apoptosis and stimulated cell growth (Li P 2007), which is consistent with the presumably induced PCD at mid-stage of ACMV infection.

Meanwhile, flux of fatty acid metabolism which represents a convergence point for defence signaling cascades involving SA, JA and NO[331] through simplified fatty acid synthesis**,** was late-enhanced by 59 and 91% at 19dpi of CBSV and ACMV infection, however it was suppressed by 14% in the CBSV samples at 12dpi and induced by 7% in the ACMV samples at 6dpi, which all together indicate the defeated innate immunity against infection at the early stage.

The defence cascade supplied by photosynthesis, transmitted by signal transduction, and mediated by carbohydrate metabolism, photorespiration, amino acid, fatty acid and sphingolipid metabolisms and transporters. Elucidation of redistributed fluxes among all these biological processes describes the detailed characterization of the mechanisms and components underlying the responses to infection progression of RNA and DNA viruses. These reactions trigger the oxidative burst and ROS production also accumulation of SA followed by the onset of HR. That in case of infection with CBSV at 12dpi results is slight observed recovery at 19dpi, in contradictory the comprehensive negative regulated fluxes are observed when they no longer needed, presumably following the defeated processes in the ACMV samples at 12 and 19dpi. Although this simulation does not necessarily measure the regulatory changes of enzyme activities and might not be in parallel with the metabolite concentration and transcript/protein contents, it is demanding for explicit description of the modulated pathway elements due to physiological perturbation.

Overview on results

What organelle? Accumulated evidence suggests that among cellular organelles, chloroplasts are a common target by plant viruses (Li Y 2016), where we indicate the most suppressed enzymatic activities occur, together within cytosol. Most of the down-regulated photosynthetic, glycolytic, phosphoribosyl pyrophosphate, salicylate and chorismate fluxes correlate with the severity of chlorosis at 12 and 19dpi of ACMV also 12dpi of CBSV infection. That extends the essential functionality of chloroplast in defence response together with peroxisome, as were the organelles the most induced

enzymatic reactions were modulated, along the pentose phosphate pathway, jasmonate, pyruvate, fatty acid biosynthesis and transporters pathways. On the other hand, according to our RNA-seq analyses in both viral infections the ribosome showed to be induced at 6dpi, besides transcriptome level in ER proteins was enhanced at 12 and 19dpi, peroxisome was highly induced at 12dpi of CBSV infection. Therefore all together may be correspondent with the possibility of modifying activity of certain primary metabolites via the leading enzymatic activity in particular organelle, for engineering resistance or developing tolerance against viral pathogens.

Concisely, although the associated fluxes were highly activated at the late stage of both viral infections, progressive pathogenicity was compromised with decreased sucrose and glucose content. Sucrose is considered as signaling molecule in plant innate immunity, while decrease in glucose content leads to defeated immunity, HR and increased ROS production. Elucidation of redistributed fluxes among all these biological processes describes the detailed characterization of the mechanisms and components underlying the responses to infection progression of RNA and DNA virus, ranging from pre-symptoms stage towards infection stability and dominance. The defence cascade is supplied by photosynthesis, transmitted by signal transduction, and mediated by carbohydrate metabolism, photorespiration, amino acid, fatty acid and sphingolipid metabolisms and transporters. At the early stage activity of fructose-1, 6-bisphosphatase was suppressed in infection with RNA virus, ribose-5-phosphate isomerase showed induction in CBSV and suppression in ACMV. Additionally, at mid-stage plastoquinol-plastocyanin reductase decreased in both infections, and more dramatically in ACMV infection. Glucose-6-phosphate isomerase in chloroplast induced activity in CBSV (higher at 12dpi) and ACMV (very high at 19dpi) like pyruvate kinase in cytosol at 19dpi (higher in ACMV). Trios-phosphate isomerase in cytosol activated at mid and late stage of both viruses, though more at mid-stage. In addition, at the late-stage of both infections induced level of major nitrogen and energy supply for immune system, glutamine and the wound healing and recovery element, proline were identified. However, it is noteworthy that they were decreased at the early stage together with alanine which is involved in inhibition of apoptosis and protein degradation. For instance, *PAD4* showed an opposite trend in response to infection with RNA and DNA virus infection, and *RBOH* was significantly elevated in both viruses but at different stages of infection, or *BARD1* which was highly repressed in CBSV infection but highly induced in ACMV infection at the early stage. Besides, the investigated viral infection process confirmed a network of cross-talk between phytohormones that alters among SA-JA/Et signalling balance. This is maintained by promoting systemic signals of defence against biotrophic pathogens SA, and a combination of JA and Et against necrotrophs. We also observed that almost all JA biosynthesis and signalling genes as well as JA content were enhanced at early and late stage of ACMV infection and late stage of infection with CBSV. Similarly, the associated enzymatic activities in peroxisome was induced at 19dpi (higher in ACMV), after a slight suppression in CBSV at 12dpi and induction in ACMV at 6dpi. On the other hand, SA biosynthesis, signaling and content was induced at mid-stage of CBSV infection also at mid- and late stage of ACMV infection, while the biosynthetic flux simulation in

chloroplast did not show any change before symptom appearance and showed decreased activity at mid and late stage of both infections. That seems hypothetically the coordination of viral entity with symptoms severity and stage of infection might cause biotrophic or necrotrophic behaviour of pathogen. These reactions trigger the oxidative burst, ROS production, and also accumulation of SA followed by the onset of HR. As one of the different features of these interaction phases, assessment of oxidative burst processes confirmed that *MEK2-SIPK* cascade is trans-activating with *RBOHB, NTF4/6* and *WIPK*, playing an essential role in response to virus infection. That in case of infection with CBSV at 12dpi resulted in presumable slight recovery at 19dpi. In contradiction, the comprehensive negative regulated fluxes are observed when they are no longer needed, presumably following the defeated processes in the ACMV samples at 12 and 19dpi. Furthermore, these data combined with metabolic modelling helped us to coordinate all central metabolic enzymes, including those not affected by significant gene expression changes, and undetectable products by chemical assays. Altogether contribute to identifying the details of a complex metabolic adaptation of Potyvirus and Geminivirus.

5. Conclusion

The diverse alteration during compatible viral pathogenicity leads to a complex modification on infected host immunity system and requires a global and detailed overview on the infection process. Here, we combined different approaches of systems biology to study this broad spectrum of changes that utilize an integrated analysis of plant-virus interaction during infection progress. This comparative, integrated systems biology of plant-virus interaction progression enables a more rapid and precise understanding of modulated activities and complex cooperative networks among a large variety of physiological processes in response to infection. Omics-based analyses and metabolic network modelling are here applied to describe the complex interplay between cassava viruses and immune system of *N. benthamiana*, suggesting a novel overview on the zigzag model of plant immunity system, which explain the presumption that depending on the infection stage, each of these viruses might show ET and PTI as well as HR. This reconstructed infection process proposes a functional approach to investigate the transcriptome and metabolome alteration associated with the characteristic disease development induced by CBSV and ACMV in the compatible host.

Also, the recent gold standard for time series transcriptome analyses RNA-seq was applied not only to gain a global insight into transcripts alteration, but for detailed identification of altered defence associated genes and biological processes during infection progression. Elucidation of the cross-talk among hormone pathways determined the modulated JA or SA responsive genes at different stages of infection. Similar to other elements of signal transduction, energy metabolism and ubiquitin proteasome system are also described in this study. That helped us to elucidate the details of infection process focusing on effect of different types of viral genomes. Furthermore, the overlap with emission of ethene during PPD, also calcium and calmodulin-binding regulation cascades in senescence process are identified. Then Results of respective bioinformatics on the modification of several key pathway genes were validated in Real-Time. More particularly, the expression pattern of functional TIR/CC-NB-LRR class of R genes for resistance to pathogens, besides of transactivation of various signaling component was described and functionally confirmed. Moreover, *HSP90* in a chaperone complex with *SGT1* and *RAR1*, and contributing in ETI was identified as the main feature of differentiating response to CBSV and ACMV infection, particularly at mid-stage of infection. In addition to the cell death phenotype induced by CBSV, infection and high accumulation of ACMV due to the *NRC3a* silencing was demonstrated. We also observed that SA deficiency that causes more severe symptomatic phenotype in RNA virus infection, as the extensive role of *RDR1* in defence responses during viral infection progression. That is also consistent with the phenocopy and ROS accumulation in *NahG* plants, which also weakens basal defence and SAR resulted by defective SA biosynthesis process. Reactive oxygen species was also triggered differently by innate immune response due to this presumed hypothesis. We also observed that localized accumulation of ROS steadily increased due to infection progression of CBSV and ACMV relative to mock. It led us to conclude that the beginning of viral infection follows the PTI pattern

followed by ETI with higher load of oxidative burst activity. This demonstrated that *MAPK* cascades are involved in transcriptional activation of RBOHB and may lead to the second burst, downstream of which *MEK2* acts to induce PCD.

From another point of view, early stage of infection with CBSV and ACMV accompanied by suppression of glutamine, serine, alanine and proline also SA, suppressed carbohydrate, amino acids, lipids and energy metabolisms. Whereas at the mid-stage of infection with CBSV and ACMV, suppressed SA and chorismate fluxes (in chloroplast), enhanced SA content and the expression of *EDS1* and *PAD4*, replication, repair and signal transduction were observed. And enhanced glutamine, induced pyruvate kinase (in cytosol) and JA fluxes (in peroxisome and chloroplast), suppressed SA and chorismate fluxes (in chloroplast), transcription and translation metabolisms was shown at the late stage of infection with CBSV and ACMV. Depending on the availability of control methods, the future studies on resistant crop development might be complemented in any of the transcript, metabolome and enzymatic flux directions. On the other hand, the infected plant surveillance was observed to be through induced accumulation of nitrogen and sulphur compounds, calcium and calmodulin-binding regulation cascades. However, it finally occurred with repressed oxidase phosphorylation and defeated defence system at the early stage of infection. Thereby providing the sufficient nutrient for the susceptible host might be considered as a practical approach, as already the soil fertility and mining in sub-Saharan Africa is one of the main causes of crop productivity loss. This might be integrated into upgrading the immunity system of plant against pathogens, particularly CBSV and ACMV. Those directly target the carbohydrate resources such as tubers of cassava as a vital staple food, is propagated vegetatively by stem cuttings mainly providing carbohydrates, deficiency of protein. Efforts have been made to increase and secure sustainable cassava production through improving agronomic practices and reducing biotic and abiotic stresses {Vanderschurena H, 2014 #214}, as well as resistance screening and genetic engineering. That could be a motivation for this sort of integrative and comparative analysis. Here, outlining various biological and computational techniques opens a new generation of analyses to simultaneously explore the mystery of host–virus interaction system globally and in details. Taken together, analyzing and modelling of transcripts and metabolites of plant during compatible viral infection process, led us to extrapolate the role of key pathway and elements affecting the viral disease progression. In contrast with the linear regression of expression data obtained from RNA-seq and qRT-PCR, the flux balance analyses is not necessarily in parallel with the metabolite concentration and transcript/protein contents. Howeverو it is demanding complementary for explicit description of the modulated pathway elements due to pathogens infections. This unravels the fundamental and detailed description of ongoing interplay during infection progress at different levels of systems biology of infected host.

Appendix

Supp1. Solutions

S1.1. Inoculation buffer

(Norit buffer): 0,05M sodium/potassium phosphate buffer (pH 7.0), 1mM EDTA, 5mM DIECA, 5mM thioglycolic acid, (Store at -20°C)

S1.2. Agrobacterium culture media

(50mL, YEB), 100 µl MgSO4, 100 µM MES[332], 125 µM acetosyringone

S1.3. Infiltration buffer

MS (PH 5.6), 10 mM MES, 10mM MgCl2, 150 mM acetosyringone

S1.4. Extraction buffer

0.05 M Tris, 0.06 M sodium sulfite (pH 8.5), (Store at 2-8 °C)

S1.5. Coating buffer

(1L, pH 9.6), 1.59 g sodium carbonate (Na2CO3), 2.93 g sodium bicarbonate (NaHCO3), 0.20 g sodium azide (NaN3), (Store at 2-8 °C)

S1.6. PBS [333]

(1L, pH 7.4), 8.0 g sodium chloride (NaCl), 0.2 g monobasic potassium phosphate (KH2PO4), 1.15 g dibasic sodium phosphate (Na2HPO4), 0.2 g potassium chloride (KCl), 0.2 g sodium azide (NaN3), (Store at 2-8 °C)

S1.7. PBS-Tween (PBST)

PBS + 0.5 ml Tween20 per litre, (Store at 2-8 °C)

S1.8. Conjugate buffer

PBST + 2% PVP + 0.2% Albumin from chicken egg white (Sigma-Aldrich A5253), (Store at 2-8 °C)

S1.9. Substrate buffer

(1L, pH 9.8), 97 ml diethanolamine, 0.2 g sodium azide (NaN3), 1 mg/ml freshly added 4-Nitrophenyl phosphate disodium salt hexahydrate (Sigma-Aldrich 71748-5G), (Store at 2-8°C)

Supp2. Protocols

S2.1. TAS-ELISA

- Dilute specific antibody in coating buffer at the recommended dilution
- Add 200µl to each well of the microtiter plate
- Cover the plate and incubate at 37 °C for 2- 4 h
- Wash plate with PBS-Tween, three times
- Add 200 µl of 2% skim milk in PBS-Tween to each well
- Cover the plate and incubate for 30 min at 37°C
- Remove blocking solution
- Extract samples 1/20 (w/v) in extraction buffer by grinding young leave tips in extraction buffer
- Add 200 µl aliquots of the test sample to duplicate wells
- Cover the plate and incubate overnight at 4 °C
- Wash plate with PBS-Tween, three times
- Add 200 µl of the MAb conjugate buffer (in appropriate dilution) to each well
- Cover the plate and incubate at 37 °C for 2- 4 hours
- Wash plate with PBS-Tween, three times
- Dilute RAM-AP 1:1000 in conjugate buffer, i.e., 20µl in 20 ml buffer. Add 200µl to each well
- Cover the plate and incubate at 37 °C for 1 hour
- Wash plate with PBS-Tween, three times
- Add 200 µl aliquots of freshly prepared substrate buffer to each well
- Cover the plate and incubate at 37 °C for 30, 60 and 90 min
- Assess results by Spectrophotometric measurement of absorbance at 405nm

S2.2. Bacterial culture

A. tumefaciens cells were grown overnight in YEP-induction medium containing appropriate antibiotics (kanamycin, 50 mg/ml and Rifampicin, 25 mg/ml), incubated at 28 ºC on a shaker-incubator (250 rpm) for about 16 hours. The cultures were centrifuged at 6000rpm for 10 min at room temperature, re-suspended in MMA to adjust the final OD_{600} to 1, and then appropriate clones were mixed equally (final volume to 50 mL) into two sterile 250 ml flasks and incubated without shaking for 2-4 hours, the top 40mL of infiltration culture were injected by syringes to the top three leaves of plants, in the temperature 18-20 ºC.

S2.3. cDNA synthesis reaction

17.8 ddH_2O, 5 µl dNTPs (of 10mM stock), 0.75 µl oligo dt18 primer (of 10µm stock), 0.75 µl random hexamer N6 primer (of 10µm stock), 0.2 µl M-MLV RT, 1 µl RNA ≈ 100ng

S2.4. Quantification of phytohormones

Plant material was weighed (around 200 mg) and frozen with liquid nitrogen and samples were kept at -80˚C until used. For phytohormone analyses, leaf material was extracted with 1.0 ml of methanol containing 40 ng of D6- jasmonic acid (HPC Standards GmbH, Cunnersdorf, Germany), 40ng D4-salicylic acid (Sigma-Aldrich), 40ng D6-abscisic acid (Santa Cruz Biotechnology, Santa Cruz, U.S.A.), and 8 ng of D6- jasmonic acid-isoleucine conjugate (HPC Standards GmbH, Cunnersdorf, Germany) as internal standards. The homogenate was mixed for 30 min, ground with the help of stainless steel balls (3mm) in a Paintshaker, and centrifuged at 14,000 rpm for 10 min at 15 ºC. The supernatant was collected. Chromatography was performed on an Agilent 1200

HPLC system (Agilent Technologies, Waldbronn, Germany). Separation was achieved on a Zorbax Eclipse XDB-C18 column (50 x 4.6 mm, 1.8 µm, Agilent). Formic acid (0.05%) in water and acetonitrile were employed as mobile phases A and B respectively. The elution profile was: 0-0.5 min, 10 % B; 0.5-4.0 min, 10-90 % B; 4.0-4.02 min 90-100 % B; 4.02-4.5 min 100 % B and 4.51-7.0 min 10% B keeping a flow rate of 1.1 mL/min.. The mobile phase flow rate was 1.1 ml/min. The column temperature was maintained at 25 ºC. An API 5000 tandem mass spectrometer (Applied Biosystems, Darmstadt, Germany) equipped with a Turbospray ion source was operated in negative ionization mode. The instrument parameters were optimized by infusion experiments with pure standards, where available. The ionspray voltage was maintained at at -4500 eV. The turbo gas temperature was set at 700 ºC. Nebulizing gas was set at 60 psi, curtain gas at 25 psi, heating gas at 60 psi and collision gas at 7 psi.

Multiple reaction monitoring (MRM) was used to monitor analyse parent ion → product ion: m/z 136.9 →93.0 (collision energy (CE)-22 V; declustering potential (DP) -35 V) for salicylic acid; m/z 140.9 →97.0 (CE -22 V; DP -35 V) for D4-salicylic acid; m/z 209.1 →59.0 (CE -24 V; DP -35 V) for jasmonic acid; m/z 215.1 →56.0 (CE -24 V; DP -35 V) for D6- jasmonic acid (D6-JA); m/z 263.0 →153.2 (CE -22 V; DP -35 V) for abscisic acid; m/z 269.0 →159.2 (CE -22 V; DP -35 V) for D6-abscisic acid; m/z 322.2 →130.1 (CE -30V; DP -50V) for jasmonic acid-isoleucin conjugate; m/z 328.2 →130.1 (CE -30V; DP -50V) for D6- jasmonic acid-isoleucine conjugate (D6-JA-Ile); m/z 225.1 →59 (CE -24V; DP -35V) for 11/12-hydroxy jasmonic acid (OH-JA); m/z 338.1 →130.1 (CE -30V; DP -50V) for JA-Ile hydroxylated form (12-OH-JA-Ile); m/z 352.1 →130.1 (CE -30V; DP -50V) for 12-carboxy jasmonic acid-isoleucine conjugate (12-COOH-JA-Ile). Both Q1 and Q3 quadrupoles were maintained at unit resolution.

Analyst 1.5 software (Applied Biosystems) was used for data acquisition and processing. Linearity in ionization efficiencies were verified by analyzing dilution series of standard mixtures. Phytohormones were quantified relative to the signal of their corresponding internal standard. For quantification of OPDA and OH-JA, the internal standard D6-JA was used applying experimental-determined response factors of 1.0 and 1.0 respectively. For 12-OH-JA-Ile and COOH-JA-Ile quantification, D6-JA-Ile was used as internal standard applying an equivalent response factor of 1.0 in both cases (Vadassery J 2012).

S2.5. Quantification of amino acids

Around 200mg of fresh leaves were weight and freeze-dried until constant weight. Amino acids were extracted with 1 ml of methanol (as for phytohormone extraction), ground with the help of stainless steel balls (3mm) in a Paintshaker, and centrifuged at 14,000 rpm for 10 min at 15 ºC and the resulting supernatant was diluted in a ratio of 1:10 (v:v) in water containing the 13C, 15N labelled amino acid mix (Isotec, Miamisburg, US). Amino acids in the diluted extracts were directly analysed by LC-MS/MS. The analyses method was modified from a protocol described by Jander et.al. (2004). Chromatography was performed on an Agilent 1200 HPLC system (Agilent Technologies, Boeblingen, Germany). Separation was achieved on a Zorbax Eclipse XDB-C18 column (50 x 4.6mm, 1.8µm, Agilent Technologies, Germany). Formic acid (0.05%) in water and acetonitrile were employed as mobile phases A and B respectively. The elution profile was: 0-1min, 3%B in A; 1-2.7min, 3-100%B in A; 2.7-3min 100% B and 3.1-6min 3% B in A. The mobile phase flow rate was 1.1 ml/min. The column temperature was maintained at 25°C. The liquid chromatography was coupled to an API 5000 tandem mass spectrometer (Applied Biosystems, Darmstadt, Germany) equipped with a Turbospray ion source operated in positive ionization mode. The instrument parameters were optimized by infusion experiments with pure

standards (amino acid standard mix, Fluka, St. Louis, USA). The ionspray voltage was maintained at at 5500 eV. The turbo gas temperature was set at 700 °C. Nebulizing gas was set at 70psi, curtain gas at 35psi, heating gas at 70psi and collision gas at 2psi. Multiple reaction monitoring (MRM) was used to monitor analyte parent ion → product ion: MRMs were chosen as in Jander et.al. (2004) except for Arg (m/z 175 →70), Lys (m/z 147 →84), Orn (m/z 133 →70), and Gly that was detected nonfragmented (m/z 76 →76). Both Q1 and Q3 quadrupoles were maintained at unit resolution. Analyst 1.5 software (Applied Biosystems, Darmstadt, Germany) was used for data acquisition and processing. Linearity in ionization efficiencies were verified by analyzing dilution series of standard mixtures (amino acid standard mix, Fluka plus Gln, Asn and Trp, also Fluka). All samples were spiked with 13C, 15N labelled amino acids (algal amino acids 13C, 15N, Isotec, Miamisburg, US) at a concentration of 10ug of the mix per mL. The concentration of the individual labelled amino acids in the mix had been determined by classical HPLC-fluorescence detection analyses after pre-column derivatization with ortho-phthaldialdehyde-mercaptoethanol using external standard curves made from standard mixtures (amino acid standard mix, Fluka plus Gln, Asn and Trp, also Fluka). Individual amino acids in the sample were quantified by the respective 13C, 15N labelled amino acid internal standard, except for tryptophan, asparagin, and ornithine: tryptophan was quantified using 13C, 15N-Phe applying a response factor of 0.42, asparagin was quantified using 13C, 15N-Asp applying a response factor of 1.0, ornithine was quantified using 13C, 15N-Lys applying a response factor of 1.0 (Jander G 2004, Crocoll C 2016).

S2.6. Quantification of flavonoids and caffeoyl ester

Around 200mg of fresh leaves were weight and freeze-dried until constant weight. Flavonoids were extracted with 1 ml of methanol (as for phytohormone extraction), ground with the help of stainless steel balls (3mm) in a Paintshaker, and centrifuged at 14,000 rpm for 10 min at 15 ºC and the resulting supernatant was analysed by HPLC-UV (Agilent HP1100 Series, Agilent Technologies, Waldbronn, Germany) equipped with a C-18 reversed phase column (Nucleodur Sphinx RP, 250 x 4.6 mm, 5 µm particle size; Macherey-Nagel, Düren, Germany). The mobile phase consisted with of 0.2% formic acid (v/v) (solvent A) and acetonitrile (solvent B) used in gradient mode at a flow rate of 1mL min-1 at 25°C. The gradient was as follows: 10-22% B (12 min), 22-100%B (0.1 min), 100% B (1.9 min), and 10% B (4 min). The eluent was monitored by a photodiode array detector at 330 nm. Caffeoyl quinates were quantified based on an external standard curve of an authentic standard of trans-5-caffeoylquinic acid applying a relative molar response factor of 1.0. The compounds were identified based on UV visible absorption and on mass spectra from LC-MS analyses on a Bruker Esquire 6000 IonTrap mass spectrometer (LC conditions were the same as for HPLC-UV analyses) in comparison to the identified metabolites in the literature (Clifford MN 2003, Clifford MN 2008).

S2.7.Quantification of free sugars

A 50 µl aliquot of the methanolic extract for phytohormone analyses (200mg fresh weight in 1mL of methanol) was diluted in a ratio of 1:10 (v:v) in water. Sugars in the diluted extracts were directly analysed by LC-MS/MS. Chromatography was performed on an Agilent 1200 HPLC system (Agilent Technologies, Boeblingen, Germany). Separation was achieved on a HILIC-HPLC-column (apHera NH2 Polymer; 15 x 4,6mm, 5µm, Supelco). Water and acetonitrile were employed as mobile phases A and B respectively. The elution profile was: 0-0.5min, 80%B in A; 0.5-13min, 80-55%B in A; 13-14min, 55-80% B in A and 14-18min, 80% B in A. The mobile phase flow rate was 1.0 ml/min. The column temperature was maintained at 25°C. The liquid chromatography was coupled to an API 5000 tandem mass spectrometer (Applied Biosystems,

Darmstadt, Germany) equipped with a Turbospray ion source operated in negative ionization mode. The instrument parameters were optimized by infusion experiments with pure standards (D-(+)-glucose, D-(-)-fructose, sucrose, all Sigma-Aldrich). The ionspray voltage was maintained at at -4500 eV. The turbo gas temperature was set at 600 °C. Nebulizing gas was set at 50psi, curtain gas at 20psi, heating gas at 60psi and collision gas at 5psi. Multiple reaction monitoring (MRM) was used to monitor analyte parent ion → product ion: m/z 178.8 →89.0 (collision energy (CE)-10 V; declustering potential (DP) -60 V) for D-(+)-glucose; m/z 178.8 →89.0 (CE -12 V; DP -60 V) for D-(-)-fructose; m/z 340.9 →59.0 (CE -46 V; DP -80 V) for sucrose. Both Q1 and Q3 quadrupoles were maintained at unit resolution. Analyst 1.5 software (Applied Biosystems, Darmstadt, Germany) was used for data acquisition and processing. Individual sugars in the sample were quantified by external standard curves generated with dilution series of authentic standards (all from Sigma-Aldrich).

Supp3. Figures

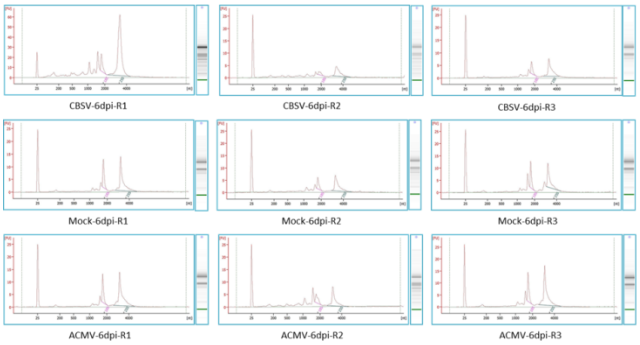

Samples	RNA Area	RNA Concentration	rRNA Ratio [25s/18s]	RNA Integrity Number (RIN)
CBSV-6dpi-R1	429.2	166 ng/µl	6.4	7.8
CBSV-6dpi-R2	55.2	21 ng/µl	4.4	6.8
CBSV-6dpi-R3	72.7	28 ng/µl	2.7	8
Mock-6dpi-R1	80.1	31 ng/µl	2.3	8.6
Mock-6dpi-R2	62.8	24 ng/µl	2.7	7.9
Mock-6dpi-R3	83.1	32 ng/µl	1.6	7.9
ACMV-6dpi-R1	83.4	32 ng/µl	2.5	9
ACMV-6dpi-R2	75.3	29 ng/µl	2.5	7.7
ACMV-6dpi-R3	103.4	40 ng/µl	2.6	8.5

Figure S1. Representative plant RNA electropherogram different time points; Degraded RNAs appear as a smear at low-molecular weights, whereas intact total RNA show sharp 28S and 18S peaks; x-axis is time(sec), y-axis is fluorescence, and the first peak is for marker (Gassmann). The integrated data analyses pipeline on the instrument will also render the electrophoretic data into a gel-like picture for users more accustomed to traditional gel electrophoresis. The table summarizes the criteria of the example samples (obtained at 6dpi) assessed by Bioanalyzer.

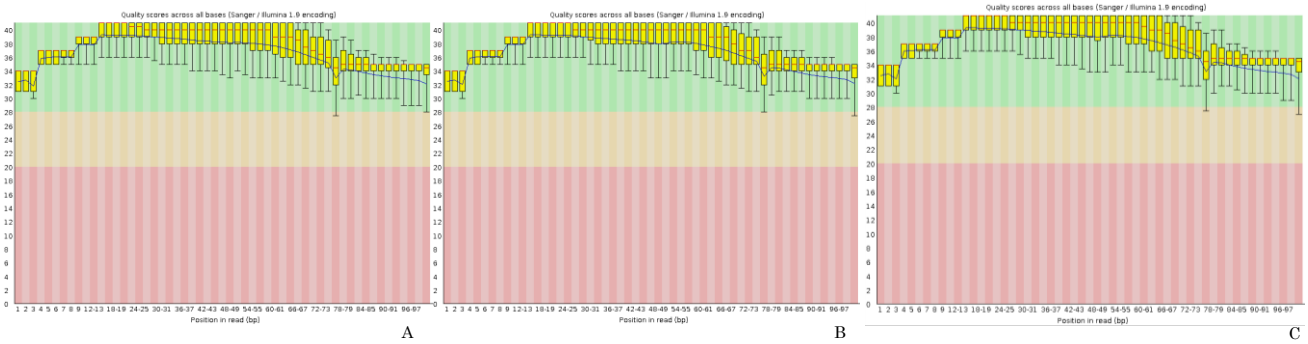

Figure S2. FastQC per base sequence quality plot; The plot summarized the base quality at each base position across all reads. The y-axis shows the quality scores, and the yellow boxes represent the interquartile range (25-74%) of base quality values for each base position. The green, orange and red background colouring indicates good, reasonable and poor quality respectively (forward reads obtained from A: Mock, B: CBSV, C: ACMV at 12dpi)

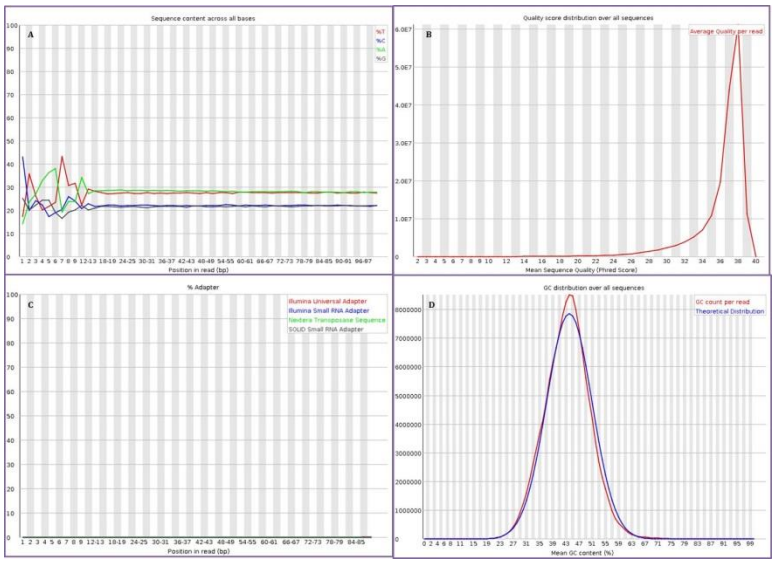

Figure S3. FastQC analyses plots; **A:** per base sequence content plot shows the first 13-base positions with sequence-specific bias typical for Illumina RNA-seq reads. The x-axis is the position in read and y-axis shows the percentage of each nucleotide. **B:** Per sequence quality score plot shows the distribution of reads' mean qualities, neither of our reads showed mean quality less than 38, as it represented in plot B, 60 million read content showed average quality of 38-40. **C:** Overrepresented sequences plot shows the adaptor content of the retrieved reads. The x-axis is the position in read and y-axis shows the percentage of each adaptor. **D:** Per base GC content plot shows the frequency and possible contamination. In this roughly normal distribution the central peak corresponds to the overall GC content of the underlying genome (forward reads obtained from Mock at 12dpi).

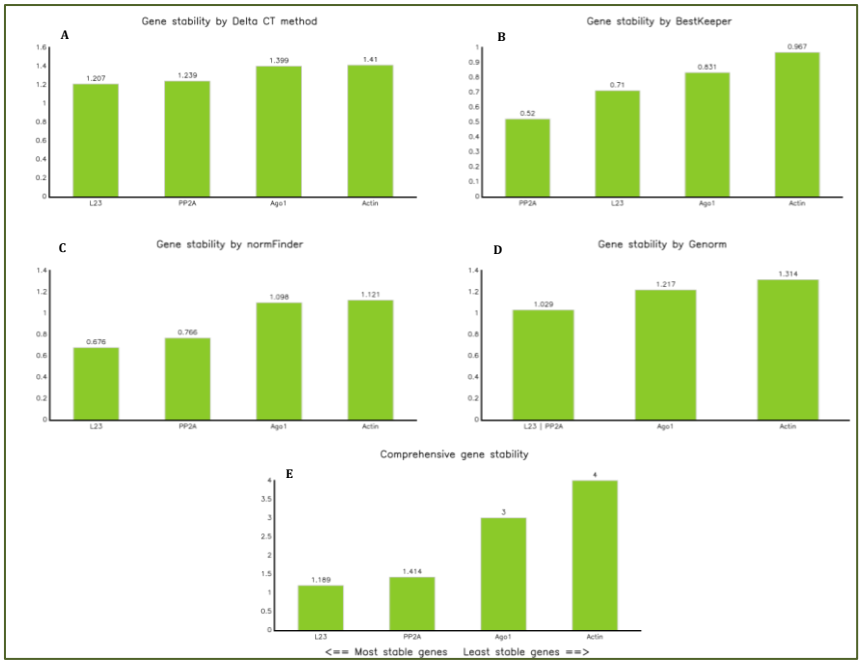

Figure S4. Determination of most stable reference gene: L23, PP2A, Ago1 and actin; Determination of Real-Time PCR efficiencies of reference genes, according to different algorithms such as Delta CT (Fig. S4A), BestKeeper (Fig. S4B), NormFinder (Fig. S4C) and Genorm (Fig. S4D), we found L23 as the most stable endogenous standard gene to apply for normalization of the target genes and verify their RNA-seq expression pattern (Fig. S4E).

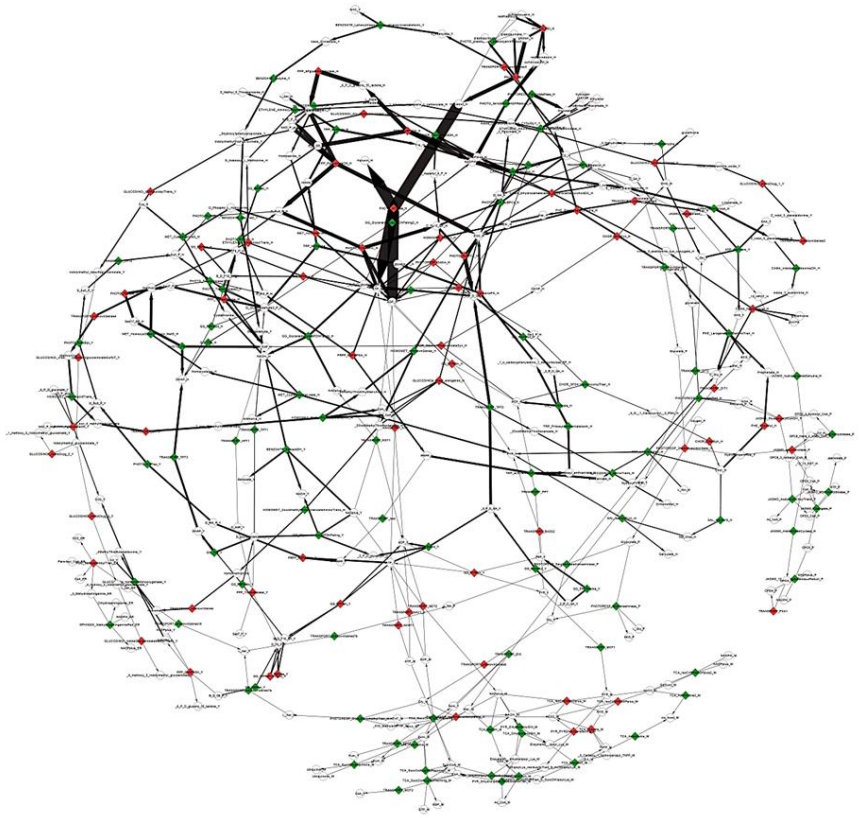

Figure S5. Metabolic network of *Arabidopsis thaliana* (Fieselmann A 2016)

Supp4. Tables

Filename	Basic Statistics	Total Sequences	Sequences flagged as poor quality	Sequence length	%GC
A_R1.fastq	pass	1.41E+08	0	101	43
A_R2.fastq	pass	1.58E+08	0	101	43
B_R1.fastq	pass	1.66E+08	0	101	44
B_R2.fastq	pass	1.66E+08	0	101	44
C_R1.fastq	pass	1.76E+08	0	101	43
C_R2.fastq	pass	1.76E+08	0	101	43
D_R1.fastq	pass	1.58E+08	0	101	42
D_R2.fastq	pass	1.58E+08	0	101	42
E_R1.fastq	pass	1.78E+08	0	101	44
E_R2.fastq	pass	1.78E+08	0	101	44
F_R1.fastq	pass	1.78E+08	0	101	43
F_R2.fastq	pass	1.78E+08	0	101	43
G_R1.fastq	pass	1.77E+08	0	101	42
G_R2.fastq	pass	1.77E+08	0	101	42
H_R1.fastq	pass	1.36E+08	0	101	42
H_R2.fastq	pass	1.36E+08	0	101	42
I_R1.fastq	pass	1.6E+08	0	101	44
I_R2.fastq	pass	1.6E+08	0	101	44

Table S1. Overview of sequencing data [334]

Query label	Target label	Virus name	Percent identity	Alignment length	Number of mismatches	Number of gap opens	Start position in query	End position in query	Start position in target	End position in target	E-value	Bit Score
comp24354_c0_seq1	AJ427911	ACMV [Nigeria-Ogo]	95.47	2497	109	4	1	2495	2603	109	0	3982
comp24354_c0_seq2	X17096	ACMV-[Nigeria] DNA-2	95.7	2046	88	0	222	2267	2306	261	0	3291
comp27204_c0_seq1	X17095	ACMV [Nigeria] DNA 1	97.38	2782	72	1	366	3147	2781	1	0	4732
comp27204_c0_seq1	X17095	ACMV [Nigeria] DNA 1	97.64	2417	57	0	3148	5564	2781	365	0	4148
comp12658_c0_seq1	fn434437	CBSV, isolate Tan_70	99.93	8963	6	0	21	8983	8995	33	0	16519

Table S2. Blastn output

	Input (left or right)	Aligned pairs	multiple alignments	discordant alignments	concordant pair alignment rate	read mapping rate
CBSV-6dpi	64857123	57373621	6294281 (11.0%)	1669205 (2.9%)	85.90%	92.50%
CBSV-6dpi	50271801	45148027	4887083 (10.8%)	1317036 (2.9%)	87.20%	93.50%
CBSV-6dpi	43226338	38829461	4243989 (10.9%)	1204676 (3.1%)	87.00%	93.60%
Mock-6dpi	52717923	47308043	5793340 (12.2%)	1592522 (3.4%)	86.70%	93.60%
Mock-6dpi	54698541	49220007	6005412 (12.2%)	1632025 (3.3%)	87.00%	93.70%
ACMV-6dpi	65200429	58454226	6258017 (10.7%)	1729802 (3.0%)	87.00%	93.40%
ACMV-6dpi	59254089	52706683	6106744 (11.6%)	1835117 (3.5%)	85.90%	93.10%
ACMV-6dpi	51271669	46075053	5011384 (10.9%)	1526916 (3.3%)	86.90%	93.60%

Table S3. Alignment summary

	L23	Ago1	PP2A	Actin
n	60	60	60	60
geo Mean [CP]	22.78	28.29	25	27.32
AR Mean [CP]	22.79	28.31	25.01	27.35
min [CP]	21.25	26.19	23.79	24.93
max [CP]	25.29	30.22	26.79	31.19
std dev [+/- CP]	0.71	0.83	0.52	0.97
CV [% CP]	3.11	2.93	2.08	3.54
min [x-fold]	-2.88	-4.29	-2.31	-5.26
max [x-fold]	5.69	3.81	3.47	14.58
std dev [+/- x-fold]	1.64	1.78	1.43	1.95

Table S4. Determination of most stable reference gene; CP data of housekeeping genes by BestKeeper

Gene name	Forward (5'-3')	Reverse (3'-5')	TAIR ID	N. benthamiana ID
4CL;CoA ligase	ACGTCGTTGCTCTGCCGTATTC	TCAACATCACACCTTTCGGCAGTC	CK299019	NbS00036814g0014
AHK2_3_4	TTGCACTGGGCTGTAGATCGTG	GGCGTTTACATCGGCATTCCTG	CN743542	NbS00011469g0014
AHP	AGCACTGCTACGGTTCAAAGAAG	GTGGACTCCTCTCTCATTCCTTGC	TA6135_4100	NbS00056949g0004
ALF5	TGTCTGGAACTGGATTTCTTGCC	AAGCGGCTACCCATGCAGATAG	DQ054581	NbS00022866g0101
ARR-B	ACACGGACATGGACATGGGTTTC	TTCCAGACCAGTCTCGCTGTTG	TA5900_4100	NbS00017224g0005
BAHD1	TCCCAGGAAATGTCACGAACGAG	GGGTCGTTGGATCGCATAAGAAAG	TA6902_4100	NbS00027775g0004
BAK1	CGGGTTCGATATCCGGGTTAACTG	TCTCGCCGTTGAGTTTGTTGGAC	CK289127	NbS00014431g0006
BKI1	ACATTGAGGCCCTTGACACAGAG	CTTCTTCCAATTGGTCACAAACCG	TA5772_4100	NbS00006555g0001
BRI1	GTGCAGTCTTCAGGAGGAGACATC	GCAGCCTCCAAAGTGGCAAATG	CK285971	NbS00007519g0002
BZR1_2	GCAATGGCCCATCCTTATTTCCTG	AACAGGCTACTGCGTCCTCATC	CK290035	NbS00028268g0004
CHIB /chitinase	TGGCAGTGGAATGGGAATGGTG	ACCGGCTTTGAGCCTCACATAATC	TA7730_4100	NbS00023821g0011
CKX1_ARATH	TCTAGACTTTGCCCTCCTTTGCC	TTGCCATTGGTGTAGCTGTGAAC	TA4722_4100	NbC25816420g0002
EDS1	AGGCCGAAGCGTTATAGGTTCAC	CAGAGCGTTCACCTGTTTGCAC	AF479625	NbS00001627g0012
EIN2	GCAGCGCTGGAATCTACAAGTC	TGGCCAGCATCAGCTTTCACAG	TA6833_4100	NbS00018665g0004
ERF1	AAACCCATGACGAAGCAGTTTGG	AATCCCGTATCTCCAGAAGCATTG	CK289127	NbS00028692g0001
ILR1; IAA	TATACATGACGGCGCTCGGAAC	TCGAACTGGTCAGAACCGAAGC	TA5777_4100	NbS00035721g0014
JAZ	AACCGAAAGGTACGCGGGTTTG	ACGCCGCCCTATCATATGCCTTAG	TA4171_4100	NbS00026688g0011
MAP2K1, MEK1	CATGGGAAGCAAGCATTCAAAGGG	TGACTCCAGGTTGAAGCAGCAC	CK297726	NbS00006857g0015
MET18, MMS19	ACAGGGTTCACCGGGAAATGAC	ACACAACTGGTCGGAGCTTTCC	TA7088_4100	NbS00057660g0006
MYC2	TCGACGTTAAGGTGATCGGATGG	TAACTTCGCGGCTGGATGGTTC	CK295587	NbS00015337g0005
NbMEK2 *	TGTACGAAGTCCGCCATAAGCG	TCACCGTGAACGACTTTGAGAGC	TA5294_4100	
NbNTF4 *	TCGCCAGAGGATTCTGATCTTGG	GAACTCGAGGGAGCTGCTTTAC	AY547494	
NbNTF6 *	TCGCCAGAGGATTCTGATCTTGG	GAACTCGAGGGAGCTGCTTTAC	AY547494	
NbrbohA/B *	TGGAGCACCAGCACAAGACTAC	TCCAATTCCAAGACCCACCAAC	AB079499	
NbSIPK *	AGGTGCACTTGCACATCCTTACC	AGTCATGCAAATGGGCTCGTCAC	TA5832_4100	
NbWIPK *	AAGCTCCACGATGCAGGTGATG	TGCTCAAAGTCGAAGGAGGATGG	AB098729	
NOA1 *	TGTTTAACGCACCACTTGGAGATG	ATTGGGCTTGTCACAGGGCTTG	TA3973_4100	
PR1	ATTGCCGGCATAGACTCCAACC	CGGAATGCTCTGAATTGCGTTGC	CN746035	NbS00061216g0001
PTI6	TTGCAACGCCACCTTCACTGAG	AGGACCGGATTCGTGATAAGTGC	TA7073_4100	NbS00002024g0006
RAR1	TTGCAACGCCACCTTCACTGAG	AGGACCGGATTCGTGATAAGTGC	TA7073_4100	NbS00013235g0013
RHF	ATTGTTCTACGATGGCGTCTGC	TCAGCATACGGAGGGTGAGTTC	TA5617_4100	NbS00036939g0001
SGT1	GATGCTGCTGTGAAGGAAAGCG	TGACTCTGCCAATCGAGTTTCG	AY206005	NbS00002728g0011
SKP1	TTGCCCTAGAGTCGCAGACAATC	AGGTAAAGGGATGCTGGTGTCG	TA6524_4100	NbS00024298g0005
TGA	AGCTATTGCCAAGCAGCCAAGC	TCGACACAAAGGTTCCGGAAGTG	TA6178_4100	NbS00025965g0001
BARD1	CAGCCCATCAAAGTGGCCAAAC	TTCCTTGCCATCCGTTCTCTTTC	CK285526	NbS00004728g0002
Cullin	GGCAACATTGGTCCGTTTGCAG	TTCAGCCGCGAGAAACCACTTC		NbS00022640g0007
E3	GTGCTCGTGCGACGAAGTATTG	AACCACACTGGACATTGAAGGC		
SAG101	AGGCCGAAGCGTTATAGGTTCAC	CAGAGCGTTCACCTGTTTGCAC	Q4F883	
RDR1-pn	AGGCCATTGGTGTTGCTGTGAG	GCTTCTTGAACCAGGTCCTTGC	Q9LQV2	NbS00009618g0001
PAD4	AAACTCCTCGTAGAGCCACTCG	GTGGCCTTTCACATGATGCAACC	Q9S745	NbS00036265g0002
NDR1	AGGACAAAGGTGTTCGTTACGATG	TGTGCTTTCTTGTCATGACCTTGG	O48915	NbS00006690g0001
FBox	TCAAGAGTGAATCGGAGGTGCTG	ACTCTCGCTCAACCTTCAACGC	K12115	NbS00009879g0004
RFWD2, COP1	GTGGCAATGAAGGCATCAATGGG	TTCCAGCATCCCAGCACATTCG	CK292531	NbS00016456g0009
H3	ATTCCCTAATGGAGGGCAAATGTC	TGACCTAATGGACCTTTCACGTTG		NbS00013740g0005
IAA	TTTGGCCTCGAACGAGAAGCTG	TTTATGCGATACGGCCAAAGCAC	CN746175	NbS00003784g0004
NPR1	GATGCTTCTGCCACCCAGTTTC	TGGGATCGCCAATAGCTTTCAAC		NbS00006539g0005
WRKY22	TGTACCGCGCCTGCATATGATAC	TCTCCGCACCCTCATCACAATAC		NbS00011597g0002
bglB	AATGACGTGCCTATGCTCATGC	TCGCCTTCGCAGTACCGTAATC		

Table S5. Primers used for gene expression quantification by real time PCR [335]

Group of DEGs	GO IDs	Term description	No. of transcripts
CBSV_6dpi_up			
	GO:0016829	lyase activity	1
	GO:0016740	transferase activity	1
	GO:0003824	catalytic activity	1
ACMV_6dpi_up			
	GO:0080008	CUL4 RING ubiquitin ligase complex	1
	GO:0051179	localization	1
	GO:0050896	response to stimulus	1
	GO:0044249	cellular biosynthetic process	5
	GO:0044238	primary metabolic process	1
	GO:0043687	post-translational protein modification	5
	GO:0043231	intracellular membrane-bounded organelle	3
	GO:0016853	isomerase activity	1
	GO:0007275	multicellular organismal development	2
	GO:0007018	microtubule-based movement	4
	GO:0005623	cell	1
	GO:0005488	binding	3
CBSV_6dpi_ down			

	GO:0044425	membrane part	2
	GO:0044238	primary metabolic process	1
	GO:0044042	glucan metabolic process	3
	GO:0016740	transferase activity	2
ACMV_6dpi_ down			
	GO:0051179	localization	3
	GO:0044425	membrane part	3
	GO:0044238	primary metabolic process	3
	GO:0043687	post-translational protein modification	2
	GO:0016740	transferase activity	3
	GO:0006811	ion transport	1
	GO:0003824	catalytic activity	1
ACMV_6dpi_up & CBSV_6dpi_up			
	GO:0051179	localization	1
	GO:0044249	cellular biosynthetic process	1
	GO:0044238	primary metabolic process	4
	GO:0016853	isomerase activity	1
	GO:0016741	transferase activity, transferring one-carbon groups	1
	GO:0016740	transferase activity	3
	GO:0005623	cell	1
	GO:0005488	binding	1
	GO:0003676	nucleic acid binding	1
ACMV_6dpi_ down & CBSV_6dpi_ down			
	GO:0070035	purine NTP-dependent helicase activity	1
	GO:0044425	membrane part	1
	GO:0044238	primary metabolic process	1
	GO:0016740	transferase activity	1
CBSV_12dpi_up			
	GO:0000271	polysaccharide biosynthetic process	1
	GO:0003676	nucleic acid binding	6
	GO:0003677	DNA binding	4
	GO:0003824	catalytic activity	35
	GO:0003950	NAD+ ADP-ribosyltransferase activity	1
	GO:0005088	Ras guanyl-nucleotide exchange factor activity	2
	GO:0005488	binding	9
	GO:0005623	cell	17
	GO:0005777	peroxisome	1
	GO:0005945	6-phosphofructokinase complex	1
	GO:0006164	purine nucleotide biosynthetic process	9
	GO:0006519	cellular amino acid and derivative metabolic process	1
	GO:0006811	ion transport	3
	GO:0007018	microtubule-based movement	4
	GO:0008134	transcription factor binding	1
	GO:0008152	metabolic process	1
	GO:0008289	lipid binding	1
	GO:0008415	acyltransferase activity	3
	GO:0009507	chloroplast	1
	GO:0016043	cellular component organization	2
	GO:0016740	transferase activity	25
	GO:0016741	transferase activity, transferring one-carbon groups	4
	GO:0016772	transferase activity, transferring phosphorus-containing groups	4
	GO:0016829	lyase activity	7

	GO:0016853	isomerase activity	1
	GO:0016876	ligase activity, forming aminoacyl-tRNA and related compounds	3
	GO:0016887	ATPase activity	4
	GO:0017076	purine nucleotide binding	4
	GO:0019538	protein metabolic process	9
	GO:0020037	heme binding	20
	GO:0022803	passive transmembrane transporter activity	2
	GO:0030244	cellulose biosynthetic process	1
	GO:0030414	peptidase inhibitor activity	2
	GO:0031327	negative regulation of cellular biosynthetic process	1
	GO:0032559	adenyl ribonucleotide binding	6
	GO:0042440	pigment metabolic process	1
	GO:0043231	intracellular membrane-bounded organelle	5
	GO:0043687	post-translational protein modification	45
	GO:0044042	glucan metabolic process	1
	GO:0044237	cellular metabolic process	4
	GO:0044238	primary metabolic process	76
	GO:0044249	cellular biosynthetic process	46
	GO:0044424	intracellular part	5
	GO:0044425	membrane part	2
	GO:0045454	cell redox homeostasis	1
	GO:0046474	glycerophospholipid biosynthetic process	1
	GO:0046872	metal ion binding	15
	GO:0048268	clathrin coat assembly	2
	GO:0048437	floral organ development	1
	GO:0050896	response to stimulus	20
	GO:0051179	localization	49
	GO:0055114	oxidation reduction	17
	GO:0070035	purine NTP-dependent helicase activity	3
ACMV_12dpi_up			
	GO:0000271	polysaccharide biosynthetic process	1
	GO:0003676	nucleic acid binding	1
	GO:0003824	catalytic activity	8
	GO:0005088	Ras guanyl-nucleotide exchange factor activity	1
	GO:0005488	binding	11
	GO:0005576	extracellular region	1
	GO:0005623	cell	8
	GO:0006164	purine nucleotide biosynthetic process	2
	GO:0006519	cellular amino acid and derivative metabolic process	1
	GO:0008415	acyltransferase activity	2
	GO:0009117	nucleotide metabolic process	1
	GO:0015932	nucleobase, nucleoside, nucleotide and nucleic acid transmembrane transporter activity	2
	GO:0016043	cellular component organization	2
	GO:0016568	chromatin modification	1
	GO:0016740	transferase activity	9
	GO:0016741	transferase activity, transferring one-carbon groups	1
	GO:0016887	ATPase activity	4
	GO:0017076	purine nucleotide binding	6
	GO:0019538	protein metabolic process	1
	GO:0020037	heme binding	6
	GO:0022803	passive transmembrane transporter activity	1

	GO:0030246	carbohydrate binding	1
	GO:0031072	heat shock protein binding	1
	GO:0043231	intracellular membrane-bounded organelle	3
	GO:0043687	post-translational-protein modification	34
	GO:0044238	primary metabolic process	18
	GO:0044249	cellular biosynthetic process	15
	GO:0044424	intracellular part	1
	GO:0045454	cell redox homeostasis	1
	GO:0046872	metal ion binding	8
	GO:0050896	response to stimulus	7
	GO:0051179	localization	11
	GO:0055114	oxidation reduction	1
	GO:0070035	purine NTP-dependent helicase activity	1
CBSV_12dpi_ down			
	GO:0000271	polysaccharide biosynthetic process	1
	GO:0003676	nucleic acid binding	1
	GO:0003677	DNA binding	2
	GO:0003824	catalytic activity	3
	GO:0005488	binding	1
	GO:0005623	cell	3
	GO:0006519	cellular amino acid and derivative metabolic process	1
	GO:0006568	tryptophan metabolic process	2
	GO:0008289	lipid binding	1
	GO:0009117	nucleotide metabolic process	1
	GO:0016043	cellular component organization	1
	GO:0016740	transferase activity	6
	GO:0016741	transferase activity, transferring one-carbon groups	2
	GO:0016772	transferase activity, transferring phosphorus-containing groups	1
	GO:0016829	lyase activity	4
	GO:0016887	ATPase activity	1
	GO:0020037	heme binding	3
	GO:0032559	adenyl ribonucleotide binding	1
	GO:0043687	post-translational protein modification	5
	GO:0044042	glucan metabolic process	1
	GO:0044238	primary metabolic process	11
	GO:0044249	cellular biosynthetic process	4
	GO:0046872	metal ion binding	3
	GO:0050896	response to stimulus	5
	GO:0051179	localization	9
	GO:0051707	response to other organism	1
	GO:0055114	oxidation reduction	4
	GO:0070035	purine NTP-dependent helicase activity	1
ACMV_12dpi_ down			
	GO:0000271	polysaccharide biosynthetic process	1
	GO:0003677	DNA binding	1
	GO:0003824	catalytic activity	1
	GO:0004888	transmembrane receptor activity	1
	GO:0005623	cell	2
	GO:0006519	cellular amino acid and derivative metabolic process	1
	GO:0016853	isomerase activity	1
	GO:0020037	heme binding	1
	GO:0032559	adenyl ribonucleotide binding	2
	GO:0043687	post-translational protein modification	8

GO:0044042	glucan metabolic process	1
GO:0044238	primary metabolic process	6
GO:0044249	cellular biosynthetic process	12
GO:0045454	cell redox homeostasis	1
GO:0050896	response to stimulus	3
GO:0051179	localization	1
GO:0055114	oxidation reduction	4
CBSV_12dpi_up & ACMV_12dpi_up		
GO:0000279	M phase	1
GO:0002376	immune system process	2
GO:0003676	nucleic acid binding	5
GO:0003824	catalytic activity	24
GO:0004888	transmembrane receptor activity	4
GO:0005488	binding	12
GO:0005576	extracellular region	6
GO:0005623	cell	14
GO:0005829	cytosol	2
GO:0005945	6-phosphofructokinase complex	2
GO:0006164	purine nucleotide biosynthetic process	2
GO:0006464	protein modification process	1
GO:0006519	cellular amino acid and derivative metabolic process	3
GO:0007018	microtubule-based movement	2
GO:0008415	acyltransferase activity	1
GO:0009117	nucleotide metabolic process	1
GO:0016021	integral to membrane	4
GO:0016701	oxidoreductase activity, acting on single donors with incorporation of molecular oxygen	2
GO:0016740	transferase activity	23
GO:0016772	transferase activity, transferring phosphorus-containing groups	12
GO:0016829	lyase activity	12
GO:0016876	ligase activity, forming aminoacyl-tRNA and related compounds	3
GO:0016887	ATPase activity	5
GO:0017076	purine nucleotide binding	10
GO:0019538	protein metabolic process	2
GO:0020037	heme binding	18
GO:0022803	passive transmembrane transporter activity	2
GO:0030246	carbohydrate binding	1
GO:0043231	intracellular membrane-bounded organelle	4
GO:0043687	post-translational protein modification	80
GO:0044042	glucan metabolic process	1
GO:0044237	cellular metabolic process	2
GO:0044238	primary metabolic process	50
GO:0044249	cellular biosynthetic process	45
GO:0044425	membrane part	2
GO:0045454	cell redox homeostasis	3
GO:0046395	carboxylic acid catabolic process	1
GO:0046872	metal ion binding	19
GO:0050896	response to stimulus	7
GO:0051179	localization	40
GO:0051707	response to other organism	3
GO:0055114	oxidation reduction	20
GO:0070035	purine NTP-dependent helicase activity	5
CBSV_12dpi_ down & ACMV_12dpi_ down		
GO:0000271	polysaccharide biosynthetic process	1

	GO:0003677	DNA binding	1
	GO:0003824	catalytic activity	11
	GO:0005488	binding	2
	GO:0005623	cell	2
	GO:0006164	purine nucleotide biosynthetic process	1
	GO:0006519	cellular amino acid and derivative metabolic process	3
	GO:0006568	tryptophan metabolic process	1
	GO:0006811	ion transport	2
	GO:0008152	metabolic process	1
	GO:0008289	lipid binding	3
	GO:0012501	programmed cell death	1
	GO:0016021	integral to membrane	1
	GO:0016740	transferase activity	5
	GO:0016741	transferase activity, transferring one-carbon groups	5
	GO:0016887	ATPase activity	1
	GO:0019538	protein metabolic process	1
	GO:0019898	extrinsic to membrane	2
	GO:0020037	heme binding	13
	GO:0030246	carbohydrate binding	1
	GO:0032559	adenyl ribonucleotide binding	2
	GO:0043170	macromolecule metabolic process	2
	GO:0043231	intracellular membrane-bounded organelle	2
	GO:0043687	post-translational protein modification	16
	GO:0044042	glucan metabolic process	2
	GO:0044237	cellular metabolic process	2
	GO:0044238	primary metabolic process	31
	GO:0044249	cellular biosynthetic process	23
	GO:0044425	membrane part	1
	GO:0045454	cell redox homeostasis	2
	GO:0046872	metal ion binding	2
	GO:0050896	response to stimulus	3
	GO:0051179	localization	15
	GO:0055114	oxidation reduction	11
	GO:0070035	purine NTP-dependent helicase activity	1
	GO:0080008	CUL4 RING ubiquitin ligase complex	1
CBSV_19dpi_up			
	GO:0008415	acyltransferase activity	2
	GO:0016887	ATPase activity	3
	GO:0005488	binding	6
	GO:0003824	catalytic activity	24
	GO:0005623	cell	7
	GO:0006519	cellular amino acid and derivative metabolic process	2
	GO:0044249	cellular biosynthetic process	1
	GO:0044237	cellular metabolic process	2
	GO:0030244	cellulose biosynthetic process	2
	GO:0048268	clathrin coat assembly	2
	GO:0003677	DNA binding	1
	GO:0048437	floral organ development	1
	GO:0044042	glucan metabolic process	5
	GO:0006541	glutamine metabolic process	1
	GO:0020037	heme binding	6
	GO:0019320	hexose catabolic process	1
	GO:0043231	intracellular membrane-bounded organelle	1
	GO:0044424	intracellular part	2

	GO:0016853	isomerase activity	1
	GO:0016876	ligase activity, forming aminoacyl-tRNA and related compounds	1
	GO:0051179	localization	34
	GO:0016829	lyase activity	5
	GO:0044425	membrane part	1
	GO:0046872	metal ion binding	12
	GO:0007018	microtubule-based movement	2
	GO:0003676	nucleic acid binding	2
	GO:0044422	organelle part	1
	GO:0055114	oxidation reduction	14
	GO:0022803	passive transmembrane transporter activity	3
	GO:0042440	pigment metabolic process	1
	GO:0000271	polysaccharide biosynthetic process	1
	GO:0043687	post-translational protein modification	26
	GO:0044238	primary metabolic process	50
	GO:0019538	protein metabolic process	4
	GO:0070035	purine NTP-dependent helicase activity	2
	GO:0006164	purine nucleotide biosynthetic process	4
	GO:0005088	Ras guanyl-nucleotide exchange factor activity	1
	GO:0051707	response to other organism	1
	GO:0050896	response to stimulus	11
	GO:0016740	transferase activity	16
	GO:0016772	transferase activity, transferring phosphorus-containing groups	1
ACMV_19dpi_up			
	GO:0008415	acyltransferase activity	2
	GO:0032559	adenyl ribonucleotide binding	1
	GO:0016597	amino acid binding	1
	GO:0016887	ATPase activity	7
	GO:0005488	binding	22
	GO:0003824	catalytic activity	34
	GO:0005623	cell	19
	GO:0045454	cell redox homeostasis	3
	GO:0044249	cellular biosynthetic process	67
	GO:0016043	cellular component organization	2
	GO:0044237	cellular metabolic process	2
	GO:0034613	cellular protein localization	1
	GO:0016568	chromatin modification	1
	GO:0003677	DNA binding	4
	GO:0005576	extracellular region	1
	GO:0010181	FMN binding	1
	GO:0044042	glucan metabolic process	3
	GO:0006541	glutamine metabolic process	1
	GO:0020037	heme binding	16
	GO:0020037	heme binding	7
	GO:0002376	immune system process	1
	GO:0016021	integral to membrane	4
	GO:0043231	intracellular membrane-bounded organelle	8
	GO:0044424	intracellular part	2
	GO:0006811	ion transport	2
	GO:0016853	isomerase activity	2
	GO:0016876	ligase activity, forming aminoacyl-tRNA and related compounds	1
	GO:0008289	lipid binding	3
	GO:0051179	localization	55

	GO:0016829	lyase activity	9
	GO:0000279	M phase	2
	GO:0043412	macromolecule modification	1
	GO:0044425	membrane part	3
	GO:0008152	metabolic process	2
	GO:0046872	metal ion binding	27
	GO:0007018	microtubule-based movement	3
	GO:0003950	NAD+ ADP-ribosyltransferase activity	1
	GO:0031327	negative regulation of cellular biosynthetic process	2
	GO:0003676	nucleic acid binding	7
	GO:0015932	nucleobase, nucleoside, nucleotide and nucleic acid transmembrane transporter activity	2
	GO:0009117	nucleotide metabolic process	2
	GO:0055114	oxidation reduction	16
	GO:0016701	oxidoreductase activity, acting on single donors with incorporation of molecular oxygen	4
	GO:0022803	passive transmembrane transporter activity	3
	GO:0000271	polysaccharide biosynthetic process	1
	GO:0043687	post-translational protein modification	108
	GO:0044238	primary metabolic process	71
	GO:0019538	protein metabolic process	4
	GO:0070035	purine NTP-dependent helicase activity	7
	GO:0017076	purine nucleotide binding	11
	GO:0006164	purine nucleotide biosynthetic process	4
	GO:0005088	Ras guanyl-nucleotide exchange factor activity	1
	GO:0043549	regulation of kinase activity	1
	GO:0000003	reproduction	2
	GO:0051707	response to other organism	4
	GO:0050896	response to stimulus	19
	GO:0023060	signal transmission	1
	GO:0016740	transferase activity	27
	GO:0016741	transferase activity, transferring one-carbon groups	7
	GO:0016772	transferase activity, transferring phosphorus-containing groups	3
	GO:0004888	transmembrane receptor activity	2
	GO:0006568	tryptophan metabolic process	1
	GO:0008270	zinc ion binding	1
CBSV_19dpi_ down			
	GO:0008686	3,4-dihydroxy-2-butanone-4-phosphate synthase activity	2
	GO:0003824	catalytic activity	3
	GO:0044249	cellular biosynthetic process	28
	GO:0051179	localization	3
	GO:0055114	oxidation reduction	3
	GO:0043687	post-translational protein modification	2
	GO:0016740	transferase activity	2
	GO:0016741	transferase activity, transferring one-carbon groups	3
ACMV_19dpi_ down			
	GO:0032559	adenyl ribonucleotide binding	2
	GO:0031225	anchored to membrane	1
	GO:0016887	ATPase activity	1
	GO:0005488	binding	10
	GO:0030246	carbohydrate binding	1

	GO:0003824	catalytic activity	7
	GO:0005623	cell	11
	GO:0045454	cell redox homeostasis	3
	GO:0006519	cellular amino acid and derivative metabolic process	2
	GO:0044249	cellular biosynthetic process	35
	GO:0016043	cellular component organization	1
	GO:0044237	cellular metabolic process	1
	GO:0009507	chloroplast	1
	GO:0006265	DNA topological change	2
	GO:0005576	extracellular region	1
	GO:0020037	heme binding	7
	GO:0043231	intracellular membrane-bounded organelle	25
	GO:0044424	intracellular part	2
	GO:0006811	ion transport	1
	GO:0016853	isomerase activity	2
	GO:0051179	localization	22
	GO:0016829	lyase activity	2
	GO:0000279	M phase	1
	GO:0044425	membrane part	1
	GO:0046872	metal ion binding	8
	GO:0007018	microtubule-based movement	17
	GO:0007275	multicellular organismal development	1
	GO:0003676	nucleic acid binding	1
	GO:0045735	nutrient reservoir activity	1
	GO:0055114	oxidation reduction	5
	GO:0009506	plasmodesma	2
	GO:0009856	pollination	1
	GO:0000271	polysaccharide biosynthetic process	1
	GO:0043687	post-translational protein modification	29
	GO:0044238	primary metabolic process	50
	GO:0017076	purine nucleotide binding	3
	GO:0005088	Ras guanyl-nucleotide exchange factor activity	3
	GO:0000003	reproduction	1
	GO:0050896	response to stimulus	8
	GO:0022621	shoot system development	5
	GO:0023060	signal transmission	1
	GO:0016740	transferase activity	7
	GO:0016741	transferase activity, transferring one-carbon groups	2
	GO:0008270	zinc ion binding	1
ACMV_19dpi_up & CBSV_19dpi_up			
	GO:0008415	acyltransferase activity	1
	GO:0032559	adenyl ribonucleotide binding	2
	GO:0016887	ATPase activity	3
	GO:0005488	binding	8
	GO:0003824	catalytic activity	20
	GO:0005623	cell	11
	GO:0006519	cellular amino acid and derivative metabolic process	3
	GO:0044249	cellular biosynthetic process	40
	GO:0016043	cellular component organization	16
	GO:0003677	DNA binding	2
	GO:0005576	extracellular region	3
	GO:0044042	glucan metabolic process	7
	GO:0046474	glycerophospholipid biosynthetic process	1

GO:0020037	heme binding	8
GO:0043231	intracellular membrane-bounded organelle	2
GO:0044424	intracellular part	1
GO:0016876	ligase activity, forming aminoacyl-tRNA and related compounds	4
GO:0008289	lipid binding	1
GO:0051179	localization	23
GO:0016829	lyase activity	3
GO:0043170	macromolecule metabolic process	1
GO:0044425	membrane part	2
GO:0046872	metal ion binding	11
GO:0003676	nucleic acid binding	3
GO:0055114	oxidation reduction	12
GO:0022803	passive transmembrane transporter activity	1
GO:0030414	peptidase inhibitor activity	1
GO:0043687	post-translational protein modification	26
GO:0044238	primary metabolic process	28
GO:0019538	protein metabolic process	2
GO:0006464	protein modification process	1
GO:0070035	purine NTP-dependent helicase activity	1
GO:0017076	purine nucleotide binding	7
GO:0051707	response to other organism	1
GO:0050896	response to stimulus	4
GO:0017171	serine hydrolase activity	1
GO:0016740	transferase activity	8
GO:0016741	transferase activity, transferring one-carbon groups	1
GO:0016772	transferase activity, transferring phosphorus-containing groups	1
GO:0004888	transmembrane receptor activity	1
ACMV_19dpi_ down & CBSV_19dpi_ down		
GO:0044249	cellular biosynthetic process	1
GO:0020037	heme binding	1
GO:0051179	localization	1
GO:0044238	primary metabolic process	3
GO:0070035	purine NTP-dependent helicase activity	1

Table S6a. Gene Ontology terms; Common and specific up-regulated (log2FC ≥+2 and Padj-value<0.05) and down- regulated (log2FC≤ -2 and Padj-value<0.05) genes during infection progression with CBSV and ACMV; up and down indicates for up-regulated and down-regulated genes

Group of sample	**No. of non-annotated transcripts**
CBSV_6dpi_up	1
ACMV_6dpi_up	21
ACMV_6dpi_low	5
CBSV_6dpi_low	4
ACMV_6dpi_up & CBSV_6dpi_up	10
ACMV_6dpi_low & CBSV_6dpi_low	2
CBSV_12dpi_up	567
ACMV_12dpi_up	189
CBSV_12dpi_low	74
ACMV_12dpi_low	42
CBSV_12dpi_up & ACMV_12dpi_up	349
CBSV_12dpi_low & ACMV_12dpi_low	142
CBSV_19dpi_up	286
ACMV_19dpi_up	2449
CBSV_19dpi_low	9
ACMV_19dpi_low	251

CBSV_19dpi_up & ACMV_19dpi_up	156
CBSV_19dpi_low & ACMV_19dpi_low	11

Table S6b. the DEGs without any GO annotation

Coefficients:

	Estimate	Std. Error	t value	Pr(>|t|)	
(Intercept)	-0.48690	0.71216	-0.684	0.4948	
variable	0.11189	0.05303	2.110	0.0358	*
replicate2	0.45226	1.00826	0.449	0.6541	
variable:replicate2	-0.04780	0.07523	-0.635	0.5257	

Residual standard error: 3.237 on 259 degrees of freedom
Multiple R-squared: 0.02271, Adjusted R-squared: 0.01139
F-statistic: 2.006 on 3 and 259 DF, p-value: 0.1135

Response: value

	Df	R Sum Sq	R Mean Sq	Iter	Pr(Prob)	
variable	1	57.34	57.342	5000	0.0076	**
replicate	1	1.22	1.217	51	1.0000	
variable:replicate	1	4.23	4.230	238	0.2983	
Residuals	259	2713.61	10.477			

Coefficients:

(Intercept)	variable	replicate1
0.82226	0.08799	0.06803

variable:replicate1 0.0239

Coefficients:

	Estimate	Iter	Pr(Prob)	
variable	0.08799	5000	0.0088	**
replicate1	0.06803	75	0.5733	
variable:replicate1	0.02390	63	0.6190	

Residual standard error: 3.237 on 259 degrees of freedom
Multiple R-Squared: 0.02271, Adjusted R-squared: 0.01139
F-statistic: 2.006 on 3 and 259 DF, p-value: 0.1135

Table S7. Summary of linear model to investigate the profiles across the two replicates (RNA-seq and qRT-PCR) and their interaction with variables (three time points)

	baseMean	log2FoldChange	lfcSE	stat	pvalue	padj
CBSV-12dpi	218.4061	6.221429	0.346418	17.95929	4.06E-72	1.31E-69
ACMV-12dpi	181.4812	5.642318	0.356673	15.81931	2.29E-56	5.35E-54
CBSV-19dpi	6.758628	1.005833	0.388497	2.589033	0.009625	0.033826
ACMV-19dpi	33.87409	3.665312	0.493163	7.432251	NA	NA

Table S8. The expression values of DOX1; alpha-dioxygenase [EC:1.-.-.-]; K10529

Name	Internal	Connectivity
ADP_H	FALSE	7
ADP_M	FALSE	1
ADP_Y	FALSE	3
AKG_H	FALSE	1
AKG_M	TRUE	3
AKG_P	FALSE	1
AMP_H	FALSE	1
AMP_P	FALSE	1
AMP_Y	FALSE	1
ATP_H	FALSE	8
ATP_M	FALSE	1
ATP_P	FALSE	1
ATP_Y	FALSE	4
Ac_CoA_M	TRUE	3
Ac_CoA_P	FALSE	1
B_D_F16_BP_H	TRUE	3
B_D_F16_BP_Y	TRUE	4
B_D_G6_P_H	TRUE	2
B_D_G6_P_Y	TRUE	2
CO_2_ER	FALSE	1
CO_2_H	FALSE	2
CO_2_M	FALSE	5
CO_2_Y	FALSE	1
Chor_H	TRUE	2

Cit_M	TRUE	2
CoA_ER	FALSE	1
CoA_M	FALSE	6
CoA_P	FALSE	3
DAHP_H	TRUE	2
DHAP_H	TRUE	4
DHAP_Y	TRUE	3
DHQ_H	TRUE	2
DHlipoylLys_residueAcTran_S_AcDHlipoylLys_M	TRUE	2
D_E4P_H	TRUE	5
D_E4P_Y	TRUE	2
D_F6_P_H	TRUE	5
D_F6_P_Y	TRUE	5
D_GA_H	TRUE	2
D_GA_P	TRUE	2
D_GA_Y	TRUE	2
D_Glyceraldehyde3_P_H	TRUE	8
D_Glyceraldehyde3_P_Y	TRUE	5
D_Ri5_P_H	TRUE	3
D_Ri5_P_Y	TRUE	2
D_Ru15_BP_H	TRUE	3
D_Ru5_P_H	TRUE	4
D_Ru5_P_Y	TRUE	3
D_Xu5_P_H	TRUE	4
D_Xu5_P_Y	TRUE	2
DiP_P	FALSE	1
Dihydrosphingosine_ER	FALSE	1
EnzymeN6_dihydrolipoyl_Lys_M	TRUE	4
EnzymeN6_lipoyl_Lys_M	TRUE	4
Fum_M	TRUE	2
GDP_M	FALSE	1
GTP_M	FALSE	1
Gly_M	TRUE	3
Gly_P	TRUE	3
Glycolate_H	TRUE	2
Glycolate_P	TRUE	2
Glycolate_Y	TRUE	2
Glyoxylate_P	TRUE	3
Hplusin_H	FALSE	1
Hplusout_H	TRUE	3
Hydrogenperoxide_P	FALSE	2
HydroxyPYR_P	TRUE	2
IDP_M	FALSE	1
ITP_M	FALSE	1
IsoCit_M	TRUE	3
Iso_Chor_H	TRUE	2
Jasmonate_P	FALSE	1
L_Glu_H	FALSE	1
L_Glu_P	FALSE	1
Linolenate_H	TRUE	2
Mal_M	TRUE	2
NADH_H	FALSE	2
NADH_M	FALSE	5
NADH_P	FALSE	2
NADH_Y	FALSE	1
NADPH_ER	FALSE	1
NADPH_H	FALSE	4
NADPH_M	FALSE	1
NADPH_P	FALSE	1
NADPH_Y	FALSE	1
NADPplus_ER	FALSE	1
NADPplus_H	FALSE	4
NADPplus_M	FALSE	1

NADPplus_P	FALSE	1
NADPplus_Y	FALSE	1
NAD_P_H_H	FALSE	1
NAD_P_H_Y	FALSE	1
NAD_P_plus_H	FALSE	1
NAD_P_plus_Y	FALSE	1
NADplus_H	FALSE	2
NADplus_M	FALSE	5
NADplus_P	FALSE	2
NADplus_Y	FALSE	1
NH3_M	FALSE	1
O2_H	FALSE	3
O2_P	FALSE	2
OAA_M	TRUE	2
OASucc_M	TRUE	2
OPC6_CoA_P	TRUE	2
OPC8_3_hydroxyl_CoA_P	TRUE	2
OPC8_3_ketoacyl_CoA_P	TRUE	2
OPC8_CoA_P	TRUE	2
OPC8_P	TRUE	2
OPC8_trans_2_enoyl_CoA_P	TRUE	2
OPDA_H	TRUE	2
OPDA_P	TRUE	2
PEP_H	TRUE	5
PEP_Y	TRUE	3
PRPP_H	FALSE	1
PRPP_Y	FALSE	1
PYR_H	TRUE	2
PYR_M	TRUE	2
PYR_Y	TRUE	2
Palmitoyl_CoA_ER	FALSE	1
Salicylate_H	FALSE	1
Sed17_BP_H	TRUE	2
Sed7_P_H	TRUE	3
Sed7_P_Y	FALSE	1
Ser	TRUE	4
Shi3_P_H	TRUE	2
Shi_H	TRUE	2
SuccCoA_M	TRUE	4
Succ_M	TRUE	4
THF_M	TRUE	2
ThPP_M	TRUE	2
Ubiquinol_M	FALSE	1
Ubiquinone_M	FALSE	1
12_13_EOT_H	TRUE	2
13_HPOT_H	TRUE	2
2_P_D_GA_H	TRUE	2
2_P_D_GA_Y	TRUE	2
2_Pglycolate_H	TRUE	2
3PHydroxyPyr_H	TRUE	2
3PSer_H	TRUE	2
3_Carboxy_1_hydroxypropyl_ThPP_M	TRUE	2
3_DehydroShi_H	TRUE	2
3_Dehydrosphinganine_ER	TRUE	2
3_P_D_GA_H	TRUE	7
3_P_D_GA_Y	TRUE	3
3_P_D_glyceroylP_H	TRUE	3
3_P_D_glyceroylP_Y	TRUE	2
510_MethyleneTHF_M	TRUE	2
5_O_1_Carboxyvinyl__3_PShi_H	TRUE	2
6_P_D_gluconate_H	TRUE	2
6_P_D_gluconate_Y	FALSE	1
6_P_D_glucono_15_lactone_H	TRUE	2
6_P_D_glucono_15_lactone_Y	FALSE	1

DHlipoylLys_resSuccTran_S_SuccDHlipoylLys_M	TRUE	2
cis_Acon_M	TRUE	2
oxFerrodoxin_H	TRUE	2
oxPlastocyanin_H	TRUE	2

Table S9. The applied metabolites in network of *Arabidopsis thaliana* (Fieselmann A 2016)

Enzyem name	Reversible?	Reaction equation
CHOR_3PShi1carboxyvinylTran_H	FALSE	PEP_H + Shi3_P_H = _5_O__1_Carboxyvinyl__3_PShi_H
CHOR_3deoxy7PheptulonateSyn_H	FALSE	D_E4P_H + PEP_H = DAHP_H
CHOR_ChorSyn_H	FALSE	_5_O__1_Carboxyvinyl__3_PShi_H = Chor_H
CHOR_DHQSyn_H	FALSE	DAHP_H = DHQ_H
CHOR_DHQdeHydra_H	FALSE	DHQ_H = _3_DehydroShi_H
CHOR_ShiDH_H	TRUE	NADPplus_H + Shi_H = NADPH_H + _3_DehydroShi_H
CHOR_ShiKin_H	FALSE	ATP_H + Shi_H = ADP_H + Shi3_P_H
GG_6PFKin_H	FALSE	ATP_H + D_F6_P_H = ADP_H + B_D_F16_BP_H
GG_6PFKin_Y	FALSE	ATP_Y + D_F6_P_Y = ADP_Y + B_D_F16_BP_Y
GG_DiPF6P1PTrans_Y	FALSE	D_F6_P_Y = B_D_F16_BP_Y
GG_FBPAldo_H	TRUE	B_D_F16_BP_H = DHAP_H + D_Glyceraldehyde3_P_H
GG_FBPAldo_Y	FALSE	B_D_F16_BP_Y = DHAP_Y + D_Glyceraldehyde3_P_Y
GG_FBPase_H	FALSE	B_D_F16_BP_H = D_F6_P_H
GG_FBPase_Y	FALSE	B_D_F16_BP_Y = D_F6_P_Y
GG_G6dpiso_H	TRUE	B_D_G6_P_H = D_F6_P_H
GG_G6dpiso_Y	TRUE	B_D_G6_P_Y = D_F6_P_Y
GG_Glyceraldehyde3PDHPating2_H	TRUE	D_Glyceraldehyde3_P_H + NADPplus_H = NADPH_H + _3_P_D_glyceroylP_H
GG_Glyceraldehyde3PDHPating_H	TRUE	D_Glyceraldehyde3_P_H + NADplus_H = NADH_H + _3_P_D_glyceroylP_H
GG_Glyceraldehyde3PDHPating_Y	FALSE	D_Glyceraldehyde3_P_Y + NADplus_Y = NADH_Y + _3_P_D_glyceroylP_Y
GG_PGAKin_H	FALSE	ATP_H + _3_P_D_GA_H = ADP_H + _3_P_D_glyceroylP_H
GG_PGAKin_Y	TRUE	ATP_Y + _3_P_D_GA_Y = ADP_Y + _3_P_D_glyceroylP_Y
GG_PGAMut_H	FALSE	_2_P_D_GA_H = _3_P_D_GA_H
GG_PGAMut_Y	TRUE	_2_P_D_GA_Y = _3_P_D_GA_Y
GG_PPYRHydra_H	FALSE	_2_P_D_GA_H = PEP_H
GG_PPYRHydra_Y	FALSE	_2_P_D_GA_Y = PEP_Y
GG_PYRKin_H	TRUE	ADP_H + PEP_H = ATP_H + PYR_H
GG_PYRKin_Y	FALSE	ADP_Y + PEP_Y = ATP_Y + PYR_Y
GG_TIM_H	FALSE	D_Glyceraldehyde3_P_H = DHAP_H
GG_TIM_Y	FALSE	D_Glyceraldehyde3_P_Y = DHAP_Y
JASMO_12_oxophytodienoateReduct_P	FALSE	NADPH_P + OPDA_P = NADPplus_P + OPC8_P
JASMO_3hydroxyacylCoADH_P	FALSE	NADplus_P + OPC8_3_hydroxyl_CoA_P = NADH_P + OPC8_3_ketoacyl_CoA_P
JASMO_AcetylCoACAcylTrans_P	FALSE	CoA_P + OPC8_3_ketoacyl_CoA_P = Ac_CoA_P + OPC6_CoA_P
JASMO_AlleneOxideCyclase_H	FALSE	_12_13_EOT_H = OPDA_H
JASMO_CoaLigase_P	FALSE	ATP_P + CoA_P + OPC8_P = AMP_P + DiP_P + OPC8_CoA_P
JASMO_acCoAOxidase_P	FALSE	O2_P + OPC8_CoA_P = Hydrogenperoxide_P + OPC8_trans_2_enoyl_CoA_P
JASMO_acylCoAHydrolase_P	FALSE	OPC6_CoA_P = CoA_P + Jasmonate_P
JASMO_enoylCoAHydratase_P	FALSE	OPC8_trans_2_enoyl_CoA_P = OPC8_3_hydroxyl_CoA_P

JASMO_hydroperoxideDehydra_H	FALSE	_13_HPOT_H = _12_13_EOT_H
JASMO_lipoxygenase_H	FALSE	Linolenate_H + O2_H = _13_HPOT_H
PHOTORESP_2hydroxyacidoxidase_H	FALSE	Glycolate_P + O2_P = Glyoxylate_P + Hydrogenperoxide_P
PHOTORESP_GAKin_H	FALSE	ATP_H + D_GA_H = ADP_H + _3_P_D_GA_H
PHOTORESP_GlyDHdecarboxylating_H	FALSE	Gly_M + NADplus_M + THF_M = CO_2_M + NADH_M + NH3_M + _510_MethyleneTHF_M
PHOTORESP_GlyhydroxymethylTran_M	FALSE	Gly_M + _510_MethyleneTHF_M = Ser + THF_M
PHOTORESP_GlyoxylateRed_H	TRUE	D_GA_P + NADplus_P = HydroxyPYR_P + NADH_P
PHOTORESP_Glytransaminase_P	FALSE	Glyoxylate_P + L_Glu_P = AKG_P + Gly_P
PHOTORESP_PglycolatePase_H	FALSE	_2_Pglycolate_H = Glycolate_H
PHOTORESP_RuBPCx_H	FALSE	D_Ru15_BP_H + O2_H = _2_Pglycolate_H + _3_P_D_GA_H
PHOTORESP_SerglyoxylatetransaminasE_P	FALSE	Glyoxylate_P + Ser = Gly_P + HydroxyPYR_P
PHOTO_ATPase_H	FALSE	ADP_H + Hplusout_H = ATP_H + Hplusin_H
PHOTO_FBPAldo2	TRUE	Sed17_BP_H = DHAP_H + D_E4P_H
PHOTO_FBPase_H	FALSE	Sed17_BP_H = Sed7_P_H
PHOTO_PSII_H	FALSE	photon_H + plastoquinone_H = Hplusout_H + O2_H + plastoquinol_H
PHOTO_PSI_H	FALSE	oxFerrodoxin_H + photon_H + redPlastocyanin_H = oxPlastocyanin_H + redFerrodoxin_H
PHOTO_PribuloKin_H	FALSE	ATP_H + D_Ru5_P_H = ADP_H + D_Ru15_BP_H
PHOTO_Ri5PIso_H	FALSE	D_Ri5_P_H = D_Ru5_P_H
PHOTO_Ri5PIso_Y	FALSE	D_Ri5_P_Y = D_Ru5_P_Y
PHOTO_RuBPCx_H	FALSE	CO_2_H + D_Ru15_BP_H = _3_P_D_GA_H
PHOTO_RuP3Epi_H	TRUE	D_Ru5_P_H = D_Xu5_P_H
PHOTO_RuP3Epi_Y	FALSE	D_Ru5_P_Y = D_Xu5_P_Y
PHOTO_Transketolase1_H	FALSE	D_Glyceraldehyde3_P_H + Sed7_P_H = D_Ri5_P_H + D_Xu5_P_H
PHOTO_Transketolase2_H	FALSE	D_F6_P_H + D_Glyceraldehyde3_P_H = D_E4P_H + D_Xu5_P_H
PHOTO_ferrodoxinNADPReduct_H	FALSE	NADPplus_H + redFerrodoxin_H = NADPH_H + oxFerrodoxin_H
PHOTO_plastoquinol_plastocyaninReduct_H	FALSE	oxPlastocyanin_H + plastoquinol_H = Hplusout_H + plastoquinone_H + redPlastocyanin_H
PPP_6Pgluconolactonase_H	FALSE	_6_P_D_glucono_15_lactone_H = _6_P_D_gluconate_H
PPP_Glc6P1DH_H	FALSE	B_D_G6_P_H + NADPplus_H = NADPH_H + _6_P_D_glucono_15_lactone_H
PPP_Glc6P1DH_Y	FALSE	B_D_G6_P_Y + NADPplus_Y = NADPH_Y + _6_P_D_glucono_15_lactone_Y
PPP_PgluconateDH_H	FALSE	NAD_P_plus_H + _6_P_D_gluconate_H = CO_2_H + D_Ru5_P_H + NAD_P_H_H
PPP_PgluconateDH_Y	FALSE	NAD_P_plus_Y + _6_P_D_gluconate_Y = CO_2_Y + D_Ru5_P_Y + NAD_P_H_Y
PPP_Transaldolase_H	TRUE	D_Glyceraldehyde3_P_H + Sed7_P_H = D_E4P_H + D_F6_P_H
PPP_Transaldolase_Y	FALSE	D_Glyceraldehyde3_P_Y + Sed7_P_Y = D_E4P_Y + D_F6_P_Y
PRPP_R5PdiPKin_H	FALSE	ATP_H + D_Ri5_P_H = AMP_H + PRPP_H
PRPP_R5PdiPKin_Y	TRUE	ATP_Y + D_Ri5_P_Y = AMP_Y + PRPP_Y
PYR_DihydrolipoylDH_M	FALSE	EnzymeN6__dihydrolipoyl_Lys_M + NADplus_M = EnzymeN6__lipoyl_Lys_M + NADH_M
PYR_DihydrolipoylLysresidueAcTran_M	TRUE	Ac_CoA_M + EnzymeN6__dihydrolipoyl_Lys_M = CoA_M + DHlipoylLys_residueAcTran_S_AcDHlipoylLys_M

PYR_PYRDHActransferring_M	FALSE	EnzymeN6__lipoyl_Lys_M + PYR_M = CO_2_M + DHlipoylLys_residueAcTran_S_AcDHlipoylLys_M
SAL_isochorPyrL_H	FALSE	Iso_Chor_H = PYR_H + Salicylate_H
SAL_isochorS_H	FALSE	Chor_H = Iso_Chor_H
SER_3PSerPhosphatase_H	FALSE	_3PSer_H = Ser
SER_PGlycerateDH_H	FALSE	NADplus_H + _3_P_D_GA_H = NADH_H + _3PHydroxyPyr_H
SER_PSerAminoTransf_H	FALSE	L_Glu_H + _3PHydroxyPyr_H = AKG_H + _3PSer_H
SPHINGO_3dehydrosphinganineRed_ER	FALSE	NADPH_ER + _3_Dehydrosphinganine_ER = Dihydrosphingosine_ER + NADPplus_ER
SPHINGO_SerCpalmitoylTran_ER	FALSE	Palmitoyl_CoA_ER + Ser = CO_2_ER + CoA_ER + _3_Dehydrosphinganine_ER
TCA_AconHydra2_M	TRUE	IsoCit_M = cis_Acon_M
TCA_AconHydra_M	FALSE	Cit_M = cis_Acon_M
TCA_CitSiSyn_M	TRUE	Cit_M + CoA_M = Ac_CoA_M + OAA_M
TCA_DihydrolipoylDH_M	FALSE	EnzymeN6__dihydrolipoyl_Lys_M + NADplus_M = EnzymeN6__lipoyl_Lys_M + NADH_M
TCA_DihydrolipoylLysresidueSuccTran_M	TRUE	EnzymeN6__dihydrolipoyl_Lys_M + SuccCoA_M = CoA_M + _DHlipoylLys_resSuccTran_S_SuccDHlipoylLys_M
TCA_Enzyme3_M	FALSE	EnzymeN6__lipoyl_Lys_M + _3_Carboxy_1_hydroxypropyl_ThPP_M = ThPP_M + _DHlipoylLys_resSuccTran_S_SuccDHlipoylLys_M
TCA_Enzyme_M	FALSE	AKG_M + ThPP_M = CO_2_M + _3_Carboxy_1_hydroxypropyl_ThPP_M
TCA_FumHydra_M	TRUE	Mal_M = Fum_M
TCA_IsoCitDHNADPplus2_M	FALSE	IsoCit_M + NADPplus_M = NADPH_M + OASucc_M
TCA_IsoCitDHNADPplus_M	FALSE	OASucc_M = AKG_M + CO_2_M
TCA_IsoCitDHNADplus_M	FALSE	IsoCit_M + NADplus_M = AKG_M + CO_2_M + NADH_M
TCA_MalDH_M	FALSE	Mal_M + NADplus_M = NADH_M + OAA_M
TCA_SuccCoALigADPforming_M	TRUE	ATP_M + CoA_M + Succ_M = ADP_M + SuccCoA_M
TCA_SuccCoALigGDPforming2_M	TRUE	CoA_M + ITP_M + Succ_M = IDP_M + SuccCoA_M
TCA_SuccCoALigGDPforming_M	TRUE	CoA_M + GTP_M + Succ_M = GDP_M + SuccCoA_M
TCA_SuccDHubiquinone_M	FALSE	Succ_M + Ubiquinone_M = Fum_M + Ubiquinol_M
TRANSPORT_MCF1	FALSE	PYR_Y = PYR_M
TRANSPORT_PLGG1	FALSE	D_GA_Y + Glycolate_H = D_GA_H + Glycolate_Y
TRANSPORT_PPT	FALSE	PEP_Y = PEP_H
TRANSPORT_PXA1	FALSE	OPDA_H = OPDA_P
TRANSPORT_TPT1	TRUE	D_Glyceraldehyde3_P_Y = D_Glyceraldehyde3_P_H
TRANSPORT_TPT2	FALSE	_3_P_D_GA_Y = _3_P_D_GA_H
TRANSPORT_TPT3	FALSE	DHAP_Y = DHAP_H
TRANSPORT_XPT1	FALSE	D_E4P_Y = D_E4P_H
TRANSPORT_XPT2	FALSE	D_Xu5_P_Y = D_Xu5_P_H
TRANSPORT_unknownGenes6	FALSE	Gly_P = Gly_M
TRANSPORT_unknownGenes8	TRUE	D_GA_Y = D_GA_P
TRANSPORT_unknownGenes9	FALSE	Glycolate_Y = Glycolate_P
simplified_fatty_acid_synthesis	FALSE	Ac_CoA_M = Linolenate_H

Table S10. The applied metabolic network of *Arabidopsis thaliana* (Fieselmann A 2016)

Bibliography

Abiri R, S. N., Maziah M, Yusof ZNB, Atabaki N, Sahebi M, Valdiani A, Kalhori N, Azizi P, Hanafi MM (2017). "Role of ethylene and the APETALA 2/ethylene response factor superfamily in rice under various abiotic and biotic stress conditions." Environmental and Experimental Botany **134**: 33-44.

Adachi H, N. T., Miyagawa N, Ishihama N, Yoshioka M, Katou Y, Yaeno T, Shirasu K, Yoshiokaa H (2015). "WRKY Transcription Factors Phosphorylated by MAPK Regulate a Plant Immune NADPH Oxidase in Nicotiana benthamiana." The Plant Cell.

Adams MJ, A. J. (2006). "DPVweb: a comprehensive database of plant and fungal virus genes and genomes." Nucleic Acids Research **34**: Database issue D382-D385.

Alamillo JM, S. P., Garcia JA (2006). "Salicylic acid-mediated and RNA-silencing defence mechanisms cooperate in the restriction of systemic spread of plum pox virus in tobacco." Plant J. **48**: 217–227.

Alazem M, L., KY, Lin NS (2014). "The abscisic acid pathway has multifaceted effects on the accumulation of bamboo mosaic virus." Mol. Plant–Microbe Interact. **27**: 177–189.

Alazem M, L. N. (2015). "Roles of plant hormones in the regulation of host–virus interactions." Molecular Plant Pathology **16**(5): 529–540.

Albersheim P, D., AG, Mc Neil M, Valent BS, Sharp JK, Nothnagel EA, Davis KR, Yamazaki N, Gollin DJ, York WS, Dudman WF, Darvill JE, Dell A (1983). "Oligosaccharins: Naturally Occurring Carbohydrates with Biological Regulatory Functions." NATO Advanced Science Institutes Series **63**: 293–312.

Alicai T, N. J., Sseruwagi P, Tairo F, Okao-Okuja G, Nanvubya R, Kiiza L, Kubatko L, Kehoe MA, Boykin LM (2016). "Cassava brown streak virus has a rapidly evolving genome: implications for virus speciation, variability, diagnosis and host resistance." Scientific Reports **6**: 36164.

Alonso JM, H. T., Roman G, Nourizadeh S, Ecker JR (1999). "EIN2, a bifunctional transducer of ethylene and stress responses in Arabidopsis." Science **284**(5423): 2148-2152.

Altschul SF, G. W., Miller W, Myers EW, Lipman DJ (1990). "Basic local alignment search tool." J. Mol. Biol. **215**(3): 403-410.

Anders S, P. P., Huber W (2015). "HTSeq--a Python framework to work with high-throughput sequencing data." Bioinformatics **31**(2): 166-169.

Andreasson E, J. T., Brodersen P, Thorgrimsen S, Petersen NH, Zhu S, Qiu JL, Micheelsen P, Rocher A, Petersen M, et al (2005). "The MAP kinase substrate MKS1 is a regulator of plant defence responses." EMBO J. **24**: 2579–2589.

W, A. S. a. H. (2010). "Differential expression analysis for sequence count data." Genome Biol. **11**(R106).

Andrews S (2010). "FastQC: a quality control tool for high throughput sequence data." Available online at: http://www.bioinformatics.babraham.ac.uk/projects/fastqc.

Apweiler R, B. A., Wu CH (2004). "Protein sequence databases." Curr Opin in Chem Biol. **8**: 76-80.

Apweiler R, B. A., Wu CH, Barker WC, Boeckmann B, Ferro S, Gasteiger E, Huang H, Lopez R, Magrane M, Martin MJ, Natale DA, O'Donovan C, Redaschi N, Yeh LL (2004). "UniProt: the Universal Protein knowledgebase." Nucleic Acids Res. **32**: D115-D119.

Arvidsson S, K. M., Riano-Pachon DM, Mueller-Roeber B (2008). "QuantPrime - a flexible tool for reliable high-throughput primer design for quantitative PCR." BMC Bioinformatics **9**(645).

Asai S, O. K., Yoshioka H (2008). "MAPK signaling regulates nitric oxide and NADPH oxidase-dependent oxidative bursts in Nicotiana benthamiana." Plant Cell **20**: 1390–1406.

Ascencio-Ibáñez JT, S. R., Lee TJ, Chu TM, Wolfinger RD, Cella R, Hanley-Bowdoin L (2008). "Global analysis of Arabidopsis gene expression uncovers a complex array of changes impacting pathogen response and cell cycle during geminivirus infection." Plant Physiol **148**: 436–454.

Ashburner M, C., Blake JA, Botstein D, Butler H, Cherry JM, Davis AP, Dolinski K, Dwight SS, Eppig JT, Harris MA, Hill DP, Issel-Tarver L, Kasarskis A, Lewis S, Matese JC, Richardson JE, Ringwald M, Rubin GM, Sherlock G (2000). "Gene Ontology: tool for the unification of biology." Nature Genetics **25**(1): 25-29.

Asselbergh B, D. V. D., Hofte M (2008). "Global switches and fine-tuning-ABA modulates plant pathogen defence." Mol. Plant–Microbe Interact **21**: 709–719.

Aubourg S, K. M., Lecharny A (1999). "The DEAD box RNA helicase family in Arabidopsis thaliana." Nucleic Acids Res. **27**(2): 628-636.

Austin MJ, M. P., Kahn K, Feys BJ, Jones JD, Parker JE (2002). "Regulatory role of SGT1 in early R gene-mediated plant defences." Science **15**(295(5562)): 2077-2080.

Azevedo C, B. S., Peart J, Takahashi A, Noël L, Sadanandom A, Casais C, Parker J, Shirasu K (2006). "Role of SGT1 in resistance protein accumulation in plant immunity." EMBO J. **25**(9): 2007-2016.

Azevedo C, S. A., Kitagawa K, Freialdenhoven A, Shirasu K, Schulze-Lefert P (2002). "The RAR1 interactor SGT1, an essential component of R gene-triggered disease resistance." Science **295**: 2073–2076.

Babu M, G. A., Brandle JE, Wang A (2008). "Association of the transcriptional response of soybean plants with soybean mosaic virus systemic infection." J Gen Virol **89**(Pt 4): 1069–1080.

Babu M, G. J., Huang TS, Wang A (2008). " Altered gene expression changes in Arabidopsis leaf tissues and protoplasts in response to plum pox virus infection." BMC Genomics **9**: 325.

Baebler S, S. K., Kovac M, Blejec A, Prezelj N, Stare T (2011). Dynamics of responses in compatible potato - Potato virus Y interaction are modulated by salicylic acid, PLos One. **6**.

Baebler S, W. K., Petek M, Stare K, Tusek-Znidaric M, Pompe-Novak M (2014). "Salicylic acid is an indispensable component of the Ny-1 resistance-gene-mediated response against Potato virus Y infection in potato." J. Exp. Bot. **65**: 1095–1109.

Baena-Gonzalez E (2010). "Energy signaling in the regulation of gene expression during stress." Mol Plant **3**: 300–313.

Bai C, S. P., Hofmann K, Ma L, Goebl M, Harper JW, Elledge SJ (1996). "SKP1 connects cell cycle regulators to the ubiquitin proteolysis machinery through a novel motif, the F-box." Cell **86**: 263-274.

Bairoch A, B. B., Ferro S, Gasteiger E (2004). "Swiss-Prot: juggling between evolution and stability." Brief Bioinform **5**(1): 39-55.

Baker B, Z. P., Staskawicz B, Dinesh-Kumar SP (1997). "Signaling in plant-microbe interactions." Science **276**: 726–733.

Bansal PK, A. R., Kitagawa K (2004). "Sgt1 associates with Hsp90: an initial step of assembly of the core kinetochore complex." Mol Cell Biol **24**: 8069–8079.

Bari R, J. J. (2009). "Role of plant hormones in plant defence responses." Plant Mol Biol. **69**(4): 473–488.

Barth C, M. W., Klessig DF, Conklin PL (2004). "The timing of senescence and response to pathogens is altered in the ascorbate-deficient Arabidopsis mutant vitamin c-1." Plant Physiol. **134**: 1784–1792.

Belkhadir Y, C. J. (2006). "Brassinosteroid signaling: a paradigm for steroid hormone signaling from the cell surface." Science **314**: 1410-1411.

Berger S, P. M., Schreiber U, Kaiser W, Roitsch T (2004). "Complex regulation of gene expression, photosynthesis and sugar levels by pathogen infection in tomato " Physiol Plant **122**: 419–428.

Berrocal-Lobo M, M. A., Solano R (2002). "Constitutive expression of ETHYLENE-RESPONSE-FACTOR1 in Arabidopsis confers resistance to several necrotrophic fungi." Plant J. **29**(1): 23-32.

Bieri S, M. S., Shen QH, Peart J, Devoto A, Casais C, Ceron F, Schulze S, Steinbiss HH, Shirasu K, Schulze-Lefert P (2004). "RAR1 positively controls steady state levels of barley MLA resistance proteins and enables sufficient MLA6 accumulation for effective resistance." Plant Cell **16**: 3480–3495.

Boddu J, C. S., Kruger WM, Muehlbauer GJ (2006). "Transcriptome analysis of the barley-Fusarium graminearum interaction." Mol Plant Microbe Interact **19**: 407–417.

Bolouri Moghaddam MR, d. E. W. (2012). "Sugars and plant innate immunity." J. Exp. Bot **63**(11): 3989-3998.

Botër M, A. B., Peart J, Breuer C, Kadota Y, Casais C, Moore G, Kleanthous C, Ochsenbein F, Shirasu K, Guerois R (2007). "Structural and functional analysis of SGT1 reveals that its interaction with HSP90 is required for the accumulation of Rx, an R protein involved in plant immunity." Plant Cell **19**(11): 3791-3804.

Boyes DC, N. J., Dangl JL (1998). "The Arabidopsis thaliana RPM1 disease resistance gene product is a peripheral plasma membrane protein that is degraded coincident with the hypersensitive response." PNAS **95**(26): 15849-15854.

Brady ST (1995). "A kinesin medley: biochemical and functional heterogeneity." Trends Cell Biol. **5**(4): 159-164.

Buchanan-Wollaston V, P. T., Harrison E, Breeze E, Lim PO, Nam HG, Lin J-F, Wu S-H, Swidzinski J, Ishizaki K, Leaver CJ (2005). "Comparative transcriptome analysis reveals significant differences in gene expression and signalling pathways between developmental and dark/starvation-induced senescence in Arabidopsis." The Plant Journal **42**: 567–585.

Camacho C, C. G., Avagyan V, Ma N, Papadopoulos J, Bealer K, Madden TL (2008). "BLAST+: architecture and applications." BMC Bioinformatics **10**(421).

Campbell JA, D. G., Bulone V, Henrissat B. (1997). "A classification of nucleotide-diphospho-sugar glycosyltransferases based on amino acid sequence similarities." Biochem J. **326**((Pt 3)): 929-939.

Cao H, G. J., Clarke JD, Volko S, Dong X (1997). "The Arabidopsis NPR1 gene that controls systemic acquired resistance encodes a novel protein containing ankyrin repeats." Cell **88**(1): 57-63.

Cecil A, h. K., Menzel T, François P, Schrenzel J, Fischer A, Dörries K, Selle M, Lalk M, Hantzschmann J, Dittrich M, Liang C, Bernhardt J, Ölschläger TA, Bringmann G, Bruhn H, Unger M, Ponte-Sucre A, Lehmann L, Dandekar T (2015). "Modelling antibiotic and cytotoxic isoquinoline effects in Staphylococcus aureus, Staphylococcus epidermidis and mammalian cells." International Journal of Medical Microbiology **305**(1): 96-109.

Cetin-Karaca H (2011). Evaluation of natural antimicrobial phenolic compounds against foodborne pathogens University of Kentucky Master's Theses. **652**.

Choe S, N. T., Fujioka S, Takatsuto S, Tissier CP, Gregory BD, Ross AS, Tanaka A, Yoshida S, Tax FE, Feldmann KA (1999). "The Arabidopsis dwf7/ste1 mutant is defective in the delta7 sterol C-5 desaturation step leading to brassinosteroid biosynthesis." Plant Cell **11**(2): 207–221.

Choi J, C. D., Lee S, Ryu CM, Hwang I (2011). "Cytokinins and plant immunity: old foes or new friends? ." Trends Plant Sci **16**: 388–394.

Christie M, B. C., Rothnagel JA, Carroll BJ (2011). "RNA decay and RNA silencing in plants: competition or collaboration?" Front Plant Sci. **2**(99).

Clark MF, A. A. (1977). "Characteristics of the microplate method of enzyme-linked immunosorbent assay for the detection of plant viruses." Journal of General Virology **34**: 475-483.

Clarke SF, B. D., Guy PL (1998). "Influence of plant hormones on virus replication and pathogenesis-related proteins in Phaseolus vulgaris L. infected with white clover mosaic potexvirus." Physiol. Mol. Plant Pathol. **53**: 195–207.

Clarke SF, G. P., Burritt DJ, Jameson PE (2002). "Changes in the activities of antioxidant enzymes in response to virus infection and hormone treatment." Physiologia Plantarum **114**.

Clifford MN, J. K., Knight S, Kuhnert N (2003). "Hierarchical scheme for LC-MSn identification of chlorogenic acids." J Agric Food Chem. **51**(10): 2900-2911.

Clifford MN, K. J., Kuhnert N, Roozendaal H, Salgado PR (2008). "LC–MSn analysis of the cis isomers of chlorogenic acids." Food Chemistry **106**(1): 379-385.

Conrath U (2011). "Molecular aspects of defence priming." trends in Plant Science **16**: 524-553.

Craig EA (1989). "Essential roles of 70 kDa heat inducible proteins." Bioessays **11**(2-3): 48-52.

Crocoll C, M. N., Reichelt M, Gershenzon J, Halkier BA (2016). "Optimization of engineered production of the glucoraphanin precursor dihomomethionine in Nicotiana benthamiana." Frontiers in Bioengineering and Biotechnology **4**(14).

Csermely P, S. T., Soti C, Prohászka Z, Nardai G (1998). "The 90- kDa Molecular Chaperone Family: Structure, Function, and Clinical Applications. A Comprehensive Review." Pharmacol. Ther. **79**(2): 129–168.

D'Auria JC (2006). "Acyltransferases in plants: a good time to be BAHD." Curr Opin Plant Biol **9**(3): 331-340.

Dangl, J. J. a. J. (2006). "The plant immune system." Nature **444**: 323-329.

De Gara L, D. P. M., Tommasi F (2003). "The antioxidant systems vis-à-vis reactive oxygen species during plant–pathogen interaction." Plant Physiology and Biochemistry **41**: 863–870.

De León IP, S. A., Hamberg M, Castresana C (2002). "Involvement of the Arabidopsis alpha-DOX1 fatty acid dioxygenase in protection against oxidative stress and cell death." Plant J. **29**(1): 61-62.

del Pozo O, L. E. (2003). "Expression of the baculovirus p35 protein in tobacco affects cell death progression and compromises N gene mediated disease resistance response to Tobacco mosaic virus." Mol. Plant-Microbe Interact **16**: 485-494.

Delaney TP, U. S., Vernooij B (1994). "A central role of salicylic acidinplant disease resistance." Science **266**: 1247–1250.

Demmig-Adams B, A. I. W. (1992). "Photoprotection and Other Responses of Plants to High Light Stress." Annual Review of Plant Physiology and Plant Molecular Biology **43**: 599-626.

Deng X-G, Z. T., Peng X-J, Xi D-H, Guo H, Yin Y, Zhang D-W, Lin H-H (2016). "Role of brassinosteroid signaling in modulating Tobacco mosaic virus resistance in Nicotiana benthamiana." Scientific Reports **6**.

Deng X-G, Z. T., Zhang D-W,Lin H-H (2015). "The alternative respiratory pathway is involved in brassinosteroid-induced environmental stress tolerance in Nicotiana benthamiana." Journal of Experimental Botany **66**(20): 6219–6232.

Després C, D. C., Glaze S, Liu E, Fobert PR (2000). "The Arabidopsis NPR1/NIM1 protein enhances the DNA binding activity of a subgroup of the TGA family of bZIP transcription factors." Plant Cell **12**: 279–290.

Díaz-Vivancos P, C.-M. M., Rubio M, Olmos E, García JA, Martínez-Gómez P, Hernández JA (2008). "Alteration in the chloroplast metabolism leads to ROS accumulation in pea plants in response to plum pox virus." Journal of Experimental. Botany **59**: 2147–2160.

Diener AC, G. R., Fink GR (2001). "Arabidopsis ALF5, a Multidrug Efflux Transporter Gene Family Member, Confers Resistance to Toxins." The Plant Cell **13**(7): 1625-1638.

Dodds PN, S. C. (2002). "A Breakdown in Defence Signaling." Plant Cell **14(Suppl)**: s5–s8.

Dombrovsky A, R. V., Antignus Y (2014). "Ipomovirus – an atypical genus in the family Potyviridae transmitted by whiteflies." Pest Manag Sci **70**: 1553-1567.

Duplan V, R. S. (2014). "E3 ubiquitin-ligases and their target proteins during the regulation of plant innate immunity." Front Plant Sci. **5**(42).

Durmuş S, Ç. T., Özgür A, Guthke R (2015). "A review on computational systems biology of pathogen–host interactions." Frontiers in Microbiology **6**(235).

Eulgem T, S. I. (2007). "Networks of WRKY transcription factors in defence signaling." Curr Opin Plant Biol. **10**: 366–371.

Fernie AR, T. R., Krotzky AJ, Willmitzer L (2004). "Metabolite profiling: from diagnostics to systems biology." Nature Reviews | Molecular cell biology **5**: 763-769.

FF, T. M. a. d. F. (2016). "Why Benthamiana Went Viral." trends in Plant Science **21**(1): 4-6.

Fieselmann A (2016). Metabolische Modellierung und systembiologische Analysen des Pathogen- und Wirtsmetabolismus : Am Beispiel von Salmonella enterica und Arabidopsis thaliana. Aachen: Shaker Verlag**:** 159.

Finn RD, C. P., Eberhardt RY, Eddy SR, Mistry J, Mitchell AL, Potter SC, Punta M, Qureshi M, Sangrador-Vegas A, Salazar GA, JTate J, Bateman A (2016). "The Pfam protein families database: towards a more sustainable future." Nucleic Acids Research **44(D1)**: D279-D285.

Fraser CM, C. C. (2011). "The Phenylpropanoid Pathway in Arabidopsis." The Arabidopsis Book / American Society of Plant Biologists **9**(e0152).

Gaffney T, F. L., Vernooij B, Negrotto D, Nye G, Uknes S, Ward E, Kessmann H, Ryals J (1993). "Requirement of salicylic acid for the induction of systemic acquired resistance." Science **261**(5122): 754-756.

Galis I, S. J., Jameson PE (2004). "Salicylic acid-, but not cytokinin induced, resistance to WClMV is associated with increased expression of SA-dependent resistance genes in Phaseolus vulgaris." J. Plant Physiol. **161**: 459–466.

Gao Q-M, Z. S., Kachroo P, Kachroo A (2015). "Signal regulators of systemic acquired resistance." Frontiers in Plant Science **6**(228).

Gassmann, S. B. a. M. "Assessing Integrity of Plant RNA with the Agilent 2100 Bioanalyzer System." Agilent technologies.

Golem S, C. J. (2003). "Tobacco mosaic virus induced alterations in the gene expression profile of Arabidopsis thaliana." Mol Plant–Microb Interact **16**: 681–688.

Gómez-Ariza J, C. S., Rufat M, Estopà M, Messeguer J, San Segundo B, Coca M (2007). "Sucrose-mediated priming of plant defence responses and broad-spectrum disease resistance by overexpression of the maize pathogenesis-related PRms protein in rice plants." Mol Plant Microbe Interact. **20**: 832-842.

Goodman RN, K. Z., Wood KR (1986). "The Biochemistry and Physiology of Plant Disease." University of Missouri Press, Columbia.

Grabherr MG, H. B., Yassour M, Levin JZ, Thompson DA, Amit I, ..., Regev A (2011). "Trinity: reconstructing a full-length transcriptome without a genome from RNA-Seq data." Nature biotechnology **29**(7): 644-652.

Grohmann U, B. V. (2010). "Control of immune response by amino acid metabolism." Immunological Reviews **236**(1): 243–264.

Gu YQ, W. M., Chakravarthy S, Loh YT, Yang C, He X, Han Y, Martin GB (2002). "Tomato transcription factors pti4, pti5, and pti6 activate defence responses when expressed in Arabidopsis." Plant Cell **14**(4): 817-831.

Gupta SK, B. E., Srivastava M, Pahlavan P, Balkenhol J, Dandekar T (2016). Improving re-annotation of annotated eukaryotic genomes. Big Data Analytics in Genomics, Springer.

Hakmaoui A, P.-B. M., García-Fontana B, Camejo D, Jiménez A, Sevilla F, and Barón M (2012). "Analysis of the antioxidant response of Nicotiana benthamiana to infection with two strains of Pepper mild mottle virus." Journal of Experimental Botany.

Hanks SK, Q. A., Hunter T (1988). "The protein kinase family: conserved features and deduced phylogeny of the catalytic domains." Science **241**((4861)): 42-52.

Hanley-Bowdoin L, B. E., Robertson D, Mansoor S (2013). "Geminiviruses: masters at redirecting and reprogramming plant processes." Nature Reviews | Microbiology **11**(11): 777-788.

Hanley-Bowdoin L, S. S., Orozco BM, Nagar S, Robertson D (1999). "Geminiviruses: Models for plant DNA replication, transcription, and cell cycle regulation." Crit. Rev. Plant Sci. **18**: 71-106.

He JX, G. J., Sun Y, Gampala SS, Gendron N, Sun CQ, Wang ZY (2005). "BZR1 is a transcriptional repressor with dual roles in brassinosteroid homeostasis and growth responses." Science **307**: 1634-1638.

Herbers K, M. P., Metraux JP, Sonnewald U (1996). "Salicylic acid-independent induction of pathogenesis-related protein transcripts by sugars is dependent on leaf developmental stage." FEBS Lett **397**: 239–244.

Hernández JA, T. J., Martínez-Gómez P, Dicenta F, Sevilla F (2001). "Response of antioxidative enzymes to plum pox virus in two apricot cultivars." Physiologia Plantarum **111**: 313–321.

Hofberger JA, Z. B., Tang H, Jones JDG, Schranz ME (2014). "A novel approach for multi-domain and multi-gene family identification provides insights into evolutionary dynamics of disease resistance genes in core eudicot plants." BMC Genomics **15**(1): 1-21.

Holm M, M. L., Qu LJ, Deng XW (2002). "Two interacting bZIP proteins are direct targets of COP1-mediated control of light-dependent gene expression in Arabidopsis." Genes Dev. 2002 May 15;16(10):1247-59. **16**(10): 1247-1259.

Hu Y, G. Y., Lei Yin, Wang X, Feng C, Feng L, Li D, Jiang X-N, Wang D-C (2010). "Crystal Structures of a Populus tomentosa 4-Coumarate:CoA Ligase Shed Light on Its Enzymatic Mechanisms." The Plant Cell **22**(9): 3093-3104.

Hubert DA, T. P., Belkhadir Y, Krishna P, Takahashi A, Shirasu K, Dangl JL (2003). "Cytosolic HSP90 associates with and modulates the Arabidopsis RPM1 disease resistance protein." EMBO J **22**: 5679–5689.

Hull, R. (2009). "Comparative plant virology." Elsevier Academic Press **second edn.**: 117-164.

Hunter LJR, W. J., Heath G, Macaulay K, Smith AG, MacFarlane SA, Palukaitis P, Carr JP (2013). "Regulation of RNA-Dependent RNA Polymerase 1 and Isochorismate Synthase Gene Expression in Arabidopsis." PLoS One **8**(6).

Iriti M, F. F. (2008). "Abscisic acid is involved in chitosan-induced resistance to tobacco necrosis virus (TNV)." Plant Physiol. Biochem. **46**: 1106–1111.

Ishihama N, A. H., Yoshioka M, Yoshioka H (2014). "In vivo phosphorylation of WRKY transcription factor by MAPK." Methods Mol. Biol. **1171**: 171–181.

Ishihama N, Y. R., Yoshioka M, Katou S, Yoshioka H (2011). "Phosphorylation of the Nicotiana benthamiana WRKY8 transcription factor by MAPK functions in the defence response." Plant Cell **23**(3): 1153-1170.

Ishihara T, S. K., Hase S, Kanayama Y, Seo S, Ohashi Y (2008). "Overexpression of the Arabidopsis thaliana EDS5 gene enhances resistance to viruses." Plant Biol. **10**(4): 451–461.

Ivanov KI, E. K., Lõhmus A, Mäkinen K (2014). "Molecular and cellular mechanisms underlying potyvirus infection." Journal of General Virology **95**: 1415–1429.

Jacob F, V. S., Maekawa T (2013). "Evolution and Conservation of Plant NLR Functions." Frontiers in Immunology **4**(297).

Jander G, N. S., Joshi V, Fraga M, Rugg A, Yu S, Li L, Last RL (2004). "Application of a high-throughput HPLC-MS/MS assay to Arabidopsis mutant screening; evidence that threonine aldolase plays a role in seed nutritional quality." The Plant Journal **39**: 465-475.

Jay F, W. Y., Yu A, Taconnat L, Pelletier S, Colot V (2011). "Misregulation of AUXIN RESPONSE FACTOR 8 underlies the developmental abnormalities caused by three distinct viral silencing suppressors in Arabidopsis." PLoS Pathog **9**(e1003435).

Jiang J, S. C.-P. (2008). "MEK1/2 and p38-like MAP kinase successively mediate H2O2 signaling in Vicia guard cell." Plant Signaling & Behavior **3**(11): 996–998.

Jin H, L. Y., Yang K Y, Kim C Y, Baker B, Zhang S (2003). "Function of a mitogen-activated protein kinase pathway in N gene-mediated resistance in tobacco." Plant J. **33**: 719-731.

Jobic C, B. A., Gout E, Rascle C, Fevre M, Cotton P, Bligny R (2007). "Metabolic processes and carbon nutrient exchanges between host and pathogen sustain the disease development during sunflower infection by Sclerotinia sclerotiorum." Planta **226**: 251–265.

Junker BH (2014). "Flux analysis in plant metabolic networks: increasing throughput and coverage." Curr Opin Biotechnol. **26**: 183-188.

Kadota Y, S. K. (2012). "The HSP90 complex of plants." Biochim. Biophys. Acta **1823**: 689–697.

Kanehisa M, F. M., Tanabe M, Sato Y, Morishima K (2017). "KEGG: new perspectives on genomes, pathways, diseases and drug." Nucleic Acids Res **45**: D353-D361.

Kanehisa M, G. S. (2000). "KEGG: Kyoto Encyclopedia of Genes and Genomes." Nucleic Acids Res. **28**(1): 27-30.

Kanehisa M, S. Y., Morishima K (2016). "BlastKOALA and GhostKOALA: KEGG tools for functional characterization of genome and metagenome sequences." J. Mol. Biol. **428**(4): 726-731.

Kanehisa M, Y., Kawashima M, Furumichi M, Tanabe M (2016). "KEGG as a reference resource for gene and protein annotation." Nucleic Acids Res. **44**: D457-D462.

Kawaide H, I. R., Sassa T, Kamiya Y (1997). "Ent-kaurene synthase from the fungus Phaeosphaeria sp. L487. cDNA isolation, characterization, and bacterial expression of a bifunctional diterpene cyclase in fungal gibberellin biosynthesis." J Biol Chem. **272**(35): 21706-21712.

Kazan K, M. J. (2009). "Linking development to defence: auxin in plant– pathogen interactions." Trends Plant Sci. **14**: 373–382.

Kazan K, M. J. (2013). "MYC2: the master in action." Mol Plant **6**(3): 686-703.

Kemmerling B, S. A., Rodriguez P, Mazzotta S, Frank M, Qamar SA, Mengiste T, Betsuyaku S, Parker JE, Müssig C, Thomma BP, Albrecht C, de Vries SC, Hirt H, Nürnberger T. (2007). "The BRI1-associated kinase 1, BAK1, has a brassinolide-independent role in plant cell-death control." Curr Biol. **17**(13): 1116-1122.

Kim D, P. G., Trapnell C, Pimentel H, Kelley R,Salzberg SL Kim D, Pertea G, Trapnell C, Pimentel H, Kelley R,Salzberg SL (2013). "TopHat2: accurate alignment of transcriptomes in the presence of insertions, deletions and gene fusions." Genome Biol. **25**(14(4)).

Kirchhausen T, B. J., Riezman H (1997). "Linking cargo to vesicle formation: receptor tail interactions with coat proteins." Curr Opin Cell Biol **9**: 488-495.

Knoester M, L. H., Bol JF, Van Loon LC (2001). "Involvement of ethylene in lesion development and systemic acquired resistance in tobacco during the hypersensitive reaction to tobacco mosaic virus." Physiol. Mol. Plant Pathol. **59**: 45-57.

Komatsu K, H. M., Ozeki J, Yamaji Y, Maejima K, Senshu H, Himeno M, Okano Y, Kagiwada S, Namba S (2010). "Viral-induced systemic necrosis in plants involves both programmed cell death and the inhibition of viral multiplication, which are regulated by independent pathways." Mol Plant Microbe Interact **23**(3): 283-293.

Koornneef A, P. C. (2008). "Cross talk in defence signaling." Plant Physiol **146**(3).

Korner CJ, K. D., Niehl A, Dominguez-Ferreras A, Chinchilla D, Boller T (2013). "The immunity regulator BAK1 contributes to resistance against diverse RNA viruses." Mol. Plant–Microbe Interact. **26**: 1271–1280.

Kørner CJ, K. D., Niehl A, Domínguez-Ferreras A, Chinchilla D, Boller T, Heinlein M, Hann DR (2013). "The immunity regulator BAK1 contributes to resistance against diverse RNA viruses." Mol Plant Microbe Interact **26**(11): 1271-1280.

Korpelainen E, T. J., Somervuo P, Huss M, Wong G (2014). RNA-seq Data Analysis: A Practical Approach, CRC Press.

Kouzarides, T. (2007). "Chromatin modifications and their function." Cell **128**.

Kovac M, M. A., Milovanovic Jarah D, Milavec M, Duchting P, Ravnikar M (2009). "Multiple hormone analysis indicates involvement of jasmonate signaling in the early defence of potato to potato virus YNTN." Biol. Plant. **53**: 195–199.

Krupovic M, R. J., Bamford DH (2009). "Geminiviruses: A tale of a plasmid becoming a virus." BMC Evol. Biol. **9**(112).

Kühn K, Y. G., Duncan O, Law SR, Kubiszewski-Jakubiak S, Kaur P, Meyer E, Wang Y, Small CC des F, Giraud E, Narsai R, Whelan J (2015). "Decreasing electron flux through the cytochrome and/or alternative respiratory pathways triggers common and distinct cellular responses dependent on growth conditions." Plant Physiology **167**(1): 228–250.

Kumagai MH, D. J., della-Cioppa G, Harvey D, Hanley K, Grill LK (1995). "Cytoplasmic inhibition of carotenoid biosynthesis with virus-derived RNA." PNAS **92**(5): 1679-1683.

Kumar S, P. A. (2013). "Chemistry and Biological Activities of Flavonoids: An Overview." The Scientific World Journal.

Kunz M, A. N., Dandekar T, Naseem M (2013). "Hormone Signaling Networks Open Multiple Routes for Immunity and Disease in Plants." Biohelikon: Immunity and Diseases **1**(2).

Laity JH, L. B., Wright PE (2001). "Zinc finger proteins: new insights into structural and functional diversity." Curr Opin Struct Biol. **11**: 39-46.

Langmead B, T. C., Pop M, Salzberg SL (2009). "Ultrafast and memory-efficient alignment of short DNA sequences to the human genome." Genome Biology **10**(R25).

Laub MT , G. M. (2007). "Specificity in two-component signal transduction pathways." Annual Review of Genetics **41**: 121-145.

Lee, W. S., Fu, S.F., Verchot-Lubicz, J. and Carr, J.P (2011). "Genetic modification of alternative respiration in Nicotiana benthamiana affects basal and salicylic acid-induced resistance to potato virus " BMC Plant Biol. 11, 41.

Lee, W. S. S. a. D. G. (2010). "Antifungal action of chlorogenic acid against pathogenic fungi, mediated by membrane disruption." Pure Appl. Chem. **82**(1): 219–226.

Li H, H. B., Wysoker A, Fennell T, Ruan J, Homer N, Marth G, Abecasis G, Durbin R (2009). "The Sequence Alignment/Map format and SAMtools." Bioinformatics **25**(16): 2078-2079.

Li P, Y. Y., Li D, Kim SW, Wu G (2007). "Amino acids and immune function." British Journal of Nutrition **98**(2): 237-252.

Li Y, C. H., Cui X, Wang A (2016). "The altered photosynthetic machinery during compatible virus infection." Curr Opin in Virol. **17**: 19-24.

Liscum E, R. J. (2002). "Genetics of Aux/IAA and ARF action in plant growth and development." Plant Mol Biol **49**(3-4): 387-400.

Liu D, S. L., Han C, Yu J, Li D, Zhang Y (2012). "Validation of reference genes for gene expression studies in virus-infected Nicotiana benthamiana using quantitative real-time PCR." PLoS One **7**(9).

Liu J, Z. Y., Qin G, Tsuge T, Sakaguchi N, Luo G, Sun K, Shi D, Aki S, Zheng N, Aoyama T, Oka A, Yang W, Umeda M, Xie Q, Gu H, Qu LJ (2008). "Targeted degradation of the cyclin-dependent kinase inhibitor ICK4/KRP6 by RING-type E3 ligases is essential for mitotic cell cycle progression during Arabidopsis gametogenesis." Plant Cell **20**(6): 1538-1554.

Liu Y, S. M., Marathe R, Dinesh-Kumar SP. (2002). "Tobacco Rar1, EDS1 and NPR1/NIM1 like genes are required for N-mediated resistance to tobacco mosaic virus." Plant J. **30**(4): 415-429.

Liu Y, S. M., Serino G, Deng X-W, Dinesh-Kumar SP (2002). "Role of SCF Ubiquitin-Ligase and the COP9 Signalosome in the N Gene–Mediated Resistance Response to Tobacco mosaic virus." The Plant Cell **14**(7): 1483-1496.

Lohse M, A., Herter T, May P, Schroda M, Zrenner R, Tohge T, Fernie AR , Stitt M, Usadel B (2014). "Mercator: a fast and simple web server for genome scale functional annotation of plant sequence data." Plant Cell Environ. **37**(5): 1250-1258.

Lorenzo O, C. J., Sánchez-Serrano JJ, Solano R (2004). "JASMONATE-INSENSITIVE1 encodes a MYC transcription factor essential to discriminate between different jasmonate-regulated defence responses in Arabidopsis." Plant Cell **16**(7): 1938-1950.

Lorenzo O, S. R. (2005). "Molecular players regulating the jasmonate signalling network." Curr Opin Plant Biol. **8**: 532–540.

Love MI, H. W., Anders S (2014). "Moderated estimation of fold change and dispersion for RNA-seq data with DESeq2." Genome Biology **15**(12): 1-21.

Lozano-Duran R, R.-D. T., Gusmaroli G, Luna AP, Taconnat L, Deng XW (2011). "Geminiviruses subvert ubiquitination by altering CSN-mediated derubylation of SCF E3 ligase complexes and inhibit jasmonate signaling in Arabidopsis thaliana." Plant Cell **23**: 1014–1032.

Lu J, D. Z.-X., Jun Kong J, Chen L-N, Qiu Y-H, Li G-F, Meng X-H, Zhu S-F (2012). "Transcriptome Analysis of Nicotiana tabacum Infected by Cucumber mosaic virus during Systemic Symptom Development." PLoS One **7**(8).

Lu R, M. I., Moffett P, Ruiz T, Peart J, Wu A-J, Rathjen JP, Bendahmane A, Day D, Baulcombe DC (2003). "High throughput virus-induced gene silencing identifies heat shock protein 90 as a cofactor of plant disease resistance." EMBO J **22**: 5690–5699.

Ludwig-Müller J. (2011). "Auxin conjugates: their role for plant development and in the evolution of land plants." J Exp Bot **62**(6): 1757-1773.

Maaroufi H, T. R. (2013). "Analysis and phylogeny of small heat shock proteins from marine viruses and their cyanobacteria host." PLoS One **8**(11).

Malinovsky FG, F. J., Willats WG (2014). "The role of the cell wall in plant immunity." Front Plant Sci. **6**(5).

Mandadi KK, S. K.-B. (2013). "Plant Immune Responses Against Viruses: How Does a Virus Cause Disease?" The Plant Cell **25**(5): 1489-1505.

Manosalva PM, P. S., Forouhar F, Tong L, Fry WE, Klessig DF (2010). "Methyl esterase 1 (StMES1) is required for systemic acquired resistance in potato." Mol Plant Microbe Interact **23**(9): 1151-1163.

Maruthi MN, B. S., Tufan HA, Mohammed IU, Hillocks RJ (2014). "Transcriptional Response of Virus-Infected Cassava and Identification of Putative Sources of Resistance for Cassava Brown Streak Disease." PLoS One **9**(5).

Mauch-Mani B, M. F. (2005). "The role of abscisic acid in plant–pathogen interactions." Curr Opin Plant Biol. **8**: 409–414.

Maxwell DP, W. Y., McIntosh L (1999). "The alternative oxidase lowers mitochondrial reactive oxygen production in plant cells." PNAS **96**.

Mayers, C. N., Lee, K.C., Moore, C.A., Wong, S.M. and Carr, J.P (2005). "Salicylic acid-induced resistance to Cucumber mosaic virus in squash and Arabidopsis thaliana: contrasting mechanisms of induction and antiviral action." Mol. Plant–Microbe Interact. 18, 428–434.

Mbanzibwa DR, T. Y., Tugume AK, Patil BL, Yadav JS, Bagewadi B, Abarshi MM, Alicai T, Changadeya W, Mkumbira J, Muli MB, Mukasa SB, Tairo F, Baguma Y, Kyamanywa S, Kullaya A, Maruthi MN, Fauquet CM, Valkonen JP (2011). "Evolution of cassava brown streak disease-associated viruses." J Gen Virol. **92**: 974-987.

McIntire SL, R. R., Schuske K, Edwards RH, Jorgensen EM (1997). "Identification and characterization of the vesicular GABA transporter." Nature **389**(6653): 870-876.

Moeller JR, M. M., Bancroft T, Skadsen RW, Wise RP, Whitham SA (2012). "Differential accumulation of host mRNAs on polyribosomes during obligate pathogen–plant interactions." Mol Biosyst **8**: 2153–2165.

Monger WA, S. S., Isaac AM, Foster GD (2001). "Molecular characterization of the Cassava brown streak virus coat protein." Plant Pathol **50**(4): 527–534.

Morkunas I, R. L. (2014). "The role of sugar signaling in plant defence responses against fungal pathogens." Acta Physiologiae Plantarum **36**(7): 1607–1619.

Mur LA, K. P., Lloyd AJ, Ougham H, Prats E (2008). "The hypersensitive response; the centenary is upon us but how much do we know?" J. Exp. Bot. **59**(3): 501-520.

Nakashita H, Y. M., Nitta T, Asami T, Fujioka S. (2003). "Brassinosteroid functions in a broad range of disease resistance in tobacco and rice." Plant J. **35**(5): 887–898.

Nakasugi K, C. R., Bally J, Wood CC, Hellens RP, Waterhouse PM (2013). "De Novo Transcriptome Sequence Assembly and Analysis of RNA Silencing Genes of Nicotiana benthamiana." PLoS One **8**(3).

Naseem M, D. T. (2012). "The Role of Auxin-Cytokinin Antagonism in Plant-Pathogen Interactions." PLoS Pathog **8**(11).

Naseem M, P. N., Hussain A, Wangorsch G, Ahmed N, Dandekar T (2012). "Integrated Systems View on Networking by Hormones in Arabidopsis Immunity Reveals Multiple Crosstalk for Cytokinin." The Plant Cell **24**(5): 1793-1814.

Ndamukong I, A. A., Thurow C, Fode B, Zander M, Weigel R, Gatz C (2007). "SA-inducible Arabidopsis glutaredoxin interacts with TGA factors and suppresses JA-responsive PDF1.2 transcription." Plant J. **50**(1): 128-139.

Neill S, D. R., Hancock J (2002). "Hydrogen peroxide signalling." Curr Opin Plant Biol. **5**: 388–395.

Noguchi T, F. S., Choe S, Takatsuto S, Yoshida S, Yuan H, Feldmann KA, Tax FE (1999). "Brassinosteroid-insensitive dwarf mutants of Arabidopsis accumulate brassinosteroids." Plant Physiol. **121**: 743-752.

Ohnishi T, G. B., Watanabe B, Fujioka S, Hategan L, Ide K, Shibata K, Yokota T, Szekeres M, Mizutani M (2012). "CYP90A1/CPD, a brassinosteroid biosynthetic cytochrome P450 of Arabidopsis, catalyzes C-3 oxidation." J Biol Chem. **287**(37): 31551-31560.

Oka K, K. M., Mitsuhara I, Seo S (2013). "Jasmonic acid negatively regulates resistance to Tobacco mosaic virus in tobacco." Plant Cell Physiol. **54**: 1999–2010.

Olive AJ, S. C. (2016). "Metabolic crosstalk between host and pathogen: sensing, adapting and competing." Nat Rev Microbiol. **14**(4): 221-234.

Ondov BD, B. N., and Phillippy AM (2011). "Interactive metagenomic visualization in a Web browser." BMC Bioinformatics **12**(1): 385.

Orth JD, T. I., Palsson BØ (2010). "What is flux balance analysis? ." Nat. Biotechnol. **28**: 245–248.

Oteng-Frimpong R, L. Y., Torkpo SK, Danquah EY, Offei SK, Gafni Y (2012). "Complete genome sequencing of two causative viruses of cassava mosaic disease in Ghana." Acta Virology **56**(4): 305-314.

Padmanabhan MS, S. H., Culver JN (2006). "The Tobacco mosaic virus replicase protein disrupts the localization and function of interacting Aux/IAA proteins." Mol Plant Microbe Interact **19**(8): 864–873.

Park J, H. H., Shim H, Im K, Auh CK, Lee S, Davis KR (2004). "Altered cell shapes, hyperplasia, and secondary growth in Arabidopsis caused by beet curly top geminivirus infection." Mol Cells **17**(1): 117-124.

Peart JR, L. R., Sadanandom A, Malcuit I, Moffett P, Brice DC, Schauser L, Jaggard DA, Xiao S, Coleman MJ, Dow M, Jones JD, Shirasu K, Baulcombe DC (2002). "The ubiquitin ligase-associated protein SGT1 is required for host and nonhost disease resistance in plants." PNAS **99**(16): 10865–10869.

Peart JR, L. R., Sadanandom A,Malcuit I,Moffett P,Brice DC, Schauser L, Jaggard DAW, Xiao S, Coleman MJ, Dow M,Jones JDG, Shirasu K, Baulcombe DC (2002). "Ubiquitin ligase-associated protein SGT1 is required for host and nonhost disease resistance in plants." Proceedings of the National Academy of Sciences of the United States of America **99**(16): 10865-10869.

Peng HT, L. S., Wang L, Li Y, Li YX, Zhang CW (2013). "Turnip mosaic virus induces expression of the LRR II subfamily genes and regulates the salicylic acid signaling pathway in non-heading Chinese cabbage." Physiol. Mol. Plant Pathol. 82, 64–7.

Pennazio S, R. P. (1996). "Plant hormones and plant virus diseases. The auxins." New Microbiol. **19**(4): 369-378.

Pfaffl MW (2001). "A new mathematical model for relative quantification in real-time RT–PCR." Nucleic Acids Res **29**(9).

Pfaffl MW (2004). A-Z of quantitative PCR, Chapter 3: Quantification strategies in real-time PCR. International University Line (IUL). B. SA**:** 87 - 112.

Pierce EJ, R. M. (2013). "Assessing Global Transcriptome Changes in Response to South African Cassava Mosaic Virus [ZA-99] Infection in Susceptible Arabidopsis thaliana." PLoS One **8**(6).

Piroux N, S. K., Page A, Stanley J (2007). "Geminivirus pathogenicity protein C4 interacts with Arabidopsis thaliana shaggy-related protein kinase AtSKeta, a component of the brassinosteroid signalling pathway." Virology **362**(2): 428–440.

Pohlert T (2014). "The Pairwise Multiple Comparison of Mean Ranks Package (PMCMR)."

Postel S, K. I., Beuter C, Mazzotta S, Schwedt A, Borlotti A, Halter T, Kemmerling B, Nürnberger T (2010). "The multifunctional leucine-rich repeat receptor kinase BAK1 is implicated in Arabidopsis development and immunity." Eur J Cell Biol. **89**(2-3): 169-174.

Postnikova OA, N. L. (2012). "Comparative analysis of microarray data in Arabidopsis transcriptome during compatible interactions with plant viruses." Virology Journal **9**(1): 101.

Pratap D, K. S., Snehi SK, Raj SK (2012). "Biological and molecular characterization of cucumber mosaic virus isolate causing shoestring disease of tomato in India which has closer affinity to European or East Asian isolates of CMV." Indian J. Virol. **23**: 57-63.

R Core Team. (2014). "R: A Language and Environment for Statistical Computing."

R Core Team. (2016). "R: A Language and Environment for Statistical Computing."

Rajamäki ML, V. J. (2009). "Control of nuclear and nucleolar localization of nuclear inclusion protein a of picorna-like Potato virus A in Nicotiana species." Plant Cell **21**(8): 2485–2502.

Rasmussen R (2001). "Quantification on the LightCycler." Rapid Cycle Real-time PCR, Methods and Applications: 21–34.

Ratcliff F, M.-H. A., Baulcombe DC (2001). "Technical Advance: Tobacco rattle virus as a vector for analysis of gene function by silencing." The Plant Journal **25**: 237–245.

Reidt W, W. R., Wanieck K, Chu HH, Puchta H (2006). "A homologue of the breast cancer-associated gene BARD1 is involved in DNA repair in plants." EMBO J. **25**: 4326-4337.

Ren D, Y. K., Li GJ, Liu Y, Zhang S (2006). "Activation of Ntf4, a tobacco mitogen-activated protein kinase, during plant defence response and its involvement in hypersensitive response-like cell death." Plant Physiol. **141**(4): 1482-1493.

Rhoads AR, F. F. (1997). "Sequence motifs for calmodulin recognition." FASEB J. **11**(5): 331-340.

Riedle-Bauer M (2000). "Role of reactive oxygen species and antioxidant enzymes in systemic virus infections of plants." Journal of Phytopathology **148**: 297–302.

Robert-Seilaniantz A, N. L., Bari R, Jones JD (2007). "Pathological hormone imbalances." Curr Opin Plant Biol. **10**: 372–379.

Robinson MD, M. D. S. G. (2010). "edgeR: a Bioconductor package for differential expression analysis of digital gene expression data." Bioinformatics.

Roitsch T, B. M., Hofmann M, Proels R, Sinha AK (2003). "Extracellular invertase: key metabolic enzyme and PR protein." Journal of Experimental Botany **54**: 513-524.

Rojas CM, S.-K. M., Tzin V, Mysore KS (2014). "Regulation of primary plant metabolism during plant-pathogen interactions and its contribution to plant defence." Front Plant Sci. **5**(17).

Rolland F, B.-G. E., Sheen J (2006). "Sugar sensing and signaling in plants: conserved and novel mechanisms." Annu Rev Plant Biol. **57**: 675-709.

RSS, F. (1987). "Biochemistry of Virus-Infected Plants." Research Studies Press, Letchworth, Hartfordshire, UK.

Ruiz MT, V. O., Baulcombe DC (1998). "Initiation and maintenance of virus-induced gene silencing." Plant Cell **10**(6): 937-946.

Sansregret R, D. V., Langlois M, Daayf F, Dunoyer P, Voinnet O (2013). "Extreme resistance as a host counter-counter defence against viral suppression of RNA silencing." PLoS Pathog **9**(e1003435).

Santamaría R, P. P. (2012). "Voronto: mapper for expression data to ontologies." Bioinformatics **28**(17): 2281-2282.

Sarris P, J. J. (2015). "Plant immune receptors mimic pathogen virulence targets." Oncotarget **6**(19): 16824–16825.

Satoh K, S. T., Kondoh H, Hiraguri A, Sasaya T, Choi IR. et al. (2011). "Relationship between symptoms and gene expression induced by the infection of three strains of Rice dwarf virus." PLoS One **6**(e18094).

Satoh K, Y. K., Kondoh H, et al. (2013). "Relationship between gene responses and symptoms induced by Rice grassy stunt virus." Frontiers in Microbiology: 2013;2014:2313.

Saurin W, H. M., Dassa E. (1999). "Getting in or out: early segregation between importers and exporters in the evolution of ATP-binding cassette (ABC) transporters." J Mol Evol. **48**(1): 22-41.

Schilling CH, L. D., Palsson BO (2000). "Theory for the systemic definition of metabolic pathways and their use in interpreting metabolic function from a pathway-oriented perspective." J. Theor. Biol. **203**(3): 229-248.

Scholthof K-BG, A. S., Czosnek H, Palukaitis P, Jacquot E, Hohn T, Hohn B, Saunders K, Candresse T, Ahlquist P, Hemenway C, Foster GD (2011). "Top 10 plant viruses in molecular plant pathology." Molecular Plant Pathology **12**(9): 938–954.

Schudoma C (2015). "ktoolu." Online available from https://github.com/cschu/ktoolu.

Schulz MH, Z. D., Vingron M, Birney E (2012). "Oases: robust de novo RNA-seq assembly across the dynamic range of expression levels." Bioinformatics **28**(8): 1086-1092.

Schulze-Lefert P (2004). "Plant immunity: the origami of receptor activation." Curr Biol. **14**: R22–R24.

Schuster S, F. D., Dandekar T (2000). "A general definition of metabolic pathways useful for systematic organization and analysis of complex metabolic networks." Nat. Biotechnol. **18**(3): 326-332.

Schwarz R, L. C., Kaleta C, Kühnel M, Hoffmann E, Kuznetsov S, Hecker M, Griffiths G, Schuster S, Dandekar T (2007). "Integrated network reconstruction, visualization and analysis using YANAsquare." BMC Bioinformatics **8**(313).

Schwarz R, M. P., von Kamp A, Engels B, Schirmer H, Schuster S, Dandekar T (2005). "YANA - a software tool for analyzing flux modes, gene-expression and enzyme activities." BMC Bioinformatics **6**(135).

Segonzac C, F. D., Gimenez-Ibanez S, Hann DR, Zipfel C, Rathjen JP (2011). "Hierarchy and roles of pathogen-associated molecular pattern-induced responses in Nicotiana benthamiana." Plant Physiol. **156**: 687–699.

Segretin ME, P. M., Franceschetti M, Chaparro-Garcia A, Bos J I B, Banfield M J, Kamoun S (2014). "Single Amino Acid Mutations in the Potato Immune Receptor R3a Expand Response to Phytophthora Effectors." Mol Plant Microbe Interact. **27**(7): 624-637

Selth L, D. S., Rasheed MS, Healy H, Randles JW (2005). "NAC Domain Protein Interacts with Tomato leaf curl virus Replication Accessory Protein and Enhances Viral Replication." Plant Cell **17**: 311–325.

Shalitin D, W. S. (2000). "Cucumber Mosaic Virus Infection Affects Sugar Transport in Melon Plants." Plant Physiology **123**(2): 597-604.

Shin B, C. G., Yi H, Yang S, Cho I, Kim J, Lee S, Paek N-C, Kim J-H, Song PS, Choi G (2002). "AtMYB21, a gene encoding a flower-specific transcription factor, is regulated by COP1." Plant J **30**: 23-32.

Shirasu K, L. T., Tan M-W, Schulze-Lefert P (1999). "A novel class of eukaryotic zinc-binding proteins is required for disease resistance signaling in barley and development in C. elegans." Cell **99**: 355–366.

Small ID, P. I. (2000). "The PPR motif - a TPR-related motif prevalent in plant organellar proteins." Trends Biochem Sci. **25**(2): 45-47.

Spielbauer G, L. L., Römisch-Margl L, Do PT, Fouquet R, Fernie AR, Eisenreich W, Gierl A, Settles AM (2013). "Chloroplast-localized 6-phosphogluconate dehydrogenase is critical for maize endosperm starch accumulation." Journal of Experimental Botany **64**(8): 2231-2242.

Spoel SH, D. X. (2012). "How do plants achieve immunity? Defence without specialized immune cells." Nat Rev Immunol. **12**(2): 89-100.

Suzuki N, M. G., Morales J, Shulaev V, Torres MA, Mittler R (2011). "Respiratory burst oxidases: the engines of ROS signaling." Curr Opin Plant Biol. **14**: 691–699.

Takahashi A, C. C., Ichimura K, Shirasu K (2003). "HSP90 interacts with RAR1 and SGT1, and is essential for RPS2-mediated resistance in Arabidopsis." PNAS **100**: 11777–11782.

Takahashi H, K. Y., Zheng MS, Kusano T, Hase S, Ikegami M (2004). "Antagonistic interactions between the SA and JA signaling pathways in Arabidopsis modulate expression of defence genes and gene-for-gene resistance to cucumber mosaic virus." Plant Cell Physiol. **45**(6): 803–809.

Talarczyk A, K. M., Borucki W, Hennig J (2002). "Effect of Yeast CTA1 Gene Expression on Response of Tobacco Plants to Tobacco Mosaic Virus Infection." Plant Physiol. **129**(3): 1032–1044.

Tameling WI, B. D. (2007). "Physical association of the NB-LRR resistance protein Rx with a Ran GTPase-activating protein is required for extreme resistance to Potato virus X." Plant Cell **19**(5): 1682-1694.

Tanaka S, I. N., Yoshioka H, Huser A, O'Connell R, Tsuji G, Tsuge S, Kubo Y (2009). "The Colletotrichum orbiculare SSD1 mutant enhances Nicotiana benthamiana basal resistance by activating a mitogen-activated protein kinase pathway." Plant Cell **21**: 2517–2526.

Tecsi LI, M. A., Smith AM, Leegood RC (1994). "Complex, localized changes in CO_2 assimilation and starch content associated with the susceptible interaction between cucumber mosaic virus and a cucurbit host." Plant J **5**: 837–847.

Tecsi LI, M. A., Smith AM, Leegood RC (1994). "Metabolic alterations in cotyledons of Cucurbita pepo infected by cucumber mosaic virus." J Exp Bot **45**: 1541–1551.

Thibaud MC, G. S., Nussaume L, and Robaglia C (2004). "Sucrose increases pathogenesis-related PR-2 gene expression in Arabidopsis thaliana through an SA-dependent but NPR1-independent signaling pathway." Plant Physiol. Biochem. **42**(1): 81-88.

Thomma BP, E. K., Penninckx IA, Mauch-Mani B, Vogelsang R, Cammue BP, Broekaert WF (1998). "Separate jasmonate-dependent and salicylate-dependent defence-response pathways in Arabidopsis are essential for resistance to distinct microbial pathogens." PNAS **95**(25): 15107-15111

Thordal-Christensen H, Z. Z., Wei Y, Collinge DB (1997). "Subcellular localization of H_2O_2 in plants. H_2O_2 accumulation in papillae and hypersensitive response during the barleypowdery mildew interaction." The Plant Journal **11**(6): 1187–1194.

Thorvaldsdóttir H, R. J., Mesirov JP (2013). "Integrative Genomics Viewer (IGV): high-performance genomics data visualization and exploration." Brief Bioinform **14**(2): 178-192.

Thran M, L. K., Sonnewald U (2012). "The Arabidopsis DCP2 gene is required for proper mRNA turnover and prevents transgene silencing in Arabidopsis." Plant J. **72**: 368–377.

Tiancong Qi, S. S., Qingcuo Ren, Dewei Wu, Huang Huang, Yan Chen, Meng Fan, Wen Peng, Chunmei Ren and Daoxin Xie (2011). "The Jasmonate-ZIM-Domain Proteins Interact with the WD-

Repeat/bHLH/MYB Complexes to Regulate Jasmonate-Mediated Anthocyanin Accumulation and Trichome Initiation in Arabidopsis thaliana." The Plant Cell **23**(5): 1795-1814.

Ton J, F. V., Mauch-Mani B (2009). "The multifaceted role of ABA in disease resistance." Trends Plant Sci. **14**(6): 310–317.

Trouvelot S, H. M., Poinssot B, Gauthier A, Paris F, Guillier C, Combier M, Trdá L, Daire X, Adrian M (2014). "Carbohydrates in plant immunity and plant protection: roles and potential application as foliar sprays." Front Plant Sci. **5**(592).

Vadassery J, R. R., Hause B, Gershenzon J, Boland W, Mithöfer A (2012). "CML42-Mediated Calcium Signaling Coordinates Responses to Spodoptera Herbivory and Abiotic Stresses in Arabidopsis." Plant Physiol **159**: 1159-1175.

Van Bel M, S., Van Neste C, Deforce D, Van de Peer Y, Vandepoele K (2013). "TRAPID, an efficient online tool for the functional and comparative analysis of de novo RNA-Seq transcriptomes." Genome Biol. **14**(12): 1474-1760X.

Van Wees SC, G. J. (2003). "Loss of non-host resistance of Arabidopsis NahG to Pseudomonas syringae pv. phaseolicola is due to degradation products of salicylic acid." The Plant Journal **33**: 733–742.

Vanderschurena H, N. E., Poona JS, Baerenfallera K, Grossmannb J, Hirsch-Hoffmanna M, Kirchgessnerc N, Nannib P, Gruissema W (2014). "Large-Scale Proteomics of the Cassava Storage Root and Identification of a Target Gene to Reduce Postharvest Deterioration." The Plant Cell **26**(5): 1913-1924

Vlot AC, K. D., Park S-W (2008). "Systemic acquired resistance: the elusive signal(s)." Curr Opin Plant Biol. **11**(4): 436–442.

Wang X, C. J. (2006). "Brassinosteroids regulate dissociation of BKI1, a negative regulator of BRI1 signaling, from the plasma membrane." Science **313**: 1118-1122.

Wang X, S. P., Goregaoker P, Culver JN (2009). "Interaction of the Tobacco Mosaic Virus Replicase Protein with a NAC Domain Transcription Factor is Associated with the Suppression of Systemic Host Defences." J of Virol **83**: 9720–9730.

Ward JL, F. S., Beckmann M, Bennett M, Miller SJ, Baker JM, Hawkins ND, Vermeer CP, Lu C, Lin W, Truman WM, Beale MH, Draper J, Mansfield JW, Grant M (2010). "The metabolic transition during disease following infection of Arabidopsis thaliana by Pseudomonas syringae pv. tomato." Plant J. **63**(3): 443-457.

Wells DR, T. R., Le H, Gallie DR (1998). "HSP101 functions as a specific translational regulatory protein whose activity is regulated by nutrient status." Genes Dev. **12**(20): 3236–3251.

Werner T, M. V., Strnad M, Schmülling T (2001). "Regulation of plant growth by cytokinin." PNAS **98**(18): 10487–10492.

Westermann AJ, G. S., Vogel J (2012). "Dual RNA-seq of pathogen and host." Nature **10**: 618-630.

Whitham SA, Q. S., Chang HS, Cooper B, Estes B, Zhu T, Wang X, Hou YM (2003). "Diverse RNA viruses elicit the expression of common sets of genes in susceptible Arabidopsis thaliana plants." The Plant Journal **33**(2): 271-283.

Whitham SA, Y. C., Goodin MM (2006). "Global Impact: Elucidating Plant Responses to Viral Infection." MPMI **19**(11): 1207-1215.

Wickham H (2009). ggplot2: Elegant Graphics for Data Analysis, Springer-Verlag New York.

Wiermer M, F. B., Parker JE (2005). "Plant immunity: the EDS1 regulatory node." Curr Opin Plant Biol. **8**(4): 383-389.

Wood DE, S. S. (2014). "Kraken: ultrafast metagenomic sequence classification using exact alignments." Genome Biol. **15**.

Wu C-H, B. K., Bozkurt TO, Birk MS, Kamoun S (2015). "Helper NLR proteins NRC2a/b and NRC3 but not NRC1 are required for Pto-mediated cell death and resistance in Nicotiana benthamiana." New Phytol **209**: 1344–1352.

Wylie SJ, Z. C., Long V, Roossinck MJ, Koh SH, Jones MGK, Iqbal S, Li H (2015). "Differential Responses to Virus Challenge of Laboratory and Wild Accessions of Australian Species of Nicotiana, and Comparative Analysis of RDR1 Gene Sequences." PLoS One **10**(3).

Xie C, Y. K., Zhong D, Yuan T, Ye F, Jarrell JA, Millar A, Chen X (2011). "Investigation of isomeric transformations of chlorogenic acid in buffers and biological matrixes by ultraperformance liquid chromatography coupled with hybrid quadrupole/ion mobility/orthogonal acceleration time-of-flight mass spectrometry." J Agric Food Chem. **59**(20): 11078-11087.

Xie F, X. P., Chen D, Xu L, Zhang B (2012). "miRDeepFinder: a miRNA analysis tool for deep sequencing of plant small RNAs." Plant molecular biology **80**(1): 75-84.

Xie Z, F. B., Chen C, Chen Z (2001). "An important role of an inducible RNA-dependent RNA polymerase in plant antiviral defence." PNAS **98**(11): 6516–6521.

Xiong Y, D. C., Williams D, Zhang X, Mou Z (2009). "Characterization of Arabidopsis 6-phosphogluconolactonase T-DNA insertion mutants reveals an essential role for the oxidative section of the plastidic pentose phosphate pathway in plant growth and development." Plant Cell Physiol. **50**(7): 1277-1291.

Xu J, D. X., Yang J, Beeching JR, Zhang P (2013). "Enhanced reactive oxygen species scavenging by overproduction of superoxide dismutase and catalase delays postharvest physiological deterioration of cassava storage roots." Plant Physiol. **161**: 1517–1528.

Yan N (2015). "Structural Biology of the Major Facilitator Superfamily Transporters." Annu Rev Biophys. **44**: 257-283.

Yang C, G. R., Jie F, Nettleton D, Peng J, Carr T, Yeakely JM, Fan JB, Whitham SA (2007). "Spatial analysis of Arabidopsis thaliana gene expression in response to turnip mosaic virus infection." Mol Plant–Microb Interact **20**: 358–370.

Yang C, G. R., Jie F, Nettleton D, Peng J, Carr T, Yeakley JM, Fan JB, Whitham SA (2007). "Spatial analysis of arabidopsis thaliana gene expression in response to Turnip mosaic virus infection." Mol Plant Microbe Interact **20**: 358-370.

Yang K-Y, L. Y., Shuqun Zhang S (2001). "Activation of a mitogen-activated protein kinase pathway is involved in disease resistance in tobacco." PNAS **98**(2): 741-746.

Yang SJ, C. S., Cole AB, Cheng NH, Nelson RS (2004). "A natural variant of a host RNA-dependent RNA polymerase is associated with increased susceptibility to viruses by Nicotiana benthamiana." Proc Natl Acad Sci USA **101**(16): 6297-6302.

Yang SJ, C. S., Cole AB, Cheng NH, Nelson RS (2004). "A natural variant of a host RNA-dependent RNA polymerase is associated with increased susceptibility to viruses by Nicotiana benthamiana." Proc. Natl. Acad. Sci. **101**(16): 6297–6302.

Yifhar T, P. I., Peled D, Friedlander G, Pistunov A, Sabban M (2012). "Failure of the Tomato trans-acting short interfering RNA program to regulate AUXIN RESPONSE FACTOR3 and ARF4 underlies the wiry leaf syndrome." Plant Cell **24**: 3575-3589.

Ying X-B, D. L., Zhu H, Duan C-G, Du Q-S, Lv D-Q, Fang Y-Y, Garcia JA, Fang R-X, Guo H-S (2010). "RNA-Dependent RNA Polymerase 1 from Nicotiana tabacum Suppresses RNA Silencing and Enhances Viral Infection in Nicotiana benthamiana." The Plant Cell **22**(4): 1358-1372.

Yoshioka H, M. K., Yoshioka M, Kobayashi M, Asai S (2011). "Regulatory mechanisms of nitric oxide and reactive oxygen species generation and their role in plant immunity." Nitric Oxide **25**: 216–221.

Yoshioka H, N. N., Nakajima K, Katou S, Kawakita K, Rowland O, Jones JDG, Doke N (2003). "Nicotiana benthamiana gp91phox homologs NbrbohA and NbrbohB participate in H_2O_2 accumulation and resistance to Phytophthora infestans." Plant Cell **15**: 706–718.

Zavaliev R, L. A., Gera A, Epel BL (2013). "Subcellular dynamics and role of Arabidopsis β-1,3-glucanases in cell-to-cell movement of tobamoviruses." Mol Plant Microbe Interact **26**(9): 1016-1030.

Zerbino DR, B. E. (2008). "Velvet: Algorithms for de novo short read assembly using de Bruijn graphs." Genome Research **18**(5): 821–829.

Zhang J, S. F., Li Y, Cui H, Chen L, Li H, Zou Y, Long C, Lan L, Chai J, Chen S, Tang X, Zhou JM (2007). "A Pseudomonas syringae effector inactivates MAPKs to suppress PAMP-induced immunity in plants." Cell Host Microbe **1**(3): 175–185.

Zhao J, P. P., Schmitz RJ, Decker AD, Tax FE, Li J (2002). "Two putative BIN2 substrates are nuclear components of brassinosteroid signaling." Plant Physiol **130**(3): 1221-1229.

Zhou X, J. Z., Yu D (2011). "WRKY22 Transcription Factor Mediates Dark-Induced Leaf Senescence in Arabidopsis." Mol Cells **31**(4): 303–313.

Zhu F, X. D., Yuan S, Xu F, Zhang DW, Lin HH (2014). "Salicylic acid and jasmonic acid are essential for systemic resistance against Tobacco mosaic virus in Nicotiana benthamiana." Mol. Plant–Microbe Interact. **27**(6): 567–577.

Zhu SF, G. F., Cao XS, Chen M, Ye GY, Wei CH (2005). "The rice dwarf virus P2 protein interacts with ent-kaurene oxidases in vivo, leading to reduced biosynthesis of gibberellins and rice dwarf symptoms." Plant Physiol. **139**: 1935–1945.

Pirasteh Pahlavan

Curriculum Vitae

Endnotes

1 PAMP-triggered immunity

2 Microbial/pathogen-associated molecular patterns

3 Pattern recognition receptors

4 Mitogen-activated protein kinase

5 Nucleotide Binding-Leucine Rich Repeat

6 Effector-triggered immunity

7 Hypersensitive response

8 Effector-triggered susceptibility

9 Reactive oxygen species

10 Programmed cell death

11 Manihot esculenta

12 Putative protease (83 kDa)

13 Putative helper component protease (51 kDa)

14 Unknown function (34 kDa)

15 Unknown function (5 kDa)

16 Cylindrical inclusion putative helicase (71 kDa)

17 Unknown function (6 kDa)

18 Genome-linked protein (20 kDa)

19 Nuclear Inclusion protease (27 kDa)

20 Nuclear Inclusion polymerase (57 kDa)

21 Double-stranded DNA

22 Post-Transcriptional Gene Silencing

23 Virus-Induced Gene Silencing

24 *Turnip vein-clearing virus*

25 *Oilseed rape mosaic virus*

26 *Potato virus X*

27 *Cucumber mosaic virus*

28 *Turnip mosaic virus*

29 *Cabbage leaf curl virus*

30 Nucleotide binding site

31 Leucine-reach repeat domain

32 *South African cassava mosaic virus*

33 RNA Integrity Number

34 Solid- Phase Reversible Immobilization

[35] Gene Expression Omnibus

36 *Cassava brown streak virus* (https://www.ncbi.nlm.nih.gov/genome/?term=NC_012698)

37 *African cassava mosaic virus*, DNA1 (https://www.ncbi.nlm.nih.gov/nuccore/NC_001467.1)

38 *African cassava mosaic virus*, DNA2 (https://www.ncbi.nlm.nih.gov/nuccore/NC_001468.1)

39 ftp://ftp.solgenomics.net/genomes/Nicotiana_benthamiana/annotation/Niben044/

40 Weighted trimmed means of M-values

41 Differentially expressed gene

42 ftp://ftp.solgenomics.net/genomes/Nicotiana_benthamiana/annotation/Niben044

43 http://www.gomapman.org/export/current/OBO/ontology.obo

44 KEGG ORTHOLOGY

45 Gene Ontology

46 Kyoto Encyclopedia of Genes and Genomes

47 The collected data provided in Supp1_Data_Heatmap.xlsx

48 Suppressor of G2 allele of SKP1

49 Required for Mla12 resistance

50 Endogenous phytoene desaturase gene

51 Triple Antibody Sandwich Enzyme-Linked Immunosorbent Assay

52 Alkaline Phosphatase AffiniPure Rabbit Anti-Mouse IgG + IgM (H+L)

53 tricarboxylic acid

54 Pentose phosphate pathways

55That is available in Supp2_IDs_For_YANA_benthi.xlsx obtained according to IDs_For_YANA_Atal.csv

56 That is available in Supp3_FluxData_YANA.xlsx

57 Require for Mla12 resistance

58 Heat shock protein 90

59 Suppressor of the G2 allele of skp1

60 Database of Plant Virus genes

61 That is available in Supp4_Niben.xlsx

62 All the DEGs including their annotation and log2FC expression value are listed in Supp8_Results_DEseq2.xlsx and Supp9_Results_edgeR.xlsx, the counting output is provided in Sup/Count folder

63 This can be accessed in Supp6_Top500_Anot.xlsx

64 The detailed annotation information which was used for plotting is provided in Supp5_top100_pfam.xlsx and PieCharts_Data.pdf

65 Pentatricopeptide repeat proteins

66 Zinc finger

67 UDP glucuronosyltransferase 1 family

68 D-dopachrome decarboxylase

69 Heat shock protein

70 Asprich, aspartic acid-rich protein family

71 Apetala 2

72 ATPases associated

73 Peptide transport protein

74 Transcription factor TGA: K14431

75 Transcription factor MYC2: K13422

76 Numbers insides the bracket indicates the number of differentially expressed genes annotated in Pfam database.

77 Jasmonate ZIM domain-containing protein: K13464

78 Jasmonic acid-amino synthetase: K14506

79 OPC-8:0 CoA ligase 1 [EC:6.2.1.-]: K10526

80 Ethylene receptor [EC:2.7.13.-], ERS: K14509

81 Ethylene-insensitive protein 2: K14513

82 Ethylene-insensitive protein 3: K14514

83 Auxin influx carrier (LAX family): K13946

84 Auxin efflux carrier family: K13947

85 Auxin-responsive protein IAA: K14484

86 Auxin response factor ARF: K14486

87 Auxin responsive GH3 gene family: K14487

88 SAUR family protein: K14488

89 Adenylate isopentenyltransferase (cytokinin synthase), Adenosine phosphate isopentenyltransferase; K10760

90 Two-component response regulator ARR-A family: K14492

91 Two-component response regulator ARR-B family: K14491

92 Histidine-containing phosphotransfer protein, Plant hormone signal transduction [PATH:ko04075]; K14490

93 Arabidopsis histidine kinase 2/3/4 (cytokinin receptor) [EC:2.7.13.3], Transferring phosphorus-containing groups; K14489

94 Cytokinin dehydrogenase, [EC:1.5.99.12], Acting on the CH-NH group of donors; K00279

95 Enhanced disease susceptibility 1 protein: K18875

96 RPM1-interacting protein 4: K13456

97 Respiratory burst oxidase [EC:1.6.3.- 1.11.1.-]: K13447

98 Calcium-binding protein: K13448

99 EC:3.2.1.1

100 EC:3.2.1.2, Glycosidases, 3.2 Glycosylases; K01177

101 EC:3.2.1.68

102 EC:3.2.1.21, bglX, β-glucosidase, 3.2.1 Glycosidases, 3.2 Glycosylases; K05349

103 EC: 3.2.1.6, endo-1,3(4)-beta-glucanase [EC:3.2.1.6], endo-1,3(4)-beta-glucanase, 3.2.1 Glycosidases, 3.2 Glycosylases; K01180

104 EC:3.2.1.26

105 EC:3.2.1.96

106 Heparanase 1 [EC:3.2.1.166], 3.2.1 Glycosidases,3.2 Glycosylases; K07964

107 EC:3.2.1.15

108 EC:3.2.1.177

109 AGO, eukaryotic translation initiation factor 2C, RISC loading complex, microRNA pathway; K11593

110 BRCA1-associated RING domain protein 1 [EC:6.3.2.19], BRCC complex, multi subunit Ring-finger type E3, Ubiquitin ligases (E3); K16280

111 COPS1,CSN1; COP9 signalosome complex subunit 1; COP9 signalosome (CSN) complex; UBL-specific proteases (ULPs); Deubiquitinating enzyme (DUB); K12175

112 DNA repair protein RAD51, BRCC complex; multi subunit Ring-finger type E3, Ubiquitin ligases (E3); K10636

113 ERI1 exoribonuclease 2 [EC:3.1.-.-], Other RNAi proteins, RNA interference (RNAi) pathway; K18417

114 DCR1, endoribonuclease Dicer [EC:3.1.26.-], RISC loading complex, microRNA pathway; K11592

115 SWC4, EAF2, DNA methyltransferase 1-associated protein 1, SWR1 complex, Chromatin remodelling factors; K11324

116 CSN3, COP9 signalosome complex subunit 3, COP9 signalosome (CSN) complex; UBL-specific proteases (ULPs), Deubiquitinating enzyme (DUB); K12177

117 SMARCAD1, SWI/SNF-related matrix-associated actin-dependent regulator of chromatin subfamily A containing DEAD/H box 1 [EC:3.6.4.12], Other chromatin remodelling factors, Chromatin remodelling factors; K14439

118 DEK, protein DEK; B-WICH complex, Chromatin remodelling factors; K17046

119 RCK, [EC:3.6.4.13]; K12614

120 RDR, RDRP; [EC:2.7.7.48], RDRC (RNA-directed RNA polymerase complex), RNAi pathway; K11699

121 RNA-directed RNA polymerase complex

122 HDAC1_2, [EC:3.5.1.98], NuRD complex, Chromatin remodelling factors; K06067

123 CHD4, MI2B, [EC:3.6.4.12], NuRD complex, Chromatin remodelling factors; K11643

124 HAT2, CAF1, MIS16; Chromatin remodelling factors; K10752

125 *Tobacco rattle virus*

126 Loss-of-Function

127 *Pseudomonas syringae* pathovar tomato

128 *Pseudomonas syringae* pv. phaseolicola strain 3121

129 Pictures in Figure 18a-c, 20a-b, 21 are representative of three independent experiments using six independent plants

130 Days after agro-infiltration

131 Pictures in Figure 19 and 21 are representative of three independent experiments using six independent plants

132 Active oxygen species

133 Wound-induced protein kinase, MAPK cascades pathway

134 Salicylic acid-induced protein kinase, MAPK cascades pathway

135 Respiratory burst oxidase homolog, NADPH oxidase

136 Postharvest Physiological Deterioration

137 That is available in Supp7_ROS-Kegg.xlsx

138 DOX1; alpha-dioxygenase [EC:1.-.-.-], alpha-Linolenic acid metabolism [PATH:ko00592], lipid metabolism, K10529

139 that is available in Supp10_arabidopsis_metabolic_model.sbml

140 EC: 5.4.4.2 4.2.99.21; mbtl

141 EC: 5.4.4.2

142 EC:1.1.1.102; 3-Dehydro-D-sphinganine

143 EC: 2.3.1.50

144 EC: 1.3.1.42 ; OPRs

145 EC: 1.1.1.35

146 EC: 1.3.3.6: Superpathway of lipoxygenase , jasmonic acid biosynthesis

147 EC: 2.3.1.9: family of transferases, specifically acyltransferases

148 EC: 3.1.2.20

149 EC 6.2.1.-

150 EC: 4.2.1.17

151 EC: 5.3.99.6

152 EC: 4.2.1.92; AOS

153 EC: 1.13.11.12; LOX2S

154 EC: 2.2.1.2

155 EC: 1.1.1.44 1.1.1.343

156 EC: 1.1.1.49

157 EC: 3.1.1.31

158 Phosphoribosyl pyrophosphate, a pentose phosphate

159 EC: 2.7.6.1

160 EC: 2.7.1.11

161 EC: 2.7.1.90

162 EC: 4.1.2.13

163 EC: 4.2.1.11

164 EC: 3.1.3.11

165 EC: 1.2.1.59

166 EC: 2.7.2.3

167 EC: 5.4.2.11

168 EC: 2.7.9.2

169 EC: 5.3.1.1

170 EC: 2.3.1.12

171 EC: 1.2.4.1

172 EC: 1.8.1.4

173 EC: 4.2.1.3

174 EC: 2.3.3.1

175 EC: 2.3.1.61

176 EC 1.2.4.2

177 EC: 4.2.1.2

178 EC: 1.1.1.37

179 EC:6.2.1.4 6.2.1.5

180 EC: 1.3.5.1

181 EC: 1.1.1.42

182 EC: 1.97.1.12

183 EC: 1.10.3.9

184 EC: 1.18.1.2

185 EC: 1.10.9.1

186 EC: 2.7.1.19

187 EC: 2.2.1.1

188 EC: 5.3.1.6

189 EC: 5.1.3.1

190 EC 4.1.1.39

191 EC: 1.4.4.2

192 EC: 1.1.1.26

193 EC: 1.1.1.29

194 EC: 1.1.1.81

195 EC: 3.1.3.18

196 EC: 2.7.1.31

197 EC: 1.1.3.15

198 EC: 2.1.2.1

199 EC: 2.6.1.45

200 EC: 2.5.1.19

201 EC: 4.2.3.5

202 EC: 4.2.1.10

203 EC: 4.2.3.4

204 EC: 1.1.1.25

205 EC: 2.7.1.71

206 3-Deoxy-D-arabinoheptulosonate 7-phosphate (DAHP) synthase; EC: 2.5.1.54

207 EC: 3.1.3.3

208 EC: 1.1.1.95

209 PSAT; EC: 2.6.1.52

210 *Soybean mosaic virus*

211 Indole-3-acetic acid

212 Ethylene Responsive Factor

213 WRKY transcription factor 33; K13424

214 Skp1-cullin-F-box protein ligase

215 No Apical Meristem

216 Replication enhancer protein

217 *Tobacco leaf curl virus*

218 BR-signaling kinase

219 Protein brassinosteroid insensitive 2

220 Eeukaryotic translation initiation factor 2-alpha kinase 4

221 Histidine-containing phosphotransfer

222 Pentatricopeptide repeat

223 Aspartyl (acid) proteases

224 The term "IQ" refers to the first two amino acids of the motif: isoleucine (commonly) and glutamine (invariably)

225 Calmodulin-binding motif

226 *Plum pox virus*

227 Decapping enzyme 2

228 DICER1; endoribonuclease Dicer [EC:3.1.26.-], RISC loading complex, microRNA pathway, RNA silencing; K11592

229 RCK, DHH1, ATP-dependent RNA helicase DDX6/DHH1 [EC:3.6.4.13], piRNA pathway; K12614

230 ELF2C, eukaryotic translation initiation factor 2C, RISC loading complex, microRNA pathway; K11593

231 *Nicotiana tabacum*

232 Toll-interleukin-1 receptor homology/nucleotide binding/leucine rich repeat

233 *Tomato yellow spot virus*, Begomovirus

234 *Beet curly top virus*, Geminivirus

235 Brassinosteroid resistant ½

236 BRI1 kinase inhibitor 1

237 Rolling circle replication

238 Recombination-mediated replication

239 RING-H2 group F

240 *Tobacco necrosis virus*

241 *White clover mosaic virus*

242 *Potato virus Y*

243 *Bamboo mosaic virus*

244 *Crucifier-infecting strain of TMV*

245 Methyljasmonate

246 Coronatine insensitive 1

247 Oxophytodienoic Acid

248 Small interfering RNA

249 Tobacco mosaic virus

250 pathogen-inducible salicylic acid glucosyltransferase [EC:2.4.1.-], Glc b1-2 SA; K13691

251 Arabidopsis response regulator 2

252 TGA1 A-Related gene 3

253 S-adenosylhomocysteine hydrolase

254 Arabidopsis histidine kinase

255 Arabidopsis histidine phosphotransfer protein

256 *Rice dwarf virus*

257 BR-insensitive 1

258 Brassinazole resistant

259 Deetiolated2
260 Cytochrome P450 monooxygenase CYP90A1
261 Leucine-rich repeat receptor-like kinase
262 1-aminocyclopropane-1-carboxylate
263 1-aminocyclopropane-1-carboxylate synthase
264 Ethylene-responsive transcription factor 106
265 Ethylene insensitive 2
266 Ethylene insensitive protein 2
267 IAA-amino acid hydrolase
268 *Tomato mosaic virus*
269 Trans-acting siRNAs
270 Auxin response factors 3
271 *Tobacco mosaic virus*
272 *Sunn hemp mosaic virus*
273 Tricyclene synthase, involved in terpenoid biosynthesis and wound responding
274 RNA-dependent RNA polymerase 1 (a salicylic acid-responsive gene)
275 9-cis-epoxycarotenoid dioxygenase [EC: 1.13.11.51],; K09840
276 Vacuolar Transporter Chaperone 1
277 Constitutive Expresser of PR Genes 1
278 Extreme resistance
279 Coat protein
280 SGT1 specific sequence
281 Tetratricopeptide repeat domain
282 Present in CHP and SGT1 proteins
283 A multiprotein ubiquitin ligase (E3) complex (Skp/Cullin/F-box)
284 Cysteine and histidine rich domain
285 The "90, 70, 33 and 22" comes from their average molecular weight of "70, 70, 33, 20 kDa"
286 Nitro blue tetrazolium
287 3,3' -diaminobenzidine
288 *Zucchini yellow mosaic virus*
289 *Tomato ringspot virus*
290 Mitogen-activated protein kinase
291 *Plantago asiatica mosaic virus*
292 Wound-inducible protein kinase
293 SA-inducible protein kinase
294 Ascorbate Peroxidase 3
295 Glutathione peroxidase [EC:1.11.1.9]; K00432
296 Peroxidase [EC:1.11.1.7]; K00430

297 katE, CAT, catB, srpA; catalase [EC:1.11.1.6]; K03781

298 BCP, PRXQ, DOT5, peroxiredoxin Q/BCP [EC:1.11.1.15]; K03564

299 Dehydrogenase ascorbate reductase

300 Monodehydroascorbate reductase

301 Monodehydroascorbate reductase (NADH) [EC:1.6.5.4]; K08232

302 Pathogenesis-related

303 Suppressor of NPR1, inducible1

304 Pathogenesis-related genes transcriptional activator PTI6

305 basic leucine zipper

306 Ethylene-Response-Factor1

307 Endoplasmic Reticulum

308 EC: 2.4.1.13, Glc a1-b2 Fru, Other glycosyltransferases; K00695

309 UDP-glucosyl transferase 73C, [EC:2.4.1.-]; K13496

310 UDP-glucoronosyl and UDP-glucosyl transferase [EC:2.4.1.-], 2.4 Glycosyltransferases; K11718

311 UDP-glucose:glycoprotein glucosyltransferase [EC:2.4.1.-], 2.4 Glycosyltransferases; K11718

312 PYG, starch phosphorylase [EC:2.4.1.1], glycogen phosphorylase, 2.4.1 Hexosyltransferases, 2.4 Glycosyltransferases; K00688

313 Alpha-glucosidase [EC:3.2.1.20], Hexosyltransferases 2.4.1.1, glycogen phosphorylase, 2.4 Glycosyltransferases; K01187

314 MAN1, mannosyl-oligosaccharide alpha-1,2-mannosidase [EC:3.2.1.113], , 3.2.1 Glycosidases, 3.2 Glycosylases; K01230

315 Pd size exclusion limit (SEL)

316 4-Coumaric acid:CoA ligase

317 Coenzyme A

318 Basic endochitinase B

319 Hexokinase 1

320 Regulator of G-protein signaling protein 1 (G-protein-coupled receptor)

321 Cell wall invertase

322 1,3,4,5-tetrahydroxycyclohexanecarboxylic acid 3-(3,4-dihydroxycinnamate)

323 ATP-Binding Cassette

324 GLUT8, MFS transporter, SP family, solute carrier family 2 (facilitated glucose transporter), member 8; Sugar porter (SP) family [TC:2.A.1.1], Sugar transporters, Major Facilitator Superfamily (MFS); K08145

325 Fatty acyl-CoA reductase [EC:1.2.1.-], Sugar transporters, Sugar porter (SP) family [TC:2.A.1.1]; K1335

326 Transmembrane domain

327 Amino acid

328 Encodes a vesicular amino butyric acid (GABA) transporter, (VGAT)

329 A N-system amino acid transporter system protein involved in methyltryptophan resistance

330 Multidrug and toxic compound extrusion

331 Nitric oxide

332 2-(4-morpholinoo)-ethane sulfonic acid

333 Phosphate buffered saline

334 All the file types are ‘Conventional base calls’ with ‘Sanger / Illumina 1.9’ encoding

335 * indicates the primers retrieved from literature Liu D, S. L., Han C, Yu J, Li D, Zhang Y (2012). "Validation of reference genes for gene expression studies in virus-infected *Nicotiana benthamiana* using quantitative real-time PCR." PLoS One 7(9).